UNIVERSITÀ DI PISA
Scuola di Dottorato in Ingegneria "Leonardo da Vinci"

Corso di Dottorato di Ricerca in
Ingegneria Meccanica

Tesi di Dottorato di Ricerca

New Methodologies in the Field of Micromanufacturing

Md. Abu Hayat Mithu

Anno 2011

UNIVERSITÀ DI PISA

Scuola di Dottorato in Ingegneria "Leonardo da Vinci"

Corso di Dottorato di Ricerca in
Ingegneria Meccanica

Tesi di Dottorato di Ricerca

New Methodologies in the Field of Micromanufacturing

Autore:

Md. Abu Hayat Mithu

Relatori:

Prof. Marco Santochi, DIMNP, University of Pisa

Prof. Giovanni Tantussi, DIMNP, University of Pisa

Anno 2011

UNIVERSITÀ DI PISA

Scuola di Dottorato in Ingegneria "Leonardo da Vinci"

Corso di Dottorato di Ricerca in
Ingegneria Meccanica

Tesi di Dottorato di Ricerca

New Methodologies in the Field of Micromanufacturing

Autore:

Md. Abu Hayat Mithu _____

Relatori:

Prof. Marco Santochi _____

Prof. Giovanni Tantussi _____

Anno 2011

Abstract

Manufacturing processes are continually improving and updating with a view towards enhancing productivity. With the rapid development of technology, the demand for miniature, lightweight and advanced products is increasing. To compensate these emerging global trends towards the miniaturization of products, the electrochemical micromachining (μECM) is a promising technique. The μECM utilizes high frequency pulses for micron to nano-scale dissolution process that can be driven by with or without feedback control systems. This thesis includes the activities performed during the last three years, as the development of electrochemical micromachining workcell, fabrication of microtools, parametric effects analysis, and fabrication of various microproducts on some noble materials. During microtool fabrication, tungsten micro shafts of 0.38 mm are electrochemically etched to fabricate the desired cylindrical tools with or without conical tips. In the fabrication of microtool, electrolyte concentrations are varied in the range to 0.08–2.0 M KOH for the applied potential differences of 3–15 V AC and different etching time. The microtool fabrication process has been monitored by measuring the size, shape and overall tool geometry. These prefabricated microtools are used in the fabrication of various microdrilling and micromilling processes, especially in the fabrication of single hole micronozzles, multiple hole micronozzles array and microhole fabrication on vitrectomy needles. A mathematical model has been developed for the analysis of material removal rate (MRR) based on pulsed electrical power applied in μECM. The parametric effects of the process are studied on applied potentials, electrolyte temperature, applied frequency and its duty cycle, the dimension of microtools. For the parametric effect analysis, material removal rate, machining time, the number of short circuits, the shape and size of the fabricated microproducts are considered as response factors. The proper experimental parameters, the relationship between the parameters and the distribution of metal removal are established from the experiments worked out. The experimental micromachining tests show that MRR increases with the increase in applied potential, duty cycle, the electrolyte temperature, and microtool diameter, whereas MRR decreases with baseline potential in a certain range, applied frequency, and tool length. Machining time shows the opposite trend of MRR for all the parameters except microtool diameter. It increases with increasing microtool diameter. The microtool feed rate also has a significant effect on the dimension of fabricated microproducts. The waveforms generated during machining are analyzed; an in-process monitoring and control process has also been developed based on the waveforms. The result shows that the shape of the waveform and its corresponding values are in good agreement with the MRR, machining time and on the dimension of fabricated microholes. The proposed monitoring technique could be employed as a predictive tool in electrochemical processing. Finally, the microtools fabricated have been used for fabricating micronozzles and micropockets on nickel plates, microholes on high grade stainless steel to realize the practical applications of microdrilling process.

Sommario (in Italiano)

Il costante sviluppo dei processi di lavorazione ha lo scopo di aumentare la produttività. L'aumento della domanda di componenti miniaturizzati, leggeri e di qualità avanzata ha spinto la rapida evoluzione delle microlavorazioni: tra queste, le microlavorazioni elettrochimiche (μECM) rappresentano una tecnica promettente. Le lavorazioni μECM utilizzano un'alta frequenza di impulsi per il processo di dissoluzione anodica (nell'ordine della nano-scala e micro-scala), con o senza sistemi di controllo remoto. Questa tesi include le attività sviluppate nei tre anni passati e tese alla creazione di una cella di lavoro, alla fabbricazione di micro-utensili, all'analisi parametrica del processo ed alla fabbricazione di alcuni micro-prodotti su materiali nobili (resistenti alla corrosione e all'ossidazione). Durante la fabbricazione di microutensili, parti di tungsteno (0.38mm) sono state attaccate elettrochimicamente per realizzare utensili completamente cilindrici o dotati di punte coniche. In questa fase la concentrazione dell'elettrolita è stata variata tra 0.08 e 2 M KOH con differenze di potenziale di 3-15 V AC e vari tempi di lavorazione. Tale processo è stato monitorato misurando le dimensioni, e la geometria degli utensili che sono stati successivamente impiegati per operazioni di micro foratura e microfresatura. Tali lavorazioni sono servite per la realizzazione di microugelli a foro singolo o multiplo e per forare aghi da vitrectomia. È stato sviluppato un modello matematico per stimare il tasso di asportazione di materiale (MRR) basato sul regime impulsato di energia utilizzato nelle lavorazioni μECM. Il processo di asportazione di materiale è stato analizzato in funzione del potenziale applicato, della temperatura dell'elettrolita della frequenza e del suo duty-cycle e delle dimensioni dei microutensili. In tale analisi sono stati considerati come output del processo: il tasso di asportazione, il tempo di lavorazione, il numero di cortocircuiti e la forma e le dimensioni dei componenti realizzati. Gli esperimenti condotti hanno reso possibile determinare la relazione tra i parametri di processo e l'uniformità del processo di asportazione. I test sperimentali relativi alle microlavorazioni hanno mostrato come il MRR aumenti all'aumentare del potenziale applicato, del duty-cycle, della temperatura dell'elettrolita e del diametro dell'utensile, mentre un aumento del potenziale di "baseline" così come della frequenza applicata e della lunghezza dell'utensile, generano un effetto opposto. Il tempo di lavorazione è caratterizzato da una dipendenza opposta rispetto ai parametri sopra descritti, escluso che per il diametro del microutensile. La velocità di avanzamento del microutensile ha inoltre un ruolo importante nel determinare le dimensioni degli oggetto prodotti. Le forme d'onda del potenziale sono state analizzate durante le lavorazioni allo scopo di implementare un sistema di monitoraggio e controllo. I risultati sperimentali hanno dimostrato, infatti, che le forme d'onda, ed le relative ampiezze, sono un buon indicatore del MRR del tempo di lavorazione e della dimensione dei micro-fori. La tecnica di monitoraggio proposta può quindi essere impiegata come strumento predittivo per il controllo delle lavorazioni elettrochimiche. Come risultato finale, i microutensili fabbricati sono stati impiegati in operazioni di micro-foratura su lamine di nichel ed acciai inossidabile.

Acknowledgments

I would like to express my sincere gratitude to all those who stood by me through my doctoral program. The endeavor to complete my Ph D in the Department of Mechanical, Nuclear and production Engineering, University of Pisa would not be possible without the support of many people.

First and foremost I would like to express my sincere gratitude to my supervisors (tutors), Professor M. Santochi and Professor G. Tantussi for providing me a wonderful opportunity to be part of this research group and to perform research activities at the Department of Mechanical Nuclear and Production Engineering (DIMNP), University of Pisa. I am indebted to these two persons for mental support, continuous guidance, productive appreciation and encouragement during my research activity. In particular, I am grateful to Prof. Tantussi who taught me by hand. He also gave me the opportunity and freedom to think, to design and allowed me to put my skills into practice. It needs to mention here that I have greatly benefited from his outstanding experience in experimental research.

My sincerest thanks go to a young and energetic researcher Gualtiero Fantoni who were always up to speed on my work, and offered perfect guidance along the way. He is such a person who never says 'No'; always embodies the inquisitive nature needed in a research environment, and have inspired me to pursue problems in the respective fields of electrochemical micromachining, and related techniques.

My sincere appreciation and special thanks to M. Muhshin Aziz Khan, DIMNP, for his continuous encouragement, guidance, mental support throughout my living period in Pisa, and special thanks for his assistance while writing the thesis and other articles. This is also true for my first friend in Pisa, Luca Romoli who stood by me for the whole journey. Without his continual support (translating Italian to English, and English to Italian), expert guidance in personal life it was not possible to survive in a foreign country.

This research work has been carried out in the Department of Mechanical, Nuclear and Production Engineering, University of Pisa, Italy. It was only possible through the financial support by Ministero dell'Istruzione dell'Università e della ricerca, Programmi di ricerca cofinanziati (COFIN), Italia. I am indebt to the technical staffs of the DIMNP, F. Antonelli, G. Moretti, S. Balistrino, A. Rossi for all kinds of technical supports, assistance during the research work.

I would also like to thank the external members of the commission; to Prof. M. Lanzetta, DIMNP, University of Pisa, his valuable feedback and critical comments helped me to improve both the quality and appeal of this thesis and presentation.

I am grateful to the authority of Shahjalal University of Science and Technology, Sylhet, Bangladesh to grant me study leave during last three years. I am thankful to the Department of Industrial and Production Engineering (IPE), to all of my colleagues, and stuffs for their constant support and inspiration.

I am thankful to my co-fighters, J. Ciampi, S. Curcio, Mauro who stood besides me during the last three years in different time span. I am greatly benefited from their experimental activities. I am also grateful to many interesting people I've come to know over the last few years. They include V. Romoli, Salvatore, Viviana, Vinicio.

I am especially grateful to my mother for her love, moral support, infinite patience and positive influence over the years. Today I have no specific word to express my gratitude to whom, if were alive, he will feel be proud for his son. This work is dedicated to his memory.... My special thanks are also due to my brothers, Dr. Z.A. Tito, A.H. Tipu, M.M.H. Masum, and my sister H.A. Joly, who constantly energized me to achieve this degree.

Last but not least, I am sincerely indebt those who stood besides me, close to my heart, my wife Shamsunnaher Aysha, and my daughter Mrinmoyee Hayat Orchi. This work would not have been possible without their mental support, patient, love, and encouragement; I could not have ended this journey without their help. I would not be able to give-back the last three years, forgive me... I love you...

'Happy Birthday to my little Angel'

Pisa, 12 March, 2011 M. Abu Hayat Mithu

Dedicated to

the memory of late father
Abdul Malek Bhuiyan

and my mother
Habiba Akter Khatun

Contents

List of Figures

List of Tables

2-D / 3-D	Two dimension / Three dimension,
µECM	Electrochemical Micromachining,
AC / DC	Alternative current / Direct current,
AFM	Atomic Force Microscopy,
AJM	Abrasive Jet Machining,
BEM	Boundary Element Method,
CAD/CAM	Computer Aided Design /Computer Aided Manufacturing,
CL	Compact Layer,
CNC	Computer Numerical Control,
DL	Electrical Double Layer,
DRIE	Deep Reactive Ion Etching,
EBM	Electron Beam Machining,
ECAM	Electrochemical Arc Machining,
ECM	Electrochemical Machining,
EDM	Electrical-discharge Machining,
FEM	Finite Element Method,
IAD	Ion Angular Distribution,
IEG	Interelectrode gap,
IFE	Image Force Effect,
IHP	Inner Helmholz Plane,
LBM	Laser Beam Machining,
LECD	Localized Electrochemical Deposition,
LIGA	Lithographie (German acronym),
MEMS	Micro-Electro Mechanical System,
MOEMS	Micro-Opto-Electro-Mechanical Systems,
MRR	Material /Metal Removal Rate,
Ni	Nickel,
OHP	Outer Helmholz Plane,
RC	Resistor–capacitor (circuit),
RCL	Resistor-Capacitor-Inductance (circuit),
SEM	Scanning Electron Microscope,
STED	Shaped Tube Electrochemical Drilling,
STM	Scanning Tunneling Microscopy,
USM	Ultrasonic machining,
W	Tungsten,
WC	Tungsten Carbide,
WEDG	Electro-discharge Grinding,

Chapter 1

Introduction

1.1 PREFACE

Manufacturing processes are continually improving and updating with a view towards enhancing productivity significantly. The machining operations are one of the most prevalent methods utilized in manufacturing systems [1]. While the growths in the functionability of electrical and electronic components in conjunction with machining equipments, have been truly opening the avenue towards the field of high precision manufacturing processes [2–6]. With the rapid development of technology, the demand for miniature, lightweight and advanced products is increasing. Such a trend of size reduction demands the enhanced precision of manufactured products not only in terms of the dimension and shape, but also in terms of the roughness quality of the machined surface [7]. To compensate these requirements industries, universities and research organizations are increasing their efforts in this field, in not only all the advanced industrial countries but also in the developing countries. Micromachining is one of the key technologies that can enable the realization of all of the above requirements for microproducts and fields with such requirements are rapidly expanding [8].

The term micromachining refers to material removal of small dimensions that range from several microns to millimeter [9]. If machining can somehow possible in micron scale (less than 1 mm) following a specific manner, changing the geometry of products to a usable product, then the process is treated as micromachining. The great dream of micromachining is to build much smaller products, which will eventually be able to create any desired end product. Therefore, micromachining has a profound impact on future developments in practically all sectors of industrial activities, with their influence spanning from consumer products to more sophisticated applications.

This chapter introduces the basic issue of micromachining, the role of micromachining, the role of several nontraditional processes and especially the role of electrochemical processes, motivation, objectives, thesis organization, etc.

1.2 THE ROLE OF NONTRADITIONAL MACHINING PROCESSES

Manufacturing processes can be broadly divided into two broad categories: (a) primary manufacturing processes, and (b) secondary manufacturing processes. The primary manufacturing provides a basic size and shape to the material whereas, the secondary manufacturing processes provide the final shape and size with closer control on dimension, surface characteristics etc. Material removal processes are mainly the secondary manufacturing processes, can further be divided into two groups: (i) conventional or traditional machining processes, and (ii) nonconventional or nontraditional manufacturing processes [10].

The nonconventional machining processes are targeted for the production of difficult-to-cut materials, new materials of very high strength, complexity in shape and size, higher demand for product accuracy and surface finish, sometimes less pollutant and environmentally safe. To meet such challenges, non conventional manufacturing techniques have been classified according to the principal type of energy utilized to remove material– mechanical, chemical, thermal and electrical, and combination of them.

Ultrasonic machining (USM) and abrasive jet machining (AJM) are the two primary members of nontraditional mechanical processes. Material is removed through erosion, where hard particles, sometimes in liquid slurry, are forced into contact with the workpiece at a very high speed. Thermoelectric processes are broadly categorized into electrical and thermal processes, such as Electrical discharge machining (EDM), electron beam machining (EBM), ion beam machining, and laser beam machining. Metal removal in electrical discharge machining is achieved through high-frequency sparks hitting the surface of a workpiece submerged in a dielectric bath. In EBM, a high-speed stream of rapidly moving electrons impinges on a very narrow focusing zone on the surface of the workpiece with a consequent development of intense heat and results in fusion and vaporization of material. A laser beam and ion beam can produce tremendous energy, which is capable of melting and vaporizing materials from the surface of the material.

Again, in chemical machining is the controlled chemical dissolution of the workpiece material by contact with a strong reagent. Special coatings called masks protect areas from which the metal is not to be removed. The process is used to produce pockets and contours and to remove materials from parts having a high strength-to-weight ratio. In this machining, the depth of etch is controlled by the time of immersion. This can favorably be used in etching shallow depths in such common as well as exotic metals as aluminum, copper, and titanium, which are vulnerable to erosion by certain chemicals. Electrochemical machining (ECM) is characterized by a high material removal rate. The machining action is due to anodic dissolution caused by the passage of high density dc current in the machining cell. Other versions of ECM include electrochemical grinding, which includes about 90 percent ECM with 10 percent mechanical action; electrochemical arc machining (ECAM), in which controlled arcs in an aqueous electrolyte remove material at a fast rate; and capillary drilling, in which acid electrolytes are used to machine very fine holes [11]. Electrochemical deburring, honing, jet drilling are also included in this group.

1.3 THE ROLE OF MICROMANUFACTURING

Developments in different conventional and nonconventional machining processes and their machine tools have continued throughout the last 70 years due to the rapid enhancements in the accuracy of products. Ingenious designs of conventional machine tools have enabled complex shapes to be produced at an accuracy of ±1 micrometers (μm) [12]. Fig. 1.1 shows the accuracy attained by different conventional and nonconventional machining processes. In this modern world where the technology is getting smaller and smaller, and there is an international consensus that micromanufacturing or microfabrication is the unparallel candidate for the development of the next generation manufacturing technologies. To keep pace with this emerging global trend towards the miniaturization of manufacturing equipments and systems, several conventional and non conventional methods are used to fabricate microparts, microproducts and microsystems. Now-a-days, the use of a broad variety of working materials, components and their complex geometries and surface integrities are directing forward towards nonconventional micromachining, which can perform unprecedented tasks or add new capabilities and performances to traditional manufacturing processes.

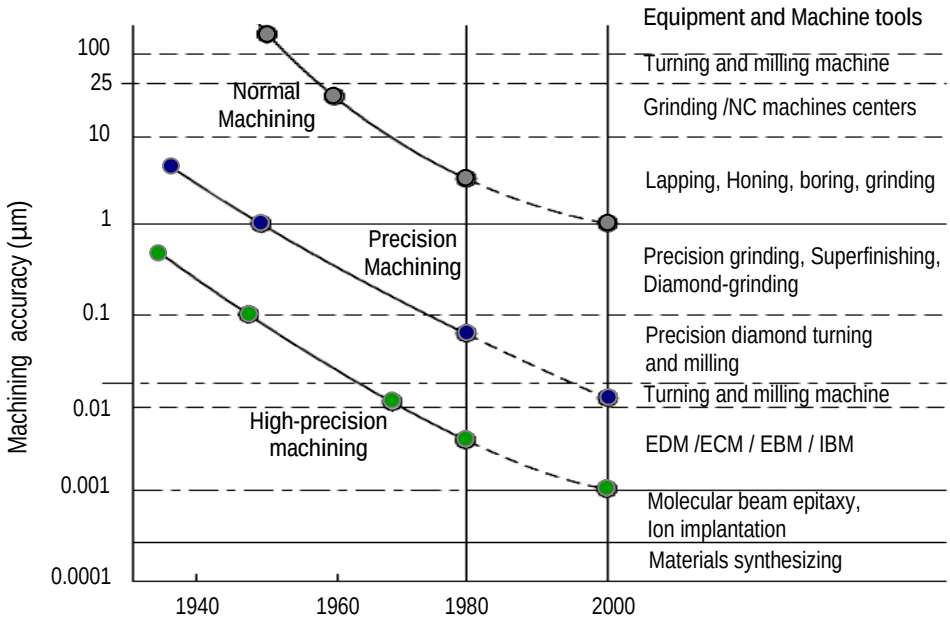

Fig. 1.1 *Machining accuracies attained by different manufacturing processes* [13].

With the advancements of various micromachining technologies for micro-manufacturing, several micromanufacturing processes are now competitors of each other. Not only this, some of these processes are combining to other processes targeting ultra precision manufacturing. For example, current computer chip transistors cannot be seen with the naked eye (they are usually micrometers in size); researchers are now attempting to make transistors even smaller called

nano-scale products. These smaller components allow manufacturers to pack more components into one useful product, say computer chips for more memory and faster speeds, where these small-scale products can be economically manufactured in a short period of time [14, 15]. Fig.1.2 displays an indication of the relevant sizes of known objects in order to visualize and understand the concept of micro and nano-devices or objects, whose outer dimensions are measured in micron to nano scale.

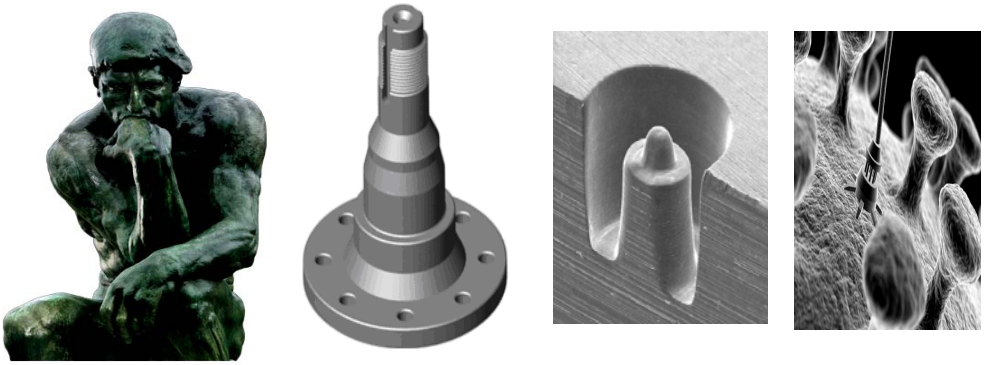

Macro (*meters*)
- Bridges
- Airplanes
- Cars
- Cranes
- Machine tools

Meso (*millimeters*)
- Cams
- Shafts
- Nozzle
- Watch gears
- Jig/Fixture

Micro (*micrometers*)
- Integrated circuits
- Micro-gears
- Needle
- Micro-nozzle
- Micro-gripper

Nano (*nanometers*)
- Viruses
- Nano-fiber
- Transistors
- Cell apparatus
- Nanofilters

Fig. 1.2 *The concept of different measurement scales.*

The nonconventional micromanufacturing processes are acquiring their importance due to some specific applications including the advantages and limitations in fabricating various shapes and sizes of microproducts. Two basic approaches, namely 'bottom-up' and 'top-down', are used in the fabrication of microproducts [16–18]. The bottom-up method involves moving atoms around to create devices, for example, electrochemical deposition process by mechanical or biological means. Besides, the top-down approach uses subtractive methods that etch away material to make the components smaller. For example, electrochemical micromachining process enabling to fabricate the micro-nozzles are now becoming increasingly important in many fields of microfluidic systems, MEMS and/or bio-MEMS, micro propulsion systems, flow control systems, printers, etc [19].

It is, therefore, envisaged as technology of choice to create complex three-dimensional shapes in various engineering materials [20]. Thus, it requires addressing the challenges for the near future [21, 22], such as: (i) to increase the knowledge related to micromachining process parameters for different materials and in consequence, increase micromachined components applications; (ii) to improve the development of microtools in order to reduce tool related errors; (iii) to devote energy to find out new techniques in microcutting process making the

process more compatible; (iv) to improve the structural rigidity and reduce the noises related to micromanufacturing; (v) to integrate CAD/CAM modules for micromachining with optimized machining strategies; and (vi) carrying out research on reliable, versatile, economical and practical sensing methods for monitoring and controlling the micromachining process. This close proximity controlling process makes the material dissolution process a bridge for the gap between the micron and nano worlds. A relational scale with various objects in order to compare the type of technology development required as well as to give body to the definition of micromanufacturing is illustrated in Fig. 1.3.

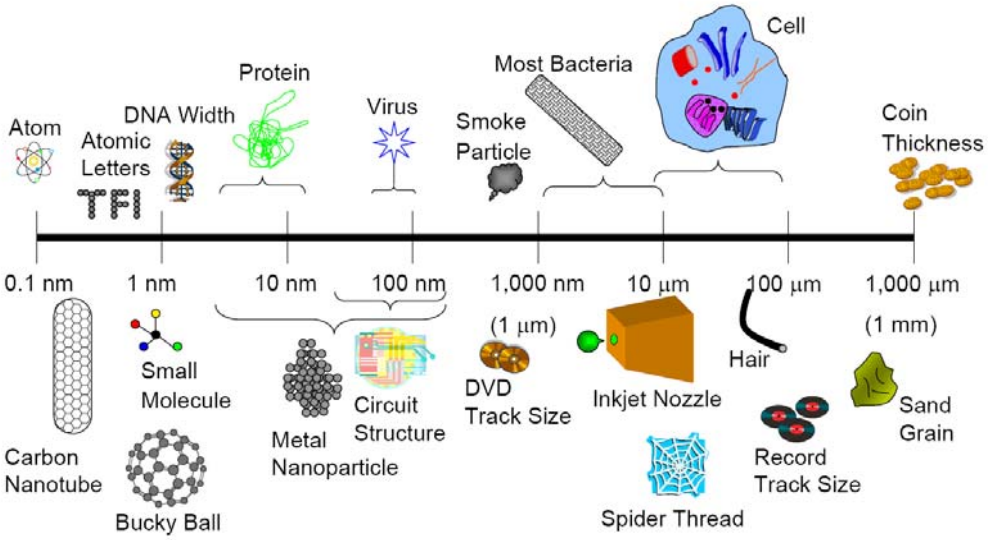

Fig. 1.3 *Relational scale showing the technological advancements* [23].

1.4 THE ROLE OF ELECTROCHEMICAL MICROMACHINING: FOCUSING AREA

Chemicals have been used for many centuries in the engraving of jewellery metals, as the use of chemical etchants are taking part in the removal of material from metal surfaces, as shown in Fig. 1.4. This process is based on the controlled removal of metal particles from a part's surface through targeted etching using acids and alkaline solutions. The substances, whose aqueous solutions allow the passage of electric current and are chemically decomposed, are termed electrolytes. Since Faraday's work in the early 1800s, it has been known that if two conductive materials are placed in an electrolyte bath and energized with a direct current, particles travel from the surface of the anode material toward the surface of the cathode material. The device in which electrolysis, chemical reaction involving oxidation and reduction, is carried out by using electricity is known as electrolytic cell. An electrolytic cell consists of a vessel for the electrolytic solution and two metallic electrodes immersed in the reaction material which are connected to a source of electric current. The phenomenon of electrolysis has wide applications. Electrochemical machining is one of the important applications.

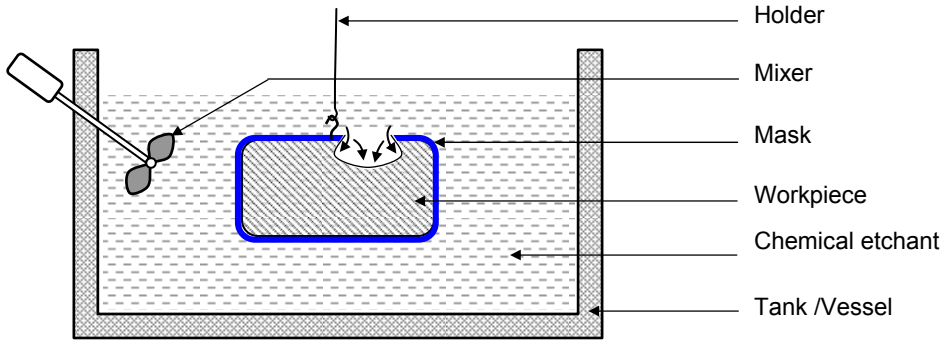

Fig. 1.4 *Chemical machining of metals.*

In electrochemical machining (ECM) processes, shown in Fig. 1.5, the workpiece is made anode (positive) and a tool is made cathode (negative). When an electric current is passed through the electrolyte, the amount of substance removed from the anode material is proportional to the quantity of electric charge passed through the electrolyte [24, 25] in order to give a desired shape to the anode or workpiece. The final shape of the workpiece is determined by the shape of the tool. Therefore, when the ECM is applicable on the manufacture of microparts, then the process is known as electrochemical micromachining (μECM). Unlike the other non conventional methods such as micro-milling, DRIE and LIGA mold processes, micro-EDM, LBM, EBM having different negative features promote electrochemical micromachining (μECM) has the promising future as the process offers better control and flexibility, requires very little monitoring and control, and can be anodically dissolved in neutral salt solutions. Therefore, the dissolved metal ions from hydroxide precipitates that remain in suspended form in solution can be easily filtered, thus significantly minimizing the problems of safety and waste disposal [26–28].

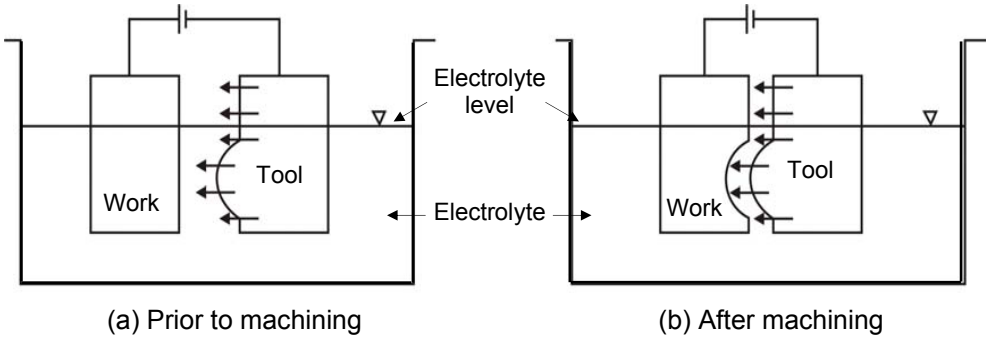

Fig. 1.5 *Electrochemical machining of metals* [10].

Today electrochemical micromachining (μECM) is standing out among all other micromaching processes due to its anodic dissolution process that effectively forms and shapes micro components from any conductive material. The dissolution process that can remove materials regardless of their hardness and toughness as

the process maintain a predefined gap between tool and workpiece. No tool wear occurs in this machining process as the process does not need any contact between the tool and the workpiece. As a result, neither residual stress nor a heat affected zone is generated offering a good quality machined surface [9, 29]. The growing popularity of μECM can also be attributed to its advantages including low setup cost, high aspect ratio of parts, and precision enhanced and large freedom in design stage [9, 30, 31]. With the advancement of newer electromechanical components and their increased rigidity and precision facilitates μECM to fabricate complex geometric parts even on various difficult-to-cut materials.

This method has proven suitable for the shaping of high corrosion resistant materials and alloys, which are not readily machined mechanically or chemically [29]. The μECM, which finds wider applications in microfabrication especially for the processing of advanced microelectronic components, medical and biomedical products (injection needle, vitrectomy needle, pacemakers, analysis equipment, sensors etc., in the field of aviation (cooling holes in jet turbine blades), space, automobile, electronics and computer, optics, miniature manufacturing etc., has also met the need for small and micro holes to be drilled with high aspect ratio in extremely hard and brittle materials. Moreover, micronozzles and other miniaturized flow control systems can be effectively fabricated on metal foils and films due to its capabilities of localizing the material dissolution, and producing the smooth and burr free surfaces.

Recently, the μECM is a versatile process that can be applied for surface profiling and texturing [32, 33], broaching [34], deburring [35], sawing, multiple hole drilling [36–38], smoothing and burnishing [39], and most importantly the fabrication of micro-probes, micro-channels used for medicine delivering systems etc. More recent, highly localized electrochemical dissolution technique is used to fabricate very precise work, thus the future of electrochemical micromanufacturing lies in the ability to convert microfabrication techniques into mass production manufacturing processes, where small-scale products can be economically manufactured in a short period of time.

1.5 MOTIVATION FOR THIS RESEARCH WORK

Micromanufacturing concerns manufacturing methods, technologies, equipment, organizational strategies and systems for the manufacture of products and/or features that have at least two dimensions that are within sub-millimeter ranges. Micromanufacturing engineering is a general term which concerns a series of relevant activities within the chain of manufacturing micro-products/features, including design, analysis, materials, processes, tools, machinery, operational management methods and systems, etc. [40].

Several conventional and nonconventional methods are used to fabricate micro-nozzles, as micro-punching [41], micro-milling, chemical etching, deep reactive ion etching (DRIE), LIGA mold process [42], laser drilling, electric discharge machining (EDM), and electron beam machining (EBM). Each method has some limitations in fabricating various shapes and sizes of micro-nozzles. Micro-punch leaves burrs and sometimes micro-cracks that restrict the flow inside the nozzle. Micro-milling,

DRIE and LIGA mold processes require several steps to make micro-nozzles having different feature sizes such as the bottom and the top diameters of the hole. Moreover, the DRIE fabrication method is not suitable for making a conical nozzle because of ion angular distribution (IAD) and image force effect (IFE), and a strong electrical field is required for the plasma glow [43]. Electro-discharge machining (EDM) is the most commonly used process for drilling fuel injector nozzles; although a typical EDM for the injector nozzle hole leaves burrs and a rough surface finish inside the hole [44]. The rough inside hole of an injector nozzle can cause geometrical variations and excessive flow restriction. Additionally, there is no mechanical tool easily accessible to the injector hole passage for deburring or polishing because of its small size and geometrical restrictions. They performed abrasive flow machining (AFM) to remove the burrs formed on the nozzle surface, surface profile and topography. However, AFM added extra cost to production. In the laser machining and EBM, very high energy density is needed for the ablation to machine the nozzle, where a machining pattern has to be programmed to manipulate the laser head at an angle of the half angle of the diverging part of the nozzle over a circular area. These processes also produce localized re-solidified affected zone, and leave microcracks on the workpiece surface where ablation occurs [29, 43].

On the contrary, electrochemical etching is a facile technique for the topographical dissolution of solids with nanometer precision through control of current density or voltage, fluid flow, etching time, and electrolyte composition, etc [45]. Besides the controlling parameters, for fabricating microproducts, the fabrication of microtool, its size and shape play an important role in μECM as the geometry of machined part is fully depends on geometry of the tool shape along with the parameters used for the process. As there is also no limitation in machining shape [46], microtools need to be machined accordingly. The shaping and sizing of microtools smaller than 200 μm in diameter by conventional machining processes is a very complex task [47], electrochemical etching, however, is the most widespread method for fabricating microtools [47– 50].

In order to achieve a meaningful implementation of micromachining technique, the research efforts seek to address on: (i) the development of machine tool, (ii) the development of process control and monitoring system, and (iii) the measurement and analysis of the micro-product to achieve the necessary accuracy and quality. The electrochemical micromachining workcell consists of an electrical function generator, an oscilloscope, computer controlled guide system for feeding the tool and the workpiece. The guides are controlled by a micro-step controller system that is interfaced with a desktop computer. To address the needs of smooth machining, it is necessary to develop a control system because a typical micro-machining is electrically and mechanically noisy and unstable due to vibrations [51] and thus the micromachining, especially electrochemical machining seeks the integration of process control systems. Among the influential factors, the potential applied and current are most prominent controllable factors. It is easier to control the dissolution process controlling the both. Taking the benefits of advanced digital electronic components in addition with visual instruments, the μECM processes can be easily monitored and controlled during the process. It would improve the accuracy [52] with no additional expenses.

Mask free electrochemical micromachining has been demonstrated by the use of ultra short voltage pulses, for appreciable polarization of the double layer only at very small electrode separations, resulting in highly localized dissolution of the workpiece [53]. High frequency pulsed voltage in electrochemical micromachining offers significant improvements in dimensional accuracy when compared with conventional or low frequency pulse electrochemical micromachining processes [54]. For this reason, ultra short voltage pulses are used to fabricate different three-dimensional micro features on corrosion and heat resistance materials commonly used in micro-technology [55]. Micronozzle with specified nozzle angle is an excellent example of for this type of applications where a controllable shape and size of entrance and exit are extremely desirable [56].

Electrochemical polishing or brightening of a surface is also achieved under rate limited conditions, where dissolution is independent of structure [57]. A very small quantity of material is removed from the product surface to give it a bright, burr free microstructure, for example micro-gripper, shown in Fig. 1.6.

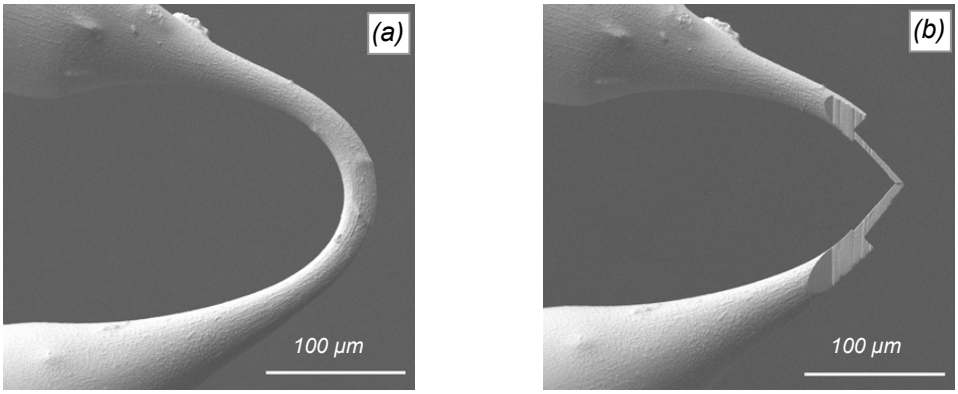

Fig.1.6 *SEM images of micro-grippers; (a) before, and (b) after microshaping* [58].

This research is, therefore, includes development of an electrochemical micromachining workcell, the fabrication of various microtools of desired shape and size, and the use of these microtools in µECM process to know on how the tool geometry and other machining parameters influence the µECM process. The study also promotes to develop an in-process control and monitoring system during microhole fabrication. In addition, it explores today's challenge of micro-nozzle and micronozzles array fabrication.

1.6 THESIS OBJECTIVES

The focus of this research work is electrochemical micromachining (µECM) process and the study is concentrated on workcell development, the functionability of various process parameters, the process monitoring and control, and fabrication of microproducts. For this perspective, the objectives of this study can be divided into following facets:

ECM machine development

The design of μECM machine demands several technical specifications to optimize the mechanical characteristics, such as stiffness, resonances etc with renouncing the compactness. From this point of view, activities associated with the development of μECM machine have been focused on:

(i) development of a rigid mechanical structure with desired number of degrees of freedom,
(ii) design and development of precision linear guide motion of the microtool holder and/or workpiece with 0.1 μm resolution in X, Y and Z directions,
(iii) design and development of the tool feeding and retreating mechanism,
(iv) fabrication of work holding fixtures for machining and post-machining measurements,
(v) improvement of damping system to prevent noises,

Fabrication of the microtools

A μECM tool electrode consists of very hard material such as tungsten, tungsten carbide, titanium, platinum, some supper alloys to satisfy high electrical and thermal conductivities, and high degree of stiffness. Microtools of different size and shape need to be fabricated depending on the geometry of the machined part. In this context, following attempts have been made:

(i) development of an integrated microtool and microproduct fabrication system,
(ii) development of a faster μECM tool fabrication system,
(iii) fabrication of a cylindrical microtool with a very high aspect ratio,
(iv) fabrication of a microtool with conical tip, and
(v) design and fabrication of single and multiple microtool holders.

Development of in-process monitoring and control system

As the fully automated manufacturing is expected to be realized in the near future, it is necessary to develop the in-process monitoring system and control the manufacturing process automatically. From a controls point of view, the μECM system can be driven in an open-loop and closed-loop fashion. Taking these facts into consideration, this study has focused on:

(i) the development of in-process monitoring system during electrochemical micromachining, and
(ii) development of a closed loop control system.

Parametric effects analysis

The aim of the paper is to study the μECM technique in particular, investigates the effects of different process parameters used in this process. Thus the goals are:

(i) optimization of the parameters (related to materials, dimensions, shapes), of the process (electrolyte, currents, topology of pulses, etc) during machining the tool material,

(ii) effect of μECM characteristic features on tool dimensions such as the diameter of tool electrodes, overall tool length, effective tool length (dipping depth), etc.
(iii) study on the effect of applied frequency on the shape and size of the fabricated micro-holes, machining time, and actual material removal rate (MRR_{act}) for various types of microtools
(iv) effect of duty cycle on machining time, MRRact, the number of short circuits and shape and size of the fabricated micro-holes.
(v) fabrication of micronozzles, micro-pockets by launching the formation of conical microtool.

Miscellaneous

(i) The common goal is to build the technology map of the μECM technologies considered within the project.
(ii) Electrochemical polishing or brightening of microproduct (micro-gripper) surfaces.
(iii) Development activity on vitrectomy needle for eyeball operation.

1.7 THESIS ORGANIZATION

The main body of this thesis is organized into eight chapters. A brief summary of each chapter is provided below.

CHAPTER 1 INTRODUCTION. This chapter introduces the basic issue of manufacturing processes, the role of micromachining, the role several nontraditional manufacturing processes and especially the role of electrochemical processes, motivation, objectives, thesis organization, and at last the summary.

CHAPTER 2 LITERATURE REVIEW. This chapter contains a review of the previous works done by different researchers on electrochemical micromachining to find out the gap in their research activities and the experiments are designed and performed accordingly. The chapter provides the idea on electrochemical process parameters, and how the process parameters influences on machining operations.

CHAPTER 3 EXPERIMENTAL. This chapter devoted to the experimental details, e.g. the design and development of electrochemical micromachining workcell, physical arrangements and architecture of electrical and electronic components, selection of different process parameters such as tool and workpiece materials, electrolytes, electrical power, procedure for fabricating different microtools and corresponding microholes, micro-cutting etc, measuring instruments and fixtures used for measurements, and at last the procedure of process monitoring and control. Experimental parameters are also presented in a tabular format.

CHAPTER 4 EXPERIMENTAL RESULTS. This chapter provides the experimental results that highlight the influence of various important electrochemical micromachining parameters like machining voltage, applied frequencies and its duty cycles, electrolyte concentration, temperature, microtool dimensions on material removal

rate, machining time, accuracy in the dimension of fabricated microproducts, and some noble issue of micromachining.

CHAPTER 5 DISCUSSIONS. The goal of this chapter is to provide an understanding of the processes involved in localized material dissolution in terms of how the process parameters affect on the machining zone. The chapter starts with the development of mathematical model developed to estimate material removal rate under pulsed power supply. In addition, an in-process monitoring system has been developed based on the waveforms generated during machining.

CHAPTER 6 CONCLUSION. This chapter provides a summary on the results and discussion found from the experiments. Recommendation for the future work is also outlined.

1.8 SUMMARY

Machining is one of the most important manufacturing processes, used to remove unwanted materials from the workpiece. Parts manufactured by other machining processes often require further operations before the product is ready for application. The conventional machining utilizes cutting tools that must be harder than the workpiece material and mechanical contact is present between the tool and the workpiece. The nonconventional machining processes are well-established in modern manufacturing industries to machine very hard difficult-to-cut materials. The need for higher machining productivity, product accuracy, and surface quality led to the nonconventional machining actions. Among the all nonconventional machining processes, μECM offers some unique advantages over competing technologies and therefore finds increasing applications in the electronics and microsystems industries, medical products, and other miniature manufacturing. Pulse electrochemical micromachining possesses attractive features compared to conventional electrochemical machining processes based on a continuous current because it allows instantaneous electrochemical reaction by applying ultrashort voltage pulses. The localization of material dissolution has been proved to be an absolutely necessarily technique in μECM to increase the replication of the surface and the precision of the part. For this reason, the uses of ultra short voltage pulses are used in the field of electrochemical micro-fabrication. More recent, the μECM is a versatile technique for surface profiling and texturing, deburring, broaching, multiple hole drilling, surface smoothing and burnishing, and the fabrication of micro-probes, microchannels etc.

Chapter 2

Literature Review

2.1 INTRODUCTION

The last twenty years have been fundamental in the development of new micro devices. The number of micro-products has increased in several fields such as biomedical, aerospace and automotive, and the rate of their growth does not seem to diminish. Beside the Micro-Opto-Electro-Mechanical Systems (MOEMS), manufactured by using silicon technologies, new hybrid microproducts emerged in the more recent past. Hybrid micro-products have complex three-dimensional structures and are composed of several components made by different materials [59]. Many of these micro-components, to resist to mechanical stress or wear and corrosion, are manufactured by using hard materials and alloys (e.g. Ti or Zr based alloys), which are difficult to be machined mechanically. Therefore new techniques have been developed to achieve high resolution, component repeatability and reduced tool wear. One of these new technologies is electrochemical micromachining (μECM).

Electrochemical machining (ECM) is a relatively old machining technique which is characterized as 'reverse electroplating' in that it removes material instead of adding it [60]. In the 19th century, the greatest researcher Michael Faraday discovered the principles of anodic metal machining. This discovery by Faraday has laid the foundation for the better known electroplating and electro polishing techniques, commonly applied today in electrochemical processes. Many years later in 1929, the Russian researcher W. Gussef developed the process to machine metal anodically that is the basis for electrochemical machining [61]. Now-a-days this technique has wide-spread applications. This chapter reviews literature on basic principles of ECM, and relative operations e.g. fabrication of microtools, micromachining environments, and some microproducts fabricated by μECM.

2.2 ELECTROCHEMICAL MICROMACHINING

Electrochemical micromachining (μECM) is a noble technique based on a very simple idea of applying voltage pulses between two conductor electrodes. Two electrically conductive materials (workpiece and tool, connected to the electrical connections) immersed in an electrolytic solution. On the application of a potential difference between the electrodes, material removal takes place from the anode workpiece. During machining, the tool and/or workpiece move relatively to each other to maintain a predefined gap between them. The schematic diagram of an ECM system is given in Fig. 2.1. Based on the same principle, μECM has a wide range of applications such as electrochemical grinding, electrochemical honing, electrochemical milling, electrochemical drilling, electrochemical deburring, and electrochemical turning, etc.

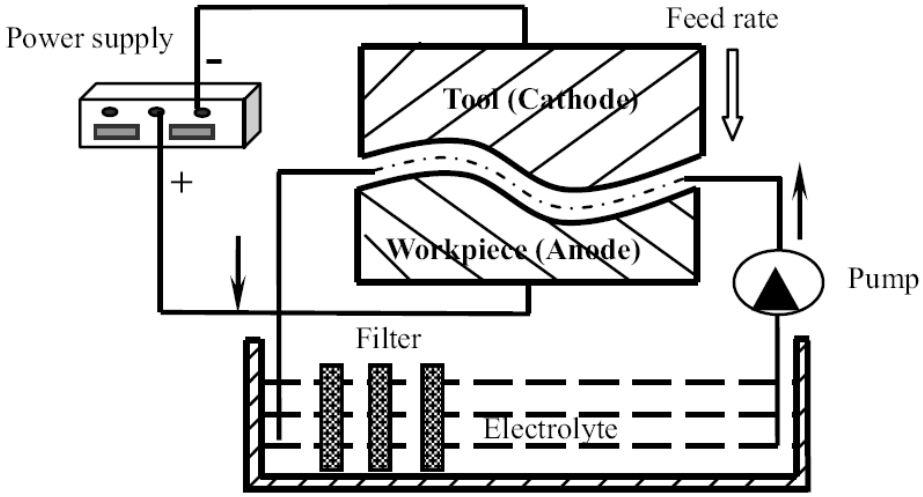

Fig. 2.1 *Schematic diagram of an ECM system* [62].

The basis of electrochemical machining is electrolysis where the metal removal is achieved by electrochemical dissolution of an anodically polarized workpiece, which is one part of an electrolytic cell [63]. In electrolytic cell, etching involves conversion of a solid insoluble material to a soluble form. The extended lattice of metal atoms in the solid state must be broken down so that these atoms can enter the solution as soluble compounds. This is accompanied by removal of electrons from the anode metal surface, and these electrons go to the electrolytes which act as an oxidizing agent during electrolysis [64]. The positively charged ions move towards the cathode and the negatively charged ions move towards the anode. Since the electrolyte must be neutral, there must be a balance between the total positive charge and the negative charge. But the current applied into the cell determines the rate at which the charged electrons movement across the electrode-solution interfaces [65]. At the end of the reaction, the amount of material lost by one of the electrodes is equal to the amount of material gained by the other [66]. Hence, this process can be better explained by the chemical reactions occurred during the electrochemical machining processes. On the application of a

potential difference across the electrodes, and subsequently when adequate electrical energy is raised to a level high enough between the tool and the workpiece, metal ions leave from the surface of the anode workpiece [67]. Since electrons are removed from the workpiece, oxidation reaction occurs at the anode which can be represented as,

$$M \rightarrow Mn^{+} + ne^{-} \tag{2.1}$$

where *n* is the valence of the workpiece metal. The electrolyte receives these electrons liberated from metal surface, and at the cathode, the reaction is likely to be the generation of hydrogen gas and production of hydroxyl ions:

$$nH_2O + ne^{-} \rightarrow \frac{n}{2}H_2(\uparrow) + nOH^{-} \tag{2.2}$$

Therefore, the metal ions (positive) combine with the hydroxyl ions (negative) in the electrolyte to precipitate out as metal-hydroxides, so that the net reaction is

$$M + nH_2O \rightarrow M(OH)_n + H_2 \uparrow \tag{2.3}$$

For example, during the fabrication of tungsten-carbide microtool with sulfuric acid, the probable chemical reactions of WC with Co binder at the anode of WC (Cobalt present in a few percentages), is dissolution of tungsten carbide and water [47]:

at anode, $$WC + 5H_2O \rightarrow WO_3 + CO_2 + 10H^{+} + 10e^{-} \tag{2.4}$$

$$WO_3 + 2H_2O \rightarrow WO_3.2H_2O$$

$$Co + WO_3 + H_2O \rightarrow CoWO_4 + 2H^{+} + 2e^{-}$$

$$Co + 2H_2O \rightarrow Co(OH)_2 + 2H^{+} + 2e^{-}$$

$$Co + 2H_2SO_4 \rightarrow CoSO_4 + 2H^{+} + 2e^{-}$$

and, at cathode, $2H^{+} + 2e^{-} \rightarrow H_2$ (gas) (2.5)

As expressed in Eq. 2.4 at the anode, W in WC reacts with H_2O to form the oxidized WO_3 (tungsten oxide), which is then attached to the specimen in the form of porous sludge. Carbon in WC forms CO_2 gas and the generation of CO_2 leads to porosity and cracking in WO_3 owing to the force of the escaping gas [68]. Then WO_3 combines with the water molecule and thus exists as the hydrated tungsten ($WO_3 \cdot 2H_2O$) [69]. Some WO_3 reacting with Co and H_2O produces $CoWO_4$. As expressed in Eq. 2.5, at the cathode a proton (H^{+}) in the electrolyte gains an electron to reduce to a hydrogen gas (H_2).

Thus the electrolysis has involved the dissolution of tungsten-carbide workpiece and the generation of hydrogen gas at the cathode. The formation of metallic hydroxyl, sometimes precipitated in the gap between the tool and workpiece electrode, is constantly flushed away from the gap between the tool and the workpiece to prevent short circuits. The process of electron movement within an electrolytic solution can be attributed to the ‘electrokinetics’, associated with the movement of an electrolyte solution, especially ‘electro-osmosis’ that is defined as

the phenomenon associated to the movement of an electrolyte solution near a charged interface under the influence of an electric field parallel to the surface [70]. The movement of charged particle depends on the types of electrolytes used; say acidic electrolyte, basic electrolyte or isoelectric electrolytes, and the current density of the electrolyte, which is primarily determined by the concentration of ions, and by the mobility of ions in a given electric field [50]. For different electrolytes, the movements of charged ions from the surfaces of metal oxides in solution are illustrated in Fig. 2.2., for which the surface charges depend on the pH of the solution.

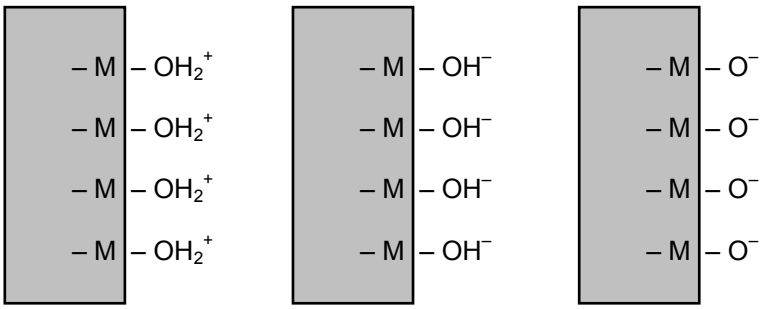

Fig. 2.2 *Surface ionization of metal oxides in aqueous solutions* [70].

2.3 BASIC PRINCIPLE OF MATERIAL REMOVAL

The amount of material removed is determined by Faraday's first law which states that the rates at which metals can be electrochemically machined is in proportion to the current passed through the electrolyte and the elapsed time for that operation, and is in inverse proportion to the electrochemical equivalent of the anode-metal which corresponds to the atomic weight of the dissolving ions over the ionic charge times the Faraday's constant [67, 69, 70]. Therefore, the volume of material removed during machining can be expressed as:

$$V_m = CIt \tag{2.6}$$

where,

V_m = volume of metal removed during machining in cube millimeter (mm^3),
C = electrochemical constant (mm^3/amp-s),
I = current (amp),
t = machining time (sec).

The electrochemical constant is a unique property, and given by

$$C = \frac{A_w}{z.F.\rho_a} \tag{2.7}$$

where, A_w = molecular mass of the work material,
z = number of valence electrons,
F = Faraday's constant (96,485 Joule per volt gram equivalent),
ρ_a = density of work material.

These parameters are now related to the current through Ohm's Law, which states that the current flowing in a conductor is directly proportional to the applied voltage. Therefore, combining the Faraday's and Ohm's law, the resultant equation comes:

$$V_m = C.\frac{E}{R}t \tag{2.8}$$

where, E = applied voltage and R = resistance of the conductor. In electrochemical machining, the electrolyte resistance,

$$R = \frac{g.r}{A_s} \tag{2.9}$$

where,

g = inter-electrode gap, i.e., gap between the tool and the workpiece,
r = resistivity of the electrolyte (ohm-mm),
A_s or A = surface area of tool electrode that taking part in machining (mm^2).

Hence, the volume of material remove during machining is given as,

$$V_m = C\frac{EA}{gr}t \tag{2.10}$$

The rate at which material is dissolve during machining is calculated as the total volume of metal removed over the machining time. This is also termed as actual material removal rate (MRR_{act}), can be expressed as,

$$MRR = MRR_{act} = \frac{V_m}{t} = \frac{CEA}{gr} \tag{2.11}$$

This equation is based on the ideal process, i.e., process efficiency is 100%.

But the engineering materials are quite often alloys rather than element consisting of different elements in a given proportion. To find out the volume of material removed, lets assume that there are n number of elements are present in an alloy. The atomic weights of different components are given as A_1, A_2, ……, A_n with valency of z_1, z_2, ……, z_n, and the weight percentages of different elements are α_1, α_2, ……., α_n (in decimal fraction).

Now for passing a current of I for a time t, the mass of material dissolved for any element j is given by,

$$m_j = V_m \rho_j \alpha_j \tag{2.12}$$

where V_m is the total volume of alloy dissolved. Each element present in the alloy takes a certain amount of charge to dissolve. The amount of charge required for the specific material is

$$Q_j = \frac{Fm_j z_j}{A_j} = \frac{FV_m \rho_j \alpha_j z_j}{A_j} \tag{2.13}$$

The total charge, Q_T passed during machining,

$$Q_T = It = \sum Q_j = FV_m \sum \frac{\alpha_j z_j \rho_j}{A_j} \tag{2.14}$$

Therefore, the MRR of an alloy (MRR_{alloy}) will be calculated as,

$$MRR_{alloy} = \frac{V_m}{t} = \frac{EA}{grF}\left(\sum \frac{A_j}{\alpha_j z_j \rho_j}\right) \tag{2.15}$$

This is a theoretical approach to find out the total volume removed during machining, or to find out the material dissolution rate. However, in practice, it is not easy to find out the actual value of MRR, as the process depends on a lot of other variables.

The behavior of the anodic workpiece in the particular electrolyte chosen also affects the rate of the reactions. The current resulting from a change in oxidation state of the electroactive species is termed the faradaic current because it obeys Faraday's law. The faradaic current is a direct measure of the rate of the redox reaction. The exact shape and magnitude of the voltage-current response is governed by the processes involved in the electrode reaction [65]. Therefore, the total current is the summation of the faradaic currents and non-faradaic current. During μECM, material removal is ascribed to current density distribution on the workpiece surface. As it is not simple to determine the current density, analytical methods are applied to estimate the current density. Therefore, factors that affect the rate of machining are type of electrolytes used, flow rate of electrolyte, temperature of electrolyte, and its pH value. It has been pointed out that in practice the feed rate and the dimension of tool affect the MRR during machining [71]. As the tool advances towards the workpiece, the workpiece dissolved electrochemically is flushed away together with generated gas bubbles and Joule heat by the flowing electrolyte. The area of the workpiece exposed in the electrolyte can be dissolved when sufficient voltage is applied [72].

2.4 PROCESS PARAMETERS

After the development of a well-balanced experimental setup, the effectiveness and productivity of a μECM process is critically dependent on certain factors termed as machining parameters. These factors have a significant influence not only on the machining performance but also on process monitoring and controlling behavior. Fig. 2.3 shows a fishbone diagram (also called Ishikawa diagram or cause and effect diagram) indicating the influential μECM process parameters. These parameters can be categorized into four groups: electrical power, electrolytes, tool material, and workpiece material. The type of electrolyte, contamination in percentage, concentration, temperature, flow rate or viscosity, electrical or thermal conductivity and mass transport capacity are the important considerations in μECM. Types of power supply, i.e. AC or DC power or pulsed power, current density, applied potential, applied frequency and its amplitude, duty cycle determines the material removal rate, surface finish and dimensional accuracy. For effective utilization of ECM in micromachining applications, extensive research efforts have been made to address the important issues associated with the process.

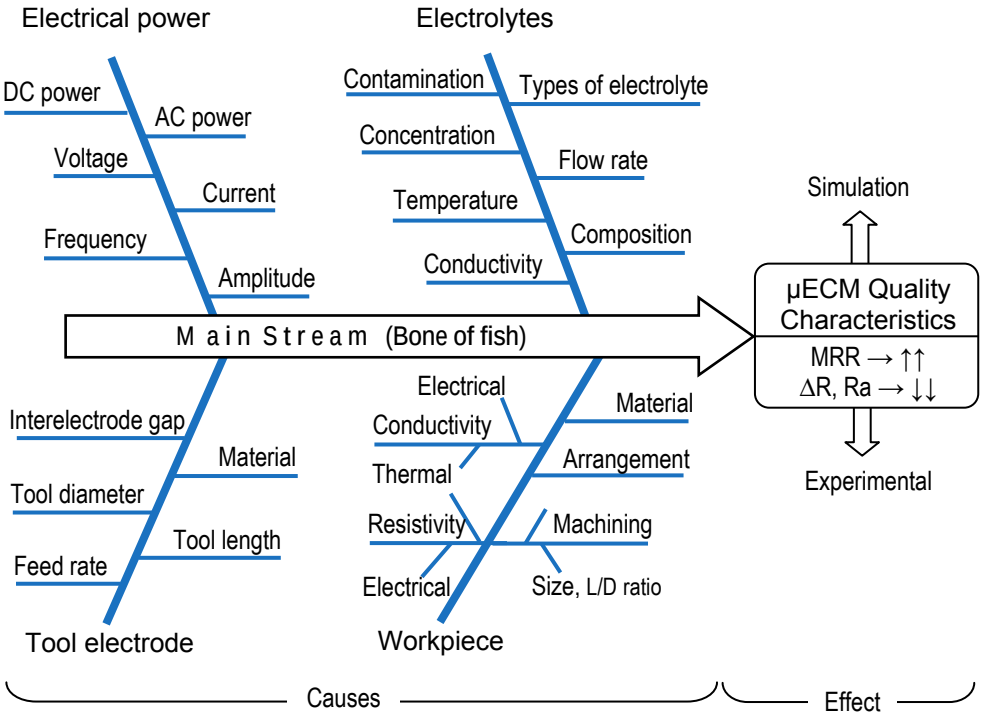

Fig. 2.3 *Major factors affecting μECM performance.*

2.4.1 Electrical Power

Electrical power is the driving force for the flow of charged particles inside the electrolyte. The electrical field strength depends on what type of electricity is passed through the electrolyte solution [73]. In electrochemical machining both AC (alternating current), where a constant or linearly changed potential is superimposed by an alternating (sinusoidal) potential signal, and DC (direct current) where the applied potential or current is constant or changed linearly or stepwise but not sinusoidal, are used. Some researchers fabricated structures like tungsten microtool using AC current [74]. A 20 V AC current was applied for initial shaping of that microstructure, and the applied potential was reduced towards zero as the tool tip shape diminished in size [75]. This technique produced a very good tungsten tool tip for atomic force microscopy. Further research attempted to improve the AC method by controlling the applied voltage, frequency, wave-shape and wave-count [76]. It was observed that the tool shape depended on the frequency or the alternative current and that low frequency was remarkably effective in reducing the radius of the wire in the case of the polishing Mo with 5% KOH solution at 12 V AC.

The most remarkable effect associated with the use of an AC voltage is the abundant formation of gas bubbles around the workpiece surface [77]. These gas bubbles propagated upwards along the side wall of the tool electrode, accumulated

near the shank part of the tool, forms a protective layer around the neck of the tool where air-electrolyte interfaced. These upcoming bubbles make a shield around the tool specimen during microtool fabrication [78]. Moreover, the bubbles distributed around the lower part of the wire yield a delocalized electrolytic attack [77]. However, it has been demonstrated [77, 79] that one can take advantage of this bubble stream to fabricate the conical shaped tools for some specific μECM applications where a sharp tool tip is needed. In this context, the cone shaped tips of AC etched tools are longer than that of the DC etched tools. An AC voltage, typically a few kHz frequency, is applied between the tool specimen and counter electrode [80]. Similar work has been done where a Pt-Ir wire tool was etched with respect to a nickel foil as the counter electrode. The applied current was 20 V AC by varying the immersed depth of the specimen. The etching proceeded faster at the air-solution interface, and a narrow neck was formed [81].

But the preferred method for electrochemical fabrication process is using DC current [82]. The DC etched tools in the shape of a hyperboloid, on the other hand, are much sharper than AC etched tools and are preferable for high-resolution scanning tunneling microscopy (STM) imaging [83]. The main problem in using DC current is that the formation of thick oxide layer (e.g. tungsten oxide, WO_3) develops on the workpiece surface regardless of the etching conditions during electrochemical etching [84, 85], but it is till now not totally known how the growth of this amorphous layer relates to the etching parameters [86, 87]. On the other hand, the neck generated by the DC current is preferable for the microtools, thus it is encouraging to use DC current for the fabrication of electrochemical tool by DC current.

The original ECM process is a procedure with DC-voltage source being mainly used for the machining of large areas [88]. Ibe [89] reported that the etching rate is virtually flat for the potential applied within 4 to 12 V. Below 4 V, etching rate drops significantly. The preferred method was DC power supply for preparing micro tool. Guise et al. [85] reported that if the power supply is DC, the tool contaminates surface oxides (WO_3) and ultimately must be removed before use in applications. Furthermore, it is important that if reversed potential is applied the contamination is lower than DC potentials as natural circulation occurs between electrodes.

A potentiostatic polarization curve of tungsten wire in 2 M KOH alkali media [90] showing the behavior of material removal rate versus cell potential during microtool fabrication is illustrated in Fig. 2.4. The result showed that it was not possible to fabricate the microtool in a reasonable period of machining time when the applied voltage was less than 2 V DC, but on increasing the potential the current density did not change sufficiently up until the onset of oxygen evolution at a cell potential of 9 V. Above 5 V, a thick black oxide film was sometimes produced. Therefore, it was advised to work with a cell potential not less than 5 V DC.

The abovementioned problems can be largely avoided by applying a pulsed voltage instead of a continuous voltage. Recently, the utilization of short pulsed power in mask-free electrochemical micromachining has been proved to be an absolutely necessary technology for the localized material dissolution process [53]. Pulsed current has three parameters: pulse-on time, pulse-off time and peak

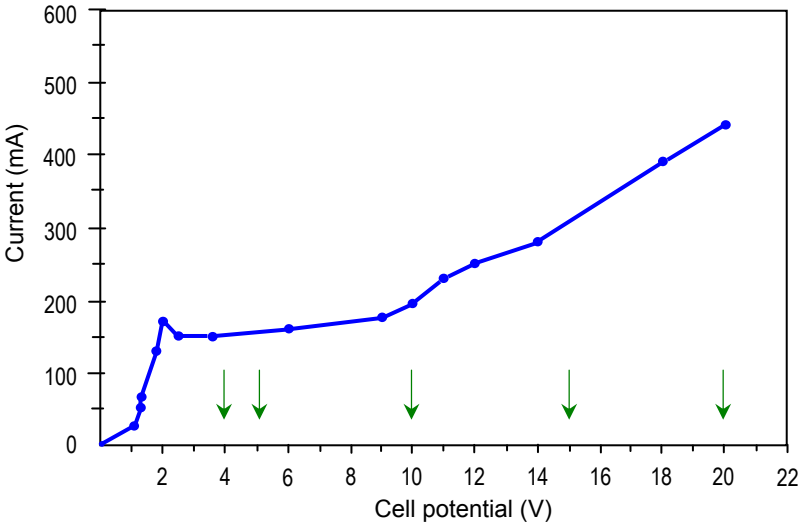

Fig. 2.4 *Current vs cell potential curve for tungsten in 2 M aqueous KOH electrolyte at 22^{0}C (Pt-wire ring cathode). Vertical arrows show cell potentials used* [90].

current density, which can be varied independently in order to achieve the desired machining rate [91]. Machining is performed during the pulse-on time and pulse-off time is kept long enough to dissipate heated electrolyte and produced gas formed during pulse-on time. The material removal is decreased due to highly confined electron motion, eventuating a major problem in ultrashort pulsed systems [27, 92]. Therefore, the useful values of the on and off-pulse times are limited by the rate of charging and discharging, respectively, of the electrical double layer, which is defined as the structure of charged ions or oriented dipoles that always forms at the interface of an electrode when it is immersed into an electrolyte solution [65]. On the application of a potential difference between two electrodes, the potential profile in the electrical double layer becomes similar to that of an equivalent circuit of capacitors and resistors [93]. However, all the current flow through an electrochemical cell is not caused by electrochemical reactions. There is reaction current called faradaic current and transient current called non-faradaic current [94]. Faradaic current determines the material dissolution rate and non-faradaic current results from current flow that charges and discharges only the double layer capacitance [95]. Novel techniques however employ pulsed voltage to reach better precisions. The applied voltage waveform plays a crucial role in defining a profile quality and surface finish of the product part [28, 53, 93, 96, 97]. The improvement of surface finish depends on the pulse duration and the interval time. In pulsed supply micromachining, periodic replacement of electrolyte makes it possible to apply a higher instant current density during the pulse-on time, leading to significant improvement of surface quality. Pulsed current enables recovery of the gap during pulse-off time, giving improved dissolution of the product part.

To investigate the machining performance of the ECM system, microhole drilling was carried out under various machining conditions [98]. The machining voltages,

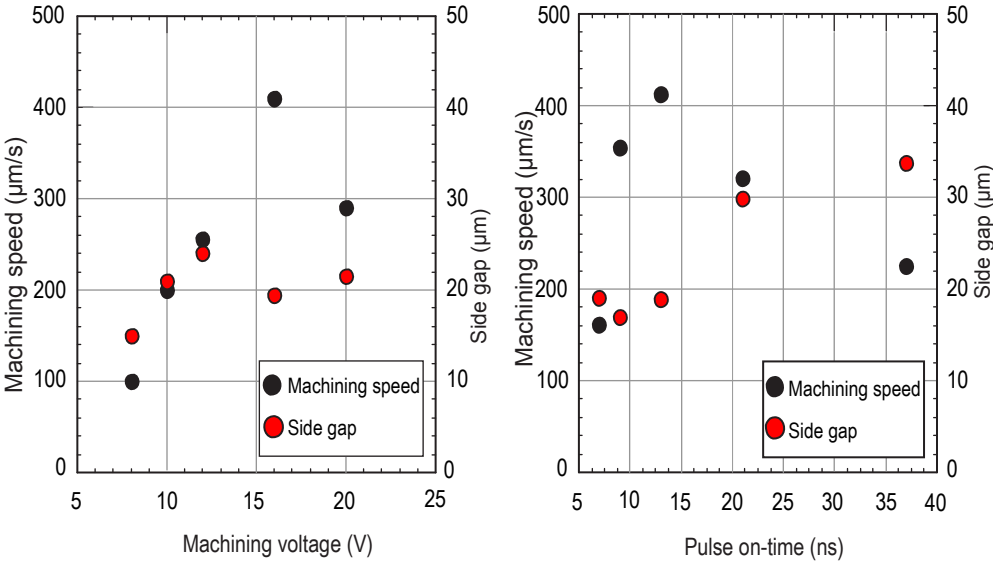

Fig. 2.5 *Machining speed and side gap versus machining voltage (left) for pulse-on time 32ms, and pulse-on time (right) for 16V pulsed power supply* [98].

pulse-on time were varied to show the machining performance under machining speed and side gap produced as shown in Fig. 2.5. It was found that the machining speed and side gap increase with the increase in the machining voltage. The machining speed reaches its maximum at the machining voltage of 16 V. Later on, the machining speed decreases with the increase in the machining voltage.

Recently many research efforts on electrochemical micromachining have been done both at theoretical and experimental level. High frequency pulsed voltage in µECM offers significant improvements in dimensional accuracy when compared with conventional or low frequency pulse electrochemical micromachining processes [99]. This technique has been proved to be an absolutely necessarily technique in µECM to increase the replication of the surfaces and the precision of the products' part [53, 100]. Mask free electrochemical micromachining demonstrated impressive results by the use of ultra short voltage pulses within narrower interelectrode gaps. For this reason, the use of very high frequency has been studied by different researchers lately. With the aid of very high frequency, three-dimensional micro features on stainless steel with 10 to about 1000 nanosecond duration pulse [101], and a micro spiral groove on a nickel sheet with a few hundred picosecond pulses [45] were successfully fabricated. To localize the dissolution area, micro holes were drilled on stainless steel plate with tens of nanosecond duration pulsed voltage [93]. With the application of very high frequency inputs, electrochemical dissolution was found close to the electrode region [92, 102]. The effects of electrode gap and pulse parameters on electrochemical micromachining with ultra short voltage pulses were also experimented [103]. Similarly, the effects of tool electrode size and insulation on µECM characteristics were also studied, and suggested that the machining rate was significantly influenced by the tool electrode area for ultra short pulses-on time

[95, 104]. In ultra short voltage pulses, non-faradaic current dominates transiently and its shape is affected by the cell impedance which is the sum of resistance and capacitive reactance. When the tool electrode diameter or the machining area increases, the cell impedance decreases because the electrolyte resistance decreases, and the double layer capacitance increases, as a consequence, the machining rate decreases with the tool electrode diameter as shown in Fig. 2.6.

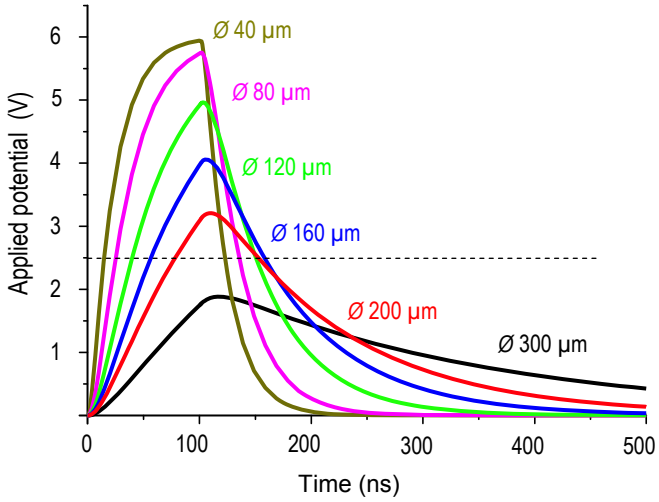

Fig. 2.6 *Double layer potentials according to tool electrode diameter (pulse: 6 V, 50 ns / 1 µs)* [95].

Furthermore, as shown in Fig 2.7, the effects of process parameters on the wire diameter in the wire etching and on the gap variation in the ultrashort pulse electrochemical cutting have been studied theoretically and experimentally [105]. The results showed that machining gap was dependent on the feed rate of the wire electrode, pulse voltage and pulse-on time. An ultra short voltage pulse based for

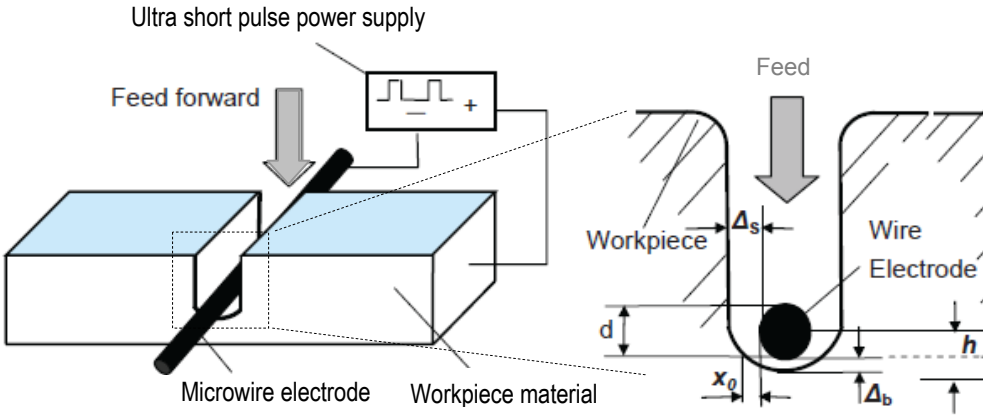

Fig. 2.7 *Schematic diagram of microwire electrochemical cutting by ultrashort pulse voltage and sketch of gap in machining zone (Insight)* [105].

mathematical model of pulse (nanoseconds) electrochemical micromachining and the micro-shaping process with taking unsteady phenomena in electrical double layer into consideration has been developed [106].

Combined effects of ultrashort voltage pulses and voltage amplitude are well studied [6]. The rate of material dissolution is affected by the conductivity of the electrolyte, which is primarily determined by the concentration of ions, and mobility of ions in a given electric field [50]. Fig. 2.8 shows the relationship between applied voltage and material removal rate at different concentration levels of acidified sodium nitrate ($NaNO_3$+H_2SO_4) electrolyte. Any increase in applied voltage results in corresponding increase in the machining current across the inter-electrode gap. This leads to increase in the material removal rate [107].

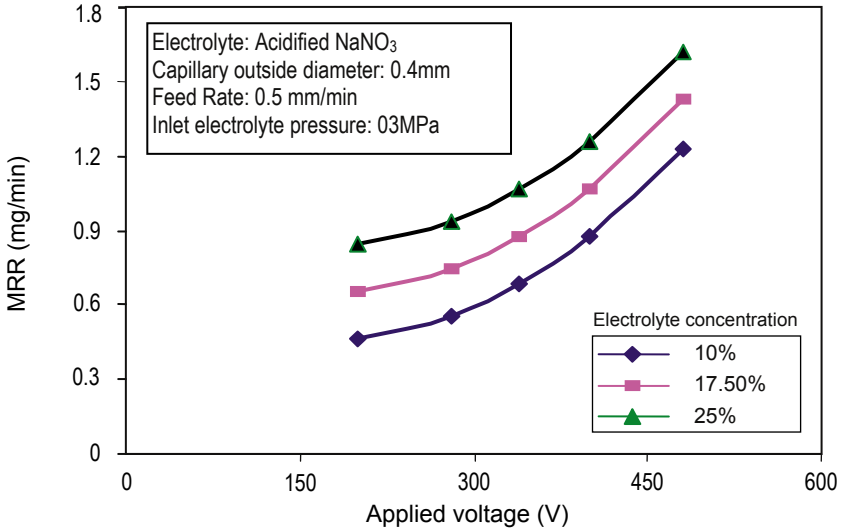

Fig. 2.8 *Effect of applied voltage on material removal rate* [107].

In ultrashort pulses, the material removal decreases due to highly confined electron motion. The electrical migration becomes dominant when the pulse duration is extremely short, such as less than 100 ns since there is no significant product buildup. An extremely small gap between the anode and cathode also makes electrical migration more prominent [108]. Because, smaller gap width allows not only higher material erosion rate, but also faster ramping-up after the pulse is turned on. Thus, on pulsed systems, during the pulse off, the relatively small inverse polarity is required to promote the dissolution of plated products on electrodes [109]. The high frequency pulsed voltage is also applied to the finishing the internal hole quality [110] controlling the pulse-on time, duty cycle and the length of un-insulated tool. So, a pulsating power supply with the polarity being reversed for a very small fraction of the cycle time is used for the shaped tube electrochemical drilling (STED) of small diameter cooling holes in turbine blades [111]. Short pulse electrochemical micromachining has been used to machine microgrooves in Ni-Ti shape memory alloy material [112]. The depth of groove for each duty factor is shown in Fig. 2.9. An increased duty factor increased the processed depth. The depth of the machined groove is increased as the current

value is increased. However, increasing the current also increases the deviation of the groove. The cause of this deviation in the depth of each groove is the characteristic focusing of the current at an edge of the electrode.

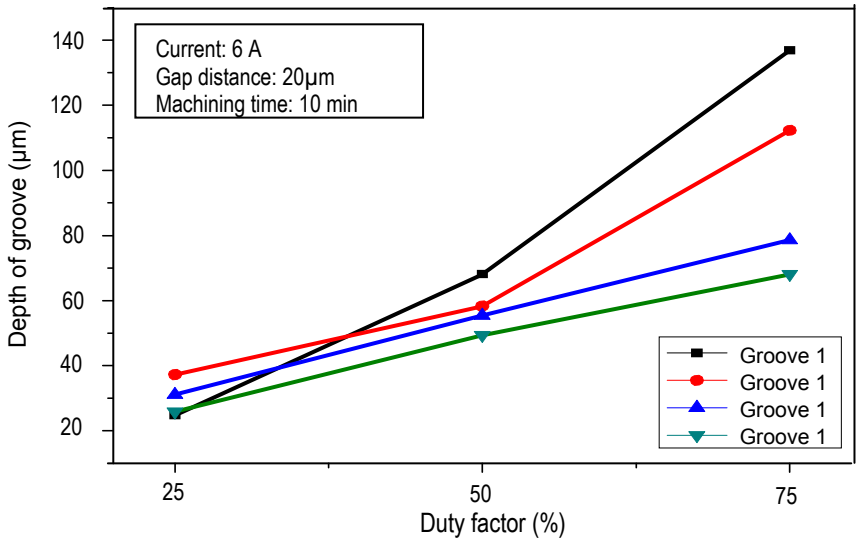

Fig. 2.9 *Effect of duty factor for depth of groove* [112].

Again Fig. 2.10 shows the effect of machining time on depth of groove. The depth of groove is increased as machining time increases, and the slope of the increased depth is reduced beginning at machining times of 10 min. The gap between each groove is reduced as machining time increases. Above aspect could be explained that initial machining gap is increased because materials are removed with the lapse of machining time.

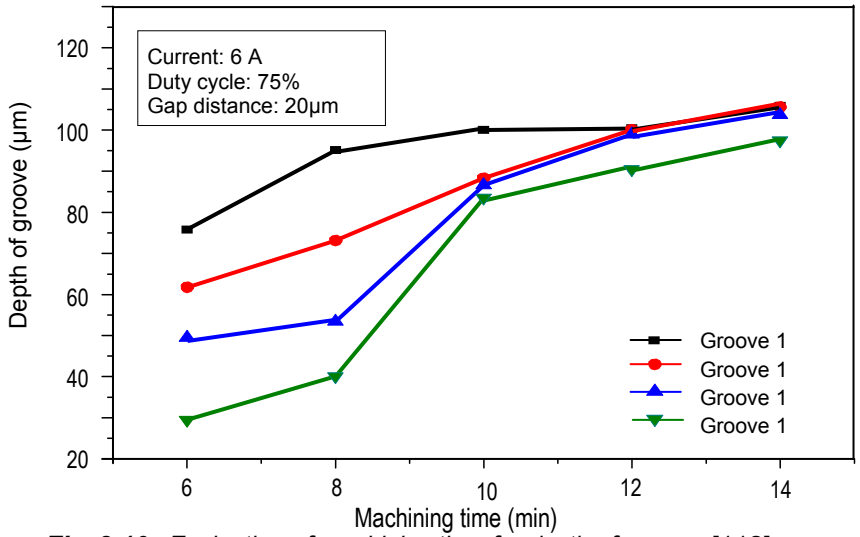

Fig. 2.10 *Evaluation of machining time for depth of groove* [112].

2.4.2 Electrolytes

Generally, pure water does not conduct electricity, but any solvated ionic species would contribute to conduction of electricity (Conductivity). An ionically conducting solution is called an electrolyte solution and the compound, which produces the ions as it dissolves, is termed as electrolyte. A strong electrolyte is a compound that will completely dissociate into ions in water, where a weak electrolyte dissolves only partially. The conductivity of an electrolyte solution depends on the concentration of the ionic species and behaves differently for strong and weak electrolytes. The electrochemical machining is primarily concerned with the interplay between the electricity and chemistry, within a chemical environment, which constitute the electrochemical cell. In general, the electrochemical processes take place at the interface of electrode-electrolyte solution, usually bulk solution [65]. But the distinction between various processes reflects the type of electrical signals used or the type of the electrolytes used. These electrochemical cells can be classified as electrolytic cell, which consumes electricity from an external source, and galvanic cell, where chemical reactions are used to produce electrical energy. Therefore, controlled potential processes transfer the charges at the electrode–electrolytic solution interface, and the electrode potential is being used to dissolve the materials in the electrolytic cell. The mass transfer inside the electrochemical cell, i.e., the dissolution of material depends on the hydrodynamic conditions for a given metal-electrolyte combination [113], and the dissolution occurs in three different modes, namely, (i) diffusion, the spontaneous movement under the influence of chemical concentration gradient, (ii) convection, transport to the electrode by a gross physical movement due to an external mechanical energy, and (iii) migration, movement of charged particles along an electrical field. In electrochemical micromachining processes, the migration mode dominating the process mostly when very low concentration electrolytes are used, and the use of electrolyte circulation system is very limited. But, the situation is quite complex when the three modes of mass transport occur simultaneously.

2.4.2.1 Types of Electrolytes Used

An electrolyte contains free ions that make the substance electrically conductive. The most typical electrolyte is anionic solution, i.e. acid solution, basic solution, salt solution etc., but molten electrolytes and fused solid electrolytes are also possible. A liquid electrolyte inherits better conductivity values than other electrolytes such as solid electrolytes and polymer electrolytes [114]. Basically, a liquid electrolyte consists of a salt dissolved in a solvent or a mixture of solvents.

In μECM, the electrolytes are chosen based on the material used, and also the process requirements. Irrespective of types, the electrolytes are classified into two categories, such as: (i) passivating electrolytes containing oxidizing anions, e.g. sodium nitrate, sodium chlorate, etc., and (ii) non-passivating electrolytes containing relatively aggressive anions such as sodium chloride [19]. Passivating electrolytes are known to give better machining precision [115–117], offering a straight microhole with less side erosions [118], schematically shown in Fig. 2.11. This is due to the formation of oxide films and oxygen evolution in the stray current region [119]. It is usual to work with $NaNO_3$ (pH ≈ 7) that can improve the

dissolution of material without affecting the microtool, because sodium nitrate has low throwing power, high and controlled metal removal, which leads to high-speed and accuracy in machining than other chemicals used in µECM.

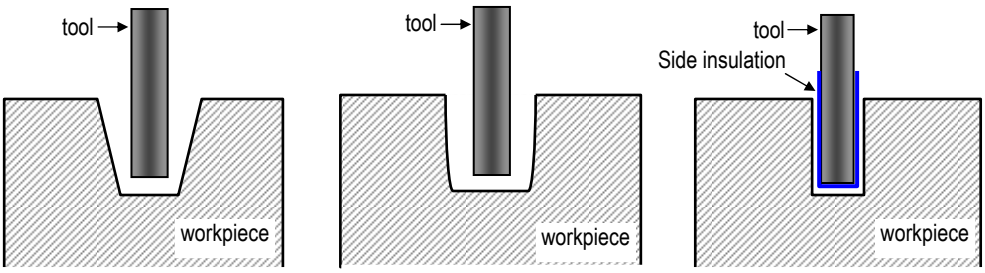

Fig. 2.11 *Forming of grooves in electrochemical micromachining with (a) non-passivating, (b) passivating, and (c) passivating with side wall insulated tool* [118].

Metals usually dissolve in acidic electrolytes when their electrode potential becomes more positive. The dissolution current density increases exponentially with the potential according to the Butler-Volmer equation [120]. At sufficiently positive potentials the formation of corrosion products becomes faster than the transfer by diffusion into the bulk electrolyte solution. As a consequence, a salt film will precipitate at the metal surface with a related potential-independent dissolution current density. When the potential becomes more positive than the passivation potential the current density drops by several orders. This effect is caused by the formation of a passivating film which consist of the oxides and hydroxides of the metal under steady state condition. The formation of faster dissolving complexes of metal ions with anions increases their transfer from the surface of the oxide matrix to the electrolyte, thus causing the increased passive current density.

The dissolution kinetics of cations depends also on the pH of the solution. When the pH reaches close to the dissolution equilibrium value of the oxide or hydroxide, cation transfer is no longer possible and the metal is passive due to the formation of a layer which is insoluble within the contacting electrolyte. In consequence one has to distinguish two causes for passivity: (a) The anodic oxide is in dissolution equilibrium and cannot dissolve or (b) the transfer of the cations from the oxide surface to the electrolyte is so slow that the dissolution rate becomes extremely small although the oxide is far from its dissolution equilibrium. The first case is found for metals like aluminum, copper, silver, or cobalt. They are not protected in strongly acidic electrolytes [121, 122].

The second case holds for metals like iron, nickel, or chromium in acidic electrolytes. They are also passive in alkaline solutions, where the dissolution equilibrium is established for their oxides. Chromium is special so far as its oxide dissolves in acidic electrolytes extremely slowly even in the presence of complexing anions like chloride. Therefore, this metal is well protected by its passive layer and does not pit at all.

In the case of iron, concentrated nitric acid will passivate the metal surface whereas diluted nitric acid does not passivate. However, diluted nitric acid may sustain passivity if the metal has been passivated before by other means.

While the etch rates of many etchants that target specific materials are commonly known, one specific electrolyte is not applicable for all types of machining, and it varies depending on the material used. Many of the chemicals used in electrochemical processes are not supplied in pure form. Acetic acid is supplied pure and sulfuric acid nearly pure (96%), while other acids normally come in lower concentrations for various reasons [123]. For example, HF is a weak acid; except when present in very small concentrations, it does not completely dissociate into H^+ and F^- ions in water [124], but a concentrated hydrofluoric acid that etches oxides very rapidly can be used to remove sacrificial oxides. The KOH solutions are made from KOH pellets. This solution contains more percentage of water because the KOH pellets normally contain 10 – 15% water [125]. Moreover, this solution is self heating. It should be allowed to equilibrate before using as KOH in unagitated solutions is found to tend to stratify resulting in etch-rate variation from the top to the bottom of the solution.

This stratification improves the etch rate, but gradually reducing the product quality [126]. The etch rate in KOH increases with temperature, finally increases the variation between experimental iterations. Variation in etch-rate may occur due to the etch setup, which is a function of 1) temperature [127]; 2) loss of liquids to evaporation [126, 128]; 3) mix up; 4) stratification of the solution; 5) elapsed time from the start of the etch; 6) applied potential [129, 130]; 7) use of same electrolyte for several times; and 8) contamination with other chemicals.

However, acidic electrolytes are advantageous due to formation of soluble reaction products, which can completely swept clean from the narrow inter-electrode gap (IEG) during machining without affecting the microtools. Moreover, the pH value of the electrolyte solution is chosen to ensure good dissolution of the workpiece material without affecting the microtool.

2.4.2.2 Electrolyte Properties

The electrolyte solution should be able to: (i) ensure a uniform and high-speed anodic dissolution, (ii) avoid the formation of a passive film on the anodic surface, (iii) not deposit on the cathode surface, (iv) have a high electrical conductivity and low viscosity to reduce the power used, (v) to have good flow conditions in the narrow interelectrode gap, (vi) be safe, nontoxic, and less erosive to the machine body, (vii) maintain its stable ingredients and pH value during machining, (viii) have small variation in its conductivity and viscosity due to temperature rise, and (ix) be less expensive and easily available [12].

Therefore, the flow of electrolyte between the microtool and workpiece facilitates the electrochemical action. The main functions of electrolytes are to [1]: (i) create an environment for anodic dissolution of workpiece material, (ii) conduct the machining current, (iii) remove the by-products formed during machining, (iv) carry away the heat generated by the machining process, (v) maintain a constant temperature in the machining region, (vi) help the shape formation of products.

2.4.2.3 Effect of Electrolyte on Machining

During micromachining, the hydrogen gas generation and evaporation of water in the small IEG due to heating increase the electrolyte concentration and viscosity. The high concentrated viscous electrolyte is not able to remove all the reaction products from the narrow machining zone. Hydrodynamic disturbance due to change in viscosity affects the distribution for diffusion layer thickness on the micromachining zone, which influence the electrochemical dissolution process to a great extent. There is a possibility of forming reaction products in-between micro-tool and workpiece that result in the generation of microsparks and short circuiting. Low-pressure electrolyte jet from two nozzles directing the flow of the electrolyte just to the micromachining zone was utilized for the present set of experiments. This type of microsparks can be avoided by using only fresh electrolyte with effective flow path design.

A mathematical model and a method for numerical modeling of two-dimensional electrolyte flow in the interelectrode gap during electrochemical machining (ECM) are presented. Programs for modeling electrolyte flow and observing the distribution of ECM parameters are designed. The hydrogen evolution in the IE gap alters the electro-conductivity, density, and viscosity of the working medium, thus altering hydrodynamic conditions due to altered distributions of pressure and electrolyte flow rate; moreover, it hinders the workpiece dissolution: the volumetric gas content increases, especially in the electrolyte exit zone, thus compromising the ECM efficiency. The electrolyte's temperature is found maximum near the electrode surfaces. The maximum temperature occurs at a minimum IE gap and varies within one vibration period, for the vibration affects hydrodynamic velocity. This is one of the factors making the temperature distribution in the IE gap asymmetric [131].

Temperature of the electrolyte also influences the machining accuracy and surface finish in EMM. The estimation methods of electrolyte temperature have already been developed, which is helpful to judge the accuracy and surface finish [132].

The surface structure of the sample and thus the occurring electrochemical reactions during ECM are strongly dependent on the electrolyte used [133]. While MRR increased as electrolyte concentration increased at low concentration, MRR dropped inversely as electrolyte concentration was larger than 1.5 M [47]. In ECM, the typical concentration of electrolytes is in the order of 20% w/v aqueous solution of $NaNO_3$ or NaCl. Although it has been stated that better accuracy can be achieved using lower electrolyte concentrations, and optimum value of concentration for industrial applications can be found by trial and error methods [134]. Furthermore, the lower concentrations generate comparatively less sludge by not only giving lower amounts of precipitates but also by minimizing the machining allowance [135]. Generally an anodic film is formed, and metal is removed by precipitation into the solution. Hence, it is advisable to use fresh and clean electrolyte for micromachining instead of recirculation [19].

More recently many progresses have been made in electrochemical micromachining. For example, Zhu et al [105] studied micro wire electrochemical

cutting by using electrochemically in situ fabricated wire electrode. As first step, microwire electrode was successfully fabricated in situ using 0.1M/l HCl electrolytes. Gamburg et al [136] studied the electrochemical deposition of nickel from a sulfate bath containing malonic or succinic acids in place of a boric acid under different current densities, pH and temperatures of the solution. They found that monolic acid as electrolytes showed good buffer properties, high values of the throwing power. Electrolytes were also found to be stable for a long time of exploitation and permitted to be used with conventional brighteners and other additives. Kim et al [47] studied micro machining of stainless steel by μECM and excellent surface quality (R_a= 0.28 μm) of machined micro structures were obtained with dilute electrolyte of 0.1 M H_2S0_4. Ryu [28] experimentally investigated the effect of organic citric acid as electrolytes on μECM. For the concentration of 0.2 M, machined time increased and short circuit was created by tool-tip and workpiece contact. ECM characteristics were found good with concentration higher than 0.3 M citric acid solutions.

As the length of flow path across the tool increases, as in case of a longer and wider work surface, the flow must be increased to sweep away the products of the machining action. Enough dilutions of the gases are required; otherwise gases will reduce the conductivity of the electrolyte towards the exit from the tool, causing a reduction in machining gap size [19]. This effect can be countered by using high flow rates, instead of compensating for it in the shape of the tool. While operating at smaller tool working gaps in order to achieve greater accuracy, a higher pressure for the same electrolyte flow is required. To have higher tool feed rates, a proportionate increase in flow is required with a corresponding increase in pressure. A rise in pressure again calls for suitable stronger and rigid tools.

In order to check the influence of the different ions in the mixture of hydrochloric and hydrofluoric acid, several experiments were performed with different electrolytes (Fig. 2.12) [6]. A flattened, cylindrical 50 μm Pt-wire served as tool electrode in these experiments and was etched into the surface with 50 ns, 2 V pulses. High acidity of the electrolyte seems to be an important precondition for successful micromachining. The necessary fluoride content is strongly dependent on the HCl concentration. The presence of high concentrations of halogenide ions together with a low pH chemically prevents the formation of thick oxide films on the stainless steel surface under particular machining conditions. Also, the presence of complexing agents might prevent the formation of thick oxide layers. On the application of 1.5 to 4 V pulses (100 to 200 ns) 10 μm deep holes can be etched within about 5 minutes. The machining rate is more than an order of magnitude slower for 3 M HCl/ 6 M HF and the process is rather sensitive towards accidental shortcuts between the electrodes upon which the surface became irreversibly passivated.

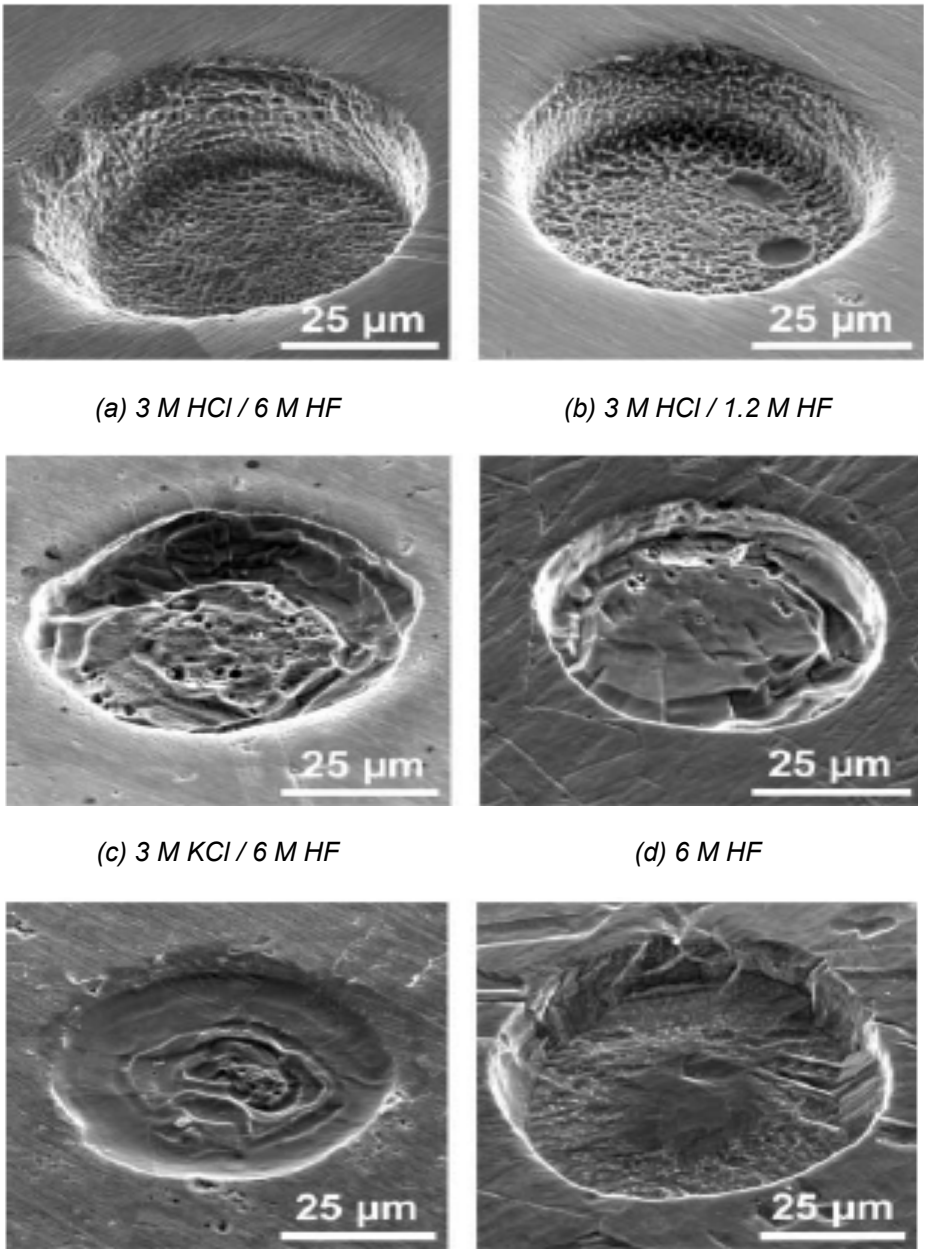

(a) 3 M HCl / 6 M HF *(b) 3 M HCl / 1.2 M HF*

(c) 3 M KCl / 6 M HF *(d) 6 M HF*

(e) 1 M HCl / 1.2 M HF *(f) 3 M HCl*

Fig. 2.12 *Comparison of holes drilled into stainless steel in different electrolytes (Tool: cylindrical platinum wire of 50 um diameter; pulses: 50 ns/2V; average potential of the workpiece V_{wp} ≈ −100 $mV_{Pd/H}$, and tool V_{tool} = 100 $mV_{Pd/H}$)* [6].

2.4.3 Microtools

For fabricating various microproducts by μECM processes, the dimension of microtool also plays an important role in micromachining as the geometry of machined part is dependent on the geometry of microtool [27, 95]. In electrochemical micromachining, the workpiece shape is expected to be the mirror image of the microtool, and be greater than the microtool size called an oversize or overcut [137,138]. The determination of microtool depend not only the accurate microtool geometry but also the choice of suitable tool material [67]. The development of microtools still remains a major challenge in micromanufacturing [117] and mainly deals with (i) selection of appropriate tool material that is application dependent, (ii) determination of the accurate tool geometry, and (iii) fabrication of the microtools for actual machining [67]. The tooling issue also plays a significant role in overall process performance and cost economics. Computer-aided design (CAD) systems are used first to design a cathode tool [139], but the choice of tool material and fabrication of microtools in micron scale are still human dependent.

2.4.3.1 Tool Materials

The μECM needs a tool electrode on micron scale, generally made of chemically inert materials [19], including high electrical and thermal conductivity, good wear (mechanical) and corrosion resistance, mechanical strength (i.e. stiffness) to withstand the pressure of electrolyte, and be easily machinable. The best choice of the materials is, therefore, limited to tungsten, platinum, titanium, and some super alloys. Other metals, such as gold, nickel, copper, silver, molybdenum, and steel are also used as electrode materials in connection with specific applications. Also, some chemically modified electrodes represent a modern approach to electrode systems. Among a wide choice of metals available, tungsten and its alloy, platinum and its alloy, titanium, some super alloys are most widely used metallic electrodes [10]. Such electrodes offer a very favorable electron-transfer kinetics, large anodic potential range and low hydrogen overvoltage. In contrast, more problematic are the high background currents associated with the formation of surface oxides and absorbed hydrogen layers [140].

Platinum wire is a soft metal but alloying with the metals iridium and rhodium increase its hardness [141]. Platinum-iridium alloy is preferred over tungsten wire in most electrochemical experiments because it is more chemically inert. Platinum-iridium alloy etched in $CaCl_2$ solution under ac voltage exhibited some of the etching characteristics of tungsten in caustic solution, but unlike the tungsten etching, an insoluble black product is formed around the wire during the etching process [141]. Therefore, the black insoluble product must be filtered and rinsed with deionized water several times after machining.

Tungsten tools are widely used as tool material because of its high rigidity, toughness and resistance to chemicals. Tungsten carbide (WC) with cobalt binder is also used as tool material, and is commonly produced by powder metallurgy. High solubility of WC in cobalt at high temperature and good wetting of WC in the liquid cobalt binder give excellent densification during liquid phase sintering and

result in a pore-free structure [47]. Considering static forces, the sudden movement of the microtool (in case of guide calibration or positioning) may initiate self excited vibrations in μECM, and to avoid this effect known as 'water hammer', there is a need for rigidity in the tool and fixtures [142]. Usually these vibrations are excited by forces acting in the direction of the tool feed, but transverse forces can cause the same effect. Therefore, titanium and its alloys have also been used in electrochemical micromachining due to the high strength, high melting point and has proven suitable for harsh environment where the corrosion resistance plays a major role [143]. Moreover, titanium is one of a few in a class of materials showing an endurance limit, which means that below a threshold stress level, the material will not fail given a near infinite number of cycles [144].

Also, though tungsten wires are commercially available in a long piece and cutting off the tungsten wire with a wire cutter or micro-grinder may leave burrs or micro-cracks as an annealed tungsten wire is brittle, tungsten (W) is a popular material for the micro tool fabrication. Good cutting made higher cut sound, whereas bad one sounds like a smashed or lower cut sound [145]. The cut end should be grind and clean in order to get a good shape tip. Sometimes, the tungsten wire contaminates with carbon due to the annealing process and hence, further processing is needed to wipe the wire surface. Moreover, as shown in Fig. 2.13, due to its poor resistance to oxidation, the tungsten tool is most likely undergo surface contamination by tungsten-oxide layer that infers the quality of the machined product, However, no single material has been proven to be superior over all others. Each material system has drawbacks, and no single material can satisfy all the microtool design purposes. Therefore it is reasonable to believe that further research is still needed in the area of microtool [19].

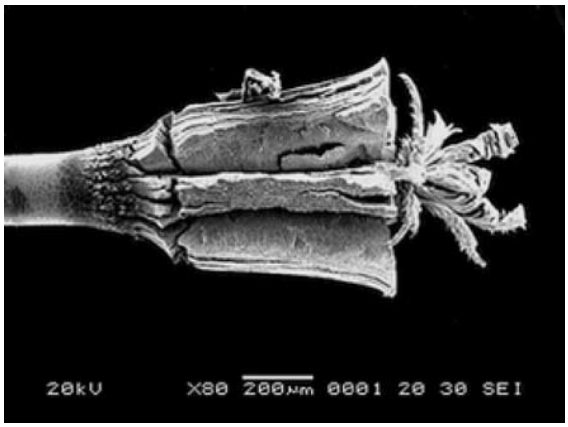

Fig. 2.13 *Sludge growth on the specimen during WC etching* [47].

2.4.3.2 Tool Design

The main problem in the electrochemical micromachining is the design of microtools. Tool design mainly deals with the determination of tool shape, which will produce a workpiece with proper dimensions and accuracy [19, 27, 29, 67]. It is

not yet successful for practical applications due to the complex gap configuration [146]. In μECM, microtool shape is a perfect negative mirror image of the workpiece to be produced, thus most researchers attempted to predict a workpiece shape machined by a given tool. This is called a direct problem, where the prediction of the tool shapes is a formidable inverse boundary problem involving Laplace equations [138, 147]. Besides, analytic techniques include the cosine method, the analogue method, and the complex variables method. Various numerical techniques, including the finite difference method, and the finite element method (FEM), have also been applied. But all the above methods are limited to consideration of the effect of the electric field only [148].

The difficulties in designing ECM tools stem from a lack of adequate understanding of the process, dissolution phenomena and mathematical complexities, which make the present methods of tool design, allow calculation of only a first approximation of the final tool shape [117, 146]. Some researchers also tried to solve the tool design problem based on the effect of thermal-fluid properties of ECM process [149]. An embedded numerical simulation technique was applied to the inverse problem. Void fraction or temperature of the electrolyte is taken into account in the majority of the articles. Recent studies have primarily been directed at numerical solutions to the inverse boundary problem instead of simple geometrical approximations [117, 137]. Jain et al. [117] simulated ECM processes in which the metal removal rate is affected by the electric and flow fields. Alder et al. [150] studied the inverse simulation technique to determine the tool profile needed for a given workpiece surface. But this method is only applicable for two dimensional tool design problems, and for equilibrium machining processes. However, the determination of the tool shape to produce a desired workpiece shape is more practical for the engineering design. Mathematically, it is an inverse problem, which is generally difficult to solve under complex boundary geometry. In recent years, studies have primarily applied numerical techniques such as the FEM and the boundary element method (BEM) [151], complex variable method [152], multigrid techniques to solve the tooling issue. The FEM and BEM methods show flexibility in the treatment of the boundary than others. Therefore the challenge pushing to continue researches to develop the understanding and modeling of process mechanics because of the non-continuous nature of the materials at micron scale and difficulties of validating model predictions [153].

2.4.3.3 Tool Fabrication Processes

When designing tool-based micromachined products, technology has strong influences on product development [154, 155]. Therefore, suitable fabrication process is needed to form the microtool for successful machining. Although the fabrication of microtools smaller than 200 μm in diameter by conventional machining processes is a very complex task because it is easily bent by the lateral force [47, 156, 157]; several conventional and nonconventional methods are used to fabricate microtools, as CNC micro-turning, [46], micro-milling, micro-grinding, chemical machining, electrochemical etching, deep reactive ion etching (DRIE), Lithographic (LIGA) mold process [42], laser machining [50], electric discharge machining (EDM), wire electro-discharge grinding, ultrasonic vibration grinding, electroforming, and electron beam machining (EBM), etc, have been tested. Each

method has some limitations in fabricating various shapes and sizes of micro-tools. The main drawback behind the conventional processes (i.e. micro-turning, micro-milling and micro-grinding) is thermal stress concentrated on the produced part [47]. Also these processes leave burrs and sometimes form micro-cracks on the machined surface. Moreover, the equipments for these processes are very expensive and their machining efficiency is very low [50]. Micro-milling, DRIE and LIGA mold processes require several steps to make micro-products. Moreover, the DRIE fabrication method is not suitable for making a microtool because of ion angular distribution (IAD) and image force effect (IFE), and a strong electrical field is required for the plasma glow [43]. Electro-discharge machining (EDM) is the most commonly used process for fabricating microtools although a typical EDM leaves burrs [44] and a rough surface finish that adversely effects on microproducts surface quality. In this case, sometimes a micro-finishing task has been required to remove the burrs formed on the tool surface [102]. To give a better finish surface, abrasive flow machining (AFM) is often used to polish the machined surface. However, AFM added extra cost to production. In the laser machining and EBM, very high energy density is needed for the ablation to machine the micro-product. Moreover, these processes also produce localized re-solidified heat affected zone, and leave micro-cracks on the surface where ablation occurs [43].

As tungsten or tungsten carbides have very high stiffness and resistance to wear, it can be machined to less than 10 μm by using electrochemical etching and wire electro-discharge grinding (WEDG) [158, 159]. A typical microtool fabricated by electro-discharge grinding is illustrated in Fig. 2.14. This process can provide excellent micro-electrodes for micromachining, but the aspect ratio is still not large enough. Therefore, a combination process is applied to fabricate microtools where the microtools are primarily formed by micro-grinding processes and then further finished by other machining processes.

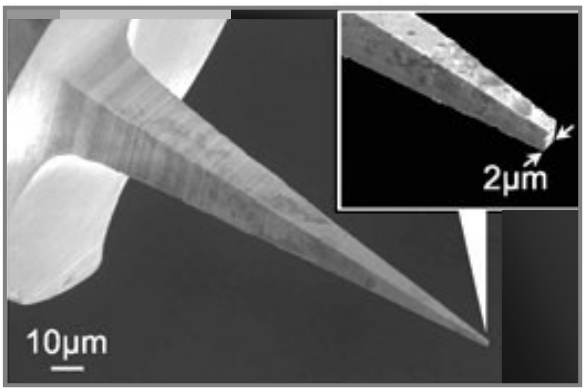

Fig. 2.14 *Microtool fabricated by electro-discharge grinding process* [160].

On the contrary, electrochemical micromachining (μECM) is standing out among all other micromachining processes due to its anodic dissolution process that effectively forms and shapes micro-components from any conductive material. A metallic workpiece is taken as anode, and another conductor is taken as cathode,

placed into an electrolytic bath maintaining a predefined gap between the electrodes while the electrolyte flows between them within the gap. Microtools can be processed to a desired micron size by varies machining time in a fixed small voltage and current. Depending on the power used, either AC [161, 162] or DC current used, this technology has potential to form a microtool of high-aspect-ratio in the nano scale machining [19]. Recently, pulsed DC current is also applied to ensure the localization of electrochemical dissolution during tool fabrication [163]. The tool specimen and the counter electrode are kept steady in the predefined electrolytic solution of fixed concentration, and on the application of a potential difference between the electrodes, a certain etching time produces a microtool of desired diameter. Hence this process does not need any contact between the electrodes; therefore, neither mechanical stress nor a heat affected zone is generated, as both are dipped into the electrolytic solution offering a good machined surface quality [29]. This process can be effectively utilized to etch any conductive metal/material irrespective of their hardness [67]. Therefore, this method has proven suitable for the shaping of high corrosion resistant materials and alloys, which are not readily machined mechanically or chemically, shows a promise as a high-resolution production manufacturing process with good throughput and excellent repeatability [164]. From these points of view the μECM is the most effective process which finds wider applications in the fabrication of microtools of very hard materials that are generally used in electrochemical micromachining techniques [47, 165]. During the fabrication of microtool by pulsed voltage, the dimension of microtools change rapidly as the concentration and applied voltage taking part in the dissolution of electrochemical processes [166]. Fig. 2.15 shows the shapes of micro-electrodes under various concentrations and of 1.8 V applied voltage, 10 mm electrode gap, 1000 rpm rotational rate, 2 mm tool depth. In this case, the tool feed rate is zero. From the same figure, revised conical shape is also observed under the same machining conditions.

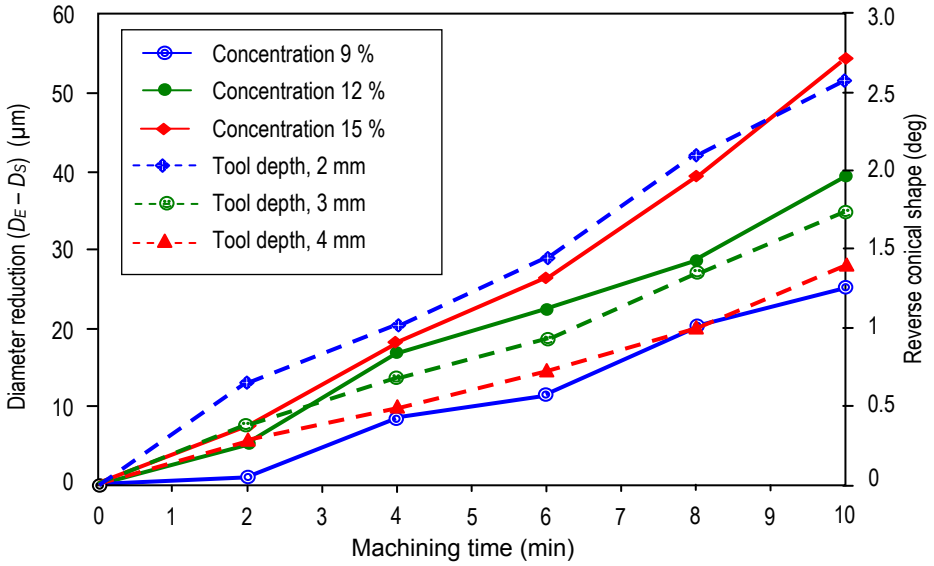

Fig. 2.15 *The shape of microtools at different electrolyte concentrations and various anodic lengths* [50].

A typical microtool formed by electrochemical process is illustrated in Fig. 2.16. Localized electrochemical deposition (LECD) technique is also a good solution for fabricating high-aspect ratio electrode of various materials where a mask is placed between the anode and cathode, and these are immersed into a mixed electrolyte [48]. Mammana and Salvadon [167] used an electrochemical etching process on a tungsten wire to form a convergent-divergent profile.

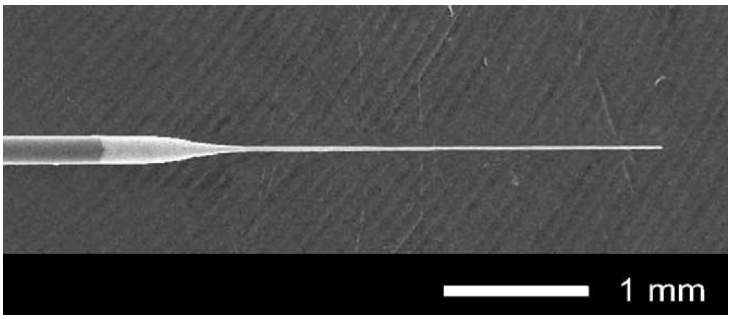

Fig. 2.16 *A cylindrical electrode with diameter of 30 μm formed by μECM* [93].

2.4.3.4 Tool Dimension

An accurate tool profile is accomplished by controlling the current density, voltage, and the concentration of electrolytes [28, 41, 78]. For fabricating microholes, usually a straight cylindrical tool is used. Experiments show that the microtools fabricated by μECM are with different end shapes can be used for different purposes in the electrochemical micromachining process [87, 98, 168, 169]. However, the end shape initially taking part in the machining processes [93]. During machining, the microtool tip approaches first and initialize the machining, and the effect of the tip shown in Fig. 2.17. So, an efficient method for fabricating microelectrodes with different end shapes is needed. Pust et al [169] modeled and developed different end shapes for effective machining, as illustrated in Fig. 2.18. Microtools with different end shapes are also fabricated by different researchers [102, 163].

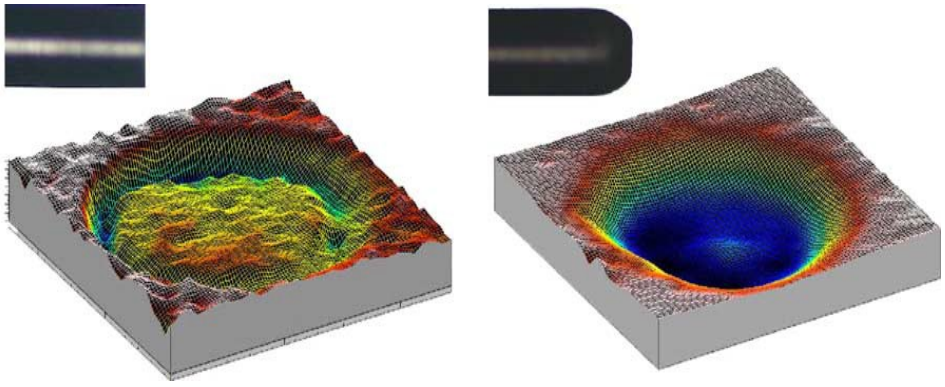

Fig. 2.17 *The machined surface according to the tool tip shape* [93].

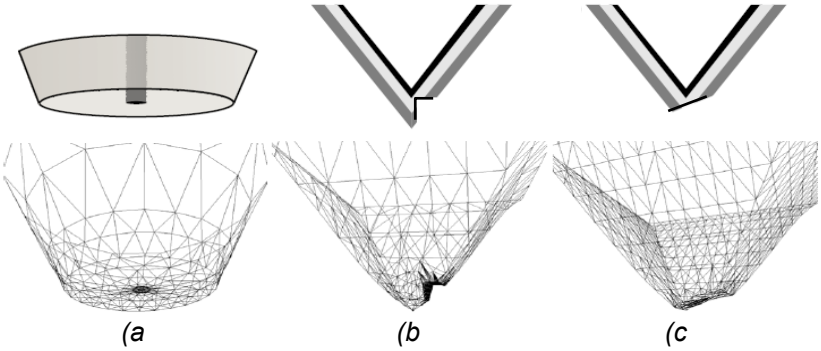

Fig. 2.18 *Schematic representation of microelectrodes with different end shapes used for scanning electron microscope; (a) disk shaped end, (b) pyramid shape thorn out, and (c) pyramid shape with angular cut* [169].

Cylindrical microtools are most widely used in electrochemical micromachining. However, it is not easy to fabricate a straight cylindrical tool by μECM process [78]. Since the invention of field ion microscope (FIM), and scanning tunneling microscope (STM), the fabrication techniques of atomically sharp tips have also been actively investigated [49]. Hard and sharp (conical shaped) tips are now an important component for many kinds of electrochemical machining, such as in the fabrication of micro nozzles, enlarging the openings of microholes, etc.

Micronozzles are becoming increasingly important in many fields such as microfluidic systems for MEMS and/or bio-MEMS, micro propulsion systems, flow control systems and printers. Each application requires an optimal shape and size for the micro nozzles and hence, a fabrication process that makes controllable shape and size of nozzles is extremely desirable [56]. The sizes, shape, physical and chemical identity of the tip apex influence not only the resolution of microscopes but also the interpretation of images and data [47]. Huge numbers of works on the fabrication of sharp tips have been performed and several techniques have been developed and experimented. Among these methods, the electrochemical etching technique is most widely used as a fast, cheap, convenient and reliable method, and there is no pre /post- treatment method involved for further finishing. The most common method for fabricating microtools is dynamic electrochemical etching in combination with 'drop-off' technique, in which the tip is continuously and slowly drawn up from the electrolyte during etching [49]. The process of conical shaped tool is shown in Fig. 2.19. A typical microtool with conical shaped tool end is illustrated in Fig. 2.20.

2.4.3.5 Tool Feed Rate

In the machining region where the workpiece directly faces the cathode tool, the anodic reaction rate is constant for a constant interelectrode gap (IEG) [170, 171]. The proper choice of feed rate maintains gap between the electrodes. Microtool feed rate should be always less than the linear material removal rate, for performing effective micromachining. Very low microtool movement in the order of

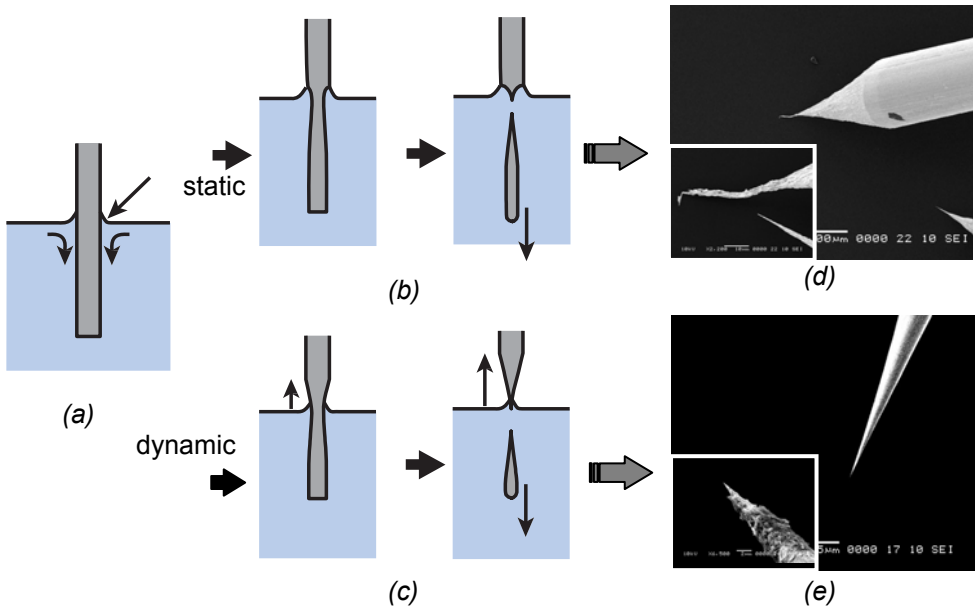

Fig. 2.19 *A schematic drawing of the electrochemical etching. (a) set up prior to etch, (b) static electrochemical etching, (c) dynamic electrochemical etching, (d) SEM image of the tip apex fabricated by static etching, and (e) SEM image of the tip apex fabricated by dynamic etching* [49].

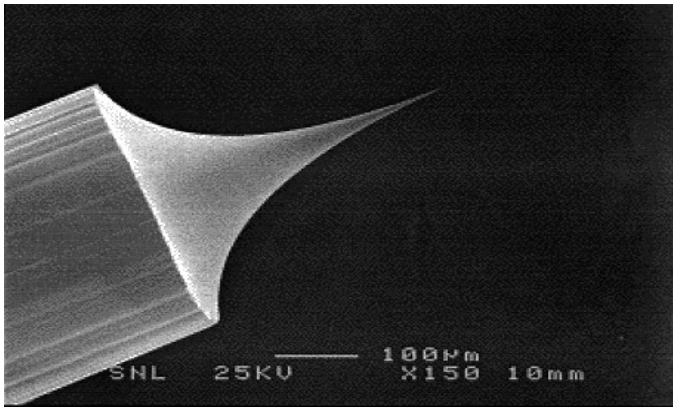

Fig. 2.20 *A large-scale SEM image of a dc-etched W tip* [87].

5–20 µm is required in µECM to increase the machining accuracy [96]. An increase in feed rate increases the material removal rate. This happens due to the reduced gap between the capillary tip and workpiece surface that increases the current density in the gap with the consequent rapid anodic dissolution. Increasing feed rate within the permissible range (feed rate matching with dissolution rate of the work material) results in lower roundness error [107]. Selection of suitable tool feed rate will reduce the chance of occurrence of microsparks [100]. Further

experiments are to be carried out by different researchers. Under the machining condition of 300 ns pulse duration and 2 μm/s feed, tool electrode cannot feed deeper than 30um on SS 304 without short circuit. This is because tool feed is quite large compared with metal dissolution rate, results the short circuit [28]. On the other hand, increase in feed rate also lead to the minimization in the formation of burrs [35]. Due to a combination of high feed rate and low applied voltages, short circuits can occur, leading to bending of microtool tip [111]. The feed rate should be control in such that the inter electrode gap will not be too narrow or too wide, as in case of too narrow interelectrode gap, the anode surface profile becomes rougher because of the non-uniformity of the electrolyte flow in the gap and also of the electrochemical discharge. On the other hand, in the case of too wide interelectrode gap, enough electrochemical reaction and localized dissolution cannot be ensured at the anode surface because the resistance between the cathode and anode is too high [172]. As shown in Fig. 2.21, in addition to front gap, side gap is also investigated under the feed rate effect [37], where the side gaps decreases when the machining speed increases. According to the theory of electrochemical machining, the distance between multiple electrodes and the material decreases as the tool-feeding speed increases. Therefore, along with the other machining parameters, the feed rate of the tool has a significant effect in the machining performance.

Experiments of the micro electrochemical cutting of a nickel plate with the thickness of 80μm were carried out to demonstrate the effects of machining parameters on the machining gap and the result shows that the high feed rate leads to the decrement of machining gap, i.e. the improvement of machining accuracy [105]. Therefore, the feed rate as high as possible under a steady machining process is suggested for the improvement of the machining accuracy.

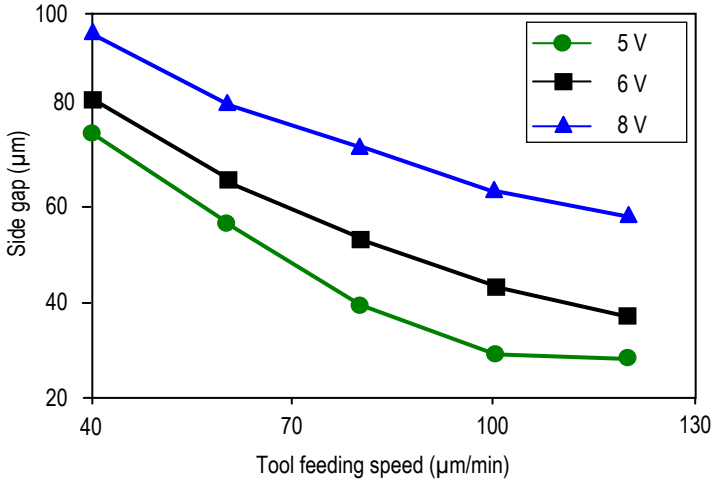

Fig. 2.21 *Variation of side gaps versus the tool-feeding speed* [37].

Micro electrodes are sometimes requiring wire feeding, which enables the use of a thinner wire [102]. Fig. 2.7 shows the schematic diagram of wire feeding against the workpiece material [105]. This type of machining is usually carried out in acidic environments in a view to dissolve the materials in the machining zone. Stainless steel and other hard materials are machined using this process. As a small machining gap is preferred [173], the machining parameters such as pulse-on time and its period, the feed rate are handled carefully. During microcutting, decreasing the feed rate leads to wider machining gaps and hence a lack of dimensional accuracy and too small of a gap causes sparking or a gap short circuit that could damage the wire-tool and workpiece surface.

2.4.4 Workpiece Materials

As electrochemical micromanufacturing process works regardless of material hardness and strength, in recent years, processes for the manufacture of small size objects have been investigated and improved for various applications in electronics, mechanical industries and, more recently, in the area of sensors and actuators [174]. These small size objects are manufactured by electrochemical machining processes of mask or maskless operations in passivated environments. For this reasons, researchers are interested on various corrosion resistant materials such as nickel, high grade stainless steel etc. for the fabrication of microproducts [175]. In electrochemical machining, the operations are carried out on nickel for several reasons. Many parts of new machines are made of pure nickel [27]. It is the main component of considerable number of superalloys, including rhenium alloys, which are electrochemically treated, and a great number of corrosion-resistant alloys [176, 177] that are used in various corrosive media such as alkaline, acidic solutions. The corrosion study [178] showed that nickel almost does not corrode in the concentrated phosphoric acid and 48% sulfuric acid solutions.

On the other hand, corrosion-resistant steels are one of the most important classes of structural materials, and finding extensive use in all leading branches of industry: chemical, petrochemical, paper and pulp, heating and atomic energy, aviation and rocket building, ship building, automobile, food, medical, cryogenic technology, consumer goods, industrial and civil building, etc. A distinguishing feature of corrosion-resistant steels is their increased resistance to uniform corrosion in a wide range of corrosion-active media or a different degree of corrosiveness [179]. An increase in chromium content facilitates passivation and increases corrosion resistance in media of an oxidizing nature. One example of that class of material is AISI 403 stainless steel that is tempered martensitic steel. It has excellent high temperature corrosion resistance, good elevated temperature mechanical properties and moderate irradiation resistance [180]. For this reason, these types of steels are used in medical applications for fabricating injection needles and vitrectomy needles. These needles body is made of AISI 403 stainless steel and finished by chromium plating. But in some cases, the needle is affixed with the plunger syringe. The vitrectomy needles having an opening closer to the tip generally made of AISI 403 steel. This straight chromium corrosion resistant stainless steel offers reasonable corrosion resistance and high mechanical characteristics.

As shown in Fig. 2.22, electrochemical wire cutting method was first patented by Kunio Chikamori [181]. After this innovation, many researchers worked on this type of cutting process where a thin wire is used to cut a metallic workpiece in a 3-D complicated profile cutting. Previously this process was restricted to cutting of heat resistant alloys and some other metals that were difficult to cut by mechanical machining. As the electrolysis is affected by the use of direct current within an unmoving electrolyte, however, the ions, gases, etc. generated in consequence of the electrolyzing action stagnate in the gap between the work blank and the cathode to interface with the effective flow of electric current at high current density and consequently cause local buildup of heat in the electrolyte. To preclude this phenomenon of stagnation and its attendant hindrances, the electrolyte is forced by some means or other to flow at a high rate of not less than 10 m/s during the machining or the cathode is provided with an injection nozzle adapted to include a local flow of the electrolyte when necessary.

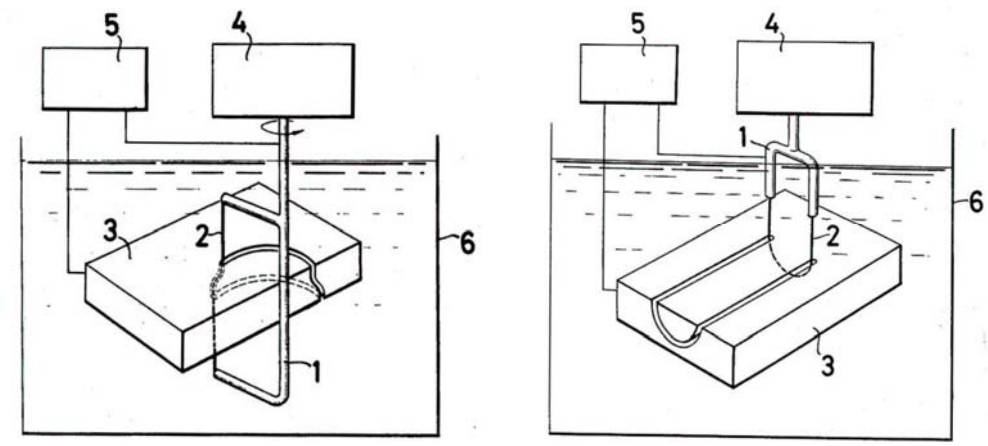

Fig. 2.22 *Schematic illustration of electrochemical wire cutting; where, (1) Wire-tool support member, (2) Wire-tool, (3) Metallic workpiece, (4) Feeding device, (5) Power source, and (6) Electrolyte reservoir* [181].

The forced flow of electrolyte, however, necessitates incorporation of an extra device for generating flow. Furthermore, the movement of the electrolyte tends to result in degradation of the machining accuracy. In the case of providing the cathode with the injection nozzle, the cathode is inevitably limited in its thickness so that an attempt to use, as the cathode a thin wire less than 0.5mm in diameter turns out to be futile.

2.5 MONITORING AND CONTROL

Process monitoring is the manipulation of measurements to determine the state of the process. In high precision machining, the monitoring is necessary for detection of a process condition to prevent machine damage by stopping the process, or to make decision about the process inputs (feeds and speeds) [182] . In μECM the difficulty in the process monitoring is the absence of accurate analytical models to

account for changes in the measured variables by variations in the machining conditions. Such changes are often attributed to process anomalies by the monitoring system, which result in false alarms [183]. Process monitoring is generally performed through the analysis of process measurements. For this purpose, a process variable or a set of variables is measured and processed online to be compared against its expected value. Any deviation from this expected value is attributed to a process anomaly. Expected values of measurements are either determined according to an analytical model of the process [184, 185] or established experimentally [186]. Therefore, successful implementation at the process control and supervisory levels requires realistic process modeling based upon a good physical understanding of the process to be controlled. After the invention of electrochemical process, some attempts have been taken by different researchers to monitor and control the process run smoothly [187, 188].

Since the early 1960s, extensive efforts have been continuously undertaken to understand the complex nature of ECM in two main directions. In this regard, eddy current was used for in-process measurement of the interelectrode gap to adjust some machining parameters [189]. The work led to the improvement of the accuracy of the produced shapes. Further research work was considered for process modeling and proper tool design. Research work and were concerned with electrolyte temperature, pressure variations in the interelectrode gap, and the choice of optimum gap voltage that would avoid the occurrence of sparking and the consequent loss of the tool and workpiece [26, 190]. A dynamic control model that considered the dynamic nature of the process was proposed [191]. The use of constant current flow to control the machining gap was recommended [192] to maintain a small and stable machining gap for better dimensional control. A high-speed data acquisition system was used to acquire the pulse current signal for developing an on-line monitoring system where the signal variance was correlated to the interelectrode gap size [100]. A computer-controlled stepper motor drive unit for providing variable and automatic feed rates besides auto-sensing of the ECM gap conditions during machining, and the electrical responses received from the machining gap, control of the tool feed rate and electrolyte flow conditions were developed [193]. A numerically controlled movement of the tool electrode was introduced [194] that can carefully handle the movement of the tool electrode, and later on, an intelligent knowledge-based system for a ready, on-line knowledge consultancy to select appropriate ECM conditions is described [195, 196].

During pulsed μECM many of the selected machining conditions must be kept unchanged as they have a direct impact on the machining process accuracy and surface finish [93]. The gap voltage affects the produced oversize, which in turn alters the dimensions of the machined part. Surface roughness depends on current density, which is affected by the tool feed rate, gap voltage, work material, gap phenomenon, and electrolyte conditions including type, concentration, temperature, pressure, pH level, and conductivity. During μECM, machining conditions leading to high process accuracy are associated with smaller surface roughness and greater machining productivity. High current densities are, therefore, recommended [12]. For further improvement of micro-machining accuracy, a piezoelectric transducer is used to vibrate the microtool so as to retract it from the workpiece during pulse-off time to enlarge the end gap to intensify the

electrolyte flushing [197]. Further investigations are still needed in the area of μECM for better understanding of the process mechanism, parametric optimization, current density and local removal rate [19].

Among all the parameters discussed above, the inter-electrode gap is a key factor for deciding precision, machining efficiency, surface quality of workpiece in μECM [198]. As there is no limitation of machining shape, the shape and size of the microtools becoming smaller and with various end shapes [98], complexity is increasing for these microtools in the μECM [47]. Hence, monitoring and controlling the interelectrode gap is very difficult [12]. While the growths in the functionability of highly sophisticated electrical and electronic components offer the opportunity to improve the level of process monitoring and control, there still have not any effective methods that can be used to on-line process monitoring and control [199, 200]. Moreover, the costs of these additional control equipments may remain a small fraction of the total machine cost including power supply.

On the other hand, a typical μECM is electrically and chemically noisy. Most of the μECM researches are carried out into toxic electrolytes like HCl, H_2SO_4, HF, $HClO_4$, HNO_3 and their mixtures. The use of toxic electrolyte in μECM has been an obstacle for the wide spread of micro-electrochemical fabrication technology [28]. Moreover, the etching process produces H_2 gas, can form bubbles that can prevent the movement of fresh etchant to the surface, and the gaseous H_2 can cause airborne fumes may result in irritation and sensitization of the lungs or other mucous membranes [201]. In addition, the tool electrode advanced towards the workpiece at a constant feed rate where the dissolution takes place into a very tiny space. Thus the formation of bubbles around the diffusion layer makes the sighting problems [78]. But, if material removal rate can not keep pace with the feed rate, the microtool touches the workpiece and cause short circuiting. The result is highly detrimental for μECM because of irreparable damage to the intricate and often costly workpiece and tools or completely shut down the machine prematurely [12], and extensive damage of workpiece and/or damage of the microtool tip [202].

2.6 SUMMARY

Electrochemical machining, an electrolytic process governed by Faraday's laws of electrolysis, uses electrical energy to remove material from electrically conductive materials. Material removal is achieved by electrochemical dissolution of an anodically polarized workpiece which is one part of an electrolytic cell. An electrolytic cell is created in an electrolyte medium, with the tool as the cathode and the workpiece as the anode. On the application of a sufficient electrical power, metal ions are removed from the anode workpiece, taken away by the vigorously flowing electrolyte through the inter electrode gap, separated from the electrolyte solution in form of metal hydroxides. Unlike conventional cutting methods, workpiece hardness is not a factor, making ECM suitable for difficult-to-cut materials, finds wider range of applications in industrial sectors.

The progress of modern miniaturized technology towards micro-devices triggered the miniaturization of mechanical components, which are becoming increasingly

important to fulfill the needs of modern world. However, methods which allow for the three-dimensional micromachining of metals are rather limited. Electrochemical micromachining has become an important issue in the miniaturization of machine parts and enables precise three–dimensional machining of different recently developed materials. Various predominant process parameters such as current density, applied frequency and its duty ratio, tool-work gap, electrolyte concentration, temperature, pH value etc, and also the anode reactions influence the machining performance of μECM. Recently, the electrochemical reactions are spatially confined with down to nanometer precision through the application of ultrashort voltage pulses. This technique helps to improve the machining performance to nanometer scale precision.

Chapter 3

Experimental

3.1 INTRODUCTION

The anodic dissolution is essentially an electrochemical oxidation process of disintegration of its surface atoms resulting finally in the liberation of cations into the electrolyte. The importance given to the anodic dissolution is easily understood if it is considered that it is the direct cause of the material decay on the application of electrical power in a chemical environment. It is usual to consider that various types of anodic mechanisms exist depending on the type and range of potentials applied with respect to the passivity domain. Active dissolution taking place at applied potentials preceding the passivation on a film-free surface is of major importance for the homogeneous corrosion in weakly oxidizing media such as acidic solutions. Today, it is well accepted that anodic dissolution involves the existence of intermediate surface bonds between the metallic state and the solution species, called double layer. The nature and kinetic behavior of these entities are inferred from transient techniques relating the time or frequency response of the current, or of the applied potential, to the relaxation of their surface concentrations. The mechanism of active dissolution of nickel remains highly controversial. It seems that there is no agreement so far even on the actual shape of the current-voltage profiles.

This chapter is aimed primarily at introducing to the experimental setup and the experimental procedure for the anodic dissolution of tungsten tool material for fabricating microtools and of nickel plate and stainless steel for fabricating different microproducts. Emphasis will be given on the applications rather than the mechanism of electrochemical micromachining techniques.

3.2 EXPERIMENTAL SYSTEM

The developed electrochemical micromachining system that used for various electrochemical micromachining processes is shown in Fig. 3.1. The machining system structure has been constructed so that the electrochemical machine is kept away from the external environment, and all the electrical, electronic instruments and all sort of hazardous chemicals are kept inside the workcell. The frame of the system is fabricated from aluminum structural bars in the form of a rectangular box, covered with transparent plastic sheets as it is possible to observe the machining process during experiments. The door of the structure is also made of transparent plastic sheet. The external dimension of the system is 1000 x 600 x1900 mm (length x width x height). The whole structure is placed on four vibration-proof pedestals to reduce the external vibrations. A suction fan is placed on the top of the structure as the gaseous products produced during experimental work can escaped out through the flexible pipe attached to the upper side of the system. Moreover, an electric lamp is placed inside to give more light inside the frame.

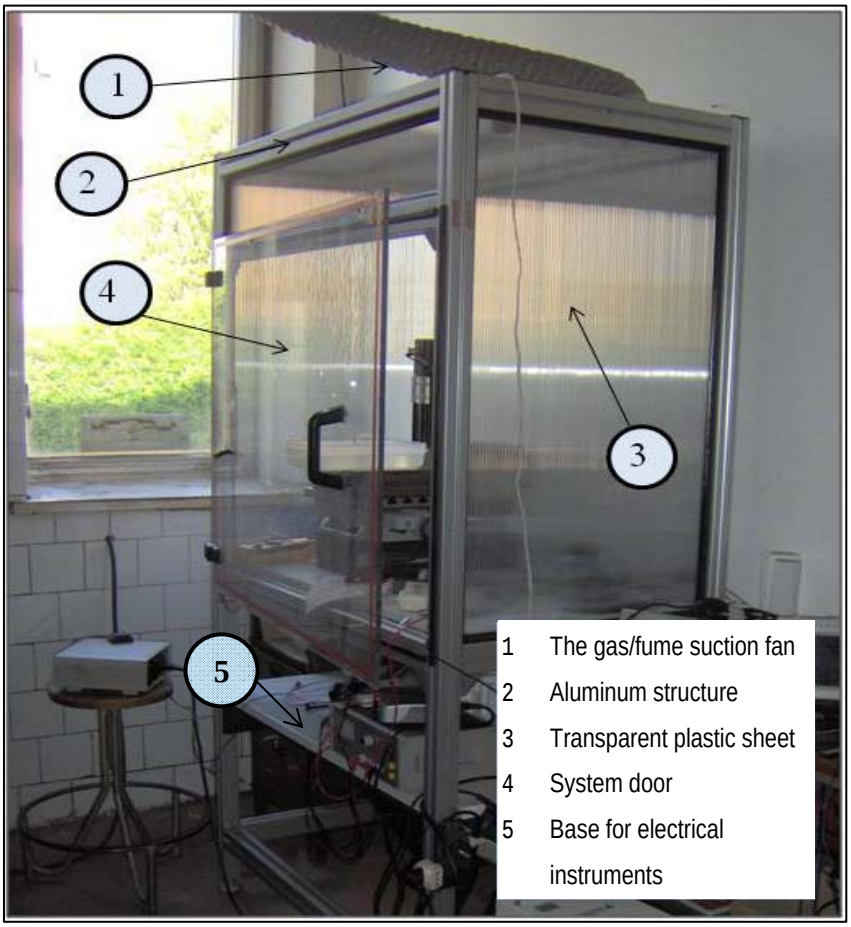

Fig. 3.1 *The electrochemical micromachining system.*

3.2.1 Electrochemical Workcell

The experimental workcell, shown in Fig. 3.2, consists of an electrical function generator, an oscilloscope, computer-controlled guide system for feeding the tool and the workpiece. The guides were controlled by a 3-axes micro-step controller system that was interfaced with a desktop computer. The controller was controlled by customized software. The maximum travel range of the precision guides were 155 mm (X) x155 mm (Y) x 40 mm (Z) with the resolution of 0.1 µm in X, Y and Z directions and full closed feedback control ensured the accuracy of submicrons. These linear stage guides also provided the facility of unidirectional repeatability lower than 0.05 µm. The specifications of the testing equipments are given in Table 3.1. To avoid the physical contact between the microtool and the nickel workpiece, a tailored electronic circuit was used that automatically stopped and retracted the tool. After the set time, the circuit automatically restarted feeding the tool maintaining the predefined gap between the workpiece and tool. Experiments were performed at room temperature. No circulation system was integrated during experimentation as µECM process involved negligible heat generation and the amount of precipitation was very small.

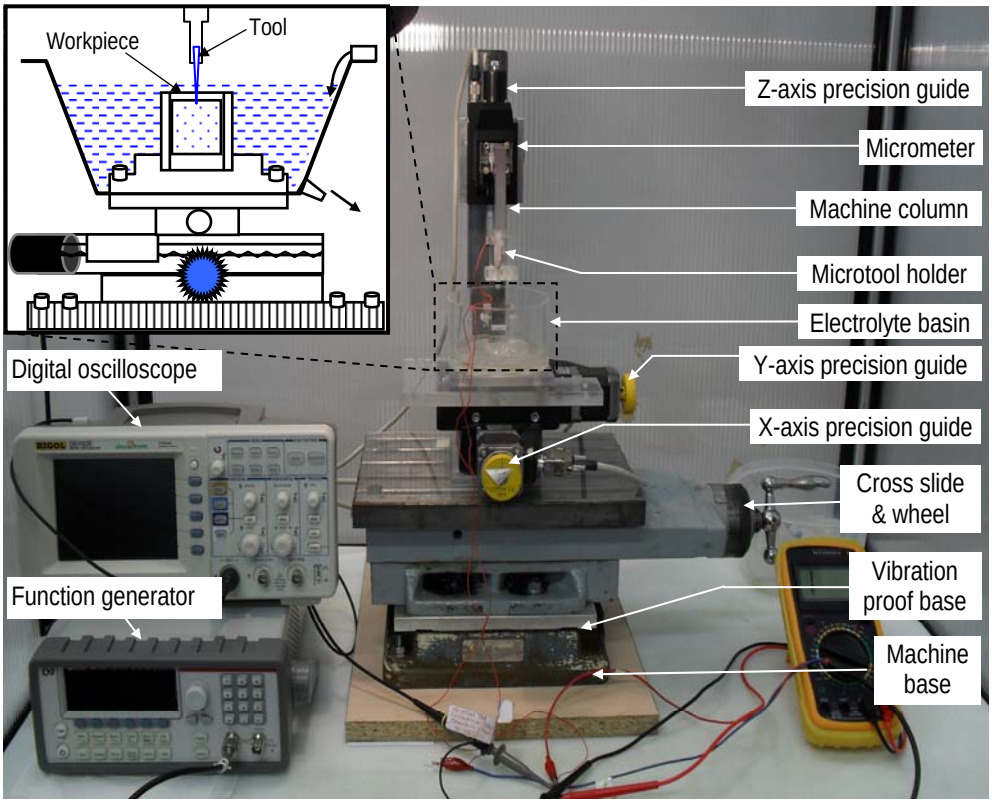

Fig. 3.2 *The electrochemical micromachining workcell and the electrolyte cell (insight).*

During microtool fabrication, the straight tungsten specimen was fixed with the holder unit, positioned vertically downward and immersed through circular electrode that was dipped into the electrolytes basin containing caustic solutions of different concentrations. The depth of immersion was controlled by the servo-controlled feed mechanism of Z stage. Again, during microdrilling, the fabricated microtool was clamped in the tool-holder, positioned vertically downward and fed along Z-axis, while the workpiece was positioned horizontally and moved by X-Y axes travel guides.

Table 3.1 Specifications of testing equipments used for electrochemical machining workcell.

Equipments	Specifications
Function generator	Keithley 3390 50 MHz; frequency resolution, 1 μHz; amplitude, 10 mV_{pp}–10 V_{pp}; 4 digits resolution; phase range, – 360° to +360°; accuracy, 8 ns
Oscilloscope	Rigol DS1000E, 1 GHz, 2 channel, digital storage, 64 K color display
Linear travel guide	PLS-85, X and Y axes, maximum travel 155 mm, resolution 0.1 μm, uni-directional repeatability 0.05 μm, maximum 100 mm/s, and
	ML- 40, Z- axis, maximum travel 40 mm, resolution of 0.1 μm, maximum 5 mm/s.
Micro-controller	SMC corvus eco, 3-axes closed loop control, velocity < 0.1 μm/s, 15 – 25 rev/s, linear interpolation, miCos GmbH.

3.2.2 Electrolytic Cell

Generally, the basin that contains the ionized conductive liquid and the two electrodes during electrochemical action is termed as electrolytic cell. This is a specially designed basin that must fulfill the requirements of: high signal to noise ratio, low dead volume, well-defined hydrodynamics, small ohmic drop, and ease of fabrication and maintenance [65]. As the materials are separated from the workpiece surface by the electrochemical action, the electrochemical cell must not be made of electrically conductive materials. Therefore the best choice of the materials for fabricating electrochemical cell is glass, plastics, teflon, quartz etc. Specially designed glass cells are commonly used as the cell material, due to its low cost, transparency, chemical inertness, and impermeability. But, some chemicals (e.g. NaOH, KOH) react with the glass; in this case, Plexiglas is the best option for cell material. For electrochemical micromachining, the cell may be (i) two electrode cell, commonly used for microtool fabrication or mask free electrochemical machining processes, and (ii) three electrode cell, commonly used in controlled potential experiments. The most widely used electrolytic cell for microtool fabrication is shown in Fig. 3.3, where two co-axial cylindrical Plexiglas shells are fitted on a thick rectangular Plexiglas plate. A circular tungsten wire is

placed in the groove (<1 mm) made on the inside wall of the inner cylindrical shell. The electrode diameter is significantly smaller than the inside wall of the Plexiglas cylinder in order to minimize the electrical field effect. Electrolytes are poured into the cell so that the circular electrode is fully dipped into the solution. The two-electrode cell usually contains an electrolyte volume of 50–500 ml. A photographic image of a two-electrode electrochemical micromachining cell is shown in Fig. 3.4.

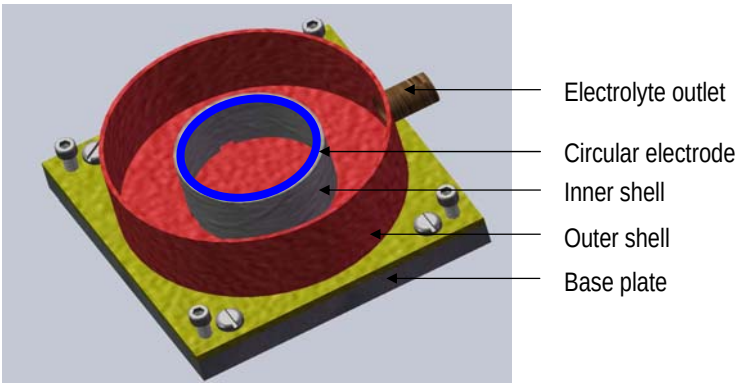

Fig. 3.3 *A schematic illustration of two-electrode electrochemical cell.*

On the other hand, a three-electrode cell contains the three electrodes, namely the working electrode, the reference electrode, and the auxiliary electrode, and all are immersed in the sample solution. While the working electrode is the electrode at which the reaction of interest occurs, the reference electrode provides a stable and reproducible potential (independent of the sample composition), against which the potential of the working electrode is compared. Commonly, calomel electrodes or silver/silver chloride electrodes are used as reference electrode, but depending on the electrolyte, Hg/HgO electrodes in strongly basic solutions, and $Hg/HgSO_4$ electrodes in sulphuric acids are used.

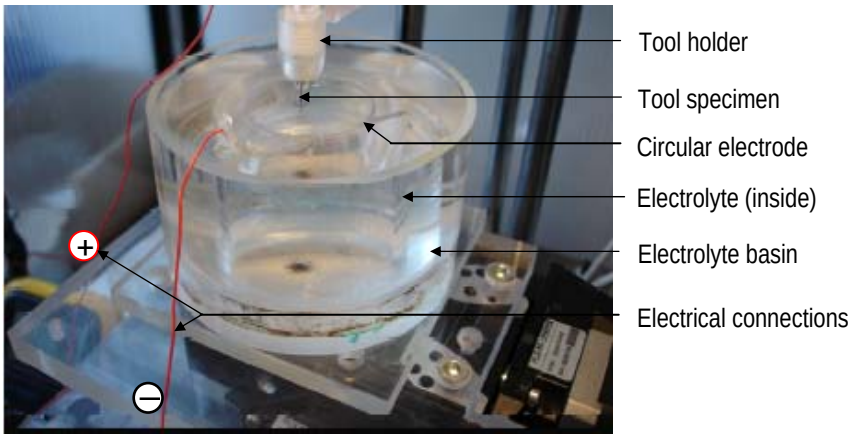

Fig. 3.4 *A photographic illustration of two-electrode electrochemical cell.*

3.2.3 Microtools

As the electrochemical micromachining process demands a microtool on micron scale, including high electrical and thermal conductivity, good wear and corrosion resistance, mechanical strength, tungsten are widely used as tool material because of its high rigidity, toughness and resistance to chemicals. To manufacture the tools, straight tungsten wire (Goodfellow Ltd., UK) of purity 99.9%, having 0.38 mm in diameter, 0.5 m in length was used. The required tungsten piece was cut from as supplied long wire. The cut end of the specimen was ground and polished to remove the warthog shapes formed during cutting process, and cleaned. The length and tool tip condition were also checked under optical microscope before etching to ensure nonexistence of flaw/crack. Some basic physical properties of tungsten wire are summarized in Table 3.2.

Table 3.2 Chemical composition and physical properties of tungsten wire.

Properties	Value
Chemical composition	99.9% tungsten (W) +
	Al < 50 ppm
	Ca < 50 ppm
	Cr < 50 ppm
	Cu < 50 ppm
	Fe < 50 ppm
	Mg < 50 ppm
	Ni < 50 ppm
	Si < 50 ppm
	Sn < 50 ppm.
Poisson's ratio	0.28
Yield strength (MPa)	550
Tensile modulus (GPa)	411
Electrical resistivity at 0–20^{0}C (μOhm-cm)	5.4
Coefficient of thermal expansion at 0–100^{0}C (K^{-1})	4.5×10^{-6}
Thermal conductivity at 0–100^{0}C (Wm^{-1} K^{-1})	173

3.2.4 Work Material

The selection of workpiece material was based on the properties of corrosion and heat resistance. Nickel, being inert against most chemicals, is a metal commonly applied in micro-technology. An uncoated nickel plate of 50 x 50 x 0.075 mm in dimension, 99.0% pure (Goodfellow Ltd., UK) was selected as work material. The chemical composition and some basic physical properties of nickel plate are summarized in Table 3.3.

Table 3.3 Chemical composition and physical properties of nickel plate.

Properties	Value	
Chemical composition	99.0% Ni +	
	Cu	< 2500 ppm
	Fe	< 4000 ppm
	Mg	< 2000 ppm
	Mn	< 3500 ppm
	Si	< 1500 ppm
	Ti	< 1000 ppm
	C	< 1500 ppm
	S	< 100 ppm.
Poisson's ratio	0.312	
Yield strength (MPa)	660	
Tensile modulus (GPa)	199.5	
Electrical resistivity at 0–20^{0}C (μOhm-cm)	6.9	
Coefficient of thermal expansion at 0–100^{0}C (K^{-1})	13.3 ×10^{-6}	
Thermal conductivity at 0–100^{0}C (Wm^{-1} K^{-1})	90.9	

Table 3.4 Chemical composition and physical properties of AISI 403 steel.

Properties	Value	
Chemical composition	Fe balanced +	
	C	0.15 %
	Mn	1.00 %
	Si	0.50 %
	S	0.03 %
	Cr	11.5–13.0 %
	P	0.04 %
Poisson's ratio	0.27 – 0.30	
Yield strength (MPa)	275	
Elastic modulus (GPa)	190 – 210	
Electrical resistivity at 0–20^{0}C (μOhm-cm)	6.9	
Coefficient of thermal expansion at 0–100^{0}C (K^{-1})	9.9 ×10^{-6}	
Thermal conductivity at 0–100^{0}C (Wm^{-1} K^{-1})	24.9	

Electrochemical micromachining is also preformed on special grade stainless steel. The material on which the μECM operations were carried out is AISI 403 steel.

Heat treatment imparts to this steel and extremely high tensile strength and hardness as well as excellent abrasion resistance and corrosion resistance facilitates this material to use in the fabrication of small medical instruments, such as injection needle, vitrectomy needles etc. The chemical composition and some basic physical properties of AISI 403 steel is summarized in Table 3.4.

3.2.5 Tool Holder

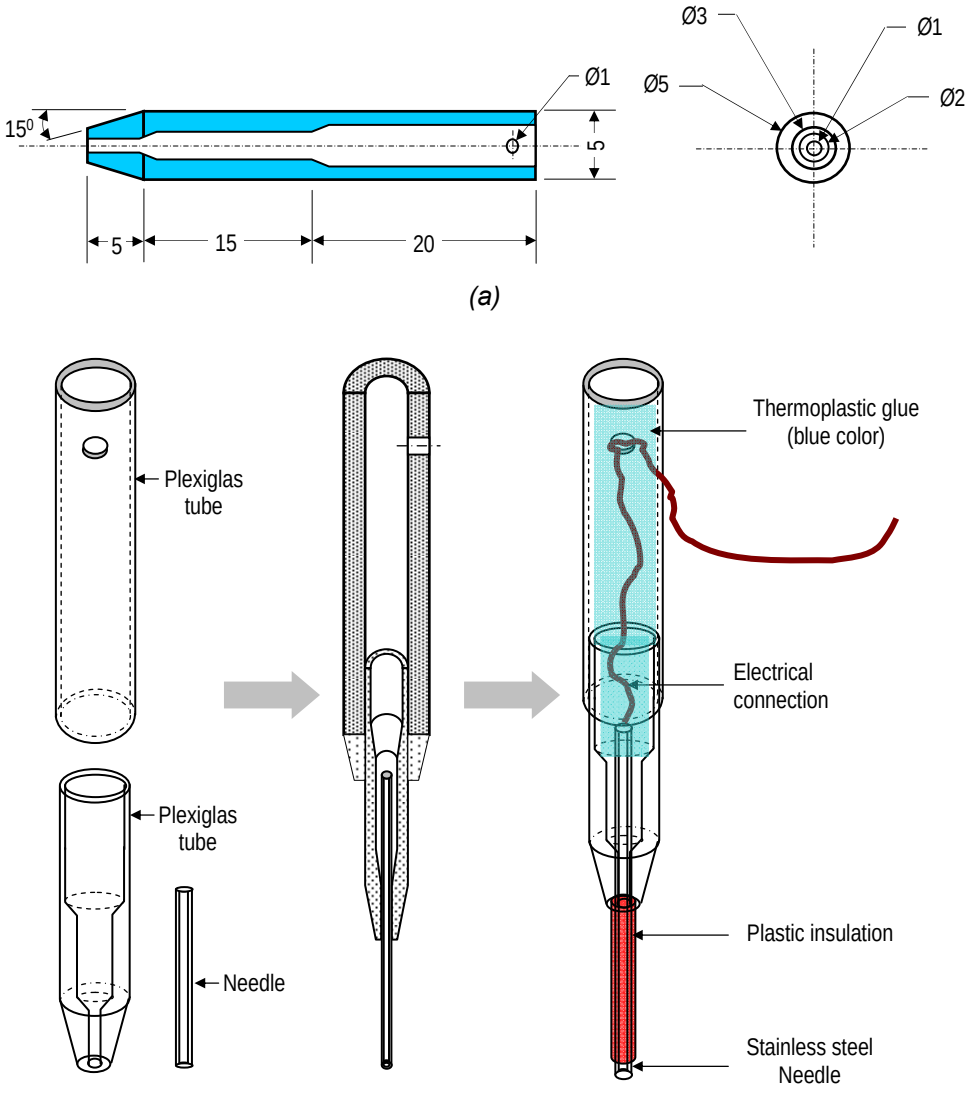

Fig. 3.5 *Different tool holders for electrochemical machining, (a) simple tool holder, and (b) different parts and assembled modified tool holder.*

The tool holder is an important connection between the linear travel guide and the microtool. The importance in choosing the optimum tool holder is substantial as the quality of the tool holder has a great influence on the results of the complete micromachining process. During the fabrication of microtool by electrochemical micromachining processes, the tool specimen is very small, where the specimen dimension is 0.38 mm in diameter and 5–10 mm in length. Therefore, there is no proven technique for clamping the tool specimen with the extended part of the linear travel guide. Sometimes the holders end part acts as a shank of the tool, as the tool is submerged into the electrolyte. The most important requirements for a microtool holder are: the gripping force that is sufficient for electrochemical machining, low weight, be co-axial, compact in size, corrosion resistance, capable of easy tool mounting and dismounting, and ease of use.

In electrochemical machining, the same tool holder is used for clamping the prefabricated microtools. Therefore, during the experiments, two different tool holders were fabricated as illustrated in Fig. 3.5. As shown in Fig. 3.5(a), the slim tool holder, which stands out with very simple in design is fabricated from a single Plexiglas plastic shell and is made leak-proof using thermoplastic plastic glue. The second one shown in Fig 3.5(b) is made of three different components and then assembled together. This tool holder offers better facilities than the simple one. Both tool holders can be used with long extensions, which make them even more flexible for different machining reaches. The main advantage of the second tool holder is its capability of holding a very short microtool. Changing a microtool can be done within seconds, and does not need any external power source and therefore can be used anywhere. To avoid chemical reaction with the stainless steel needle, this steel portion is insulated with plastic/rubber insulation.

The tool holder support for multiple positioning, shown in Fig. 3.6, is attached to the linear travel guide via the extended support part. These tool holders were inserted into the tool holder support in vertically downward and upward directions depending on the machining conditions during the fabrication of microtools or microdrilling, micro-cutting etc.

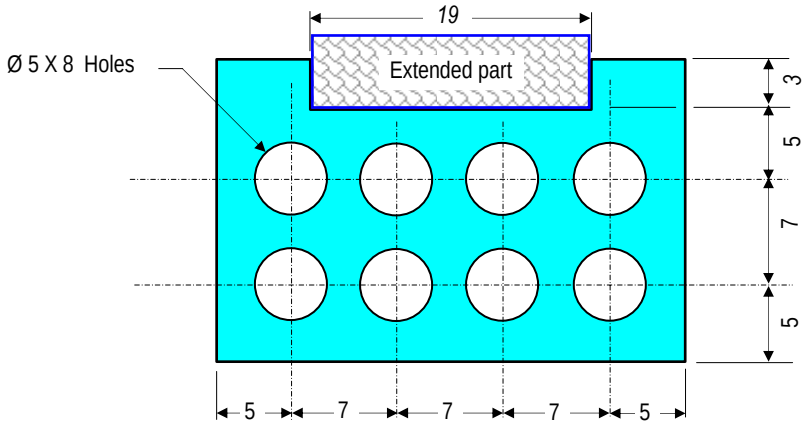

Fig. 3.6 *The tool holder support for multiple positioning of the tool holder.*

3.2.6 Work Holding Device

During electrochemical machining, the nickel plate was fixed with the wok holding device, called work fixture as illustrated in Fig. 3.7. The material for the fixture was so chosen that it must be corrosion resistant. The fixture was so precise that it can hold the nickel workpiece of thickness 0.075 mm. The workpiece is clamped by two rectangular Plexiglas sheet, and screwed to the main base plate of the electrolytic basin. On one side of the clamp, a nickel plate is connected for electrical power.

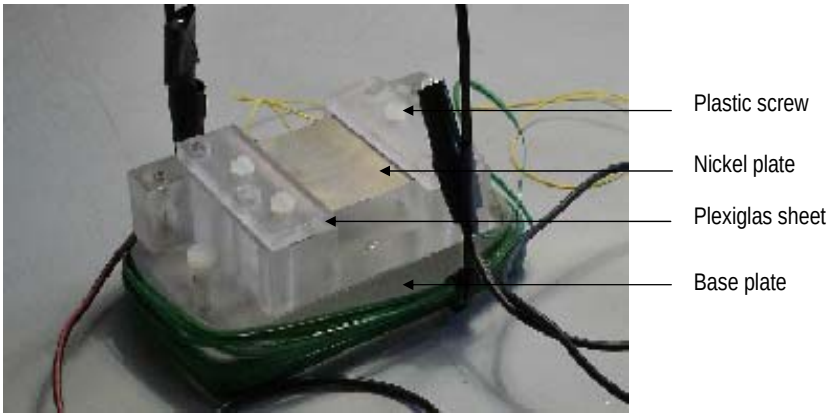

Fig. 3.7 *The workpiece holding fixture.*

The same work holding device was used to work on the injection needle and the vitrectomy needle. But when a small workpiece (20 x 20 x 0.075) was used, the fixture was modified as shown in Fig. 3.8.

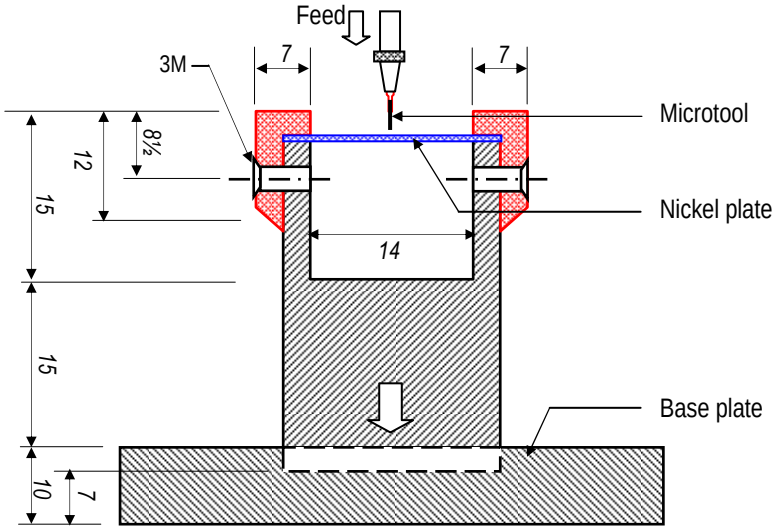

Fig. 3.8 *The workpiece holding fixture for small workpiece.*

During the fabrication of microtools from vertically upward direction, it was very complicated task to put the tungsten tool specimen in the electrolytic cell. In this case the tool holder was placed in the specially designed electrolytic cell where the height of the circular electrode was possible to control by turning the rotary part of the electrolytic cell. The special designed electrolytic cell is shown in Fig. 3.9.

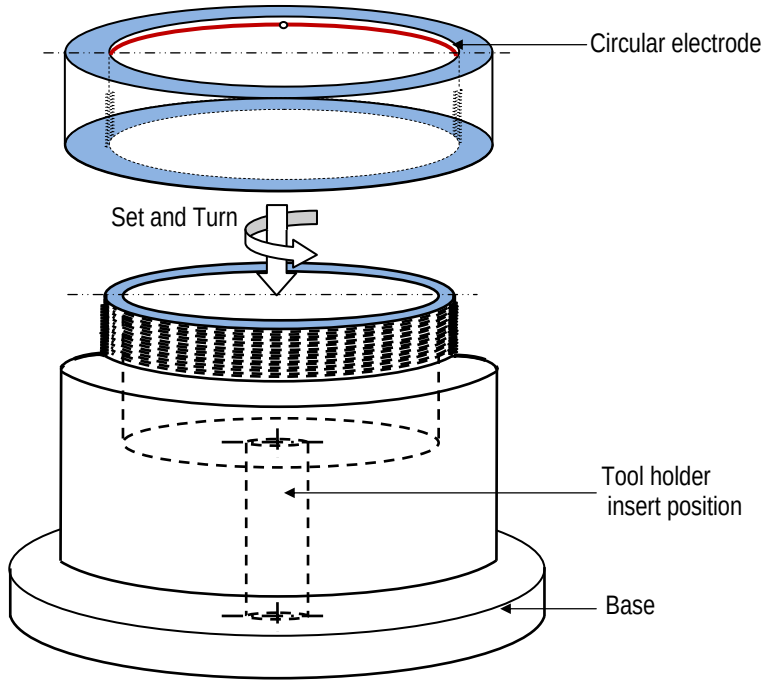

Fig. 3.9 *The workpiece (microtool specimen) holding fixture during tool fabrication.*

3.2.7 Electrolyte Selection

In the fabrication of tungsten microtool with electrochemical etching, the electrolyte must be capable of dissolving tungsten wire to give it a desired shape. In this context, solutions of KOH or NaOH were able to serve the purpose of dissolving the material like tungsten, but the use of sodium rather than a potassium cation have no direct influence on the rate of reaction, tool tip angle and the tool length. In the fabrication of microtool 0.08–1.4 M KOH electrolytes were prepared with fresh deionized aqueous solution. In order to keep a homogeneous concentration of the solution, it is required to stir the KOH solution more than three times before use if the prepared solution was kept unmoved or unused for more than one week because the concentration is low at upper solution and high at lower solution. Moreover, the quality of the solution changed due to the carbon dioxide dissolved from air. It is also recommended that not to shake the bottle too much to avoid the carbon dioxide contamination. It is better to prepare a new solution if the KOH solution is older than one month.

On the other hand, less toxic and dilute electrolyte, 0.2 M HCl was selected during microholes fabrication. Hence, the acidic electrolyte allowed easily refreshing electrolyte in the machining area because the acid electrolyte usually produced by-product much less than common salt electrolytes. Fresh and clean electrolytes were used with a view to reduce the effects associated with the precipitation that formed during etching process. This experiment was performed at room temperature. As the slender electrode was used, it was very difficult to pump electrolyte throughout the machining area because of its tendency to bend on application of forced flow of electrolyte. Therefore, no circulation system was integrated as the μECM process involved negligible amount of heat generation and precipitation formation. The electrolyte conductivity depends on the concentration; therefore, the proper choice of the electrolyte can be determined from the graph given in Fig. 3.10.

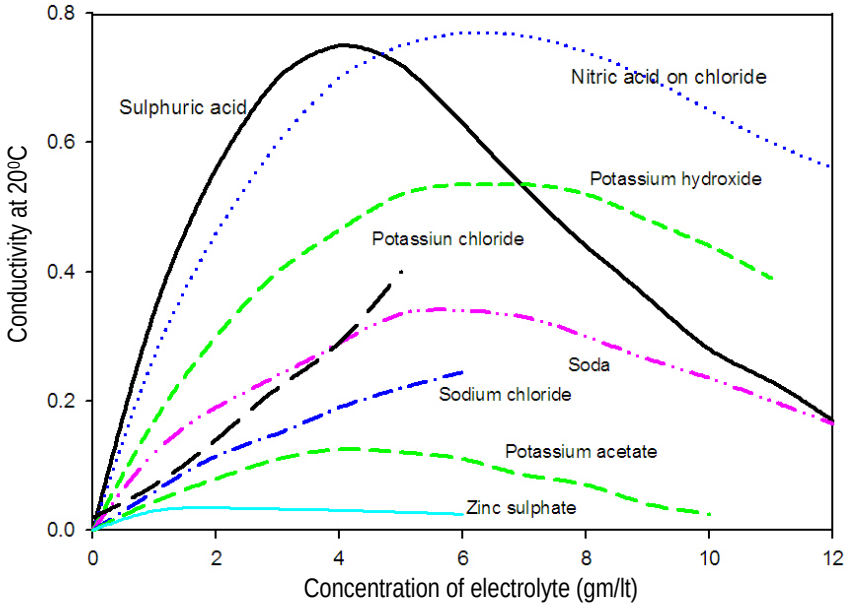

Fig. 3.10 *Variation of conductivity of electrolytes with the concentration.*

3.2.8 Electrical Power

Electrochemical micromachining conventionally utilizes DC input as power source. But, in this experimental works, AC power has been used for microtool fabrication processes and pulsed DC power has been used for microdrilling and micro-cutting processes. The applied voltage waveform plays a crucial role in the quality and surface finish of microproducts' part. To understand the electrochemical cell model based on voltage pulses, it is important to define the electrical double layer, or simply double layer (DL) and short-pulse behavior in material dissolution process.

3.2.8.1 Electrical double layer

The electrical double layer is the array of charged particles and/or oriented dipoles existing at every material interface [65, 140]. But, in electrochemical process, the electrical double layer is the structure of charge accumulation and charge separation that always occurs at the interface when an electrode is immersed into an electrolyte solution. Such a layer reflects the ionic zones formed in the solution to compensate for the excess of charge on the electrode. The excess charge on the electrode surface is compensated by an accumulation of excess ions of the opposite charge in the solution. Thus, a positively charged electrode attracts a layer of negative ions, and vice versa, as illustrated in Fig. 3.11. A counter-layer consists of ions of sign opposite that of the electrode, therefore, and the amount of charge is a function of the electrode potential.

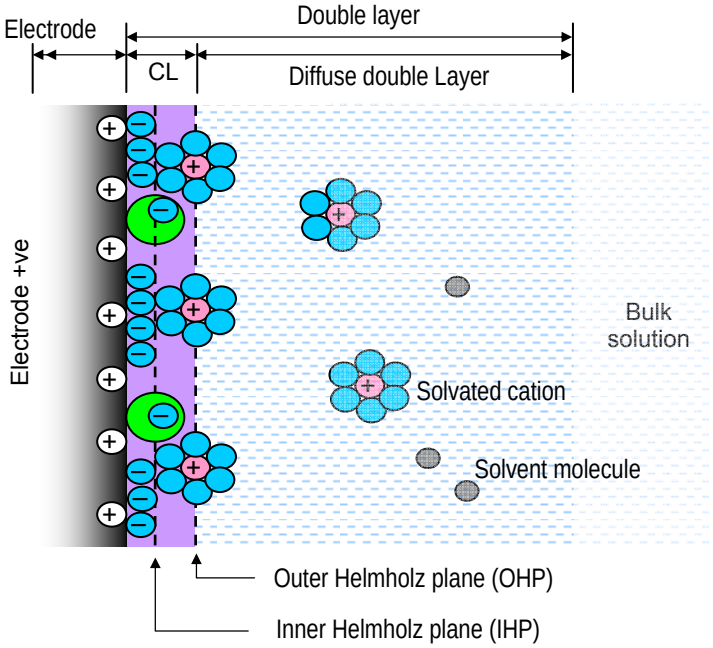

Fig. 3.11 *Schematic representation of the electrical double layer.*

As illustrated in figure, the electrical double layer has a complex structure of several distinct parts. The inner layer, which is the closest to the electrode, is known as the inner Helmholz plane (IHP). It contains solvent molecules and specifically adsorbed ions that are not hydrated in the aqueous solutions. It is defined by the locus of points for the specifically adsorbed ions. The next layer, the outer Helmholz plane (OHP), reflects the imaginary plane passing through the center of solvated ions at their closest approach to the surface. The solvated ions are nonspecifically adsorbed and are attracted to the surface by long-range coulombic forces. Both Helmholz layers represent the compact layer (CL). This compact layer of charges is strongly held by the electrode and can survive even when the electrode is pulled out of the solution.

This outer layer, beyond the compact layer, is loosely associated with the object, because it is made of free ions which move in the fluid under the influence of electric attraction and thermal motion rather than being firmly anchored, called the diffuse layer, or Gouy layer. This is a three-dimensional region of scattered ions, which extends from the OHP into the bulk solution. The total charge of the compact and diffuse layers equals (and is opposite in sign) to the net charge on the electrode side. Depending on the ionic strength, the thickness of the double layer may extend to more than 10nm. In electrochemical micromachining system, the electrodes are separated on the micron scale, the voltage pulsing of the tool in an electrolyte leads to the charging and discharging of electrochemical double layers at both the tool and workpiece. Electrically, this system can be thought of as two equi-potential surfaces, in contact with spatially varying double layer capacitances, connected by the resistance of the electrolyte [203].

For voltage pulses, the evolution of both the electric field and polarization of the double layers can be determined by applying basic circuit theory elements. The electrical double layer resembles an ordinary parallel-plate capacitor, and the capacitance of the double layer consists of a combination of the capacitance of the compact layer in series with that of the diffuse layer. As both capacitors are in series, the total capacitance is found adding the capacitance of the compact layer (C_H) and capacitance of the diffuse layer (C_G). Depending on the strength of the solution used, the capacitance of the double layer per unit area, C_{dl} values are usually in the range of 10–40 μF/cm^2 [65]. The smaller of these capacitances determines the observed behavior.

The capacitance of the compact layer increases with decreasing separation between the electrode surface and the counter-ionic layer, and the value of diffusion layer capacitance is strongly affected by the electrolyte concentration, where the compact layer is largely independent of the concentration. During electrochemical machining, on the application of a potential difference between two electrodes, the potential profile in the electrical double layer becomes similar to that of an equivalent circuit of capacitors and resistors [93]. This time constant is given by the product of the electrolyte resistance along the current path and the double layer capacitance, and therefore varies linearly with the separation between the electrodes. As the rate of electrochemical reactions is exponentially dependent on the voltage drop in the double layer, the reaction at the workpiece is strongly confined to the charged region. However, all the current flow through an electrochemical cell is not caused by electrochemical reactions. There is reaction current called faradaic current and transient current called non-faradaic current [94]. Faradaic current determines the material dissolution rate and non-faradaic current results from current flow that charges and discharges only the double layer capacitance [95]. Such a charging process is non-faradaic process because electrons are not transferred across the electrode–solution interface. It occurs when a potential is applied across the double layer, or when the electrode area or capacitances are changing.

Electrocapillary is the study of the interfacial tension as a function of the electrode potential, results from a reduction of the surface energy at the solid/liquid interface due to an applied electrical potential [204]. The effect causes the contact angle of a

hydrophobic liquid droplet to decrease and wet the solid surface. Such a study can shed useful light on the structure and properties of the electrical double layer. A plot of the surface tension versus the potential is called an electrocapillary curve. The more highly charged the interface becomes, the more the charges repel each other, thereby decreasing the cohesive forces and lowering the surface tension. Experimental electrocapillary curves have a nearly parabolic shape around the zero potential.

3.2.8.2 Characteristics of pulsed voltage

The potential profile across the double layer is similar to that of a parallel resistor–capacitor (RC) circuit. According to electrical dissolution theory, dissolution of solid materials take place during the pulse on time, and the pulse-off time affects machinability characteristics. The double layer is charged during pulse-on time, is removed during the pulse off-time. Moreover, the ions which have been depleted during the pulse-on time are replenished by convection and diffusion of the electrolyte. If the pulse off is not long enough to remove the charged ions, the machining zone increases continuously similar to the machining characteristic with DC voltage. To get a clear idea about the waveform generated during machining, the voltage value that is provided by the oscilloscope is depicted in Fig. 3.12.

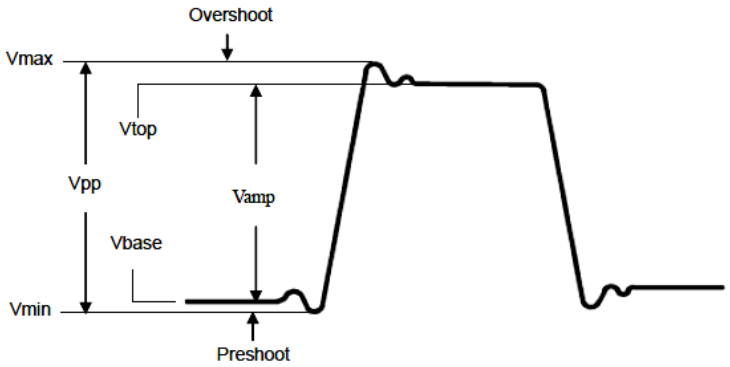

Fig. 3.12 *The measurement of voltage parameters of a digital oscilloscope.*

where,

V_{pp}:	Peak-to-peak voltage.
V_{max}:	The maximum amplitude. The most positive peak voltage measured over the entire waveform.
V_{min}:	The minimum amplitude. The most negative peak voltage measured over the entire waveform.
V_{top}:	The median voltage value of the waveform's flat top.
V_{base}:	The median voltage value of the waveform's flat base.
V_{amp}:	Voltage between V_{top} and V_{base} of a generated waveform.
Overshoot:	Defined as $(V_{max}–V_{top})/V_{amp}$, useful for square and pulse waveforms.

Preshoot: Defined as $(V_{min}–V_{base})/V_{amp}$, useful for square and pulse waveforms.

Average: The arithmetic mean over the entire waveform.

The oscilloscope provided the automatic measurements of some time parameters that include applied frequency, period, duty cycle, width, rise time, fall time, delay, etc. These values can also be displayed with the waveform generated during machining. The nomenclatures of the time based parameters are depicted in Fig. 3.13.

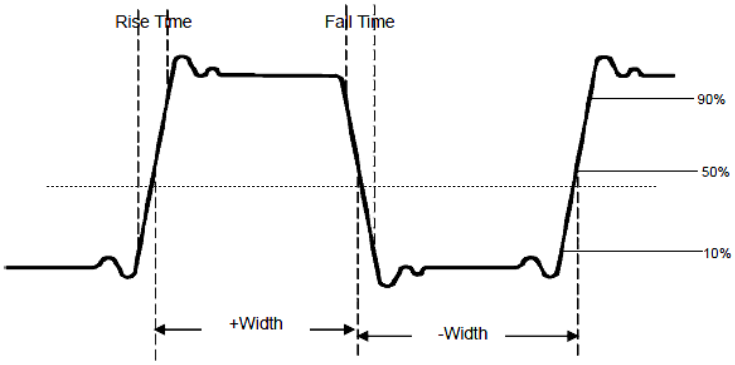

Fig. 3.13 *The automatic measurement of time parameters of a digital oscilloscope.*

where,

Rise Time: Time that the leading edge of the first pulse in the waveform takes to rise from 10% to 90% of its amplitude.

Fall Time: Time that the falling edge of the first pulse in the waveform takes to fall from 90% to 10% of its amplitude.

Width (+/–): The width of the first positive/ negative pulse in 50% amplitude points.

Duty (+/–) Duty Cycle is defined as +ve/-ve Width divided by the period.

Delay 1→2: The delay between the two channels at the rising edge or falling edge.

During every pulse period, the double layer is charged and discharged periodically over the two electrodes, since the charging and discharging time depends on the constant RC circuit, material removal generally occurs in areas where electrolyte resistance is lower, i.e. where the tool-workpiece gap is very small. As it is not simple to determine the faradaic current duration and its initial time, t^*, the amount of faradaic current can be estimated from the waveform generated during machining. A representative waveform that generated during machining is shown in Fig. 3.14.

But, on the application of ultra short voltage pulses between the electrodes, faradaic dissolution current flows only in the very confined region, and during the pulse-off time, the electrode polarity interchanges. Therefore, the RC circuit has been modified to resistor-capacitor-inductance (RCL) circuit for better machining facilities. Electrolyte resistance, inductance and electrical double layer provide an

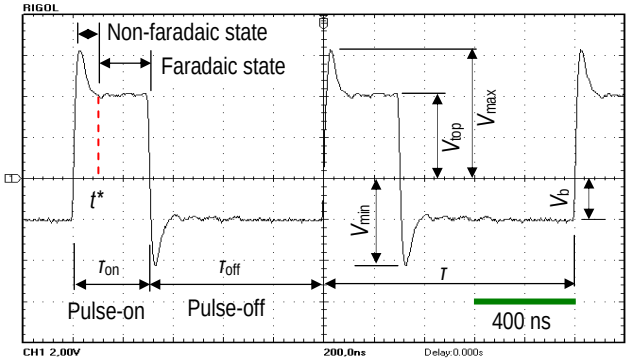

where,

T = frequency period

T_{on} = pulse-on time

T_{off} = pulse-off time

t^*= initial time to start faradaic current, i.e., the mean value of flat voltage

Fig. 3.14 *A representative waveform that generated during machining.*

equivalent RCL circuit in electrochemical cell is shown in Fig. 3.15, where, C_{dl}, is the capacitance of the double layer, R_P, is polarization resistance of the double layer, R_s is short path resistance and R_l is long path resistance of the equivalent circuit, L_i is the inductance of the electric wires, R_u is the internal resistance of the pulse supplier, V_u is the exit tension of the pulse supplier, I_t is the total current, and G_l is the ideal pulse supplier. The inductance prevents instantaneous reversal of the current, while an appropriate value of negative voltage applied to the workpiece during the pulse-off time accelerates the creation of the double layer without the dissolution of the tool. While the pulse duration of machining current is shortened to a few nanoseconds, the electrochemical process cannot achieve stationary condition owing to the extremely short pulse duration.

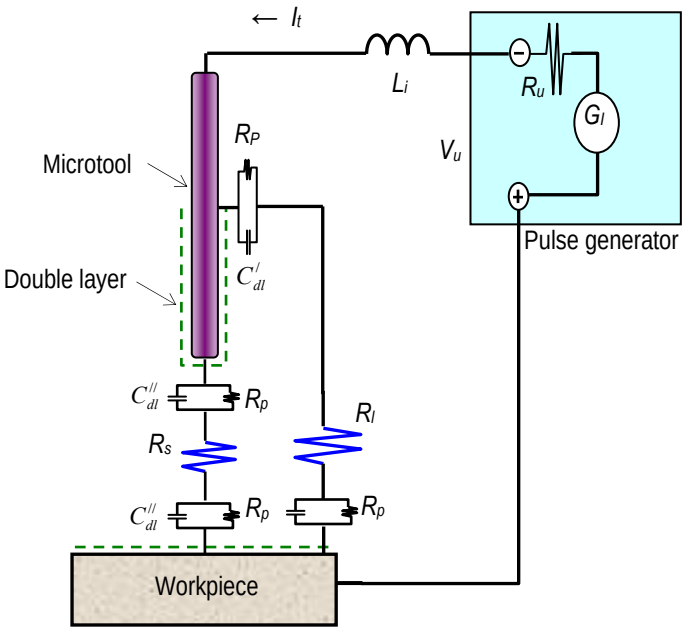

Fig. 3.15 *Equivalent circuit model for electrical double layer potential.*

The local charging is a complex function of tool–substrate geometry, electrolyte resistance, double-layer capacitance, pulse height, and pulse duration. The specific electrolyte resistivity and the double-layer capacity are determined by the electrolyte concentration, which can be locally altered in a time-varying electric field. Little is known about the complex dynamics of charging and discharging, therefore the direct characterization of the material dissolution is very difficult. While no direct measurement of dynamic electrochemical processes is possible, the rate of material dissolution can be estimated from the experimental techniques.

3.3 MACHINING PROCESSES

During the experimental scheme, microtools of different dimensions were fabricated and these microtools were used to drill microholes and micro-cutting on nickel plate and stainless steel needles. Parametric effects on machining performance were also tested. Material removal rate (MRR), machining time, taper angle of the microtool and microhole were considered as performance measures of μECM characteristics. The succeeding sections describe on how microtools were fabricated and the application of microtools on microdrilling and micro-cutting processes in brief.

3.3.1 Fabrication of Microtools

In the μECM, selection of electrode polarity is important. The straight tungsten specimen was clamped inside of the microtool holder, immersed in vertically downward at the center of Plexiglas basin with an uncovered length of 3 mm into the electrolyte containing caustic solutions of different concentrations. A circular tungsten wire was mounted around the inner wall of the basin. As the tools used for this experiment were fabricated by reversed ECM process, the tool specimen was connected as anode and the circular tungsten electrode was used as counter electrode (cathode). Electrolytes were poured into the small basin so that the circular electrode was fully submerged into the solution as shown in Fig. 3.16. A constant potential difference of 3–15V AC was applied. As the dissolution process proceeds, a straight micro-shaft with a certain diameter forms after a certain etching time. In-process measurement of the tool diameter was very difficult because the tool was submerged in the electrolyte solution, and the tool specimen was thin as well. Creation of bubbles around the dissolution area was another problem in sighting the reduction of tool diameter in process. Variations in diameter and length of the electrodes were, therefore, measured in a specified time interval by an optical microscope (Nikon SMZ800).

The uniformity in the variation of diameter of the microtool was monitored by measuring the diameters at different locations in between the points slightly away from the tool tip and shank. The dissolution of tool material was recorded by a stopwatch, and the process of dissolution continued until the tool diameter was reduced to about 50 –150 μm. Each of the tools was rinsed in the hot water to remove foreign particles and the formed oxides. After cleaning, tool tips were characterized under optical microscope and scanning electron microscope (SEM) to see the roundness error that is defined by difference of maximum and minimum

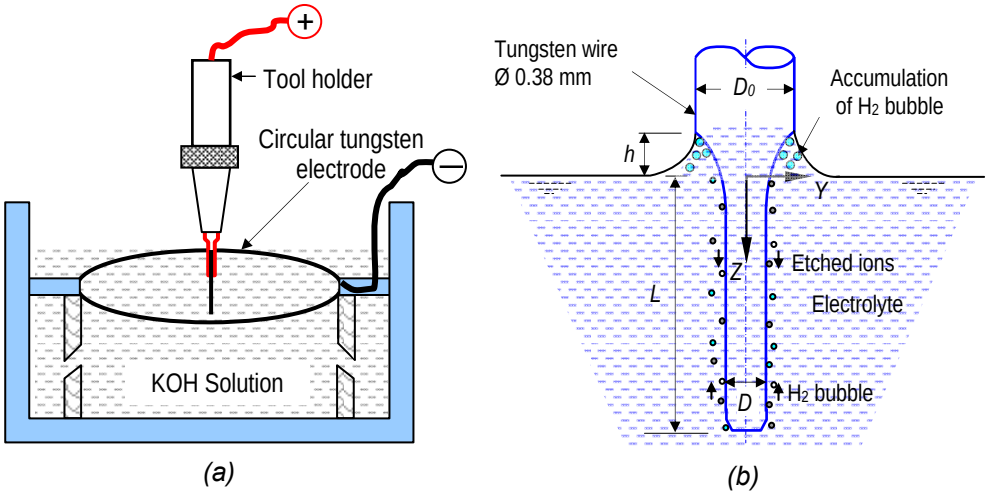

Fig. 3.16 *Electrochemical tool etching (a) setup, and (b) etching mechanism.*

diameters at the entrance of the hole. The same experimental procedure was also applied for the tool specimens were placed in vertically upward direction, horizontal to the electrolyte basin and the tool placed very near to the circular electrode, shown in Fig. 3.17. Experimental conditions for tool sizing and shaping are summarized in Table 3.5.

Table 3.5 Experimental conditions for tool sizing and shaping.

Material:	Anode: Straight tungsten specimen (5–8 mm), Ø 0.38 mm, ground and polished Cathode: Circular tungsten wire (Ø 0.38 mm), 5, 10, 20 and 40 mm ring diameter
Polarity	AC, 50 Hz
Potential applied	3 V, 6 V, 9 V, 15 V AC
Electrolyte type	KOH aqueous solution
Electrolyte concentration	0.08, 0.1, 0.4, 0.5, 0.6, 0.7, 1.0, 1.2 and 1.4 M/l
Uncovered tool length	3 mm
Tool insert position	Vertical (downward and upward), Horizontal to the basin, vertically downward, and Very near to the circular electrode
Temperature of solution	Room temperature
Electrolyte circulation	No circulation

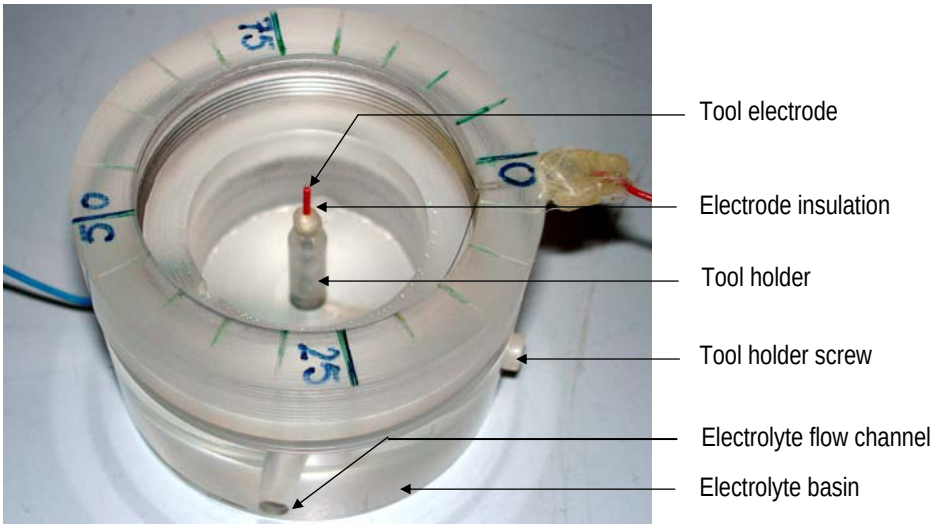

Fig. 3.17 *Electrochemical tool etching, specimen set in vertically upward direction.*

The etched tungsten electrode was brought out from the plastic basin and placed vertically downward direction into KOH electrolytic solution to a desired depth to prepare conical shaped tip as illustrated in Fig. 3.18. During preparation of tool tip,

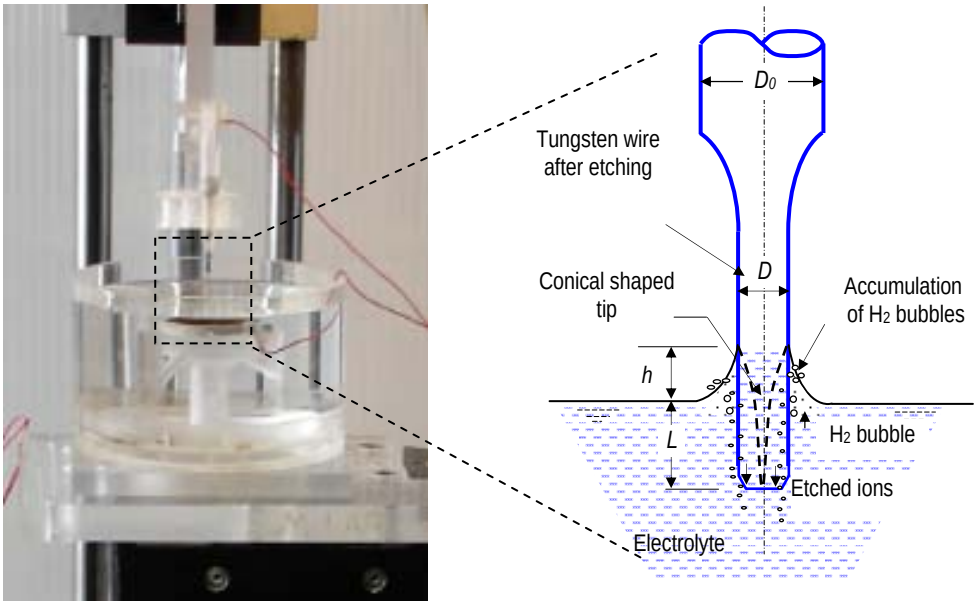

Fig. 3.18 *The electrochemical micromachining for the preparation of microtool tip and the schematic illustration of the fabrication process (insight).*

the dissolution of electrode also took place slightly above of the electrolyte level when dipped into electrolyte. The cylindrical tool thus immersed by surface tension and the electrolyte raised along the tool body forming a shape very similar to the parabolic shape. The electrochemical reaction took placed when the potential is applied between the two electrodes. Conical/tapered shape was formed on the cylindrical tool part that was dipped into the electrolyte solution, where *L* is depth of immersion, and *h* is the elevation of solution due to surface tension. The dotted line (in Fig. 3.18) indicates the conical shape that formed at the tip of the cylindrical tool. Experimental conditions for tip preparation are listed in Table. 3.6.

Table 3.6 Experimental conditions for microtool tip formation.

Material:	Anode: Prefabricated straight tungsten tool (5–8 mm long), 0.38 mm shank diameter, different size Cathode: Circular tungsten wire (Ø 0.38 mm), 20 and 40 mm ring diameter
Polarity	AC, 50 Hz
Potential applied	9 V, 15 V AC
Electrolyte type	KOH aqueous solution
Electrolyte concentration	0.4, 0.5, 0.6, 0.7, 1.0 and 1.4 M/l
Uncovered tool length	1 mm (approximately)
Tool insert position	Vertically downward
Temperature of solution	Room temperature
Electrolyte circulation	No circulation

3.3.2 Fabrication of Microhole

Microholes are the most basic machined features of micromachining. A series of experiments were conducted using different machining conditions to investigate the parametric effect of micromachining during microdrilling and micro-cutting. The machining conditions for microdrilling and micro-cutting by pre-fabricated microtools are summarized in Table 3.7. Each of the microproducts was rinsed in the hot water to remove foreign particles and the formed oxides before measurement.

The vitrectomy needle body is made of AISI 403 steel and finished by chromium plating. The channels of that needle are permanently affixed with the needle. Therefore, some modification is needed in the experimental setup, to put firmly in the electrolytic basin. The same parameters are used for the development of vitrectomy needle, and special care needs to place the needle inside the basin. The chromium plating offers special advantage to the machining processes in protecting the needle body from the acidic environment.

Table 3.7 Machining conditions for microhole fabrication.

Factors	Parameters/Value
Materials	Tool material : Prefabricated tungsten microtool Work material : Nickel plate, 50 x 50 x 0.075 mm, uncoated, 99.0% pure, annealed
Electrolyte concentration	: 0.2 M HCl solution (without circulation)
Electrical parameters	Frequency (MHz) : 0.5, 1.0, 1.5, 2.0, 4.0, 8.0 Duty cycle (%) : 15, 25, 30, 35, 40 V_{pp} (volt) : 16.1 V_{max} (volt) : 10.6 V_{base} (volt) : – 5.0
Tool insert position	: Vertically downward , perpendicular to the workpiece
Tool feed rate (μm/s)	: 0.05 to 0.5, computer controlled
Tool advancement (μm)	: 80 to 200, vertically downward

3.4 MEASUREMENTS

Image analysis application software, Easy Analysis, integrated with the optical microscope (Nikon SMZ800) was used to measure the diameter and length of the tool produced by μECM. After a specified time interval, the diameter of the tool was measured under that microscope to measure the reduction in diameter. Entrance and exit diameters of each fabricated microhole were also measured using the same microscope. The specially designed fixture used to assist in the measurement of microtool under optical microscope is shown in Fig. 3.19 and 3.20. In addition, scanning electron microscope (SEM) was used to acquire better picture of the fabricated microtools and their tips, and fabricated micro-drilled holes and micro-pockets.

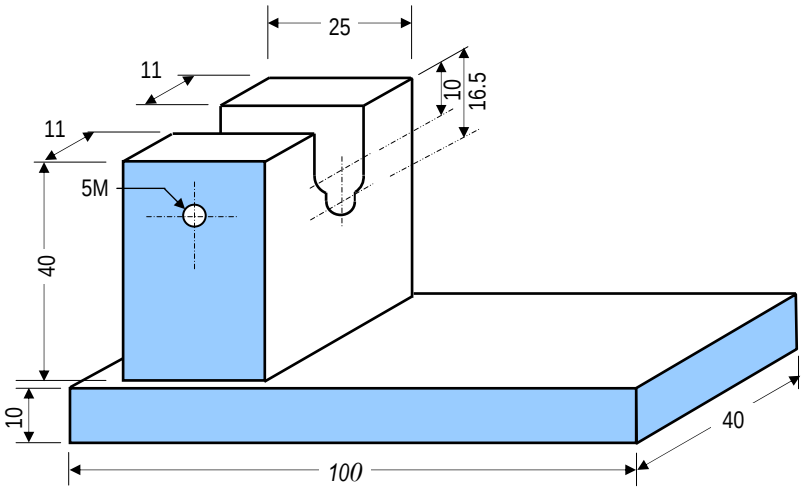

Fig. 3.19 *The fixture used under microscope for microtool measurements.*

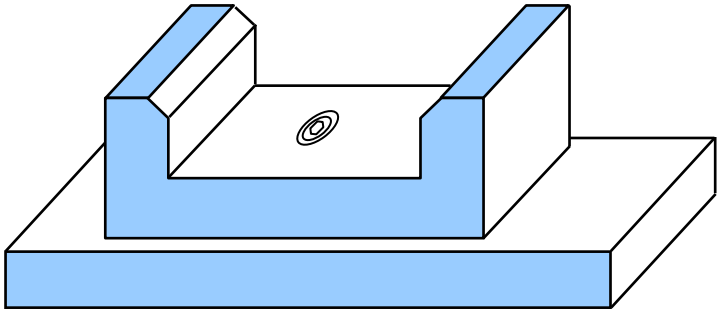

Fig. 3.20 *The fixture used for measuring microtools with the electrolyte basin.*

Although tool electrodes were cylindrical, the entrance and exit diameter of the machined microhole were not same due to: (i) shape restriction, (ii) etching process in case of non-insulated tool, and (iii) corner etch of the hole entrance in addition with the linear etching, and the result is the tapering of the side wall. Therefore, to evaluate the total material removed during machining, both entrance and exit diameters were measured. The amount of material removed from the workpiece can be calculated from the truncated cone equation (3.1).

$$V_m = \frac{\pi h}{12}\left(\phi_{ent}^2 + \phi_{ent}.\phi_{exit} + \phi_{exit}^2\right) \qquad (3.1)$$

where, $Ø_{ent}$, $Ø_{exit}$ and h were hole entrance diameter, hole exit diameter and thickness of the metal plate, respectively, shown in Fig. 3.21. The actual material removal rate (MRR_{act}) is calculated as the total volume of material removed from the workpiece over the total machining time which is expressed as cubic millimeter per minute (mm^3/min).

The gap ratio (g_{ent}/g_{exit}), an important factor showing the effect of tool diameter on the formation of taper angle during machining, is measured as a ratio of side gap at the entrance to side gap at the exit of the hole. The gap ratio and the taper angle

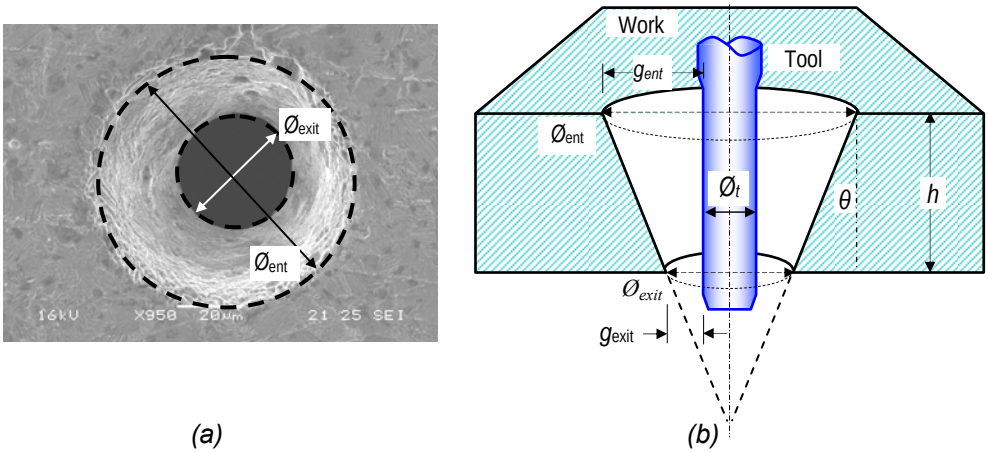

Fig. 3.21 *(a) SEM image, and (b) schematic illustration of the fabricated microhole.*

The gap ratio (g_{ent}/g_{exit}), an important factor showing the effect of tool diameter on the formation of taper angle during machining, is measured as a ratio of side gap at the entrance to side gap at the exit of the hole. The gap ratio and the taper angle formed in micro-drilled hole can be calculated from the equation (3.2) and (3.3), as:

$$\text{gap ratio, } \frac{g_{ent}}{g_{exit}} = \left(\frac{\varphi_{ent} - \varphi_t}{\varphi_{exit} - \varphi_t} \right) \tag{3.2}$$

$$\text{and, taper angle, } \theta = tan^{-1}\left(\frac{2h}{\varphi_{ent} - \varphi_{exit}} \right) \tag{3.3}$$

where, g_{ent}, g_{exit}, $\varnothing_t$, and θ are the side gap at the entrance, side gap at the exit of the microhole, microtool diameter, and microhole taper angle, respectively.

3.5 PROCESS MONITORING AND CONTROL

To address the needs of smooth machining, it is necessary to move the tool electrode along the workpiece electrode maintaining a constant gap (predefined) between them. The function generator, the oscilloscope and a tailored circuit were used as signal source, signal analyzer and tool feeding controller, respectively. Function generators provided the signals during machining and these signals were analyzed with the aid of oscilloscope. The screen image of the oscilloscope, produced during machining, were recorded and transferred to the PC for storage and further processing. The digital storage oscilloscope facilitated this operation. The software of control system performed two functions: the track control and the gap control. To avoid the physical contact between the workpiece (nickel plate) and the tool (tungsten), the tailored electronic circuit automatically stopped and retracted the tool. After the set time, the circuit automatically restarted feeding the tool maintaining the predefined gap between the electrodes. The flow chart of the gap control system is illustrated in Fig. 3.22.

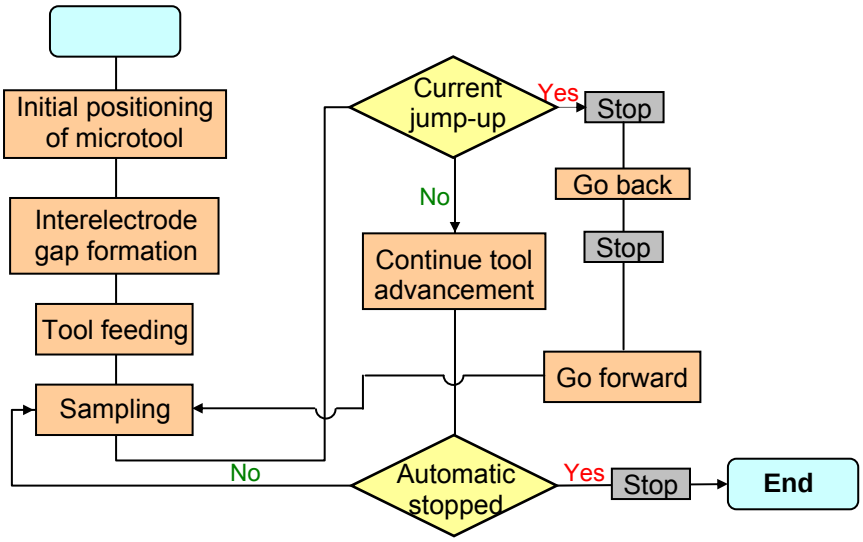

Fig. 3.22 *Flow chart of feedback control system.*

Chapter 4

Experimental Results

4.1 INTRODUCTION

Electrochemical micromachining offers some unique advantages over competing technologies. It is being widely used in the micromanufacturing industries because of its capability of machining broad variety of materials regardless of their mechanical properties. Tungsten wires are extensively used for the fabrication of microtools due to its high mechanical, chemical and thermal properties, which are essential for fabricating microtools. On the other hand, nickel is a corrosion resistant material used for in the fabrication of microproducts. Recently, chromium plated high grade stainless steels have wide-spread applications in medical and biomedical microproducts for its corrosion resistance and other high mechanical characteristics. The need for microholes or microcutting with high aspect ratio in extremely hard and brittle materials demands a suitable micromachining process, and μECM can fulfill these requirements.

To deal with this micromachining technique, it is necessary to study the effects of the parameters used in μECM process. The aim of this work is to present experimental investigation on different process parameters, and to establish a relationship with the parameters to the outcomes for different work materials. The range of the parameters was selected based on the state of the arts and recommendations given by different researchers. The results obtained from different experiments are analyzed in terms of material removal rate, machining time, frequencies of short circuits, and dimensions of the fabricated micro-products. An attempt has also been made to develop an in-process monitoring and control system discussed in the next chapter.

This chapter will highlight the influence of various important electrochemical micromachining parameters like machining voltage, applied frequencies and its duty cycles, electrolyte concentration, temperature, and microtool dimensions on material removal rate, machining time, accuracy in the dimension of fabricated microproducts, and some noble applications of micromachining.

4.2 FABRICATION OF MICROTOOLS

The microtools of desired shape and size were fabricated by electrochemical etching techniques, and used to produce some microproducts through micro-drilling and micro-cutting. Two types of microtools were made: (i) the cylindrical microtool, and (ii) microtool with conical tip.

4.2.1 Sizing and Shaping of Cylindrical Microtools

During the shaping and sizing of microtool from tool specimen, the effects of some μECM parameters such as applied potential, electrolytic concentration, and etching time etc were investigated. Microtool diameter and length are considered as output factors.

4.2.1.1 Etching characteristics according to applied potentials

Experiments were performed to investigate the etching characteristics according to applied potentials where a specified electrolyte concentration of 1.0 M KOH was selected and potentials applied were varied from 3 to 15 V AC. The uniformity in the variation of diameter of the microtool was monitored by measuring the diameters at different locations in between the point slightly away from the tool end (D_E) and the shank (D_S). At the end of the process, D_S was found to be larger than D_E. The difference between D_S and D_E indicates that conicity exists in the fabricated microtool as shown in Fig. 4.1. The variation in diameter of tungsten tool shape for different applied potentials is illustrated in Fig. 4.2. From Fig. 4.2, it is evident that variation in diameter between tool end and shank increases with the increase of both etching time and applied potentials. When the applied potential was 3 V, the rate of change in diameter (D_S — D_E) was very slow. As the MRR was low, it took a long time to fabricate a microtool of desired size, which was practically not feasible. Rapid deterioration of electrolytic solution was also observed due to formation of black precipitations at the lower applied potential. For the applied voltage of 6 V AC, change in diameter (D_S — D_E) with time was found to be a possible solution to these aforestated problems. In this case, the minimum diameter of the tool end was obtained at about 5 minute of machining. After 5 min of machining, the tool length decreased with no change in its shape over time. Over these applied potentials, the rate of dissolution was faster and it was possible to make a tool within 3 min of etching. It was observed that higher potentials were

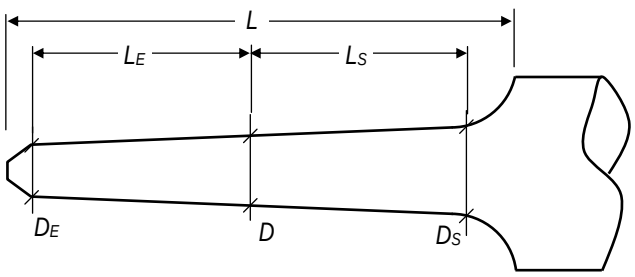

Fig. 4.1 *Conceptual model of taper formation during microtool fabrication.*

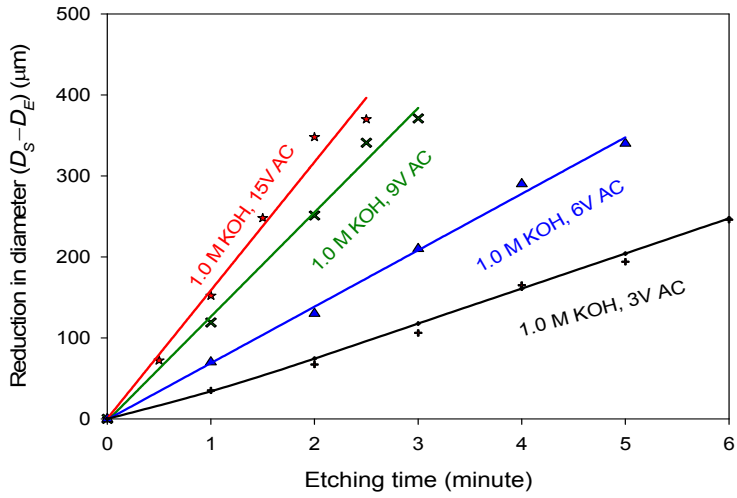

Fig. 4.2 *Variation in microtool diameter (D_S — D_E) with etching time for different applied potentials.*

very much sensitive to tool shape as the solid angle of conically-shaped microtool became larger with higher potentials. Also, higher dissolution and sometimes neck formation were evident for higher applied potential.

4.2.1.2 Etching characteristics according to electrolyte concentration

During experiment, electrolyte concentrations were varied from a very low concentration (0.08 M) to a moderately high concentration (1.4 M KOH). At the initial stage of the machining, the change in diameter with etching time and/or MRR

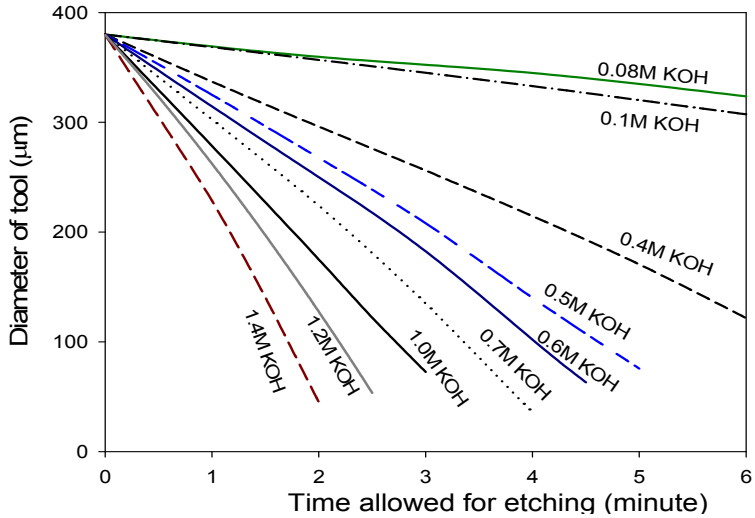

Fig. 4.3 *Variation in microtool diameter with etching time for various electrolyte concentrations and a constant 9 V applied potential.*

was approximately linear for all the concentrations. For a certain etching time, the dissolution over the entire tool length was uniform making a straight micro-shaft with a certain diameter. After that certain time period, the deviation in diameter between the tool end and shank increased with the increase in etching time forming a conically-shaped microtool as shown in Appendix A.

Due to the electric charge concentration at the shaft portion of tool, intensive dissolution occurred at the lower end of the tool formed a conical shape. From Fig. 4.3 and 4.4, it was found that variation in tool diameter depended on machining time and concentration of the electrolyte used. The tool diameter decreased and its conical angle became larger for higher concentrations of the electrolyte and with increasing machining time as well. The tool length remained constant over a certain period of time depending on concentration of electrolyte and a rapid reduction of tool length was observed after that limiting etching time.

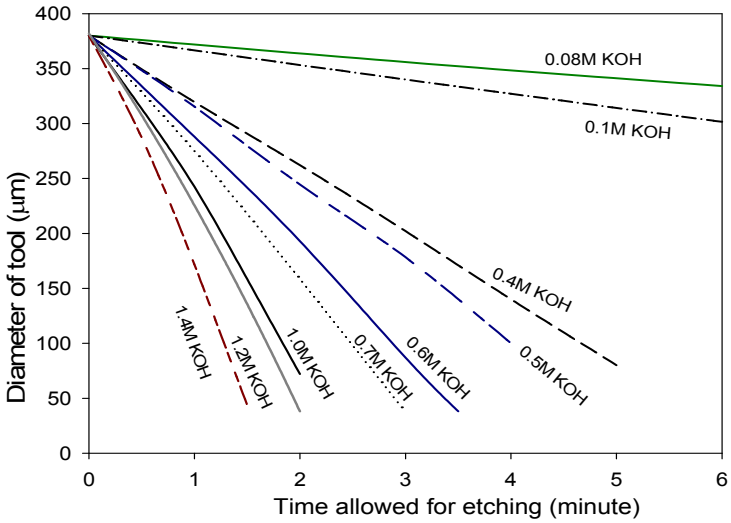

Fig. 4.4 *Variation in microtool diameter with etching time for various electrolyte concentrations and a constant 15 V applied potential.*

4.2.1.3 Etching characteristics according to arrangement of the electrolyte basin

Tool specimens were set into the electrolyte basin in different arrangements such as (i) vertically downward, (ii) vertically upward, and (iii) horizontally at the center of the circular electrode. Tool specimens were also placed at (iv) a position very near to the circular electrode, and (v) the centre of a reduced diameter circular electrode. After the etching of tool specimens, it is found that tool body remains circular for all types of tool arrangements but the arrangement of the electrolyte basin and the diameter of the circular electrode have a significant effect on the conicity of the tool. The tool specimen set in vertically downward direction caused larger taper on the fabricated microtool. A parabolic shape was also evident in between tool body and the shank part as shown in Fig. 4.5. No such parabolic shape existed near the shank part when the tool is set either in vertically upward

direction or horizontally in the electrolyte basin. Sometimes, neck formations were observed in the microtool fabricated using vertically upward setting. There were no change in the fabricated microtool shapes when tool specimens were set at the center of the reduced diameter circular electrodes ($Ø_{CE}$ = 20 mm, 10 mm, 5 mm). The tools fabricated by different arrangements are exhibited in Fig. 4.6.

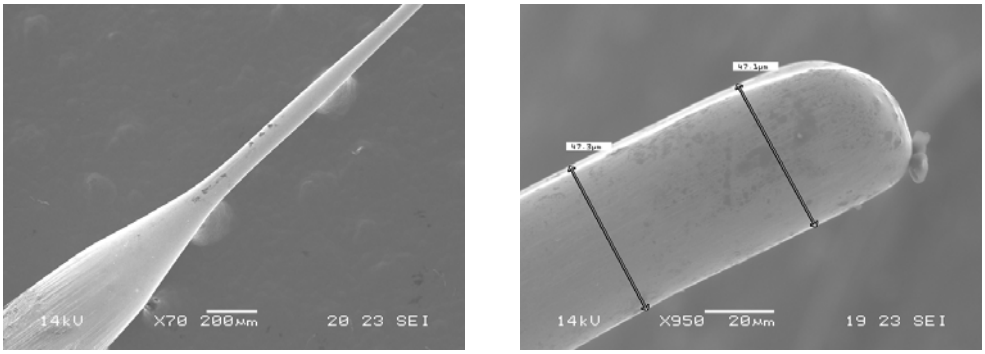

(a) *(b)*

Fig. 4.5 *SEM image of the fabricated microtool: (a) the part remain in air-electrolyte interface (i.e. shank-tool interface), and (b) tool end part.*

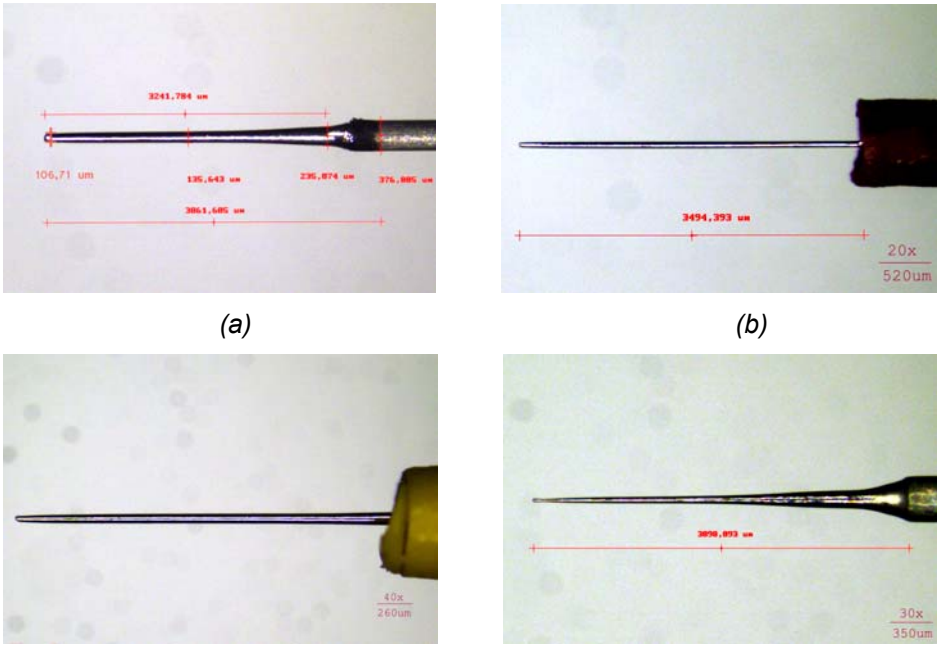

(a) *(b)*

(c) *(d)*

Fig. 4.6 *Microscopic images of the fabricated microtool for the arrangements when the tool specimen set in: (a) vertically downward direction, (b) vertically upward direction, (c) horizontal to the electrolyte basin, and (d) very near to the circular electrode, during microtool fabrication.*

4.2.1.4 Etching characteristics according to pulsed voltages

The pulsed electrical power was applied with a view to control the tool diameter and to observe the condition for bubble formation during the fabrication of microtools. This experiment revealed that the material removal rate and the bubble formation were depended on the applied frequency and its duty cycle. This experimental study showed that a microtool could be fabricated without the formation of hydrogen bubble when the applied frequency and its duty cycle were set in the range of 12 – 13 KHz, and to 30% respectively. A fabricated microtool is illustrated in Fig. 4.7.

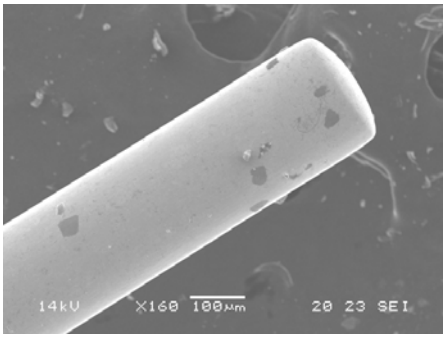

Fig. 4.7 *SEM image of a microtool fabricated by pulsed µECM process.*

4.2.2 Tool Tip Formation

For this experiment, pre-shaped tungsten tools were dipped into an aqueous KOH electrolyte solution by 1 mm and a potential difference of 15 V AC was applied between the electrodes so that the dissolution could occur. Tungsten wire and stainless steel plates were used as circular electrodes. Each of the prefabricated tools was etched to form an angle at the tip submerged into the electrolyte. The tips thus obtained were rinsed in the hot water after etching to remove foreign particles and the formed oxides. The angle of tool tip varied with variation in electrolyte concentration and with the material used as counter electrode during tool tip preparation. Fig. 4.8 shows the variation of tool tip angle with the concentration of electrolytic solutions after complete etching for 15 V AC. During etching, for both tungsten and stainless steel counter electrodes, the tool tip angle increases with the increase in electrolyte concentration. It is possible to fabricate tools with a wider range of tip angles for applied potential of 15 V AC, and the tool tip angles range was 6^0 to 28^0.

Fig. 4.9 shows that etching time to complete dissolution decreases exponentially with increase in electrolyte concentration for both tungsten and stainless steel circular electrodes. Etching time to complete dissolution reduces very rapidly for KOH solutions with concentration up to 0.5 M. After that concentration, further increase in electrolyte concentration results in gradual decrease in etching time to complete dissolution. It is, therefore, evident that electrolytic concentration has individual and substantial effects on the dissolution of tool material determining the

microtool tip angle. As shown in Figs 4.8 and 4.9, the material of the circular tool electrodes has a significant effect on the conicity of the fabricated microtool tip. Tip angle of the microtool fabricated using stainless steel circular electrode larger than that of the fabricated tool using a tungsten wire electrode. The etching time to complete dissolution is also found longer for stainless steel than for the tungsten circular electrode. The conical shaped microtools fabricated by μECM process are exhibited in Fig. 4.10. A comparative study on the effects of applied potentials and electrolyte concentrations are also given in Appendix B. From the illustrated results, it is apparent that the higher the applied potential the larger the tool tip angle for a particular electrolyte concentration.

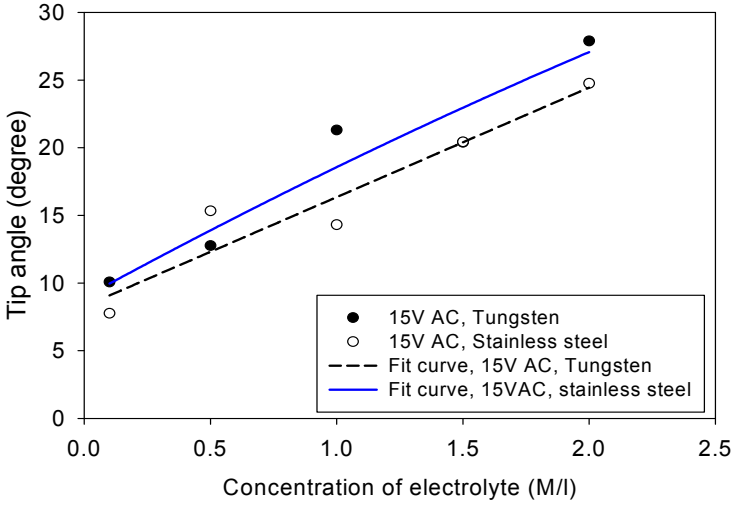

Fig. 4.8 *Effect of electrolyte concentration on fabricated microtool tip angle.*

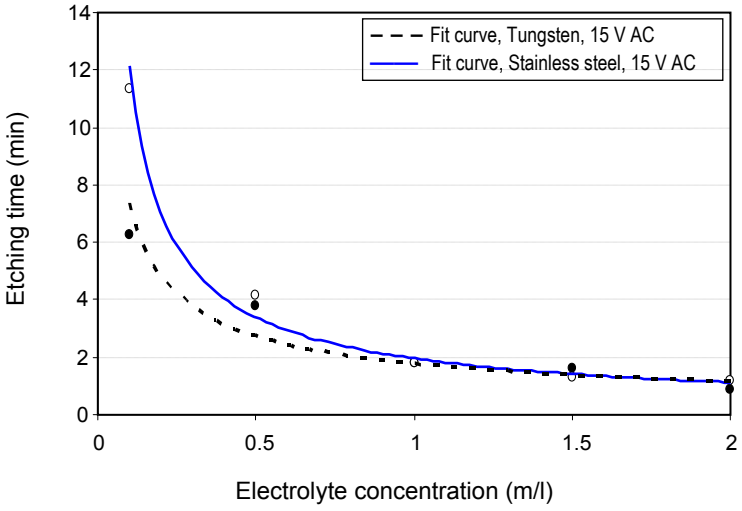

Fig. 4.9 *Effect of electrolyte concentration on etching time in the formation of microtool tip angle.*

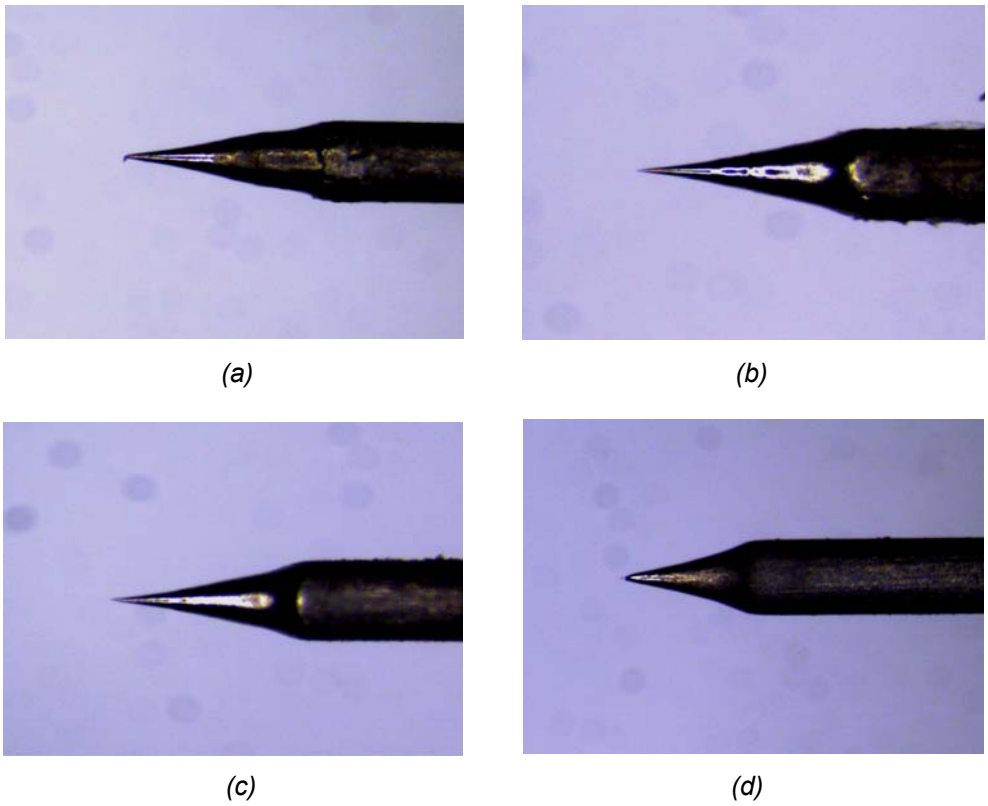

Fig. 4.10 *Microscopic image of fabricated microtool tips for (a) 0.6 M KOH, (b) 0.72 M KOH, (c) 1.0 M KOH, and (d) 1.4 M KOH electrolytes.*

4.3 PARAMETRIC EFFECT

This section describes the effect of some important parameters such as the peak-to-peak voltage and the baseline potential, applied frequency and its duty cycle, the electrolyte temperature, and the microtool dimensions on the μECM process. During machining, the machining time and the frequencies of short circuits are counted, and MRR is calculated from the microholes dimension.

4.3.1 Effect of Peak-to-peak Voltage

Experiments were conducted with pulse amplitude in range of 4.6 –17.2 V and pulse duration time of 1 μs. In spite of the transpassive dissolution region, electrochemical dissolution did not occurred under 4.0 V. The experiment was, therefore, started from above 4.6 V. Three different values of peak-to-peak voltage (V_{pp}) were employed to drill on the nickel plate. Fig. 4.11 shows the influence of peak-to-peak voltage on the faradaic effect, machining time, actual material removal rate (MRR_{act}) and side gap ratio. With increasing applied potential, both the amount of faradaic current and the MRR increased, whereas the machining

time and the side gap ratio expectedly decreased. When the applied potential was low (V_{pp} = 4.6V), the number of short circuit was found to be very high (15 times) at a moderate feed rate of 0.05 μm/s and total time required for making a single hole was around 80 minutes which was not feasible in practice. However, when the applied potential was made double, it was possible to increase the feed rate three times leading to reduction of the total machining time by more than 60% and a few short circuits. Though reduction in total machining time was insignificant, no short circuit was observed for the same feed when the applied was increased to 17.2 V. Also, the waveform shown in Fig. 5.18 demonstrate that the amount of faradaic current was very low for lower applied potentials and reached to a considerable range for higher applied potentials. Therefore, the increase in the applied voltage, and the peak-to-peak voltage increased the machining rate calculated from the microhole dimensions. The entrance and exit diameter of the fabricated microholes are shown in Fig. 4.12.

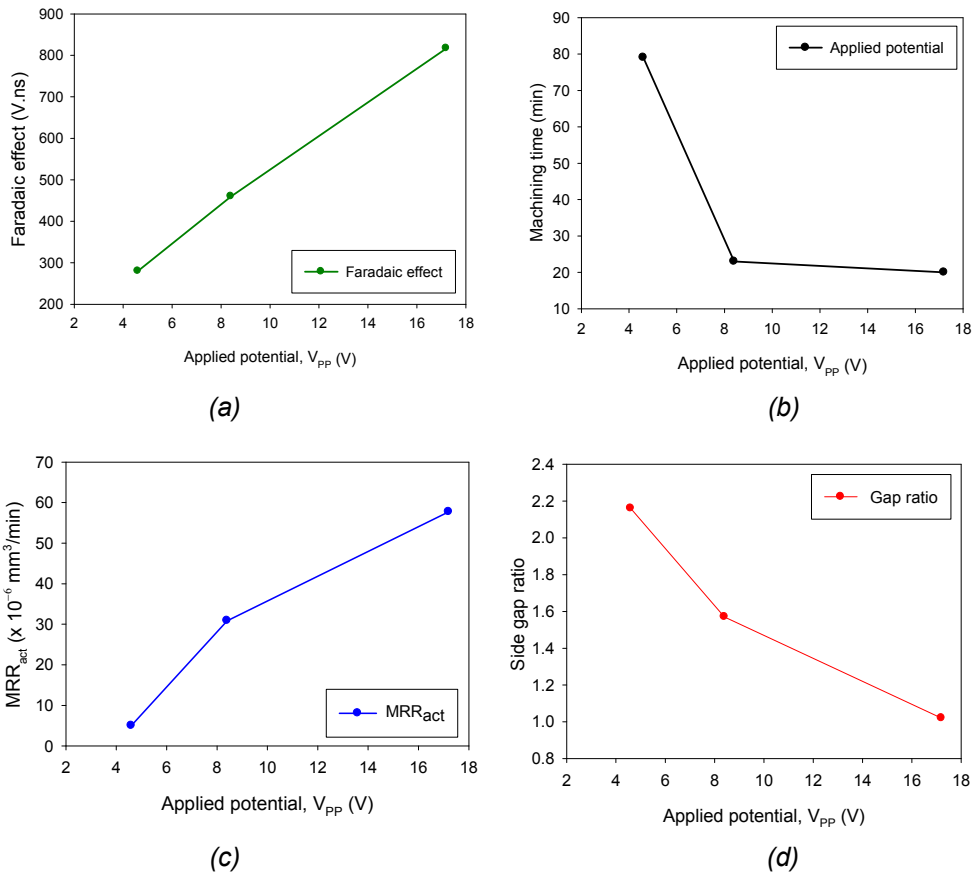

Fig. 4.11 *Effect of peak-to-peak voltage on (a) the amount of faradaic effect, (b) machining time, (c) actual material removal rate (MRR_{act}), and (d) the side gap ratio of the fabricated microhole for f = 1 MHz, pulse time, τ = 1.0 μs, duty cycle, δ_τ= 30%, 0.2 M HCl electrolytes.*

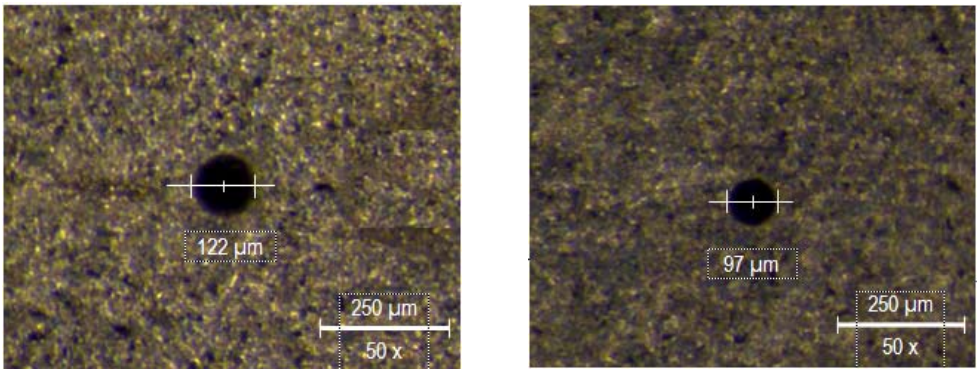

(a) *(b)*

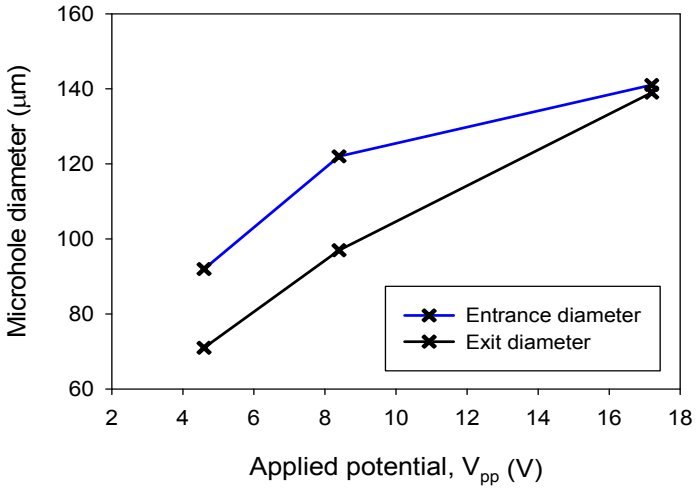

(c)

Fig. 4.12 *Microscopic image of (a) entrance and (b) exit of the same microhole for applied voltage of 8.4 V, and (c) variation in microhole diameter for different applied voltages for the same machining conditions.*

Tool electrode baseline potential also plays an important role in the determination of microhole diameter. From Fig. 4.13, it is observed that the MRR decreases with the increase in the baseline potential during µECM. When the baseline potential was in the range of −1.5 to −2.0 V, machining rate was quite high.

Machining was possible for the baseline potential up to −2.5 V. However, after this limit, the amount of faradaic current decreased rapidly and the resulting MRR was very low. Moreover, dissolved metal was deposited on the work zone. Therefore, the baseline potential in the range of −1.5 to −2.0 V is recommended as a working range for µECM. The entrance and exit diameter of the fabricated microholes are shown in Fig. 4.14.

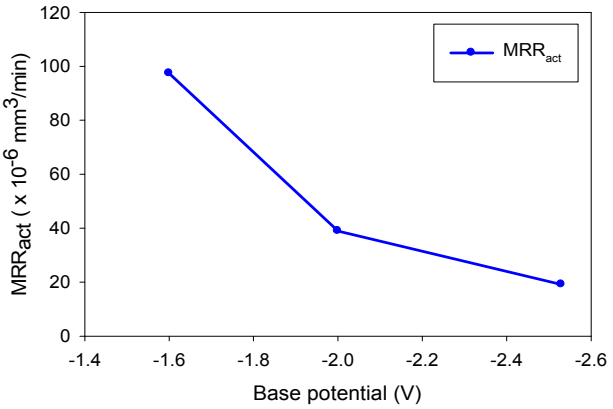

Fig. 4.13 *Effect of baseline potential on MRR during μECM on nickel plate.*

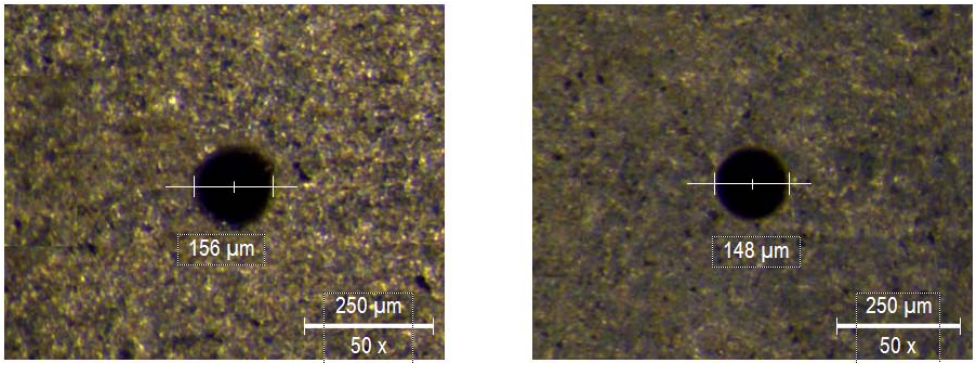

(a) *(b)*

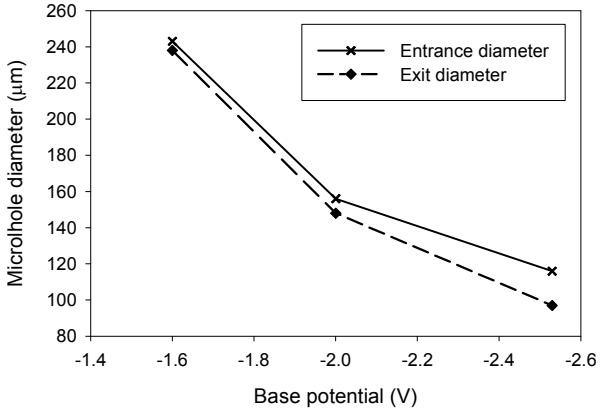

(c)

Fig. 4.14 *Microscopic image of (a) entrance and (b) exit of the same microhole for baseline potential of −2.0 V, and (c) variation in microhole diameter for different baseline potential for other parameters kept fixed.*

4.3.2 Effect of Applied Frequency

A 52 μm mean diameter tool of length 3700 μm has been positioned above the workpiece in a vertical etch position, and allowed to machine on nickel plate. During this experiment, only the applied frequencies were varied while other parameters were kept constant. Fig. 4.15 exhibits the influence of applied frequency on actual material removal rate (MRR_{act}), machining time and the number of short circuits occurred during microdrilling processes. From Figs. 4.15(*a*)–(*b*), it is evident that MRR_{act} decreases and the machining time increases with an increase in electrical frequency where the pulse on/off ratio of 1: 2.3. This is can be attributed to decrease in MRR_{act} with the increase in applied frequency.

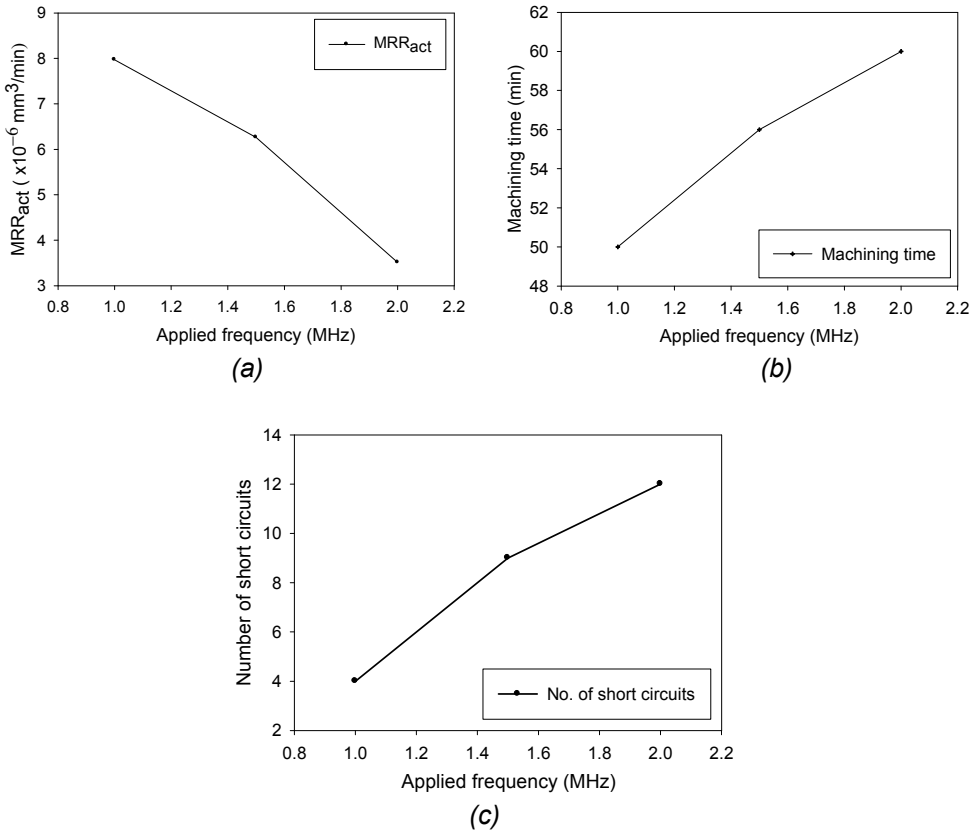

Fig. 4.15 *Effect of applied frequency on (a) MRR_{act}, (b) machining time and (c) number of short circuits occurred during microdrilling on nickel plate.*

It is also observed that the number of short circuits increases with the applied frequency. With the increasing frequency, the tool electrode fails to maintain a constant gap during machining for the same feed rate and results in increased number of short circuits. On the other hand, when high frequency is applied, entrance and exit diameters are found to be smaller. This is due to the less amount

of side erosion that occurs during machining resulting in reduction of entrance and exit of hole diameter. The entrance and exit of fabricated microholes, and the corresponding side erosions for different applied frequencies are shown in Fig. 4.16.

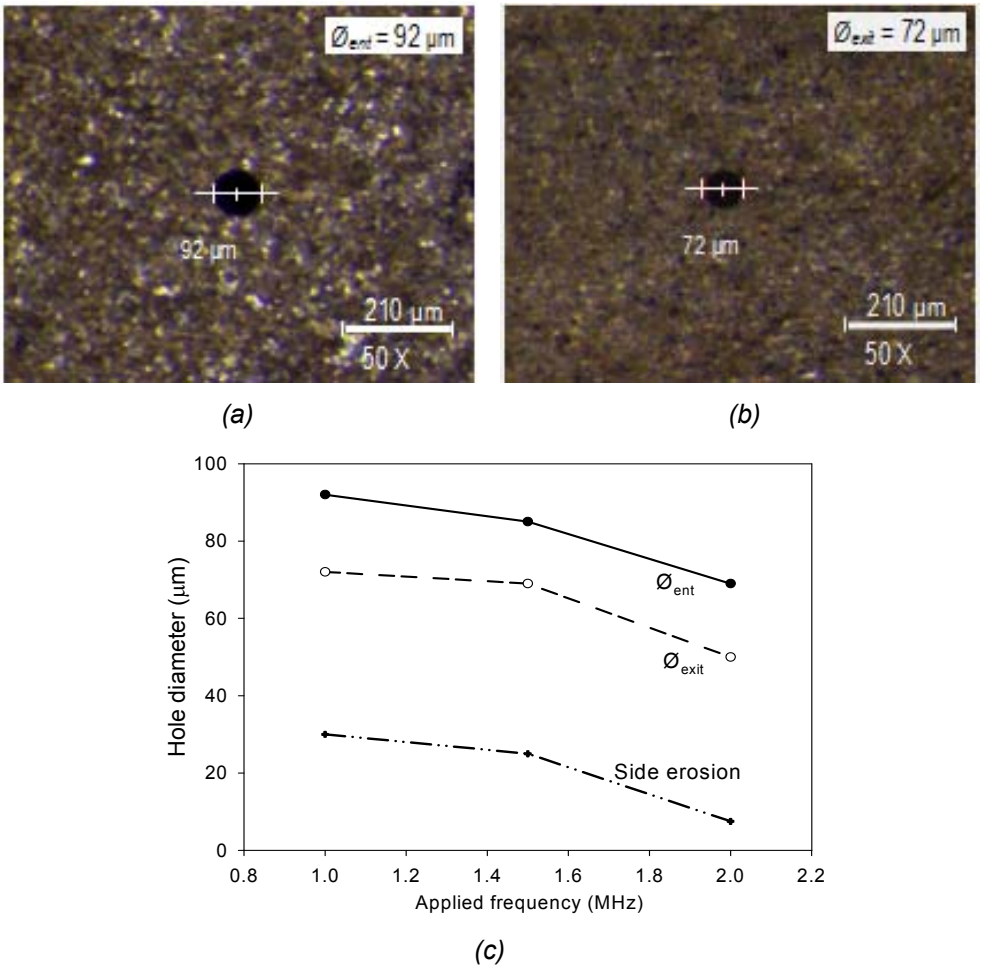

Fig. 4.16 *Microscopic image of (a) entrance and (b) exit of the same microhole, and (c) variation in side erosions for different frequencies.*

Again, a microtool with 76 µm in diameter and 690 µm in length was selected and then machining was carried out keeping all other parameters fixed. Fig. 4.17 exhibits the influence of frequency on actual material removal rate (MRR_{act}) and machining time in microdrilling processes. From the figures, it is clear that MRR_{act} and the machining time also respectively decreases and increases with an increase in applied frequency. However, it is also observed that for the same range of pulse-on time, actual MRR is found to be much higher for the lower applied frequency for a short tool.

Again, from Fig. 4.17(*c*), it is found that no short circuit occurs for applied frequency of 0.5 MHz even at a very high feed rate ranging from 0.2–0.8 μm/s. This is because of MRR increases rapidly with decreasing applied frequency or a high pulse-on time, as shown in Fig. 4.17(*a*). Moreover, gradual decrease and increase in actual MRR and machining time respectively are observed with increase in frequency ranging from 2 MHz to 8 MHz. Though hole diameter can be controlled precisely for frequency of 8 MHz, requirement for higher machining time and frequent occurrence of short circuits at this applied frequency make it inappropriate for micromachining. The microholes fabricated on the nickel plate are found almost straight up to a certain limit of applied frequency of 1.0 MHz and after that limit, conicity of the hole increases with the increase applied frequency, as illustrated in Fig. 4.18.

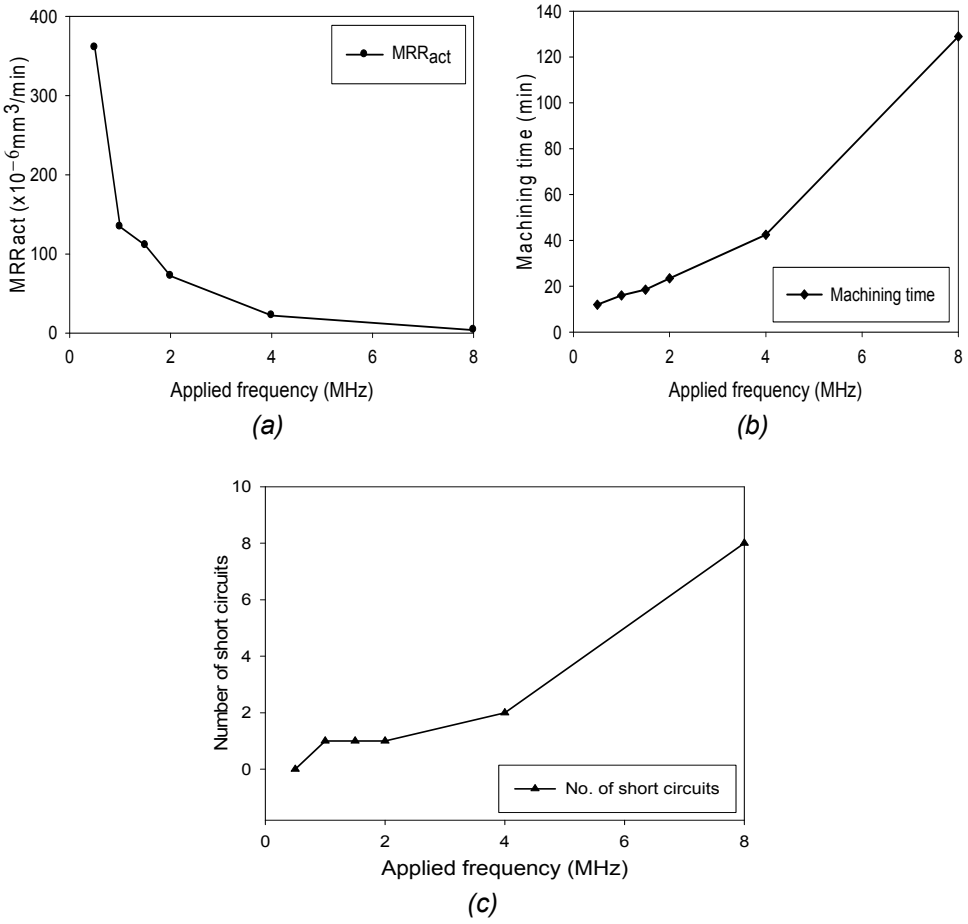

Fig. 4.17 *Effect of applied frequency on (a) material removal rate (MRR_{act}), (b) machining time, and (c) number of short circuits for short microtool.*

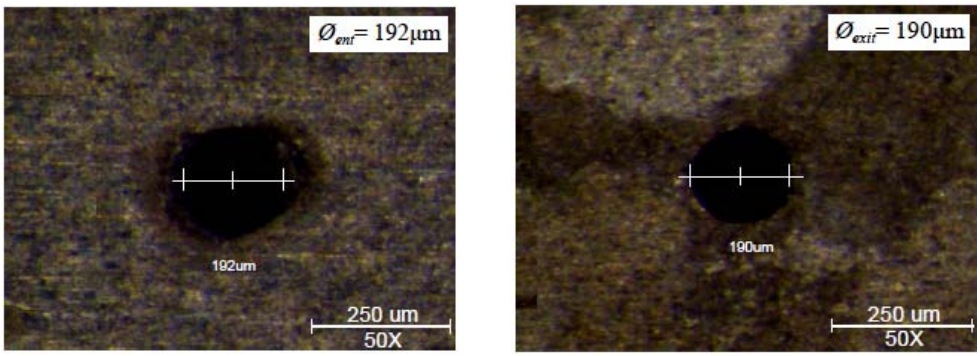

(a) (b)

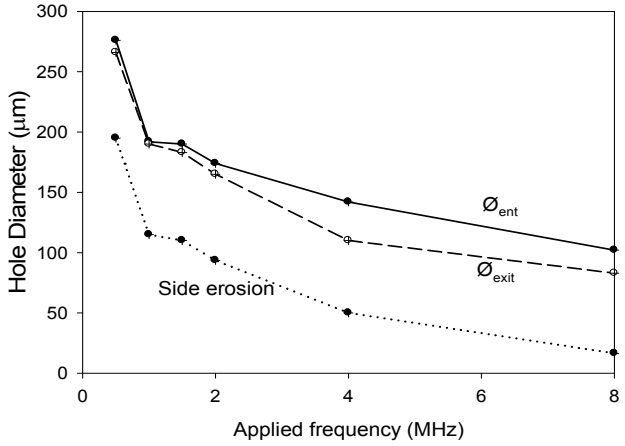

(c)

Fig. 4.18 *Microscopic image of (a) entrance, and (b) exit diameter of the hole fabricated at 1MHz, and (c) entrance and exit diameters of microholes and side erosions for various applied frequencies.*

4.3.4 Effect of Duty Cycle

Together the on-time (τ_{on}) and off-time (τ_{off}) pulses comprise a single cycle, and duty cycle is the ratio of pulse-on time and total cycle time. As the frequency determines the pulse period, this section describes the effect of duty cycle with applied frequency during microdrilling on nickel plate. The prefabricated short microtool (L= 690 µm) was employed for this study and the machining carried out keeping the other parameters fixed. Fig. 4.19 exhibit the influence of duty cycle on actual material removal rate (MRR_{act}), machining time, frequencies of short circuit occurrences and amount of faradaic effect (V_{top} *x* (τ_{on} –*t**)) during microdrilling processes. From these figures, it is found that MRR_{act} and the machining time respectively increases and decreases with an increase in duty cycle. However, for the same applied frequency, MRR_{act} is found to be much higher for high percentage of pulse-on time.

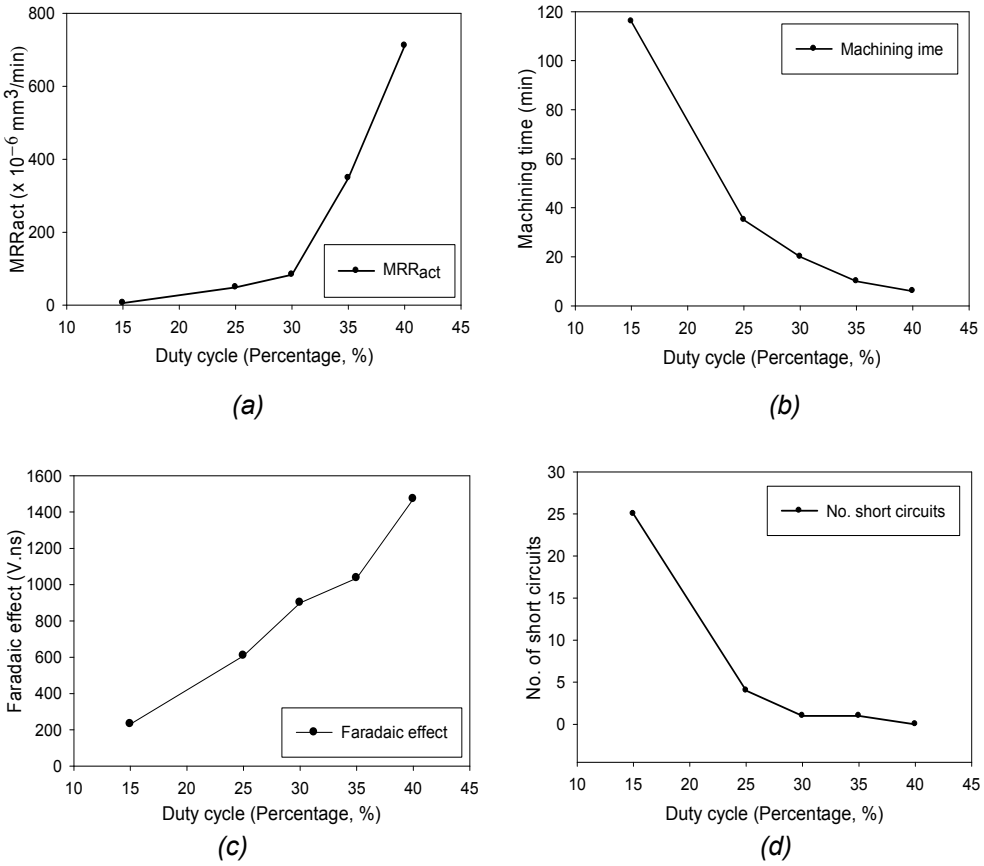

Fig. 4.19 *Effect of duty cycle on (a) MRR_{act}, (b) machining time, (c) the amount of faradaic effect generated, and (d) number of short circuits occurred during machining for the short microtool.*

From Figs. 4.19(c)–(d), it is found that no short circuit occurs for higher duty cycles even for a high feed rate ranging from 0.3 to 0.4μm/s. This is due to rapid increase in material removal rate with increasing duty cycles for the same applied frequency of 1.0MHz. Consequently, as shown in Fig. 4.19(b) rapid decrease in machining time are observed with increase in duty cycle. Thus the diameter of the hole cannot be controlled precisely for higher duty cycles as the side erosion rapidly increases for the higher duty cycles and their corresponding machining times are very low compared to the lowest duty cycle applied in this study. Figs. 4.20(a)–(c), illustrating the diameters of the holes fabricated on the nickel plate for numerous applied duty cycles, it is found that the microhole diameter is small for lower duty cycles applied and gradually increases with an increase in duty cycle. This can be attributed to the lower and higher side erosions for lower and higher applied duty cycles, respectively.

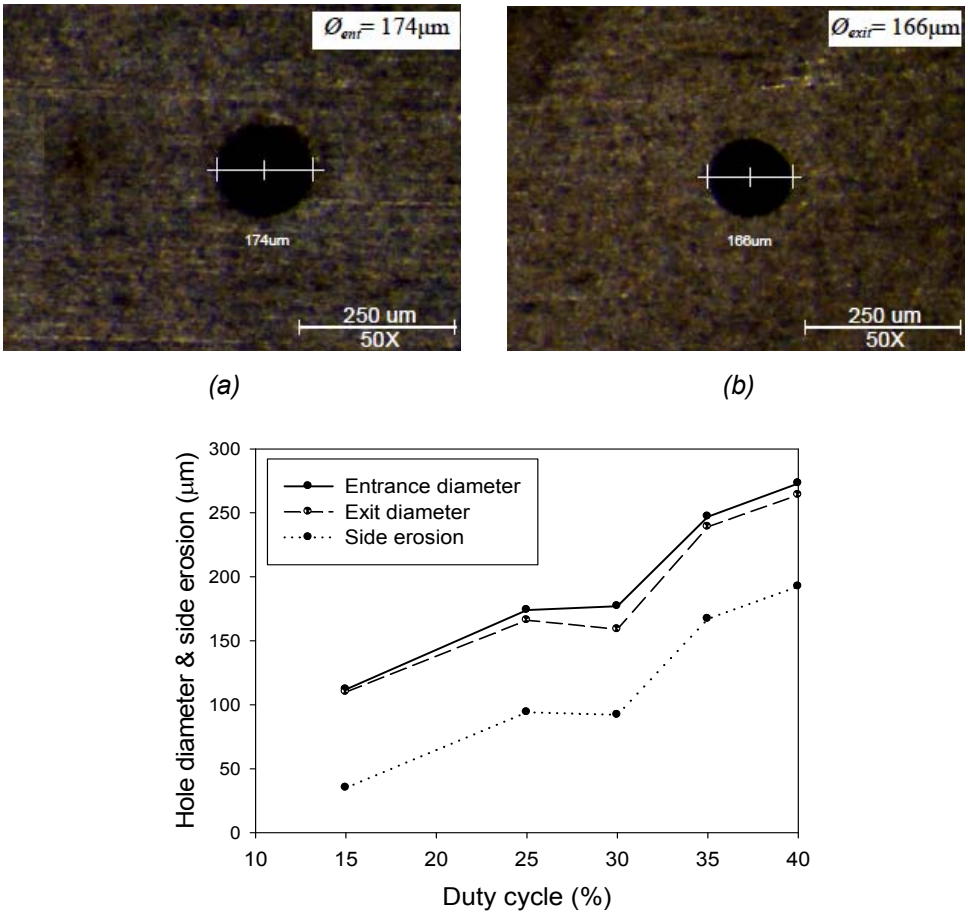

Fig. 4.20 *Microscopic image of (a) entrance, and (b) exit diameter of the hole fabricated for a duty cycle of 25%, 1 MHz applied frequency, and (c) entrance and exit diameters of microholes and side erosions for various applied frequencies.*

4.3.5 Effect of Electrolyte Temperature

A cylindrical microtool of 43 µm in diameter near to the tip, 53 µm mean diameter, and 861 µm in length was selected. During machining, only the electrolyte temperature was varied keeping all other parameters constant. Table 4.1 shows the influence of electrolyte temperature on MRR_{act}, machining time and the taper angle formed on the fabricated micro-holes during microdrilling on nickel plate. Similarly Fig. 4.21(*a*)–(*d*) relates electrolyte temperature with MRR_{act}, machining time, hole taper angle, and side gap ratio respectively. From the figures, it is evident that the MRR_{act} and machining time respectively increases and decreases with an increase in the electrolyte temperature. It is also observed that both the

side gap ratio and the taper angle increase with the electrolyte temperature. However, for the same parameters, both the entrance and the exit diameters of the fabricated microholes decrease with the electrolyte temperature, as illustrated in Fig. 4.22.

Table 4.1 Results showing effects of electrolyte temperature on μECM.

Electrolyte temperature	Machining time (min)	Tool feed (μm/s)	MRR (mm^3/min)	Taper angle (degree)	Hole diameter (μm)		Gap ratio†
					$Ø_{ent}$	$Ø_{exit}$	g_{ent}/g_{exit}
14^0C	20	0.1– 0.2	85.18×10^{-6}	12	178	162	1.13
28^0C	14	0.25– 0.4	103.1×10^{-6}	9.8	163	150	1.12
56^0C	7	0.5	142.4×10^{-6}	13.5	139	121	1.23

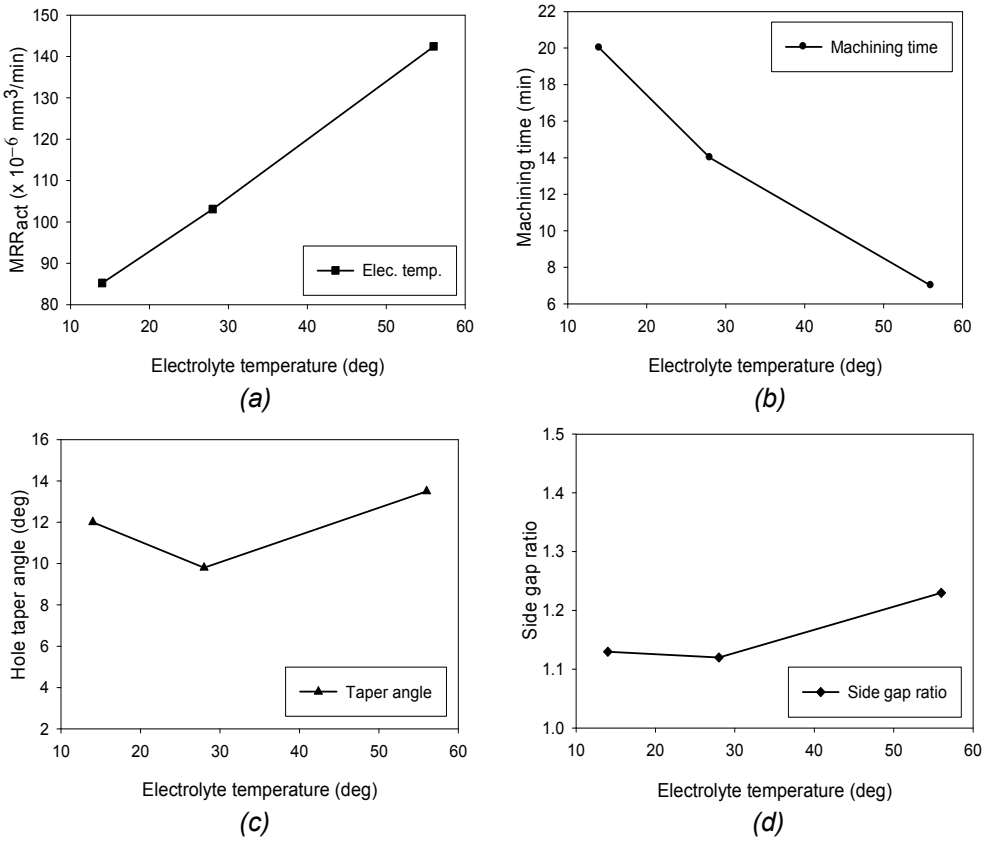

Fig. 4.21 *Effects of electrolyte temperature on (a) MRR_{act}, and (b) machining time, (c) microhole taper angle, and (d) side gap ratio of the fabricated microholes.*

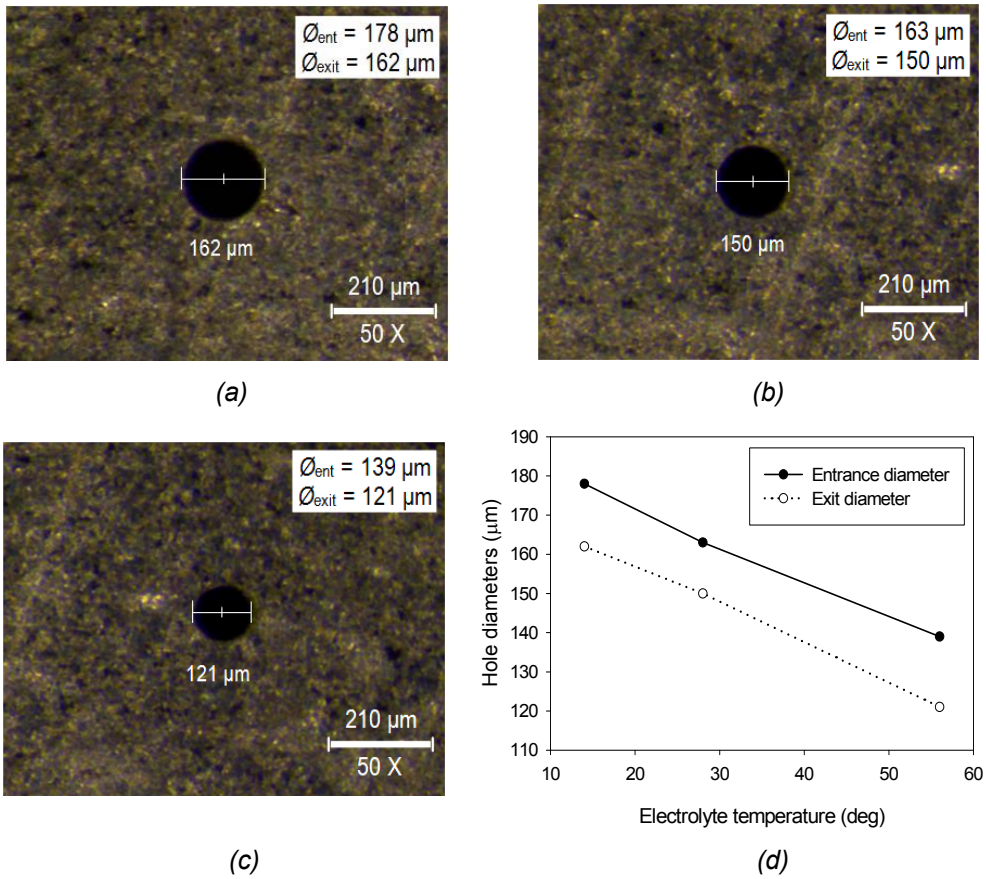

Fig. 4.22 *Microscopic image of fabricated microholes for electrolyte temperature of (a) 14^0C, (b) 28^0C, (c) 56^0C, and (d) entrance and exit diameters of fabricated microholes for electrolyte temperature variation.*

4.3.6 Effect of the Microtool Dimensions

This experimental scheme is mainly focused on the observations related to the effects of microtools' dimension in µECM process for pulsed applied voltages on the size and shape of the fabricated microholes, machining time, and actual material removal rate (MRR_{act}) for various types of microtools, i.e. (*a*) the effect of microtool diameter on MRR_{act}, machining time and the hole shape fabricated, (*b*) the effect of the microtool length (total tool length and effective tool length) on MRR_{act}, machining time and the hole shape, and (*c*) the effect conical shaped tool. Three microtools were fabricated and used for each set of experiment. Microtools of length 1369 µm and diameter of 21 µm, 41µm and 74 µm were employed to investigate the effect of tool size (diameter). Similarly, microtools of different lengths (*L*= 598 µm, 1369 µm, and 3725 µm) with approximately the same mean diameter were used to examine the effect of tool length, and a single microtool of length 3725 µm was used to explore the effect of dipping length. Two different sets of conical microtools were employed for exploring the effect of conical microtools.

4.3.6.1 Effect of the microtool diameter

Three cylindrical tungsten microtools of different diameters with approximately same length were employed. Table 4.2 shows the influence of tool shape on actual material removal rate (MRR_{act}), machining time and the taper angle formed inside the fabricated micro-holes during microdrilling. Similarly Fig. 4.23(a)–(d) relates tool shape with the described factors respectively. It is evident that the MRR_{act} and machining time increase with an increase in the diameter of microtools used for microdrilling at a particular combination of machining parameters.

The frequent occurrence of short circuit for higher diameter/size also increases the machining time. Side erosion is also considered as one of the performance factors, as it is found to be related with the machining time. Fig. 4.23(d) shows the relationship between tool diameter and side erosion. Again, from Table 4.2, the ratio of entrance gap to exit gap decreases as machining time increases. As a result, the taper angle of the fabricated microholes decreases with microtool diameter. The change in the entrance and exit diameter of the fabricated microhole is shown in Fig. 4.24.

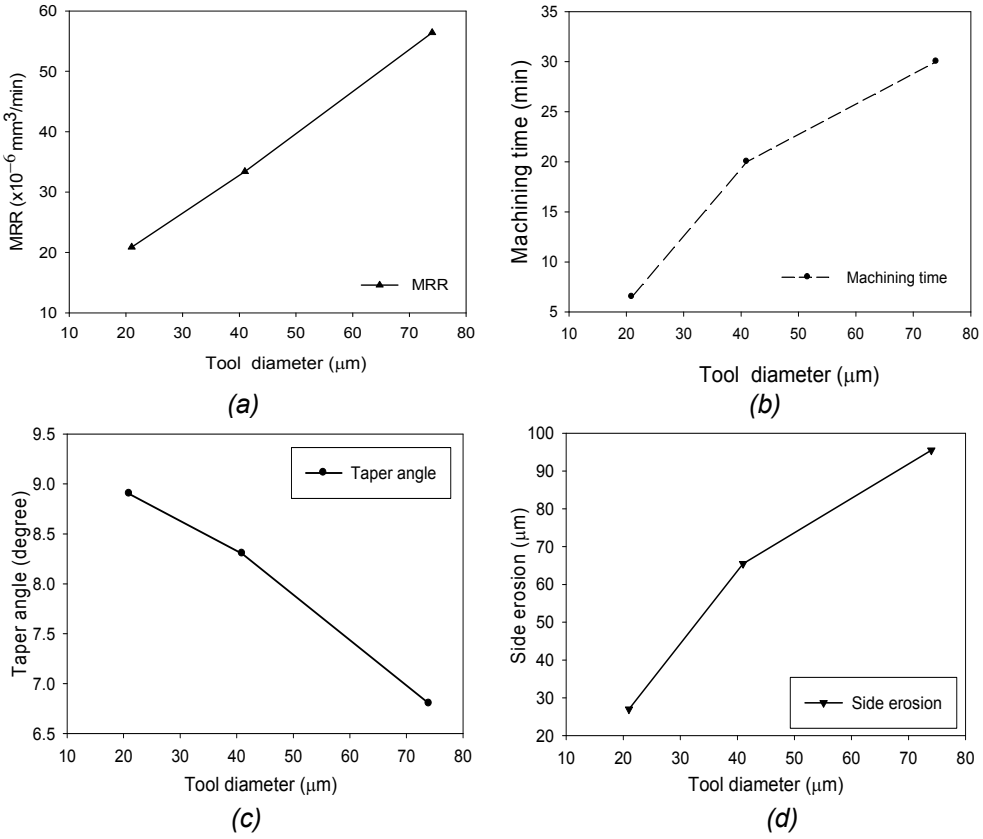

Fig. 4.23 *Effects of tool diameter on (a) MRR_{act}, (b) machining time, (c) taper angle, and (d) side erosion.*

Table 4.2 Results showing effects of tool diameter on μECM.

Tool shape and size (μm)	Machining Time (min)	Tool feed (μm/s)	Taper angle (degree)	MRR (mm^3/min)	Hole diameter (μm)		Gap ratio† g_{ent}/g_{exit}
					$Ø_{ent}$	$Ø_{exit}$	
Cylindrical $Ø_{tool}$ = 21	6.5	0.3	8.9	20.9×10^{-6}	54	42	1.57
Cylindrical $Ø_{tool}$ = 41	20	0.1– 0.15	8.3	33.4×10^{-6}	112	101	1.18
Cylindrical $Ø_{tool}$ = 74	30	0.1	6.8	56.4×10^{-6}	174	165	1.10

† g_{ent} = machining gap at entrance of the hole, g_{exit} = machining gap at the exit of the hole

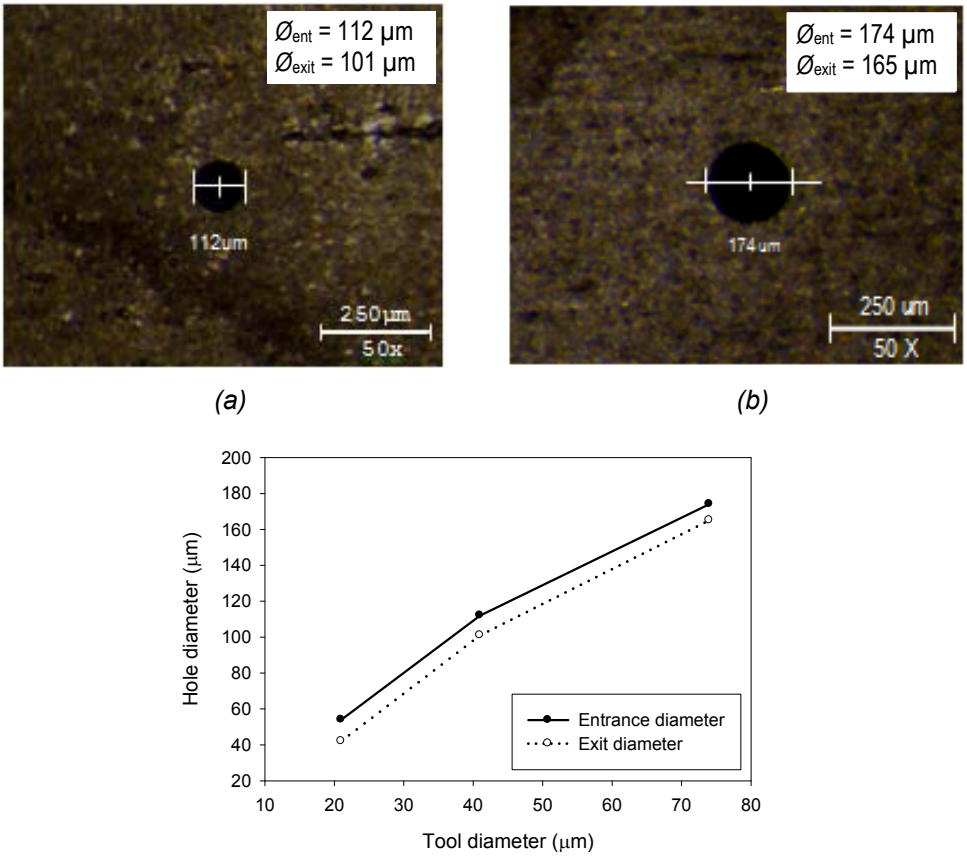

Fig. 4.24 *Microscopic image of fabricated microholes for a microtool diameter of (a) 41μm, (b) 74 μm, and (c) entrance and exit diameters of microholes.*

4.3.6.2 Effect of the overall tool length

Three microtools of different lengths with approximately the same mean diameter were employed and classified into three groups: short tool, medium tool and long tool are smaller than 1000 µm (i.e. $L \leq 1000$ µm), medium length $1000 < L \leq 3000$ µm, and long ($3000 \text{ µm} < L$) respectively. Table 4.3 and Fig. 4.25 show the effects of overall tool length on MRR, machining time and taper formation of micro-holes. From these table and figure, it is evident that the MRR_{act} and machining time respectively decreases and increases with the increase in tool length. Number of short circuits is also found to increase with the increase in microtool length. Moreover, the entrance and exit diameters are found larger for shorter tool length, i.e. overcut is higher for shorter tools. The effects of overall tool length on microhole formation during microdrilling are graphically shown in Fig. 4.26.

Table 4.3 Results showing effects of overall tool length on µECM.

Tool size (µm)	Tool feed (µm/s)	Number of short circuits	Taper angle (degree)	MRR (mm^3/min)	Hole diameter (µm)		Gap ratio g_i/g_0
					$Ø_{ent}$	$Ø_{exit}$	
Short [L<1 mm] 598	0.1 – 0.2	0	13.5	97.9×10^{-6}	177	159	1.15
Medium [1 < L <3 mm] 1369	0.1– 0.15	1	8.3	33.4×10^{-6}	112	101	1.18
Long [L > 3mm] 3725	0.05 – 0.1	4	14.0	7.97×10^{-6}	92	72	1.64

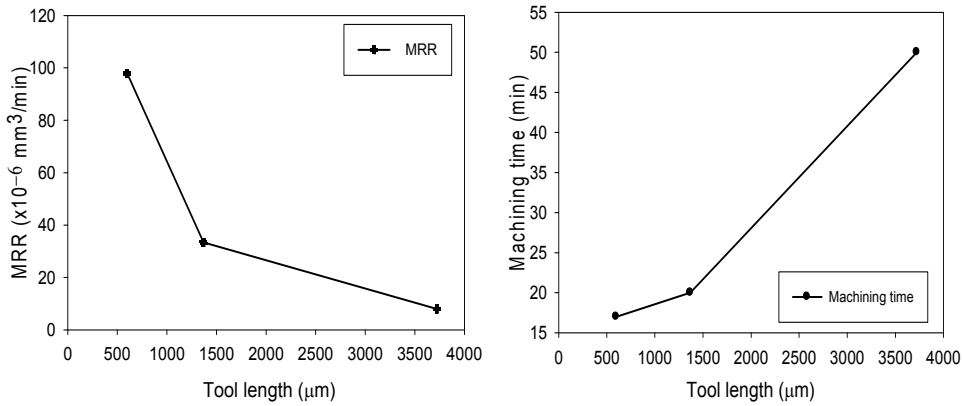

(a) *(b)*

Fig. 4.25 Effects of overall tool length on (a) MRR_{act}, and (b) machining time.

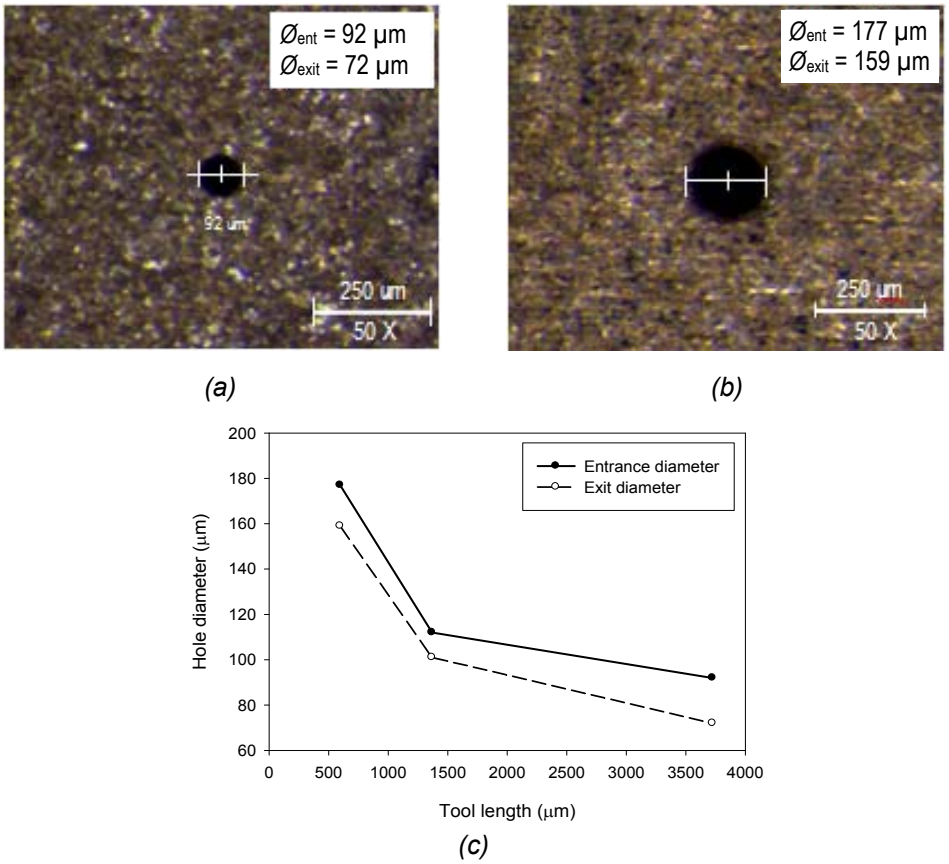

Fig. 4.26 *Microscopic image of fabricated microholes for a microtool of (a) long microtool, (b) short microtool, and (c) entrance and exit diameters of fabricated microholes.*

4.3.6.3 Effect of the tool dipping length into electrolyte

The selected long microtool was positioned vertically into different electrolyte level, i.e. tool was dipped vertically at different depth into acidic electrolyte. Table 4.4 and Fig. 4.27 exhibit the influence of effective tool length, the dipping length taking part effectively in micromachining, on actual material removal rate, machining time and number of short circuits during microholes fabrication. From the aforestated table and figure, it is evident that MRR_{act} decreases and the machining time increases with an increase in tool dipping length for a particular combination of micromachining parameters. The fully dipped tool needs longer machining time to make a smaller diameter hole and also causes maximum number of short circuits even at lower feed rates.

On the contrary, a short dipping length results higher side erosion, higher material removal, less precision on microhole, but makes the process faster than a long effective tool length. The diameters of microholes produced for different effective

tool lengths are shown in Fig. 4.28. A short dipping length of tool produces a precise hole with low conicity along with faster machining but the greater side erosion.

Table 4.4 Results showing effects of tool dipping length (effective length).

Tool size (μm)	Tool feed (μm/s)	Number of short circuits	Taper angle (degree)	MRR (mm3/min)	Hole diameter (μm)	
					$Ø_{ent}$	$Ø_{exit}$
Short dipped L_3 = 650	0.2	0	0.8	185.83×10^{-6}	169	168
Medium dipped L_2 = 1600	0.1– 0.2	1	12.5	52.56×10^{-6}	142	125
Fully dipped L_1 =3725	0.05	14	6.0	9.37×10^{-6}	108	100

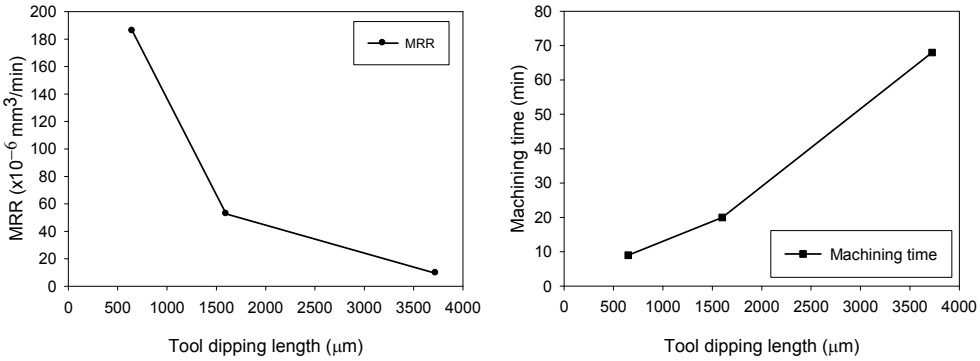

Fig. 4.27 *Effects of effective tool length on (a) MRR_{act}, and (b) machining time.*

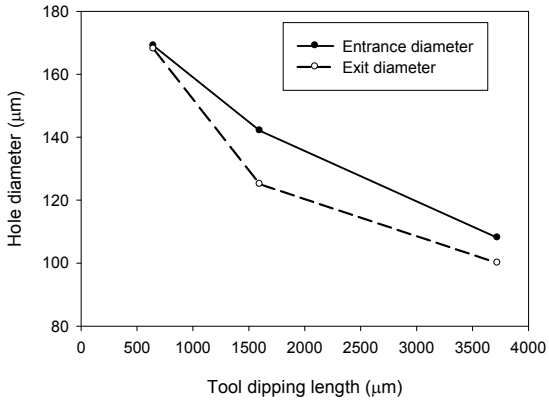

Fig. 4.28 *Entrance and exit diameters of fabricated microholes.*

4.3.6.4 Effect of Conical Shaped Tool

Two different sets of microtools such as (i) one cylindrical and one conical shaped tool, and (ii) both conical but different sized and tip angles, are fabricated for this experiment.

Two different shaped microtools, cylindrical and conical, with approximately the same length and mean diameter are employed. The effects on the MRR, machining time, number of short circuits are tabulated in Table 4.5. From the table, it is found that the material removal rate and the number of short circuits are approximately same for both cylindrical shape tool and conical shaped tool. But a conical shaped tool fabricated a microhole in a less machining time than a cylindrical tool. The microholes fabricated by a conical shaped microtool are illustrated in Fig. 4. 29.

Table 4.5 Results showing effects of tool shape (Cylindrical or conical).

Tool size (µm)	Tool feed (µm/s)	Number of short circuits	Machining time (min)	MRR (mm3/min)	Hole diameter (µm)	
					$Ø_{ent}$	$Ø_{exit}$
Cylindrical	0.05 – 0.1	5	50	7.96×10^{-6}	92	72
Conical	0.1	4	33	8.05×10^{-6}	78 71	66 53

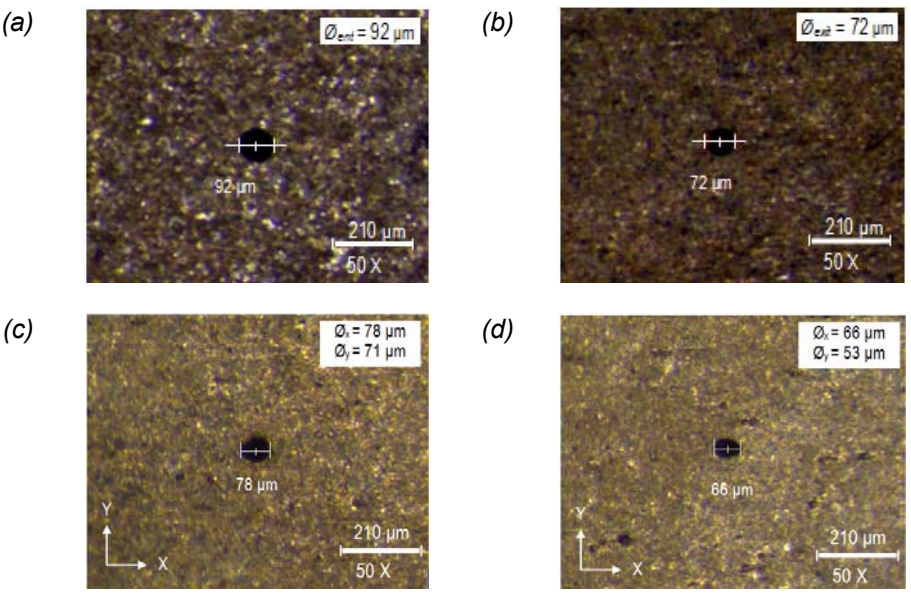

Fig. 4.29 *Microscopic image of microholes for (a) entrance, (b) exit of cylindrical tool, (c) entrance, (d) exit diameter of conical shaped tools.*

Again, Table 4.6 and Fig. 4.30 illustrate three different conical micro-holes with different diameters. First microtool was fed into the nickel plate by 200 µm from its surface. The tool tip came out of the workpiece making a conical shaped hole in it. The entrance and exit microhole diameters were found to be 212 µm and 175 µm respectively making the hole with an angle of 26^0 for the tool with the tip angle of 19^0. Second tool was fed by 120 µm at two feed rates 0.1– 0.3 and 0.5 µm, for the microtool tip angle of 18^0. The fabricated hole was found to be 31^0 and 18^0 for lower and higher feed rates respectively.

Table 4.6 Results showing effect of different conical microtools on µECM.

Tool shape	Machining Time (min)	Tool feed (µm/s)	Taper angle (degree)	MRR (mm^3/min)	Hole diameter (µm)	
					$Ø_{ent}$	$Ø_{exit}$
$A_1 = 19^0$ L_1= 478 µm $Ø_{tool}$= 170 µm	27	0.1– 0.2	26	81.94×10^{-6}	212	175
$A_2 = 18^0$ L_2= 346 µm $Ø_{tool}$= 110 µm	11.8	0.1– 0.3	31	17.92×10^{-6}	81.6	35.3
	5.2	0.5	18	10.38×10^{-6}	41.6	17.3

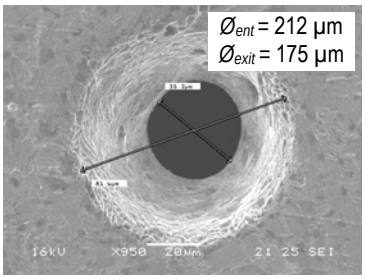

(a) feed rate 0.1–0.2µm/s, machining time 27 min

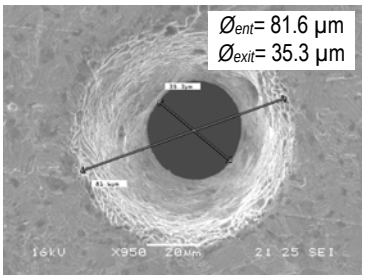

(b) feed rate 0.1–0.3µm/s, machining time 12 min.

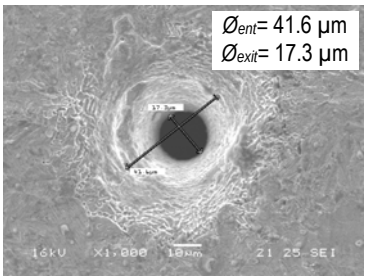

(c) feed rate 0.5µm/s, machining time 5.2 min

Fig. 4.30 *SEM images of microholes for (a) tip angle 19^0, and feed 0.1–0.2 µm/s, (b)and (c) tip angle of 18^0, and feed 0.1–0.3µm/s, 0.5µm/s, respectively.*

4.4 MICROMACHINING USING FABRICATED MICROTOOLS

4.4.1 Machining on Nickel Plate

The prefabricated microtools were used for machining on the nickel plate. Cylindrical and conical, both types of microtools were tested for micromachining, as well as microdrilling and microcutting. The nickel workpiece was placed into 0.2 M HCl acid electrolyte basin, the prefabricated microtool that was fixed with the tool-holder was fed along the Z-axis for micro drilling, and X & Y-axes for positioning of workpiece that is placed into fixture. During microcutting, the tool was fed along Z axis, and the workpiece was moved along X or Y axis according to the path of travel.

4.4.1.1 Microdrilling

4.4.1.1.1 Microdrilling a single-hole

The machining parameters given in Table 3.7 were applied for microdrilling in nickel plate. During single-hole drilling, machining was done on two different places very near to each other, to view the effect of tool geometry and feed rates. In general, μECM induces side erosion resulting in micro-holes with diameters larger than the tool electrode. Fig. 4.31 illustrates two different micro-holes, where one is blind hole and another is through hole. Fig. 4.31(a) illustrates a blind hole, the entrance and exit hole diameters were measured. Again, Fig. 4.31 (b) illustrates a tapered micro-hole with different diameters. The entrance and exit hole diameters were about 201 μm and 151 μm respectively, so the fabricated hole angle was about 33^0 coming from a tool with a tip angle of nearly 19.5^0. The angle of the tapered hole was greater than the tip angle of the microtool used as theory foresees. The tool feed was kept constant at 0.3μm/s for the whole machining process.

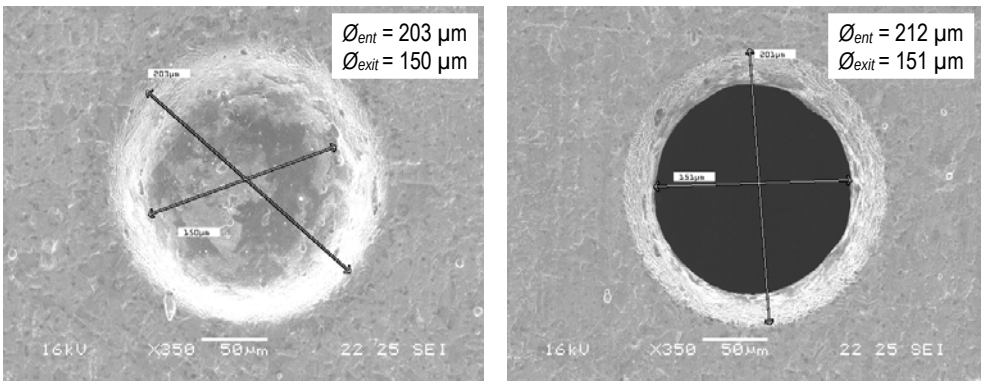

(a) *(b)*

Fig. 4.31 *SEM images of fabricated microholes on nickel plate, (a) blind hole, and (b) through hole.*

4.4.1.1.2 Microdrilling multiple holes (Micronozzle array)

The micro-nozzles with multiple holes array, which have been prepared by μECM, are represented in Fig. 4.32 and Fig. 4.33. Fig. 4.32 illustrates a micro-nozzle with five single holes arranged 500 μm apart each other on the face of the plate. The center hole is slightly larger than the others. The center hole entrance and exit diameters were about 48 μm and 19 μm respectively, so the fabricated hole angle was about 21^0 coming from a tool with a tip angle of nearly 18^0. The angle of the tapered hole was slightly larger than the tip angle of the microtool used. Similarly, the surrounding holes are approximately same dimensions where hole entrance diameter is 41 μm and the outlet diameter is 17 μm for the same tool. The nozzle angles of the surrounding holes were found about 18^0. During the operation, the tool was fed at 0.5 μm/s and immediately withdrawn at 10 μm/s. The entire machining operation was not involved any dismounting of the microtool. Total time required for machining was only 59 min including the set up time and tool positioning on five predefined places. Tool was fed 150 μm from the position where the tool set zero and continued the tool feed 0.5 μm/s.

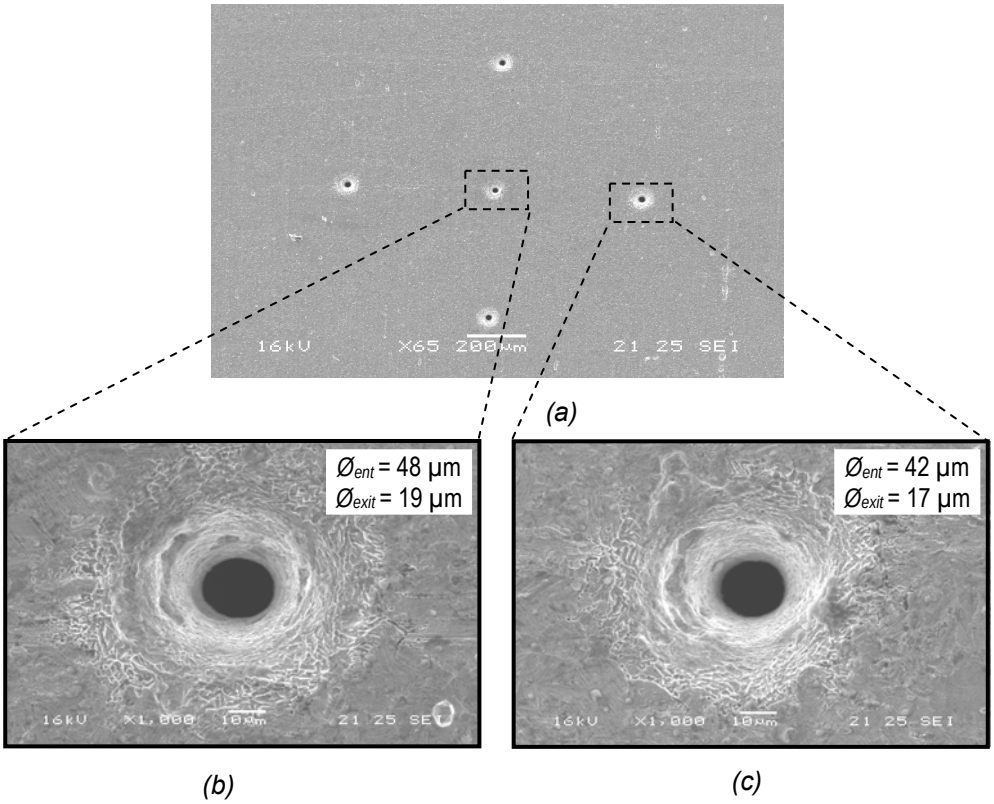

Fig. 4.32 *SEM images of fabricated micro-nozzle array (a) multiple holes on the plate (b) central hole, Ø$_{ent}$= 48μm, Ø$_{exit}$ =19 μm, nozzle angle 21^0 and, (c) surrounding hole, Ø$_{ent}$= 42 μm, Ø$_{exit}$ =17μm, nozzle angle 18^0.*

Fig. 4.33 illustrates a micro-nozzle holes array of 13 holes. The diamond shaped arrangement of micro holes are approximately 500 µm apart to each other. The diameter of entrance of micro holes is about 95 µm and the exit diameter is about 30 µm, nozzle angle was found about 40^0. Operating speeds were varied for different tool positions. When machining started, the feed rate was 0.5 µm/s and the tool was fed 90 µm continuing this speed. After this position of tool, the speed was decreased to 0.3µm/s for 30 µm. Total tool advancement was fixed to 120 µm, and then the tool was withdrawn back 200 µm in opposite direction within few seconds, with a speed of 1.0 µm/s. The same procedure was applied for rest of the holes. Total time required for machining the micro-nozzle array with 13 holes was only 119 min, including the tool positioning time.

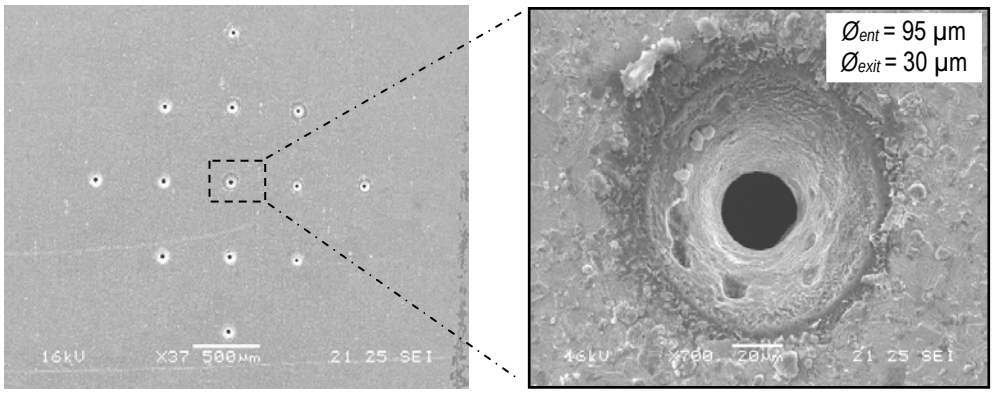

(a) *(b)*

Fig. 4.33 *SEM images of fabricated micro-nozzle array of 13 holes (a) multiple holes on the nickel plate, (b) central hole, $Ø_{ent}$= 48µm, $Ø_{exit}$ = 30 µm, nozzle angle 40^0.*

4.4.1.2 Microcutting and micromilling

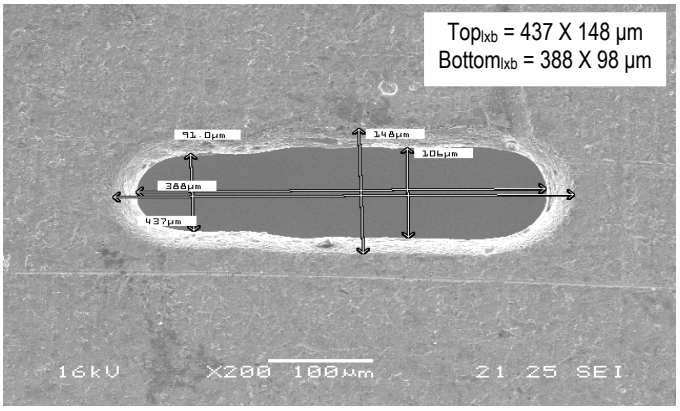

Fig. 4.34 *SEM image of micropocket on the nickel plate, nozzle angle 33^0.*

A series of successful microcutting (micro-contouring, micro-milling etc) experiments has been carried out on the nickel plate. During micro-pocket formation, the parameters used are given in Table 3.7; the nickel plate was first drilled to a specified depth and then micro-milled immediately towards the longitudinal direction of the workpiece at a constant speed. The taper shaped cut obtained was 437 X 148 µm on upper face of the plate and 388 X 98 µm on the opposite side of the plate. The taper of the cut was about 33^0 around the cut, as shown in Fig. 4.34.

During microcutting, a microtool of 21 µm in diameter without tool insulation was fixed with the holder unit, and machining was carried out on nickel plate with an electrolyte concentration of 0.1M HCl, applied frequency of 1 MHz, duty cycle 10% (pulse-on: 100 ns, pulse-off: 900 ns), applied potential of 4.2 V, base potential of –0.8 V were applied. During the microcutting process, the tool feed rate was fixed to 0.1 µm/s. There was no short circuit during the whole cutting process. The resulted microproduct was 527 µm in length, and in width, without taper formation. The microproduct is shown in Fig. 4.35.

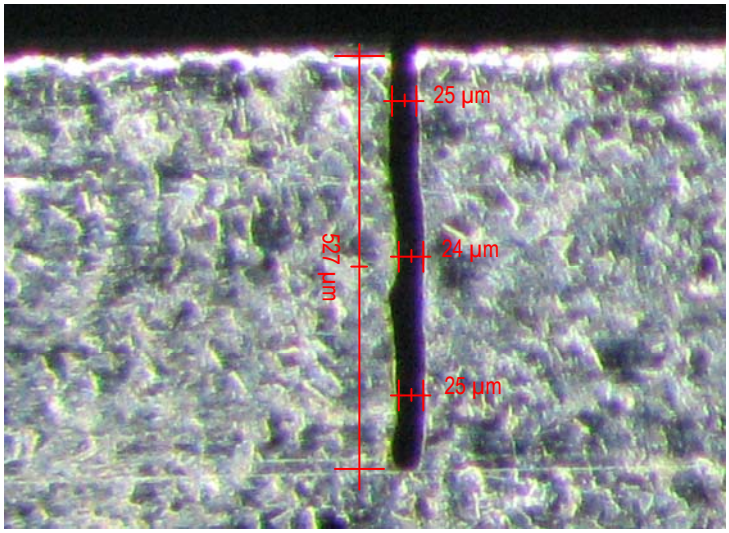

Fig. 4.35 *Microscopic image of microcutting on the nickel plate.*

The same procedure was the applied for micromilling shown in Fig. 3.36, where the electrical power was changed for each of three machining steps. The selected electrolyte concentration was 0.1 M HCl, whereas applied frequency was fixed to 1 MHz with 14% (pulse-on time: 140 ns, pulse-off time: 860 ns) duty cycle. The applied potentials chosen for first step, second and third steps of machining were 3.4V, 4.5 V, and 5.5 V respectively and the baseline potential was kept constant at –0.8 V. Machining was conducted at a fixed feed rate of 0.1 µm/s, where the tool dimension was 21 µm. Machining was done upto 1473 µm long and the width of the machined part was varied in the range of 37.5 – 63.7 µm in the first step, 63.7–73.6 µm in the second step, and 73.6 –80.0 µm in the third step.

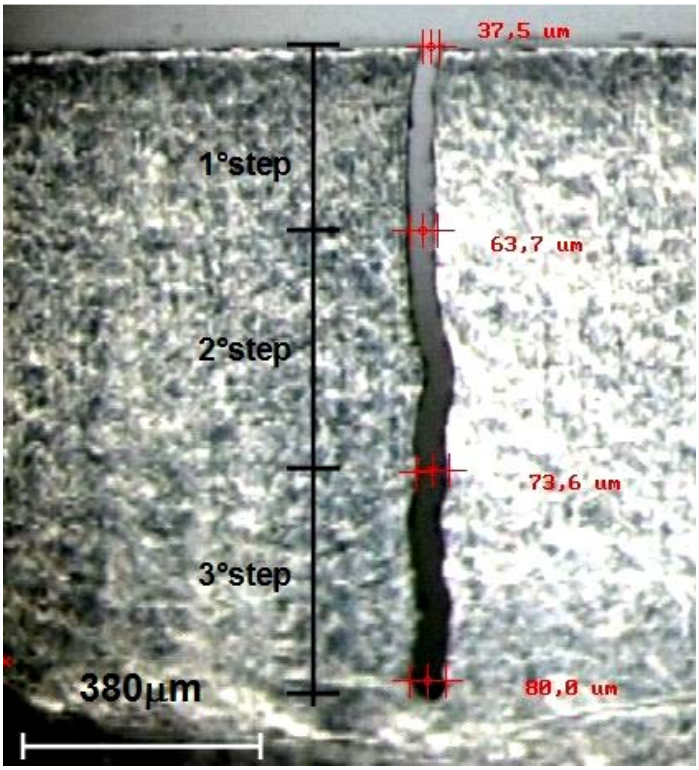

Fig. 4.36 *Microscopic image of micromilling on the nickel plate.*

4.4.2 Machining on Stainless Steel

The needle is the part of the injection syringe that actually pierces the layers of the human body to inject or extract liquid medicines or harmful fluids, respectively. Depending on how deep the injection or fluid extraction will be, the needle orifice can be thinner or wider, and its length varies. These needles are generally made of very high grade corrosion resistant stainless steels. These needles body is made of stainless steel and finished by chromium plating. The development work done on the vitrectomy needles were mode of AISI 403 steel.

4.4.2.1 Microdrilling on injection needle

Fig. 4.37 exhibits the microholes on injection needle (0.5 mm) fabricated as a test experiment for microdrilling on stainless steel. During machining, 0.2 M HCl electrolytes were used with applied frequency of 1 MHz, 30% duty cycle (pulse-on time 300 ns, pulse-off time 700 ns), V_{pp} of 7 V, baseline potential of –2 V. The diameter of the first microhole was found 70 µm for a tool feed rate of 0.05 µm/s. Time required for the microhole fabrication was 27 minute. The diameter of the second hole was found 45 µm for a tool feed rate of 0.1 µm/s. Time required for this microhole fabrication was 19.25 minute.

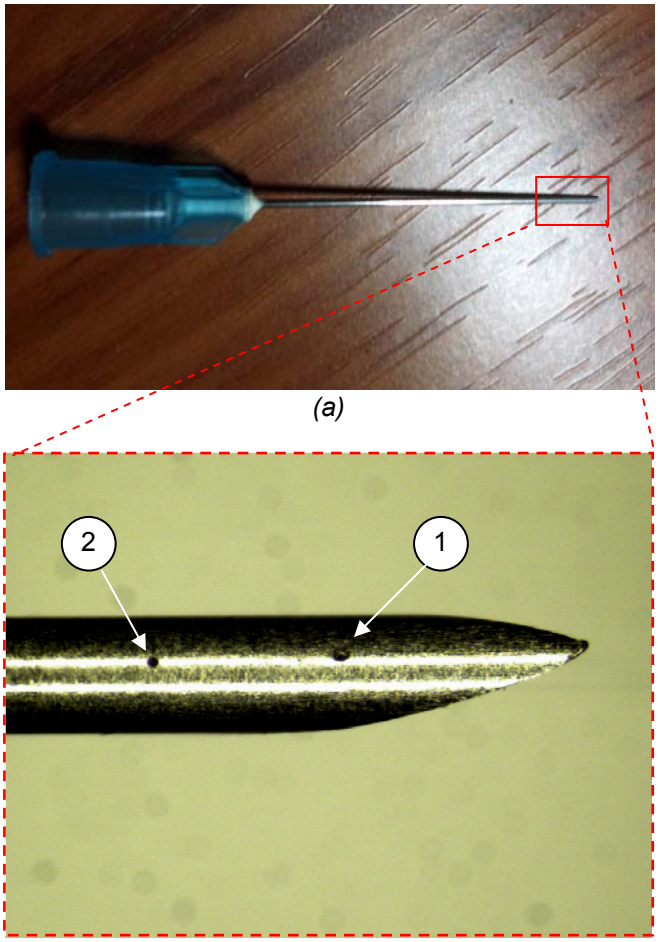

(a)

(b)

Fig. 4.37 *(a) Photographic image of injection needle (0.5 mm), and (b) microscopic image of microdrilled hole on injection needle.*

4.4.2.2 Microdrilling on vitrectomy needle

A cylindrical short microtool with 53 µm in diameter and 860 µm in length was selected and then machining was carried out on vitrectomy needle. The needles were fixed in the electrolyte basin in specially designed fixture, and the tool was fixed with the holder unit, feed along the vertical axis. The parameters selected for microdrilling on vitrectomy needles were as follows: applied frequency, f = 500 KHz, peak-to-peak voltage, V_{pp} = 15 V, V_{max} = 10 V, V_{min} = 5 V, duty cycle, δ_r = 30%, and electrolyte of 0.2 M HCl. Fig. 4.38 (a)–(b) illustrate two different microdrilled hole on two vitrectomy needles (Bausch & Lomb and Alcon).

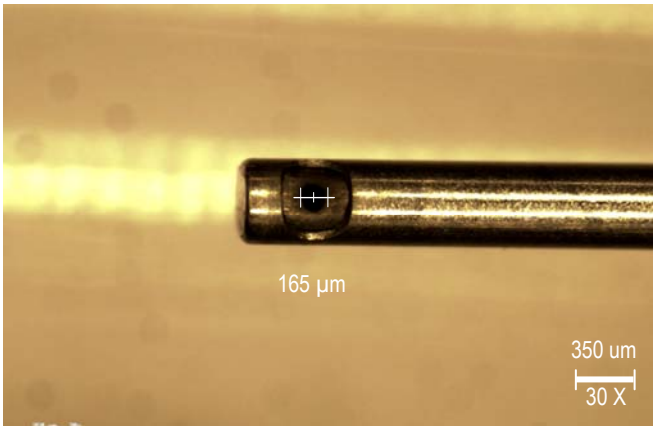

(a)

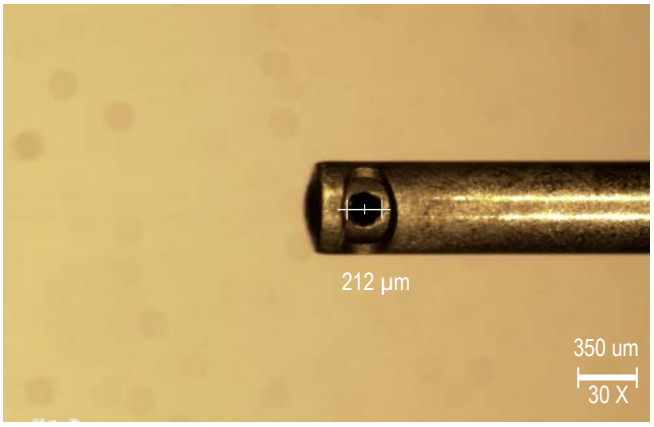

(b)

Fig. 4.38 *Microscopic images of microdrilled hole on two different vitrectomy needles, (a) hole diameter = 165 µm (Bausch & Lomb), and (b) hole diameter = 212 µm (Alcon).*

4.5 CONCLUSION

As the micromachining technologies have been extensively used to miniaturize highly precision machines and equipments necessitate the development of manufacturing processes, performance of micromachining can only be achieved by proper choice of the parameters used. To fabricate these microproducts, the equipments used for machining also should be properly designed and fabricated. This chapter details the results found from the experiments conducted for the last three years in DIMNP. In the fabrication of micro tool, tungsten micro shafts of 0.38 mm are electrochemically etched, applied potentials, electrolyte concentrations, etching time are varied for different arrangements of electrolyte basin. The results found from the experiments are stated in different sections of this chapter. The

result of parametric analysis of electrochemical process has also been declared. This chapter ends with the results obtained from some development works in the field of electrochemical process, which will give a new concept of micromachining process and its applications.

Chapter 5

Discussions

5.1 INTRODUCTION

The applications of pulsed power supply lead to the localized anodic dissolution of the workpiece material in electrochemical micromachining region. However, the use of high frequency short pulse power supply can greatly influence the machining zone that offers improved dimensional accuracy and surface quality of the workpiece material. While localized dissolution occurs in many forms, the results are the same. The amount of metal dissolved would usually be considered insignificant if uniformly distributed across the entire surface rather than accumulated around the working zone. Since current density is an important factor in assessing machining rates, the accumulated by-products unevenly increases the current density around the machining zone, which can result in perforation or other failures deteriorating the surface quality. Moreover, the localized material dissolution often appears to have a stochastic nature, varies material to material, hence it is very difficult to design with correct machining parameters. Another difficulty with localized dissolution is associated with its detection and in-process monitoring under operating conditions. Since the machining zone is very much tiny and confined in some cases, an in-process monitoring and control system will be helpful to enhance the products' quality.

The µECM process has a potential to machine a large variety of materials with suitable machining parameters. The choice of these machining parameters largely depends on what type of material needs to be machined, the dimension of electrode materials, machining environment (electrolyte used), external power supply, and arrangement of machining set up. The range of machining parameters can be determined based on the results obtained from the experiments conducted in micromachining range on different working materials. The goal of this chapter is to clarify the mechanism involved in localized material dissolution process and discuss the effects of process parameters on µECM. The first section introduces the mathematical model developed for the estimation of material removal rate under pulsed power supply. In addition, an in-process monitoring system has been developed based on the waveforms generated during machining.

5.2 DEVELOPMENT OF MATHEMATICAL MODEL FOR MRR

The amount of material removed during μECM can be determined by combining Faraday's first law and Ohm's law as stated in Chapter 2, Eq. (2.10):

$$V_m = \frac{CEA}{gr}t \tag{5.1}$$

where, V_m = volume of material removed,
C = the electrochemical constant,
E = voltage value acquired by oscilloscope,
A = electrode area under electrochemical process,
g = inter-electrode (tool-work) gap,
r = electrolyte resistivity, and
t = time allowed for machining.

For pulsed μECM, the volume of material removed for each voltage pulse is based on the assumption that material is removed only during the pulse-on time, and pulse-off time is kept large enough to heat dissipation, and to flush away the dissolved materials from the machining area. Considering that in the etching process, material removal takes place only for all pulse on-time durations; a mathematical model has been proposed to calculate the material removal rate during the pulse on-time with a good approximation [205]. Therefore, the volume of material removed ($V_{m\text{-}on\ time}$) could be obtained as:

$$V_{m-ontime} = \int_0^{\tau_{on}} \frac{CEA}{gr} dt \tag{5.2}$$

where, τ_{on} is pulse on-time during each pulsed period.

During every pulse period, the double layer is charged and discharged periodically over the two electrodes. The charging and discharging waveform attained during machining is shown in Fig. 3.13. As it is not simple to determine the faradaic current duration during the pulse-on time and its initial time, t^* (shown in Fig. 3.13), the only way to estimate the value of the charging and discharging time is from the waveform generated during the stable machining. Recalling the Fig 3.13, it is possible to distinguish the value of the faradaic state and transient state, and the value of the initial time is marked as the start time of the almost flat voltage or the median value of the almost flat voltage. Since the material removal acts only during the time corresponding to faradaic-currents, the integral has to be rearranged accordingly for better approximation as follows:

$$V_{m-faradiac} = \int_{t^*}^{\tau_{on}} \frac{CEA}{gr} dt = \frac{CA}{gr} \int_{t^*}^{\tau_{on}} E dt = \frac{CAE^*}{gr}\left(\tau_{on} - t^*\right) \tag{5.3}$$

where, t^* is the start time of the almost flat voltage and $E^* = V_{top}$ is the median value of almost flat voltage from t^* to τ_{on}. Now the MRR for a single pulse is calculated as:

$$MRR = \frac{V_{m-faradiac}}{\tau_{on} + \tau_{off}} \tag{5.4}$$

where, $V_{\text{m-faradiac}}$ is the volume of material removed for a single pulse (faradaic state) and τ_{off} is the pulse off duration.

The Eq. 5.3 implies the generalized equation for the voltage pulses, but this experimental scheme is focused on the observations related to the effects of applied frequency and duty cycle used in µECM process. As the applied frequency determines the pulse period, the Eq. (5.3) needs to be modified including the different variables related to frequency applied frequency during microdrilling, as:

$$V_{on-time} = \int_{t^*}^{\tau_{on}} \frac{CEA}{gr} dt = \int_{t^*}^{\tau_{on}} \left[\int_s \frac{CA}{gr} E ds \right] dt$$

$$= CE^* \int_{t^*}^{\tau_{on}} \left(\frac{S'}{g'.r'} \right) dt = \frac{CS'E^*}{g'.r'} \left(\tau_{on} - t^* \right) \tag{5.5}$$

where, S is the surface immersed into the electrolyte, t^* is the start time of the flat voltage and E^* is the flat voltage from t^* to τ_{on} and S', g', r' are the average values of S, g and r, respectively, coming from the surface integral. The values of g and r vary along the surface and have a minimum value in the closer part of the tip that supplies the higher contribution to the surface integral.

Again, τ_p is the time taken for one complete oscillation and δ_τ is the fraction of τ_p, called duty cycle in percentage (%), and γ^* is the percentage of pulse-on time to start almost flat voltage (median value of $E^* = V_{\text{top}}$ becomes almost flat voltage) and is measured with the aid of a digital oscilloscope. Putting these in Eq. (5.6),

$$V_{on-time} = \frac{CS'E^*}{g'.r'} \delta_\tau \left(1 - \gamma^* \right) \tau_p$$

$$V_{on-time} = \frac{CS'E^*}{g'.r'.f} \delta_\tau \left(1 - \gamma^* \right) \tag{5.6}$$

where, f is the applied frequency in hertz (cycles per second). However, this approximation by excess of MRR was calculated as

$$MRR \cong \frac{V_{on-time}}{\tau_{on} + \tau_{off}} = \frac{V_{on-time}}{\tau_p} \tag{5.7}$$

where, $V_{\text{on-time}}$ is the volume of material removed for a single pulse time. Thus, the material removal rate in the unit of cubic millimeter per minute (mm^3/min) is found as the material removal rate for a single pulse multiplied by 60 times of the applied frequency in the unit of cycles per second. Finally, the MRR is calculated as:

$$MRR_{\text{theoretical}} = V_{\text{on-time}} \times 60\, f = 60\, V_{\text{on-time}}.\, f \ (mm^3/min) \tag{5.8}$$

5.3 FABRICATION OF MICROTOOLS

5.3.1 Sizing and Shaping of Cylindrical Microtools

From Figs. 4.2, 4.3, and 4.4, it is observed that the variation of microtool diameter is a function of applied potential, electrolyte concentration, and the etching time. The shape of the microtool diameter also depends on the arrangement of the electrolyte basin, and the nature of the electrical power used. The diameter of the microtool body decreases with the increase in applied potential, electrolyte concentration, and etching time. Fig. 4.2 represents that the variation of the microtool diameter with the applied potentials and etching time for a fixed electrolyte concentration of 1 M KOH. When the applied potential was 3 V AC, the tool diameter decreased with etching time and resulted in very low rate of material removal. The material removal rate being very low, it took a long time to fabricate a microtool. Moreover, the sludge growth in the electrolyte solution was observed. When the applied potential was increased to 6 V AC, the rate of diameter reduction increased considerably and it was made possible to fabricate a microtool of same dimension within 5 minutes. After these 5 minutes of machining, the shape of the microtool remained same, whereas the length of the tool decreased with time and the shape of the microtool changed from cylindrical to conical form. At an applied potential lower than 6V and concentration of 1.0 M KOH, the charge induced intensive dissolution at the shaft end and a tapered shape of the shaft was observed. However, machining was carried out at higher applied potentials of 9 V AC and 15 V AC. For these two applied potentials, it was possible to fabricate a microtool of desired diameter within 3 minutes. But, for higher applied potentials, the rate of material dissolution was very fast and resulted in a microtool of conical shape as at high applied potentials excessive diffusion layers of dissolved ions hindered chemical reaction at the shaft end [68]. The reason behind this phenomenon is the diffusion layers that have a greater density than the electrolyte and thus tend to sink downward. Therefore, at higher applied potentials the charge concentrated near the shank portion of the tool results high activity in that region lead to the rapid dissolution leaves a neck near the shank part and air-electrolyte interface of the tool.

Fig. 4.3 and Fig. 4.4 exhibit the effect of electrolyte concentration in the fabrication of microtools. During experiment, the electrolytic concentrations were varied from a very low concentration of 0.08 M KOH to a moderately high concentration of 2.0 M KOH under two moderately high applied potentials of 9 V and 15 V AC. As shown in the aforementioned figures, the diameter of tungsten tools decreases with concentrations and etching time. At the initial stage of machining, the reduction in the diameters was found approximately linear for all electrolyte concentrations. The uniformity of microtool diameter was observed without taper formation as shown in Fig. 5.1. After that certain etching time, the variation in microtool diameter was observed, and found increased with the concentration and etching time. The curves describing relationships between the etching time and the reduction in microtool diameter for different electrolyte concentrations had parabolic shape. From these figures, it also observed that the rate of diameter reduction was very fast for the concentrations higher than 1.0 M KOH. Therefore, it was very difficult to

fabricate a microtool of predefined diameter for these concentrations and higher applied potentials due to rapid dissolution rate. On the other hand, when the electrolyte concentration was very low (0.08 –0.1 M KOH), the rate of material removal was too low to be practically viable for micromachining. Hence, microtools can be fabricated easily in the range of electrolyte concentration of 0.4–1.0 M KOH, applied potential of 6–15 V AC, within an accepted time period.

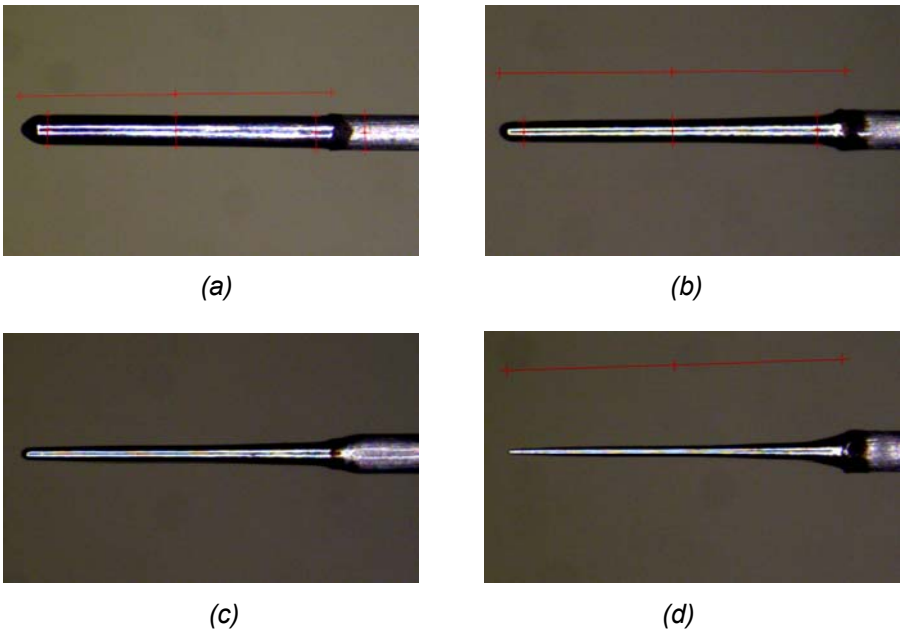

Fig. 5.1 *Microscopic image of fabricated microtools for different etching time, and 0.6 M KOH electrolyte, applied potential of 9 V AC; (a) after 1 min, $Ø_{mean}$ = 314.5 µm, (b) after 2 min, $Ø_{mean}$ = 250 µm, (c) after 4 min, $Ø_{mean}$ = 102 µm, and (d) after 5 min, $Ø_{mean}$ = 41.5 µm.*

Among the influential factors stated above, the initial shape of the tool specimen decides the final shape of the geometry, as the electrochemical machining of solid materials into an aqueous solution usually takes place preferentially in an area that is more protrusive, i.e., an area with a larger local curvature [78]. Moreover, the arrangement of the electrochemical basin and the length of the tool specimen influence the final shape of the fabricated microtool. The tungsten tool electrode that is immersed vertically downward into the electrolyte with the desired depth *L*, shown in Fig. 3.16 (b), after etching it was found that the length of material dissolution is higher to some extent. It is reputed that this extension in the dissolution length is due to the surface tension of the electrolyte solution, where the immersion depth of the tool specimen extends by *h*. From the experimental evidence, the shape of that extended portion that was submerged into the electrolyte due to surface tension becomes parabolic, and formed at the air-electrolyte interface.

Formation of this parabolic shape can be attributed to both bubbling effect and field effect that occurs during etching. Hydrogen bubbles formed around the tungsten wire considered as the key factor in the bubbling theory. The smallest amount of bubbles formed at the lower end of the tungsten wire. These bubbles propagated upward along the sides of the wire and accumulated near the shank of tool where air-electrolyte interfaced. As a result, the density of the bubbles became the highest near the shank of tool. These upcoming bubbles make the curved shaped shank part of the tool. Besides, tool electrode set at the centre of a circular cathode electrode caused path-resistance to vary positively with point-to-point distance between the two electrodes as described in field effect theory. As the circular electrode radius was high enough as compared to the tungsten tool diameter, the electric field-driven repulsive force was same for whole length of tool and hence, etching occurred at the same rate for both electrodes, where the circular electrode reduces its diameter for the whole immersed portion and the tool electrode reduces its diameter along its length. But the reduction in diameter is not same for the whole range of the tool and conical shaped tool was observed. The reason behind this is due to the effect of the diffusion layer that was not possible to keep to a constant value for the whole length of the tool specimen during machining, hence, the fabricated microtool becomes a conical shape during the etching period. The region of the diffusion layer depends on net flow rate of particles entering and leaving boundary layer, and the effect of the diffusion layer depends on the dissolution rate from the unit surface area of tool material.

In order to obtain a thin cylindrical microtool of desired dimension, two new techniques have been proposed. In these proposed techniques, arrangement of the electrolyte basin is modified where the tool specimen is inserted from the bottom of the basin or the tool specimen is placed in horizontal position in the electrolyte basin. The resulted microtool was thin and cylindrical for the whole range of the microtool length, as illustrated in Fig. 4.6.

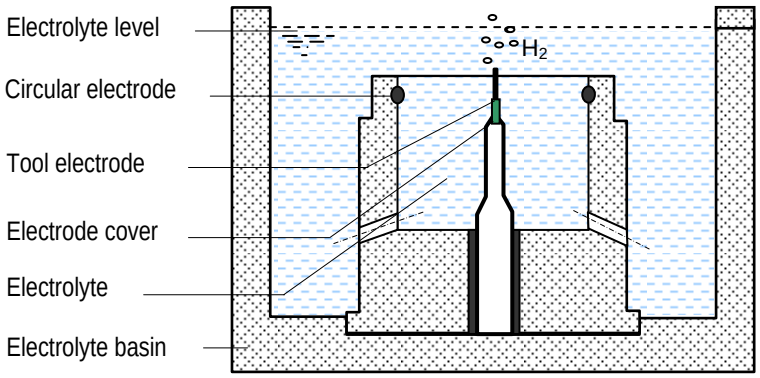

Fig. 5.2 *Fabrication of microtools by electrochemical etching process where the tool specimen is set in vertically upward direction.*

Fig. 5.2 illustrates the schematic arrangement of proposed electrochemical etching process for microtool fabrication. The overall microtool profile formed by this

process become cylindrical and it is possible to control the diameter of the tool through the entire length. The reason is that the hydrogen bubbles formed during machining propagated upwards and the dissolved ions come to downward direction. This two opposite direction movement of hydrogen bubbles and ions do not effect on the microtool shape. However, no such parabolic shape exists near the shake part of the tool.

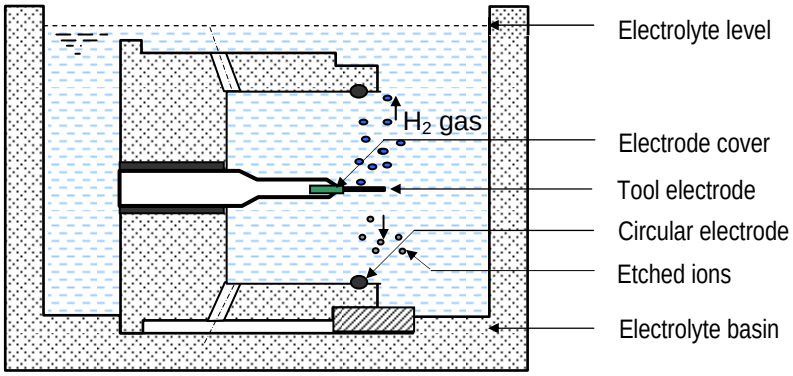

Fig. 5.3 *Fabrication of microtools by electrochemical etching process where the tool specimen is set in horizontal to the electrolyte basin.*

Again Fig. 5.3 illustrates the schematic arrangement of proposed electrochemical etching process for the microtool specimen set in horizontal to the electrolyte basin. The microtools fabricated from this technique were also found cylindrical through out whole length of the tool electrodes. The tool specimen was fully dipped into the electrolyte, and the portion which was covered by the rubber cover insulation was acted as tool shank part. To check the roundness of the tools fabricated by this process, SEM images have been taken, shown in Fig. 5.4, are found cylindrical and approximately circular in shape.

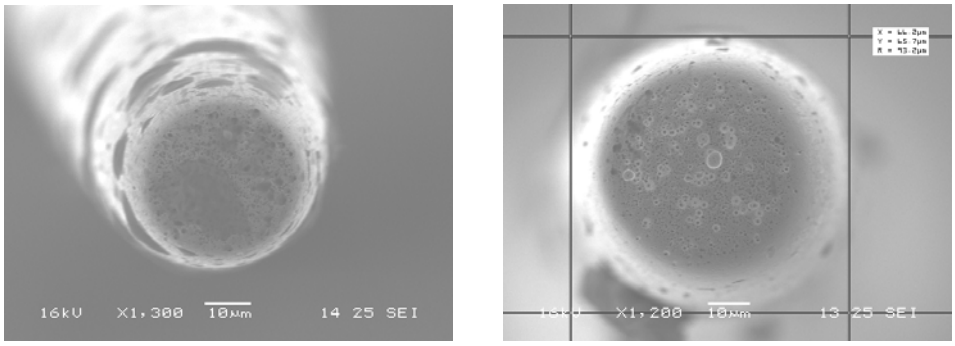

Fig. 5.4 *SEM image of the fabricated microtools formed in horizontally to the electrolyte basin during machining.*

5.3.2 Microtool Tip Formation

Referring to Fig. 4.8, it is observed that the microtool tip angle varies with the concentration of electrolytic solutions for applied potentials of 15 V AC. For both tungsten and stainless steel counter electrodes, the microtool tip angle increases with the increase in electrolyte concentration. Formation of this conical shape can be attributed to the surface tension of electrolytes, bubbling effects and field effects occurred during the tip etching process. The bubbles formed during etching propagated upward along the sides' walls of the specimen wire and accumulated in the extended surface of the electrolyte due to surface tension. These upcoming bubbles acted as a shield for the wire and reduced the contact between the KOH solution and tungsten resulted in retardation of etching reaction. Besides, the electric field-driven repulsive force was higher at the sharper edge of tool; the surfaces of the bottom perimeter of the emerged tungsten wire initially had the highest etching rate and resulted in a nice and smooth tip with commonly observed cone shape [206].

The phenomena of microtool tip formation can be broadly described according to the following general observations made during the etching process of tungsten wires. At applied potentials above the breakdown for etch metal, aggressive gaseous evaluation ensured during the reaction along the immersed specimen wire, disrupting the solution at the meniscus. As the reaction process proceeded, the meniscus lowered on the microtool shaft portion revealing a polished surface, angled from the base of the cylindrical part (shaft). The reaction terminated when the portion of the shaft in the solution completely dissolved, with the tip ending in a fine point at the air-solution interface as shown in Fig. 5.5. However, as the etching takes place on a narrow diameter shaft of tungsten wire of 0.38 mm, the final geometry of the tip depends on the shape of the meniscus formed on the wire at an air-solution interface because only that portion of the shaft in the solution can take part in the etching process. The contact angle between solution and wire has been determined by balancing forces of liquid–liquid cohesion and liquid–metal adhesion [207]. As the reaction proceeded, the meniscus lowers its position on the wire. Three proposed theories are put forth to explain the phenomena.

The first theory modeled in Fig. 5.6, assumes that etching occurs faster in the bulk solution due to the availability of reactant ions necessary to etch the metal. During the etching process, reactant ions are depleted, yielding a concentration gradient between the bulk solution and the top of the meniscus. Also, gaseous evolution causes bubbles to flow up the length of the shaft which continuously reduces the amount of solution in the contact with the metal at the top of the meniscus. A combination of the two effects induces a conical shaped tip with the least amount of etching occurring at the top of the meniscus.

A second theory proposed that a balance of the force on the solution, surface tension acting in the upward direction and gravity acting downward, is maintained throughout the etching process. Assuming the meniscus remained in its initial position after some portion of the wire was etched away, then more solution would be contained by the meniscus in the void made by the loss of metal. The additional weight of this solution would increase the effective gravitational force. These forces

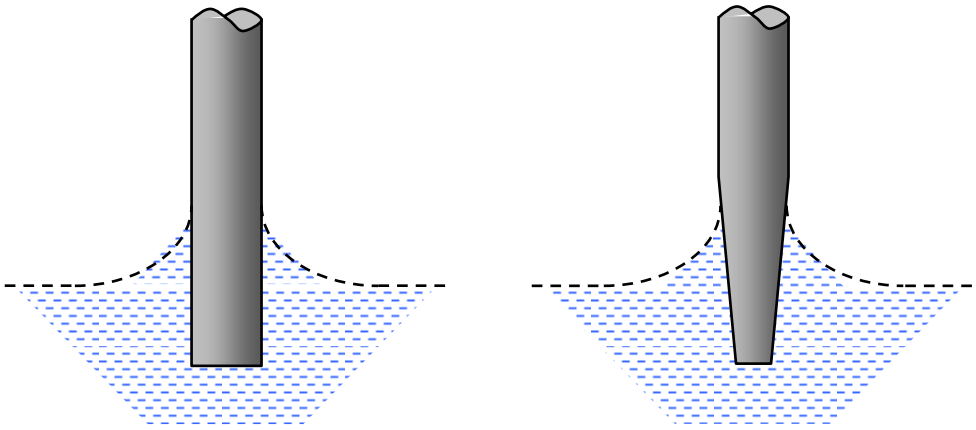

(a) Prior to etch (b) During etch

Fig. 5.5 *Model of tip formation during an electrochemical etching process.*

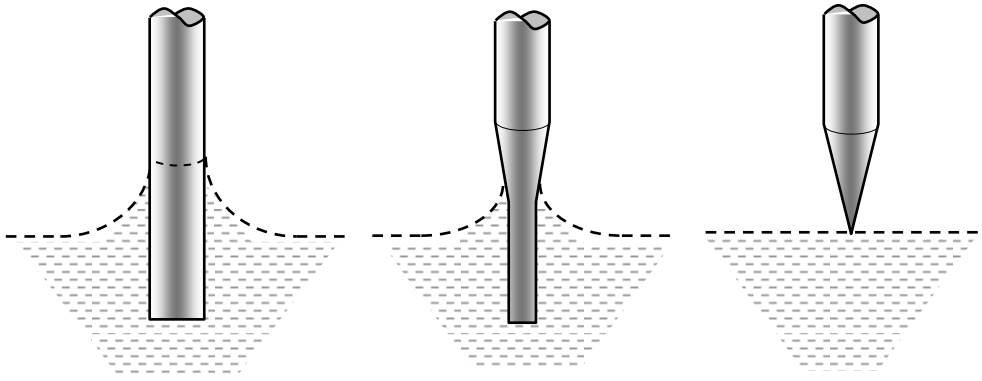

(a) Prior to etch *(b) During etch* *(a) After etch*

Fig. 5.6 *Model of meniscus shape at the air-solution interface (a) prior to etch, (b) during etching, and (c) after the etch in an electrochemical etching process.*

would change the overall balance of the forces. To decrease the gravitational force, regaining a force balance, some of the solution weight would need to be removed from the meniscus. To lose solution weight, the meniscus must lower in proportionately with the amount of the metal lost during etching. Therefore, as metal is removed during the course of etching, the meniscus must continue to lower until the etching terminates in a point at the air-solution interface.

A third theory is proposed assuming that the microtool shaft etches uniformly in the solution. During etching, cylindrical portion of the tool specimen incrementally

decreasing diameter are formed as shown in the model in Fig. 5.7. As the reaction progresses, the cylinder diameter decreases, affecting the gravitational force on the meniscus and decreasing the area of the metal solution interface, thus reduces the interfacial tension. These changes result in lowering the meniscus. Incremental steps continue throughout the reaction as the cylinder immersed in the solution decreases. This theory is supported much by experimental evidence during fabrication of microtool tip, as illustrated in Fig. 5.8.

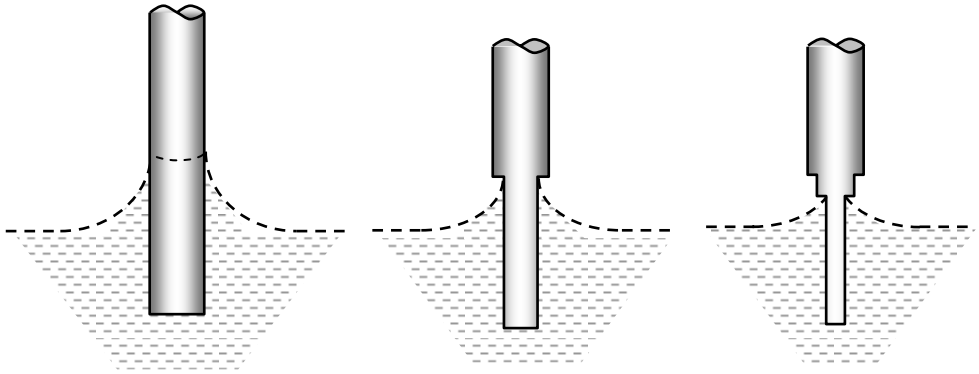

(a) Prior to etch (b) During etch, 1st step (c) During etch, 2nd step

Fig. 5.7 *Model of meniscus shape as a function of shaft diameter at the air-solution interface (a) prior to etch, (b) during etch, first step, (c) during etch, second step in the electrochemical etching process.*

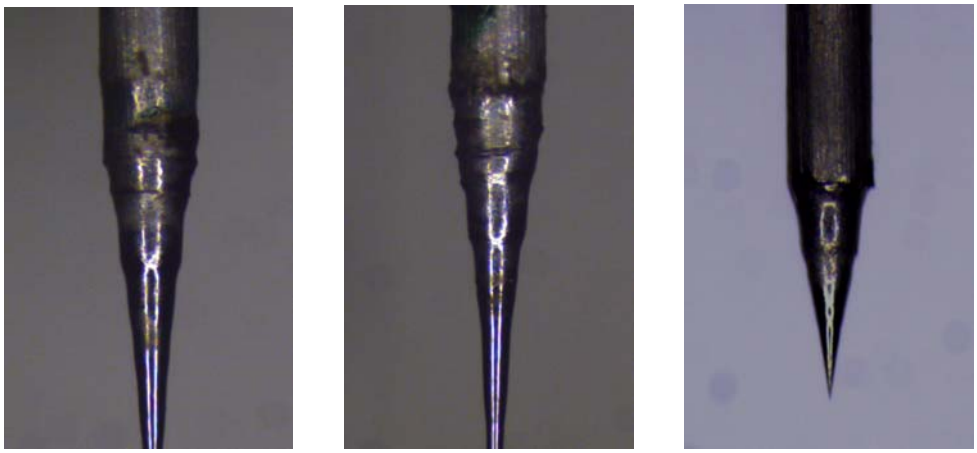

(a) *(b)* *(c)*

Fig. 5.8 *Microscopic images of the microtool tip shape, (a) during etch, first step, (b) during etch, second step, and (c) final shape of the tool tip.*

5.4 PARAMETRIC EFFECT

5.4.1 Effect of Peak-to-peak Voltage

When sufficient electrical energy is available between tool and workpiece, metallic ions may be pulled out of the workpiece surface. In pulsed electrochemical process, the peak-to-peak voltage is the dominating factor, and the amount of material dissolve depends on the value of peak-to-peak voltage applied during machining. The positive metallic ions will react with negative ions present in the electrolyte solution forming metallic hydroxides and other compounds, and thus the metal will be anodically dissolute with the formation of sludge and precipitates. Referring to Fig. 4.11, it is found that with the increase in peak-to-peak voltage, the amount of faradaic current increases, and consequently the MRR increases.

This phenomenon can be easily described according to the combined theory of Faraday's law and Ohm's law, as stated in Eqs. (5.1) – (5.3). When the electrodes are connected to an electric supply source, flow of current in the electrolyte is established due to positively charged ions being attracted towards the cathode and vice versa. Current density depends on the rate at which ions arrive at respective electrodes which are proportional to the applied voltage, concentration of electrolyte, the gap between the electrodes and tool feed rate. Due to application of pulsed electrical power that is frequently applied to the electrochemical process, material removal takes place only during the pulse-on time, and heat formed during pulse-on time is dissipated in the pulse-off time. Therefore, the amount of faradaic current formed during machining is largely dependent on the peak-to-peak voltage applied.

It is worth mentioning that machining with lower MRR needs reduction in tool feed rate to prevent from the microsparks and short circuits. Referring to Fig. 4.11 (b), machining time decreases with the increase in peak-to-peak voltages. As a consequence, the side gap ratio decreases as shown in Fig. 4.11(d).

From Fig. 4.13, MRR is found to decrease with the increasing baseline potential. This is because transient state enlarges with the baseline potential. As a result, total time to remove the same volume of material increases and MRR decreases. From the results, it is recommended that the baseline potential should be in the range of 1.0 –2.0 V for better machining as can also be found in [28]. Moreover, machining is not possible for the baseline potential higher than 2.6 V.

5.4.2 Effect of Applied Frequency

Fig. 4.15 relates the effect of applied frequency on actual material removal rate, machining time and the number of short circuits occurred during electrochemical microdrilling on nickel plate with the long tool. Referring to Figs. 4.15(a)–(b), it is observed that that MRR_{act} decreases and the machining time increases with an increase in electrical frequency. These phenomena can be explained in accordance with the general theory of pulsed electrochemical processes. Minimum pulse-on time needed to overcome the effects associated with double layer

capacitor is found to be in the range of 10~30 ns for the electrodes with the diameter ranging 40~80 µm in diameter [96]. In this work, the applied pulse-on time is fixed to 300 ns (30% duty cycle) which is much higher than the required ultra short voltage pulses. Consequently, effect of non-transient current becomes negligible and faradaic current dominates the material dissolution process. As the applied frequency increases, the electrical double layer capacitance decreases and electrolytic resistance increases. The increased electrolytic resistance causes increased cell impedance, which in turn, decreases the current density into the electrolyte. Therefore, the amount of faradic current decreases with the increase in applied frequency and causes gradual decrease in MRR_{act} and increase in machining time.

Again, referring to Fig. 4.15(c), it is seen that the number of short circuits increases with the applied frequency. As the MRR decreases with the increase in applied frequency, the tool electrode fails to maintain the predefined gap between the electrodes caused higher short circuits. The MRR cannot keep pace with the linear tool feed rate resulted several numbers of short circuits. This reduced MRR for higher applied frequencies dissolve materials less around the microtool. Therefore, less amounts of frontal and side erosions occurs during machining resulting in reduction of micro hole diameter in both entrance and exit of hole, which is also found in a similar work [47].

On the other hand, when the short tool is used, the MRR_{act} and the machining time also respectively decreases and increases with an increase in applied frequency, as stated in Fig. 4.17. It is found that no short circuit occurs for low applied frequency (500 KHz) at a moderately high feed rate for micromachining, and maximum number of short circuits occurred for high applied frequencies. Again, comparing to Fig. 4.15 and Fig. 4.17, it is clear that for the same range of pulse-on time, actual MRR is much higher for the lower applied frequency for a short tool. This observation can be explained in accordance with the Ohm's law. Referring to the equivalent circuit model for electrical double layer potential shown in Fig. 3.15, the time constant τ for charging the double layers is the product of electrolyte resistance and double layer capacitance, C_{dl}. Because of the shorter tool, short path resistance R_s is smaller than the long path resistance R_l and the double layer charging time constant τ_s of the shorter path is relatively small compared to charging time constant for long path τ_l. On the other hand, time constant τ_l of the longer path is bigger than τ_s due to the larger electrolyte resistance, R_l. Again, faradaic current decreases with the increase in tool length. As a consequence of this reduction in faradaic current, the material removal rate decreases proportionately to the rate of increase in electrolyte resistance. As for short tool length, the machinable area is restricted to the adjacent region of the tool as the electric current flows through the shorter path with the electrolyte resistance R_s. However, for long tool, the dissolution of material takes place over a large space from the surface of anode material producing a small hole as the dispersed materials cannot be measured during machining. This phenomenon is schematically shown in Fig. 5.9. Hence, microholes fabricated on the nickel plate are found almost straight for lower applied frequencies (up to 1.0 MHz) and after that conicity of the hole increases with the increase applied frequency, as the tool feed rate is reduced to keep pace with the reduced MRR. However, the diameter of

the microhole can be controlled precisely for higher applied frequencies, but the time required for machining with very high applied frequency make the process inappropriate for micromachining.

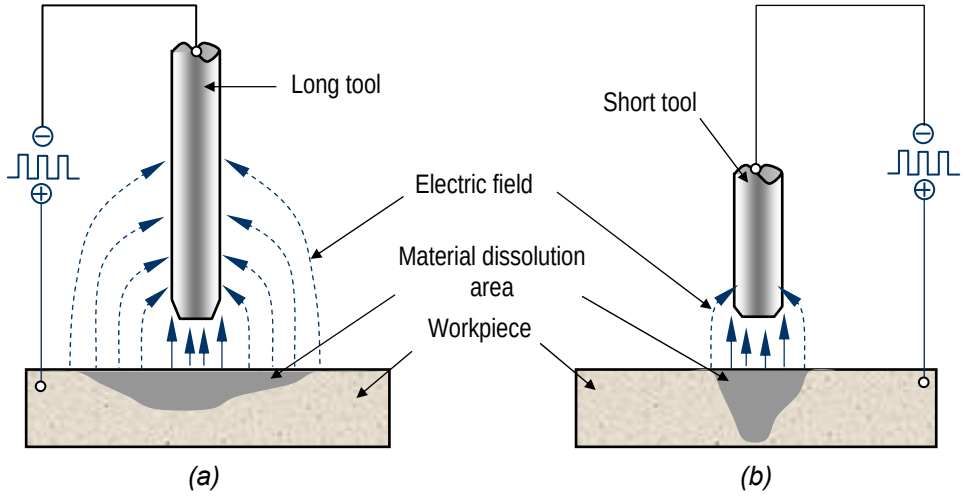

Fig. 5.9 *Schematic representation of the material dissolution region in pulsed electrochemical process for (a) long microtool, and (b) short microtool.*

5.4.3 Effect of Duty Cycle

Fig. 4.19 exhibit the effect of duty cycle on MRR_{act}, machining time, number of short circuit occurred, and the amount of faradaic effect formed during microdrilling on nickel plate. Referring to this figure, it is observed that MRR_{act} and machining time respectively increases and decreases with an increase in duty cycle, and the number of short circuit diminishes for high percentage of pulse-on time.

The effect of duty cycle for applied frequencies can be explained by the existence of the faradaic effect created during microdrilling processes. Referring to Eq. (5.5) and (5.6), volume of material removed is proportional to the product of the almost-flat voltage value acquired by oscilloscope ($E^*=V_{top}$) and time for remaining the voltage value at this level. When the small tool was used, both the voltage values acquired by the oscilloscope (E^*) and time to remain the voltage value on the same level, ($\tau_{on} - t^*$) gradually increased with the increase in the duty cycle. Therefore, the product of voltage value and the corresponding time determining the faradaic effect increases rapidly with increase of the duty cycle and results in rapid dissolution of material during machining. It was found that the material removal rate increases drastically for the applied duty cycle set to 30% and above. At this value of applied duty cycle, material dissolution was so high that no short circuit occurs even at a feed rate of 0.4 µm/s. As a consequence, the side gap increases very rapidly and it was not possible to control the diameter of the microhole.

To perform micromachining effectively, microtool feed rate should have a linear relationship with the material removal rate. Therefore, the feed rate needs to be adjusted with MRR, which affects on the machining time. When the duty cycle was reduced to a value less than 30%, frequent occurrences of short circuit restricts the machining process that eventually rises the machining time. On the contrary, the MRR increase with the increase in duty cycle, this rapid increase in material removal rate facilitates the machining process without short circuit. However, rapid decrease in machining time is problematic for the control of microhole diameter. Moreover, the side erosion rapidly increases for the higher duty cycles leaves the diameters of the fabricated holes are very large compared to the microtool diameter.

5.4.4 Effect of Electrolyte Temperature

The electrolytes are solutions not only complete the electric circuit between the microtool and work piece, but also offers an environment for machining to occur. The conductivity of an electrolyte solution depends on concentration of the ionic species and behaves differently for strong and weak electrolytes. Regardless of the concentration, the electrolyte temperature has a significant effect on electrochemical machining, as shown in Fig. 4.21. Referring to Table 4.1 and Fig. 4.21, it is observed that the MRR_{act} increases and machining time decreases with an increase in the electrolyte temperature. The side gap ratio and taper angle also increase with the electrolyte temperature. These phenomena can be explained in accordance to the concentration of ions present into the electrolyte and the movement of ions within the solution.

The charge is normally considered to be evenly distributed over the surface of the ion and these small charged ions have a strong polarizing power because of the intense field around them and have a very strong effect in producing induced dipoles or aligning permanent dipoles in the solution. These ions gathered together in an alignment to form an array of particles and/or dipoles in every material interface when the material is dipped in the electrolyte solution, termed as electrical double layer, shown in Fig. 3.11. In electrochemical process, such a layer reflects the ionic zones formed in the solution, to compensate for the excess of charge on the electrode. Referring to mentioned figure, the compact layer of charges is strongly held by the electrode and can survive even when the electrode is pulled out of the solution. But the outer layer is a three-dimensional region of scattered ions distributed in the bulk solution by a random thermal motion. The concentration of ionic species at a given distance from the surface decays exponentially with the ratio between the electrostatic energy and the thermal energy, in accordance with the Boltzmann equation. The total charge of the bulk solution equals to the net charge on the electrode side. But, a chemical reaction can only happen when the ions dissociate and bump inside the solution. In the galvanic cell, the reactions can happen by itself without the external power. Besides, in electrochemical machining cell, an external power needs to supply for the reaction to occur. In electrochemical process, machining takes place during pulse-on time, and pulse-off time is kept long enough to dissipate the heat generated and the gas formed during pulse-on time. Moreover, the material dissolution is affected by the conductivity of electrolyte, which is primarily

determined by the concentration of ions, and mobility of ions in a given electric field [55]. In ultrashort pulses, the material removal decreases due to highly confined electron motion. The electrical migration becomes dominant when the pulse duration is extremely short, such as less than 100 ns since there is no significant product buildup. As the temperature raises the movement of ions inside the solution; the rate of reaction increases with the increase in the electrolyte temperature during electrochemical machining. The reason is the increase in electrolyte temperature decreases the molecular bond strength, increases the ion movement, and speeds up the reaction rate. Again, in μECM the reactions involve in mass transport of the electroactive species to the electrode surface can be occurred by three different modes, such as diffusion, convection and migration. The raise in the electrolyte temperature also accelerates the mass transfer modes of all kinds. The viscosity of electrolyte decreases progressively with increasing temperature. This decrease in viscosity facilitates easily migrating the ions with the bulk solution, and help to reduce the effect of double layer. But at a very high temperature the dynamic viscosity reduced, shown in Appendix C, to a level where machining is sometimes impossible. Therefore, the value of the temperature needed for machining to take place is still an open question.

On the other hand, lower duty cycle, short pulse-on time increase the machining time, and high electrolyte temperature generates hydrogen gas much higher than the machining in room temperature, and evaporates the water in the small interelectrode gap due to heating increases the electrolyte concentration and viscosity make the process inconvenient. The resulted high concentrated viscous electrolyte is not able to remove all the reaction products from the narrow machining zone. As there was no flushing system integrated to the micromachining system, some of the by-products remain in that narrow interelectrode gap retard the machining rate in the tool-workpiece working zone. Hydrodynamic disturbance due to change in viscosity affects the distribution for diffusion layer thickness on the micromachining zone, which influence the electrochemical dissolution process to a great extent. Finally, there is a possibility of microspark or short circuit in-between the microtool and work piece that ultimately increases the machining time.

5.4.5 Effect of the Microtool Dimension

5.4.5.1 Effect of tool diameter

From Fig. 4.23 and Table 4.2, both MRR_{act} and machining time increase with an increase in the diameter of microtools used for microdrilling for the particular combination of machining parameters. These phenomena can be explained in accordance to Eqs. (5.1) and (5.5). The volume of material removed is proportional to the surface immersed into the electrolyte solution during machining. As the diameter of microtool increases, the total surface area under electrolytic solution increases resulting increased in dissolution rate. To overcome the effects associated with the double layer capacitor is found minimum of 10~30 ns for the electrodes 40~80 μm in diameter as reported [96]. In this experiment, the applied frequency of 1 MHz with a duty cycle of 30% was selected for machining, which sufficiently high for material dissolution to occur. As a result, the effect of non-

transient current will be negligible. Therefore, the faradaic current dominated the machining process. Moreover, the increase in surface area under electrolyte decreases the electrolyte resistance, and with the decrease in electrolyte resistance, the electrical double layer capacitance increases. This decrease in electrolyte resistance reduces the cell impedance, in turn, increases the current density into the electrolyte. As a result, the MRR increases with the increase in the microtool diameter.

Moreover, as the microtool approaches the workpiece, the length of the conductive current path decreases and consequently, magnitude of current increases. This increase in current density causes the removal of metal at a rate equivalent to the rate of decrease in electrolyte resistance. So the feed rate needs to be adjusted in such a way to control the MRR, which eventually increases the machining time as illustrated in Fig. 4.23 (b). These frequent occurrence of short circuit for higher diameter/size effects in the calculation of MRR because the occurrence of short circuit increases the machining time. A sudden jump in current density also observed. This means that the tool was approaching the workpiece and possible corrective measure demands. The corrective action can be done by holding the tool in stand-by mode until the current density reaches to the previous state and stopping the tool feeding and setting a reduced value for tool advancement. Otherwise, the microtool touches the workpiece results microspark and the distortion of the microtool tip or bending the microtool. These practical difficulties in machining increase the machining time.

Again, as shown in Figs. 4.23(c)–(d), the angle decreases and side erosion increases with the increase in tool diameter. This phenomenon can be explained according to the basic mechanism of electrochemical machining process. The μECM is a layer-by-layer dissolution process. It is already said that the machining gap increases as the machining time increases. The machining gap at the entrance of the microhole, g_i is larger than that of the exit of the microhole, g_0. This difference in the machining gap causes the tapering of the side wall [102], shown in Fig. 5.10. Moreover, the taper angle of the fabricated microholes decreases with microtool diameter is observed. This is due to Ohm's law i.e. the electrolyte resistance increases and hence side erosion rate decreases with the increase in gap. Again, if the inter-electrode gap is narrowed down to a bare minimum level then the machined shape becomes better. Both these effects though opposite in nature, plays vital role in side erosion. At the same time machining process is slowed down to avoid short circuit. During this period, the incidental side erosion could not be stopped.

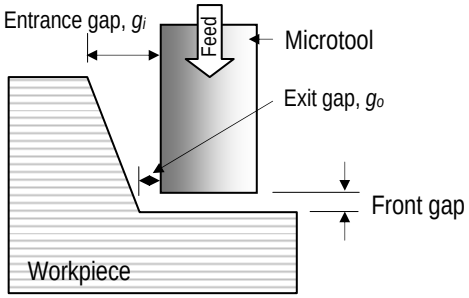

Fig. 5.10 *The effect of cylindrical microtool shape on the side wall profile.*

5.4.5.2 Effect of tool length

From Table 4.3 and Fig. 4.25, MRR decreases and machining time increases with the increase in the overall tool length. The table also shows that the number of short circuits increases with tool length. As the MRR decreases, the same microtool produces a microhole of relatively smaller diameter during microdrilling i.e. overcut is found to be higher for shorter tools.

Again, From Table 4.4 and Fig. 4.27, the MRR_{act} decreases and machining time increases with the increase in microtool dipping length or effective length. As stated earlier in section 5.4.2, these phenomena can be explained according to Ohm's law. The fully dipped tool needs longer machining time to make a reduced diameter hole and also causes maximum number of short circuits even at lower feed rates. The phenomenon has already been discussed in section 5.5.1. Moreover, this is due to the small gap between the front face of the tool and the workpiece surface, the current density inside the gap is much higher than in the neighborhood. Therefore, the workpiece is preferentially etched more within the gap region when a short dipping length is employed. Besides, increase in the dipping length increases the inhomogeneity of the current density distribution, therefore, improves the localization of the etching process. But, at the same time machining process is slowed down to avoid short circuit. During this period, the incidental side erosion could also not be stopped.

5.4.5.3 Effect of conical shaped tool

From Table 4.5, it is observed that the conical shaped tool requires less time for machining a microhole than a cylindrical microtool. The numbers of short circuits are also found less for conical shaped microtools. On comparing Figs. 4.29(a) – (b), microdrilling with a conical shaped tool, and (c)–(d), drilling with a cylindrical tool, it becomes apparent that the conical shaped tool results in significantly higher drilling speeds. This can be explained by noting that in the conical shaped tool the mean drilling speed in the hydrodynamic regime is faster than the speed attained with a cylindrical tool. For conical shaped tool, the discharge regime increases due to the concentration of the discharge activity at the electrode tip. This results in enhanced chemical etching and as a consequence in sharper microhole sidewalls compared with the microholes drilled under the same conditions using a cylindrical tool. However, for the cylindrical microtool the drilling time increases.

Again referring to Table 4.6 and Fig. 4.30, the dimension of conical shaped microholes depends on the both tool length and the diameter, i.e. the angle of the tool tip. During machining the feed rate largely affects on the microhole diameters. It is observed that. The forward feed during machining and the backward after machining both have a significant influence in the products quality. At a lower feed rate, more material was removed from the entrance part of these microholes and the dissolution was extended over the surface of the nickel plate. On the other hand, the amount of material dissolved maintain a regular ratio from the top face and vertically downward of the nickel plate for a higher feed rate. This phenomenon can be attributed to the combined effects of tool shape and the tool feed rate, graphically shown in Fig. 5.11.

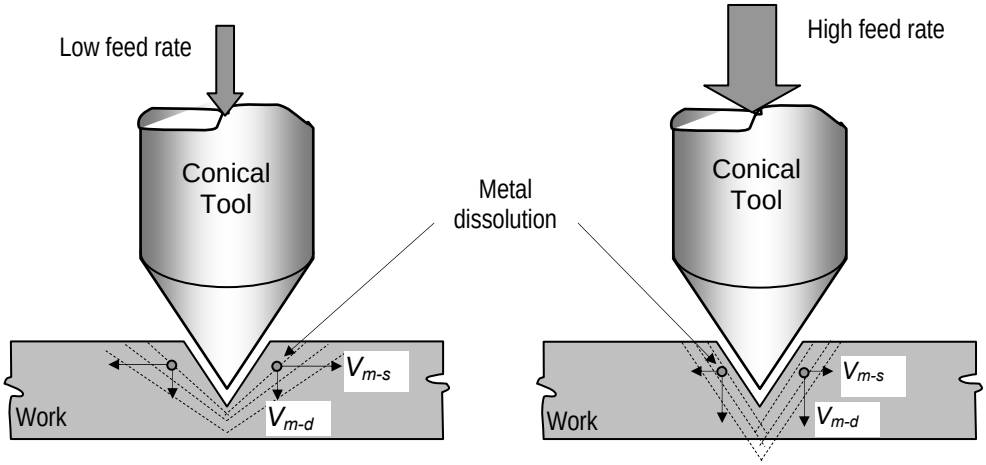

(a) Low tool feed, $V_{m-s} > V_{m-d}$ *(b) High tool feed*, $V_{m-s} < V_{m-d}$

Fig. 5.11 *Schematic illustration of metal dissolution phenomena on feed rate for the conical shaped microtools.*

5.5 MICROMACHINING

5.5.1 Micromachining on nickel plate

The encouragement of electrochemical chemical etching during machining can be achieved by optimizing the parameters, fresh and clean electrolyte supply, controlling its concentration and temperature, also the arrangement of the tool and workpiece into the machining zone. This aspect is particularly important during microdrilling where the tool electrode advances in vertically downward direction. But, along with the physical arrangement of the equipments used, the precision movement of these equipments also enhances the products quality during microcutting or micromilling. Otherwise the quality of the microproduct deteriorates, shown in Fig. 5.12. The channel shown in figure is not perfectly straight.

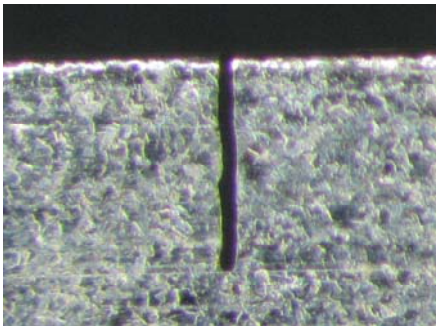

Fig. 5.12 *Microscopic image of microcutting on nickel plate.*

The electrochemical machining process is an oxidation reaction process that removes metal atom by atom. In practice the precision of µECM is limited by the stray machining of unwanted areas of workpiece. On the application of pulsed voltage, the material is removes from the confined space, and the workpiece get oxidized for the application of lower concentration of passivity electrolyte. Nickel plates are usually machined under HCl electrolytes. Chloride is one of the most aggressive halide anions commonly associated with corrosion and pitting. Therefore, after machining the fabricated product needs to clean immediately. Fig. 4.13 illustrates two different microdrilled parts. From these figures one can easily realize the difference between the products. Hence, each of the microproducts needs to rinse in the hot water to remove foreign particles and the formed oxides.

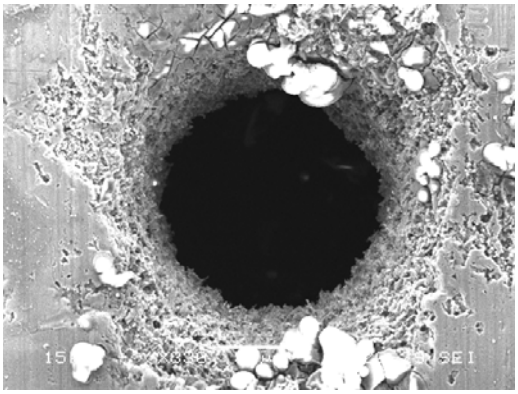

(a)

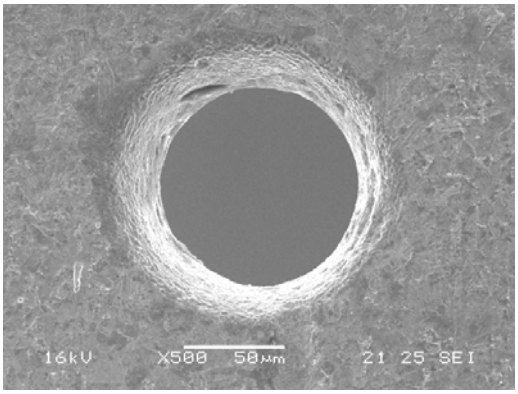

(b)

Fig. 5.13 *SEM images of two different microproducts formed on nickel plate by µECM process, (a) without rinse, (b) after rinse.*

As stated in different sections of this work, machining performance of µECM depends primarily on applied potentials, applied frequency and related duty cycle, concentration and temperature of the electrolyte, tool dimension, and tool feed rate and physical configuration irrespective of the workpiece materials. In most applications, a high feed rate of machining is maintained by feeding the tool

towards the workpiece with a constant feed rate. However, if the tool feed rate is too high, the tool would come in contact with the workpiece and cause short circuit. This short circuit is very much detrimental for a conical shaped microtool since short circuiting seriously damages conical micro tool. Till now, and most of the researchers discuss about the vertically downward feed rate that directly affects on the microproducts quality. During multiple hole array microdrilling, it was observed that the vertically upward feed rate is also affects on the microproducts quality. Referring to Fig. 4.32 and 4.33, in the diamond shape micronozzle array, the microholes are 500 µm apart to each other. In that case the tool needs to travel from one position to other withdrawing the tool at a distance above the nickel plate. If the upward feed rate is not sufficiently high, then the extra time of upward moving enlarges the microhole to some extent. This effect is extensively visible for the entrance diameters of the microholes, and very less for exit diameter. The exit diameter remains close to the tool tip diameter but the entrance diameter enlarges compared to tool shank diameter.

On the contrary, the forward feed rate, the movement of microtool from one drilling position to another predefined drilling position, is also bears the same effect on the workpiece surface. As stated in Fig. 5.14, a channel type microgroove formed on the nickel plate during the tool movement from one drilling position to another drilling position. These types of microchannels are observed when: (i) the microtool moves from one machining position to another position with a low feed rate over the workpiece surface, and (ii) the tool remains very close to the workpiece surface during forward motion. In worst case this type of channels may exists even for high feed rate. To overcome this detrimental effect of surface deterioration, the tool must pull up from the electrolyte solution at a higher backward feed rate. After proper positioning to the vertical axis (Z- stage for microdrilling), tool will move for a new microdrilling.

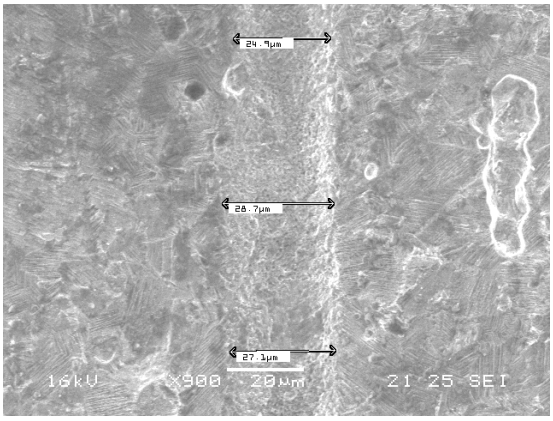

Fig. 5.14 *SEM image of microchannel of 26 µm formed on the nickel plate.*

The shape and surface finish of the microtool directly affects the workpiece accuracy and surface finish. In many applications, a smooth surface is desirable, especially for medical or biomedical applications, in flow control systems. Each application requires a microproduct of optimal shape and size (burr free). Hence,

the fabrication process needs a tool that makes a polished product. Experiments proved that the machined surface quality can be affected by the microtool end shape (for cylindrical tool), as the tool tip initiates the machining process. This surface quality is clearly visible for a blind hole, shown in Fig. 4.31(a).

Moreover, a round shaped or conical shaped tool shows good machinability than a flat ended tool because the electrolyte can enter easily in the machining area. At the beginning of the process, the material dissolution rate is higher, and no short circuit usually observed. The rate of machining decreases as the tool advances into the workpiece material. Hence, it is recommended to use a microtool of round end shape. One of the microtools used in this experiment is illustrated in Fig. 5.15.

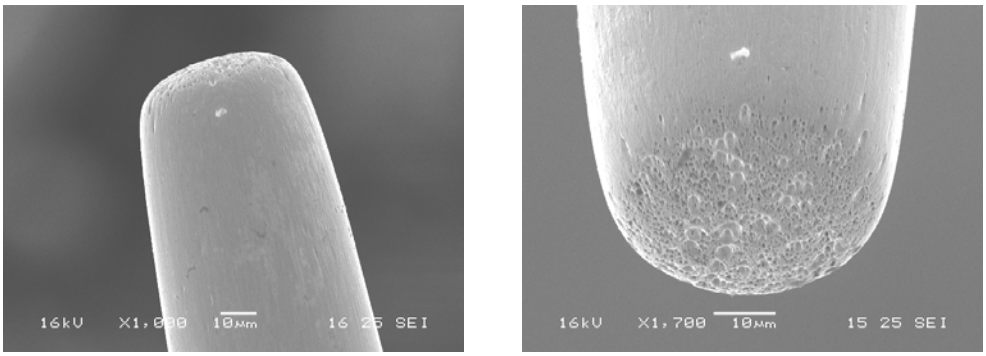

(a) *(b)*

Fig. 5.15 *SEM image of fabricated microtool used for microdrilling, (a) front side of microtool ($Ø_t$ = 48 μm), and (b) tool tip rear view.*

The common form of localized attack is sometimes observed during localized electrochemical process. The use of aggressive chemicals in connection with the electrical power attacks the workpiece surface locally. This local deterioration of workpiece, called pitting, involves a very strong bifurcation of the surface into two different zones: one zone remaining passive, and the other dissolving at a very high rate. Therefore, pitting is an electrochemical process in which small holes grow rapidly in a metal surface under the influence of a specifically aggressive electrolytic anion and an electric field. The reason for pitting is that of setting working potential higher than that at which passivation sets in. For pitting not to occur at all, the applied potential must be set below its equilibrium oxidation potential, and it is therefore will not be capable of oxidizing over the entire surface. The phenomenon has led to the notion of a pitting potential, the potential is conventionally defined as the minimum potential below which the metal will not undergo pitting process. They occur because of the action of a specific aggressive anion, commonly chloride. The high molar volume of metal chlorides, and the presence of the salt at the metal interface cause expansive stresses to form, ultimately to rupture the metal surface. During microdrilling on the nickel plate with sodium chloride solution, and applied frequency was set to 500 KHz, 15 % duty cycle, the machined surface ruptured, shown in Fig. 5.16. The applied potential higher than the equilibrium potential not only forms pits on the metal surface, it unevenly enlarges the machining area on nickel plate, shown in Fig. 5.17.

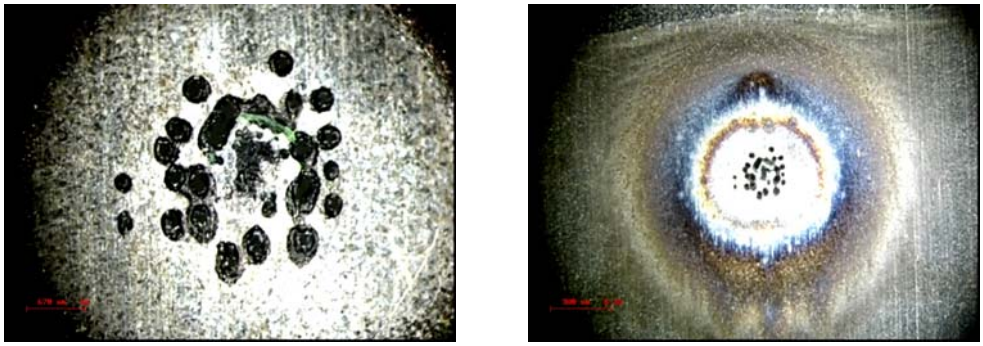

(a) *(b)*

Fig. 5.16 *Microscopic images of metal surfaces after machining, (a) pit formed on copper, and (b) pit formed on nickel plate.*

Fig. 5.17 *Overcut formed on nickel plate for higher applied potentials.*

5.5.2 Micromachining on Stainless Steel

Recently we introduced some development activities, where µECM technique is applied in practical field. To explore the application field of µECM, machining operation is performed on special grade stainless steel (AISI 403) materials. To meet the challenge of machining in a very confined zone, first machining on injection needles is tested. After successful machining on injection needle, micromachining operations are worked out on two commercially available vitrectomy needles of 23 gauge, and 25 gauge, shown in Fig. 4.37 and Fig. 4.38(*a*)–(*b*). Machining is performed on the inner cylinder of the 25 gauge vitrectomy needle. During etching with short voltage pulses, a short microtool of 53 µm in diameter was used with other appropriate machining parameters. To reduce the side gap ratio, and to fulfill the requirements (of diameter) a low feed rate was selected for the whole machining period. The needles are successfully tested, and found that the performance of the vitrectomy needle increases 40 % than prior to development work. This method has been experimented several times with the same parameters and with different parameters for reliably and reproducibly, which is expected to be a noble work.

5.6 PROCESS MONITORING AND CONTROL

To establish the in-process monitoring system, the shapes of the waveforms that formed during microdrilling on nickel plate were captured, and stored. These stored waveforms were sub-grouped into eight categories: (i) waveforms for different peak-to-peak voltage, (ii) waveforms for different baseline potentials, (iii) waveforms for various applied frequencies, (iv) waveforms for different applied duty cycles, (v) waveforms for different microtool diameters, (vi) waveforms for different microtool lengths, (vii) waveforms for variations in electrolyte temperatures, and (viii) waveforms for different microtool feed rates, to see how the shape of the waveform and different values of the corresponding wave-shape influenced on the machining rate (MRR), and also on the microproduct's quality.

Experience demonstrates that the applied potential strongly affects the kinetics of reactions occurring in electrochemical process. During machining, the anode material dissolves from a metallic sample in a clearly defined potential range. In pulsed process, the material is dissolve during the pulse-on time. In this pulsed process, the double layer charges and discharges for every pulse period. The current resulting from a change in oxidation state of the electroactive species is termed the faradaic current because it obeys Faraday's law. The faradaic current is a direct measure of the rate of the redox (oxidation) reaction. The resulting time–potential plot is a display of potential signal (vertical axis) versus the time for each pulse period. The exact shape and magnitude of the potential profile represents the amount of faradaic and non-faradaic current generated, that practically governs material dissolution process. As the faradaic effect, the product of voltage value acquired by oscilloscope, ($E^*=V_{top}$) and the time for remaining the voltage value at this level, determined how much material was dissolved for a single pulse during microdrilling processes; the total faradaic effect was calculated from the product of faradaic effect and the total time required for that particular machining, determined the total amount of material dissolved during that particular machining process.

5.6.1 Peak-to-peak Voltage

From the Fig. 5.18(a)–(c), it is observed that the value of faradaic effect increase with the increase in the peak-to-peak voltage. As a result the MRR increases with the microtool diameter, as shown in Fig. 4. 23. This observation can be explained in accordance with the equations (5.3) and (5.5), where the selected applied frequency is 1MHz, and pulse-on time is fixed to 300 ns (30% duty cycle) which is much higher than the required ultrashort voltage pulses. Therefore, effect of non-transient current becomes negligible and faradaic current dominates the material dissolution process. From the figure, the voltage values acquired by oscilloscope (V_{top}) and the time for remaining for faradaic current both increase with the increase in microtool diameter. Therefore, the faradaic effect is amplifying, and the

result is that the MRR increases rapidly with the microtool diameter. This is due to the fact, as the surface of electrode area increases, the electrical double layer capacitance increases and electrolytic resistance decreases. The decreased electrolytic resistance increases the current density into the electrolyte. Therefore, the amount of faradaic effect increases with the increase in the current density into the electrolyte, and causes rapid increase in material dissolution rate.

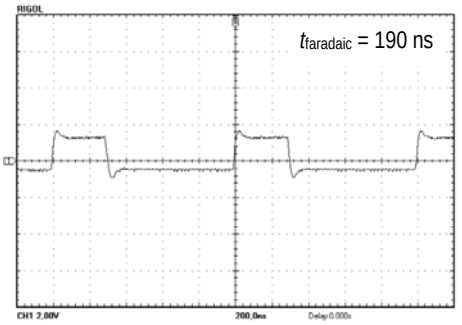

(a) V_{max}= 1.7V, V_{min}= –0.9V, V_{top}=1.27V, V_b = –0.5V

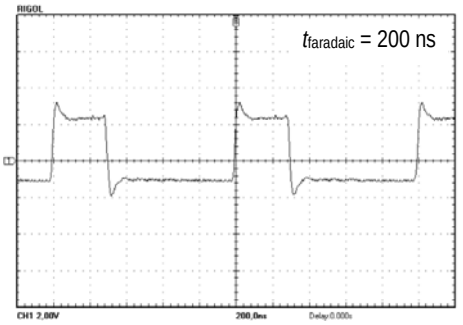

(b) V_{max}= 3.2V, V_{min}= –1.9V, V_{top}= 2.3V, V_b= –1.0V

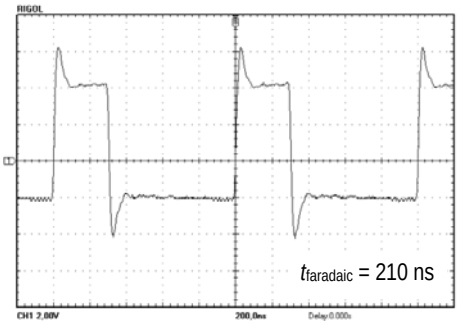

(c) V_{max}= 6.2V, V_{min}=–4.1V, V_{top}= 4.3V, V_b= –2.1V

Fig. 5.18 *Waveforms generated during machining for applied frequency, f = 1.0 MHz, τ_p = 1 µs, τ_{on} = 0.3 µs, τ_{off} = 0.7 µs, and peak-to-peak voltage of (a) 4.6 V, (b) 8.4 V, and (c) 17.2 V.*

5.6.2 Baseline Potential

Fig. 4.13 and Fig. 4.14 exhibit the influence of baseline potential on MRR and the dimension of fabricated microholes for different baseline potentials. Fig. 5.19 exhibits the waveforms generated from different baselines potentials. From fig 5.19, it is observed that the amount of faradaic current decreases and non-transient current increases with the increase in baseline potential. In this case the non-transient current is governing the process, resulting rapid reduction in the MRR. In the last figure (when V_b= 2.18 V), the amount of non-transient current is sufficiently high, therefore, no dissolution occurs in this case.

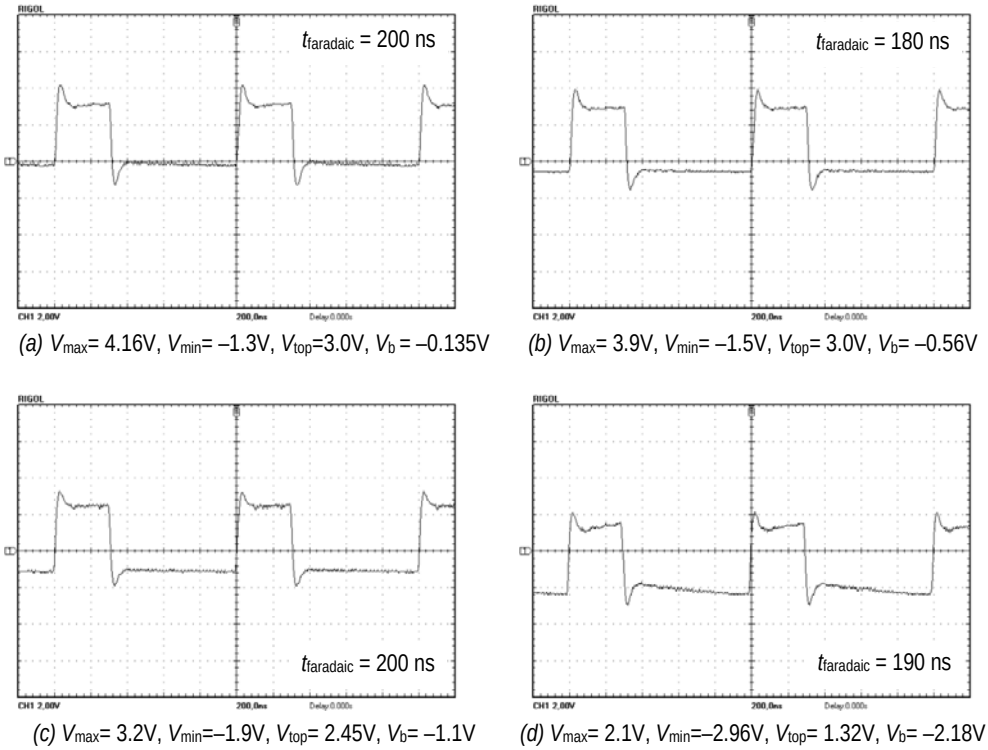

(a) V_{max}= 4.16V, V_{min}= –1.3V, V_{top}=3.0V, V_b = –0.135V

(b) V_{max}= 3.9V, V_{min}= –1.5V, V_{top}= 3.0V, V_b= –0.56V

(c) V_{max}= 3.2V, V_{min}=–1.9V, V_{top}= 2.45V, V_b= –1.1V

(d) V_{max}= 2.1V, V_{min}=–2.96V, V_{top}= 1.32V, V_b= –2.18V

Fig. 5.19 *Waveforms generated during machining for frequency, f = 1.0 MHz, τ_p = 1 µs, τ_{on} = 0.3 µs, τ_{off} = 0.7 µs, and peak voltage, V_{pp} = 15 V, and baseline potential of (a) –1.6 V, (b) –2.0 V, (c) –2.53 V, and (d) –3.6 V.*

5.6.3 Applied Frequency

Fig. 5.20 exhibits the influence of applied frequency on faradaic effect and the corresponding MRR occurred during machining. Fig. 5.21 also shows the waveforms generated during microdrilling processes. From the figure, it is clear that the amount of faradaic current decreases with an increase in applied frequency.

From the abovementioned figure, it is observed that the voltage values acquired by the oscilloscope are not in a regular manner. But the time for faradaic current ($t_{faradaic}$) is very high for low applied frequency, and decreases rapidly with an increase in applied frequency. Therefore, the faradaic effect, as well as, the total faradaic effect, decreases with applied frequency. This faradaic effect influencing on the MRR_{act}, machining time, and the dimensions of the fabricated microholes, as illustrated in Fig. 4.16 and 4.18. From these figures, it is also clear that the MRR is higher for short tool compared to long tool.

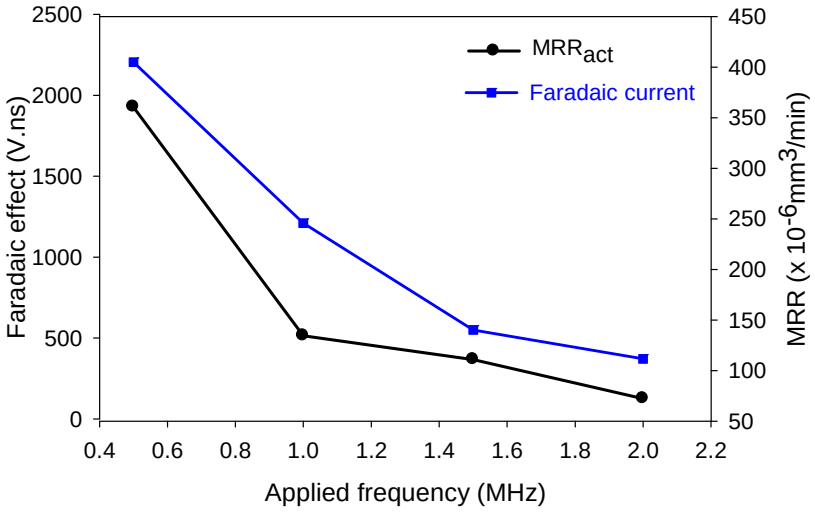

Fig. 5.20 *The effect of applied frequency on faradaic current and MRR.*

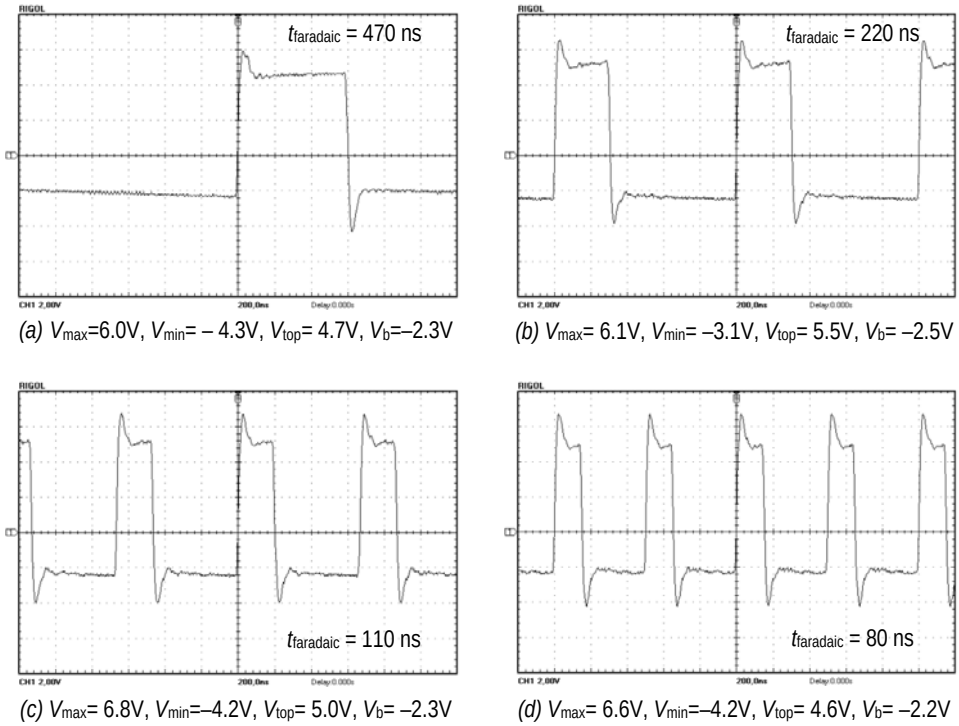

(a) V_{max}=6.0V, V_{min}= – 4.3V, V_{top}= 4.7V, V_b=–2.3V

(b) V_{max}= 6.1V, V_{min}= –3.1V, V_{top}= 5.5V, V_b= –2.5V

(c) V_{max}= 6.8V, V_{min}=–4.2V, V_{top}= 5.0V, V_b= –2.3V

(d) V_{max}= 6.6V, V_{min}=–4.2V, V_{top}= 4.6V, V_b= –2.2V

Fig. 5.21 *Waveforms generated during machining for (a) f = 0.5 MHz, τ_p = 2 µs, τ_{on} = 0.6 µs, τ_{off} = 1.4 µs; (b) f = 1 MHz, τ_p = 1 µs, τ_{on} = 0.3 µs, τ_{off} = 0.7 µs; (c) f = 1.5 MHz, τ_p = 0.67 µs, τ_{on} = 0.2 µs, τ_{off} = 4.7 µs; and (d) f = 2 MHz, τ_p = 0.5 µs, τ_{on} = 0.15 µs, τ_{off} = 0.35 µs.*

5.6.4 Duty cycle

Fig. 4.19 exhibit the influence of duty cycle on actual material removal rate and the amount of faradaic effect, and Fig. 5.22 exhibit the waveforms generated during microdrilling on nickel plate. From Fig.4.19, it is found that the amount of faradaic effect increases with duty cycle, as a consequence, the MRR_{act} increases with an increase in duty cycle. The amount of faradaic effect and MRR_{act} are found to be much higher for high percentage of duty cycle and decades with the decrease in duty cycle. This observation can be explained in accordance to the ion migration theory. The electrochemical machining is affected by the conductivity of the electrolyte which is primarily determined by the concentration of ions, and mobility of ions in a given electric field. The mobility of ions increases with the increase of pulse-on time, and smaller interelectrode gap, which ultimately increases the amount of faradaic current in the electrolyte. This increased amount of faradaic current allows not only higher material erosion rate, but also faster ramping-up when the pulse is turned on. Therefore, with the increase in the duty cycle, the MRR_{act} increases, machining time decreases, and the dimensions of microhole size increase.

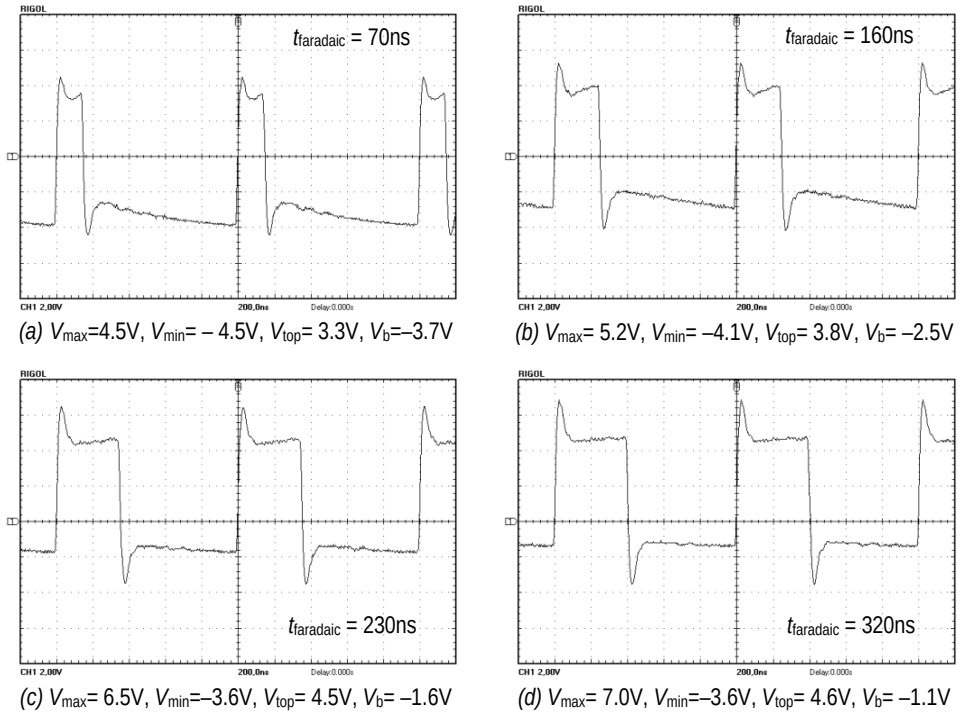

(a) V_{max}=4.5V, V_{min}= – 4.5V, V_{top}= 3.3V, V_b=–3.7V

(b) V_{max}= 5.2V, V_{min}= –4.1V, V_{top}= 3.8V, V_b= –2.5V

(c) V_{max}= 6.5V, V_{min}=–3.6V, V_{top}= 4.5V, V_b= –1.6V

(d) V_{max}= 7.0V, V_{min}=–3.6V, V_{top}= 4.6V, V_b= –1.1V

Fig. 5.22 *Waveform generated for applied frequency, f = 1MHz, τ_p= 1 µs, and duty cycle of (a) δ_τ = 15%, (b) δ_τ = 25%, (c) δ_τ = 35%, (d) δ_τ = 40%.*

5.6.5 Tool Diameter

From the Fig. 5.23, it is observed that the value of faradaic effect (V_{top}× $t_{faradaic}$) increase with the increase in the microtool diameter. As a result the MRR increases with the microtool diameter, as shown in Fig. 4. 23. This observation can be explained in accordance with the equations (5.3) and (5.5), where the selected applied frequency is 1MHz, and pulse-on time is fixed to 300 ns (30% duty cycle) which is much higher than the required ultrashort voltage pulses. Therefore, effect of non-transient current becomes negligible and faradaic current dominates the material dissolution process. From the figure, the voltage values acquired by oscilloscope (V_{top}) and the time for remaining for faradaic current both increase with the increase in microtool diameter. Therefore, the faradaic effect is amplifying, and the result is that the MRR increases rapidly with the microtool diameter. This is due to the fact, as the surface of electrode area increases, the electrical double layer capacitance increases and electrolytic resistance decreases. The decreased electrolytic resistance increases the current density into the electrolyte. Therefore, the amount of faradaic effect increases with the increase in the current density into the electrolyte, and causes rapid increase in material dissolution rate.

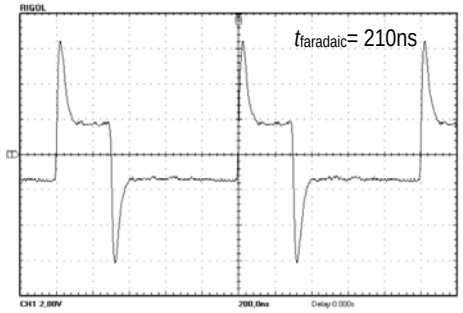

(a) V_{max}= 6.5V, V_{min}= –6.2V, V_{top}= 1.8V, V_b= –1.4V

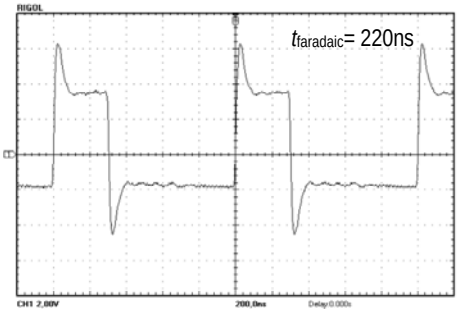

(b) V_{max}= 6.3V, V_{min}= –4.6V, V_{top}= 3.5V, V_b= –1.8V

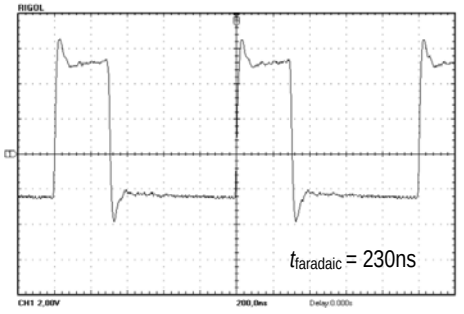

(c) V_{max}= 6.6V, V_{min}= –3.8V, V_{top}= 5.1V, V_b= –2.3V

Fig. 5.23 *Waveforms generated during machining for a microtool of (a) 21 µm, (b) 41 µm, and (c) 74 µm in diameter.*

5.6.6 Effect of Tool Length

Fig. 4.25 and Fig. 4.28 show the effects of overall tool length and the effective tool length on microdrilling process. Fig. 5.24 exhibits the waveform generated during machining. From the figure, it is evident that the amount of faradaic effect decreases with the increase in the tool length.

From Fig. 5.24, the voltage value acquired by the oscilloscope (V_{top}), and time of that voltage value at this level, ($t_{faradaic} = \tau_{on} - t^*$) both are decreasing with the increase of tool length, and the result is the gradual decrease in the faradaic current. The decreased faradaic current decreases the MRR, and increases machining time. Therefore, it is clear that MRR_{act} decreases and the machining time increases with the increase in tool length.

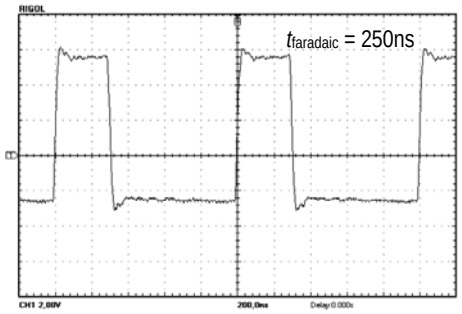

(a) V_{max}= 6.1V, V_{min}= –3.1V, V_{top}= 5.5V, V_b= –2.5V

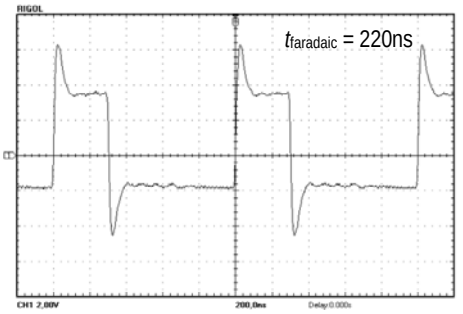

(b) V_{max}= 6.3V, V_{min}= – 4.6V, V_{top}= 3.5V, V_b= –1.8V

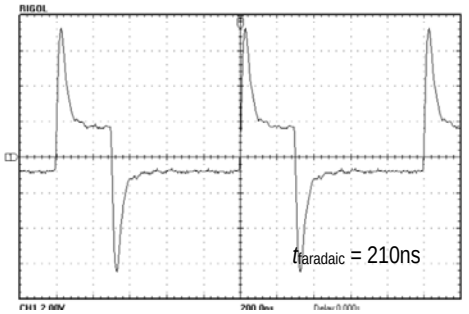

(c) V_{max}= 7.4V, V_{min}= –6.6V, V_{top}= 1.7V, V_b= –0.88V

Fig. 5.24 *Waveforms generated during machining for (a) short, (b) medium, and (c) long microtools.*

5.6.7 Effect of Electrolyte Temperature

From Fig. 5.25 it is observed that the amounts of faradaic effects are approximately same for the increases of electrolyte temperature, and non-transient effects are dominating on MRR and machining time. As the baseline potentials are

decreasing with the temperature, MRR increases and machining time decreases, as illustrated in Fig. 4.21. This phenomenon can be explained in accordance of the experience of baseline potential. The exact shape and magnitude of the time vs

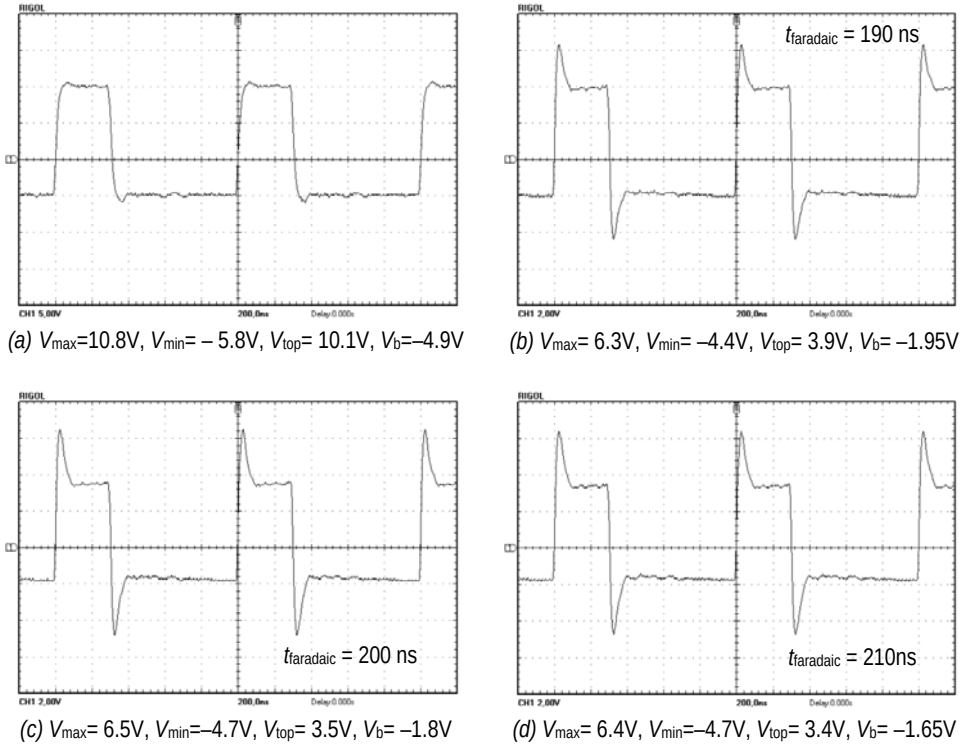

(a) V_{max}=10.8V, V_{min}= – 5.8V, V_{top}= 10.1V, V_b=–4.9V

(b) V_{max}= 6.3V, V_{min}= –4.4V, V_{top}= 3.9V, V_b= –1.95V

(c) V_{max}= 6.5V, V_{min}=–4.7V, V_{top}= 3.5V, V_b= –1.8V

(d) V_{max}= 6.4V, V_{min}=–4.7V, V_{top}= 3.4V, V_b= –1.65V

Fig. 5.25 *Waveform generated for different electrolytic temperatures of (a) waveform prior to machining, (b) 14^0 C, (c) 28^0 C, (d) 56^0 C.*

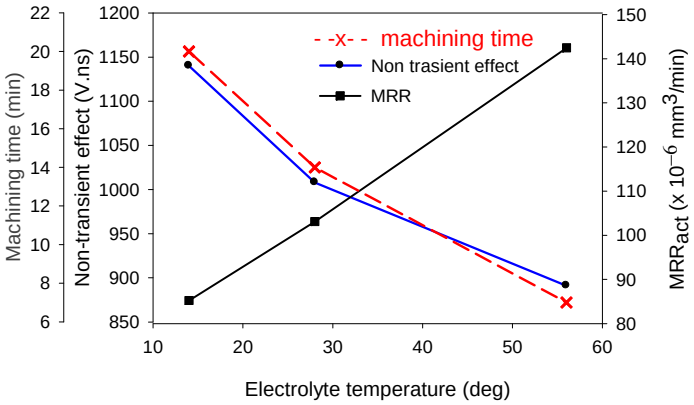

Fig. 5.26 *Effect of electrolyte temperature on non-transient current, machining time and material removal rate during microdrilling on nickel plate.*

voltage response is governed by the processes involved in the electrochemical process, and the total current is the summation of the faradaic currents for the sample and blank solutions, as well as the non-faradaic charging background current, this phenomenon can be greatly simplified by the calculation of non-faradaic non-transient state of the waveforms generated during machining. The pattern of the change of the non-transient effect, corresponding MRR, and machining time is shown in Fig. 5. 26.

5.6.8 Effect of Feed Rate on the Waveform

To perform micromachining effectively, microtool feed rate should have a linear relationship with the material removal rate. Therefore, the feed rate needs to be adjusted with MRR, which effects on the machining time. During experiment, when the applied frequency was high, and/or duty cycle was set a to reduced value, and tailored circuit was not integrated to the feed control device, a sudden jump in the current density occurred, shown in Fig. 5.27 (b), that could be monitored with the digital storage oscilloscope. This jumping in waveform indicates that possible corrective action is needed by holding the tool in stand-by mode until the current density drops under a certain value, or stop feeding and setting a reduced value for the tool feed rate to prevent the microtool tip. The attempt has been made until a

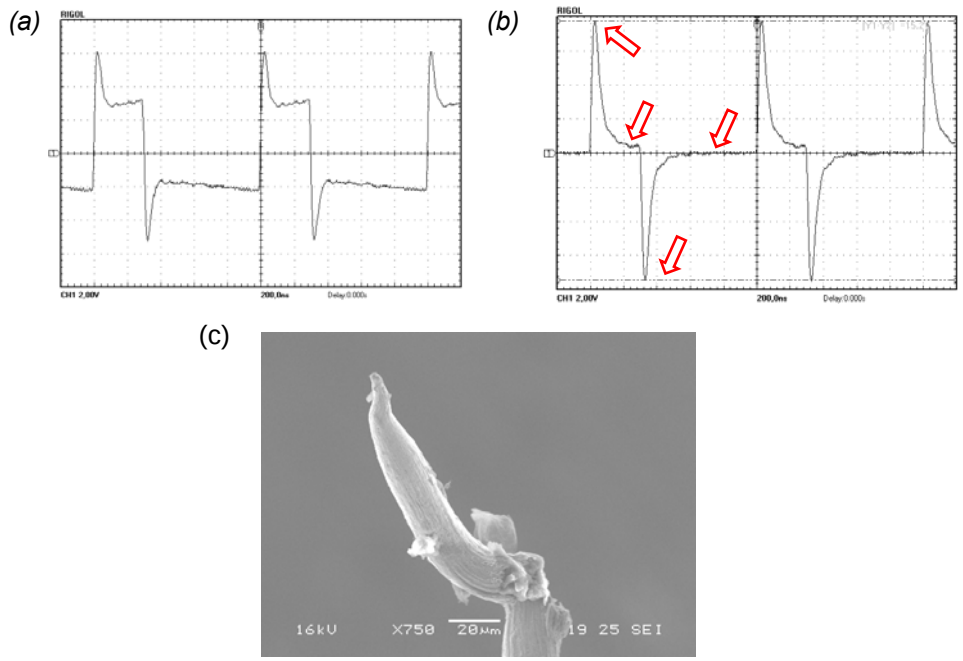

Fig. 5.27 *Effect of feed rate in micro electrochemical process, (a) waveform during machining, (b) waveform during microspark, and (c) SEM image of distorted microtool.*

stable current density is achieved. Otherwise, the high feeding rate is very much detrimental both for microtool and the workpiece, results the distortion of the microtool tip or bending the microtools in a few micrometers range of tool length. A typical short circuit state has been recorded and the distorted microtool tip is shown in Fig. 5.27(c).

5.7 CONCLUSION

This chapter presents the discussion on mathematical modeling of electrochemical micromachining material dissolution process and parametric analysis of the some important parameters how they effect on the machining process. In pulsed electrochemical process the material removal takes place during the pulse-on time only, especially in the faradaic state. Therefore, the mathematical model has been developed based on the faradaic state, and the effects of non-transient state are also discussed. During the experimental process, microtools of different size and shape are also fabricated by electrochemical process. These various shaped microtools are fabricated from a tungsten wire of 0.38 mm in diameter by reversed electrochemical process. During microtool fabrication, the effects of applied potential, electrolytic concentration, etching time, the arrangement of electrolyte basin are investigated. These pre-fabricated microtools are then used in microdrilling and microcutting process to investigate the effect of peak-to-peak voltage, baseline potential, electrolyte temperature, applied frequencies and related duty cycle, the dimension of microtool, and the feed rate used for micromachining.

At the end of this chapter, a detail study on the development of in-process monitoring system based on a digital data storage oscilloscope has also been given. The outcomes of microdrilling process, i.e. material removal rate, machining time, the dimensions of the fabricated microholes are predicted from the waveforms generated during machining and control action has been taken accordingly. Number of short circuits is also recorded. From this chapter it can be concluded that: (i) the rate of machining increases with the increase of peak-to-peak voltage with a suitable value of baseline potential; (ii) MRR and machining time respectively decreases and increases with the applied frequency; (iii) the MRR increases with the increase in duty cycle for the same applied frequency, (iv) a microtool of large diameter takes more time for machining with higher rate of MRR, (v) the rate of machining decreases with the increases in microtool length, and a short microtool makes the process faster, on the other hand, a long microtool leaves better precision than a short microtool during microdrilling, (vi) the raise in the electrolyte temperature makes the process faster, (vii) the tool feed rate has a substantial effect on the dimension of fabricated microhole. The equipment used in micromachining process has also a big influence on the precision of the final product. Prior to machining, the cleaning (removing foreign particle) and washing of fabricated microtool offers a better finished product. The development activity on vitrectomy needle and injection needle has also discussed.

Chapter 6

Conclusion

This section comprises an overall conclusion based on the outcomes from the experimental work done during last three years, research gap and limitations of work, and scope and recommendation for future work. The conclusion section combines the overall findings in relation to this experimental research scheme. The research gap will try to find out the lacking or bottlenecks of this research and finally further research ideas and directions are suggested.

6.1 CONCLUSION

This study details the development of experimental setup with precision control for electrochemical micromachining and investigates the effects of machining parameters that control the machining performance at micron scale. Based on the experimental activities performed during the last three years, the following conclusion can be drawn:

Fabrication of microtools:

(i) Microtools of desired dimension can be formed by reverse electrochemical process. During the fabrication of microtools by μECM process, it is observed that the applied potential electrolytic concentration, etching time, and the arrangement of electrolyte basin have substantial effects on the diameter of fabricated microtools. Variation in diameter with time increases with the increase in both electrolyte concentration and applied potentials. Tool length remains constant over a certain period of time depending on concentration of electrolyte. The lower the concentration the higher the time period over which the tool length remained constant. The microtools fabricated from vertically upward and horizontal directions have less taper angle than that of the microtools fabricated in vertically downward direction. The use of AC applied potential needs shorter machining time to fabricate a microtool. Machining by AC current contaminates less than the DC or pulsed power supply.

(ii) During the fabrication of conical shaped microtools, electrolytic concentration has substantial effects on the dissolution of tool material determining the shape of microtool tip angle. It is possible to control the angle of the tip by changing either the concentration of electrolyte or the etching time. The angle of the microtool tip changes with the counter electrode (circular electrode) is also observed.

Parametric effect

From the results of experiments conducted to check the effects of applied potentials, applied frequency and duty cycles, electrolyte temperature, and the dimension of microtools on electrochemical microdrilling, following conclusions can drawn:

(i) The MRR increases and machining time decreases with the increase in the peak-to-peak voltage. The side gap ratio of the fabricated microholes decrease with the increase in peak-to-peak voltage. The number of short circuits increases with the decrease in applied voltage.

(ii) Micromachining with an applied potential higher than the equilibrium potential in a corrosive environment is very much sensitive for thin metal plates. The use of aggressive chemicals in connection with the electrical power source attacks the workpiece surface, produces a ruptured surface.

(iii) The tool electrode baseline potential has a considerable effect on the MRR, machining time and number of short circuits. MRR decreases and machining time increases with the increase in the baseline potential. The baseline potential needs to be in a suitable range for micromachining.

(iv) The MRR and machining time decreases and increases respectively with the increase in applied frequency for both the long and short microtool for a particular combination of micromachining parameters. The number of short circuits also increases with the increase of applied frequency. The entrance and exit diameters are found to be smaller because of less amount of side erosion. For the same range of pulse on-time and applied frequency, the MRR_{act} is much higher and machining time is smaller for the short tool as compared to long tool.

(v) The MRR increases and the machining time decreases with an increase in duty cycle. No short circuit occurs for higher duty cycles even at a very high feed rate used for μECM. For higher duty cycles, the microhole diameters cannot be controlled precisely as the side erosion increases rapidly and the machining time is very low compared to lower duty cycles.

(vi) The MRR increases and the machining time decreases with an increase in electrolyte temperature. Machining is possible at a sufficiently high feed rate for higher electrolyte temperature. For higher electrolytic temperature, the diameters of fabricated microholes are found to be smaller that add to precision in products' dimension.

(vii) As the microtool diameter becomes larger, the electrolyte potential decreases resulting in higher MRR and higher machining time but lower

taper angle of machined hole. The ratio of the entrance gap to exit gap decreases with increased machining time and results in the reduced taper angle of the microholes.

(viii) The MRR and machining time decreases and increases respectively with the increase in overall tool length. The number of short circuits is also found to increase with the increase in microtool length. The entrance and exit diameters are found larger for shorter tool length, i.e. overcut is higher for shorter tools.

(ix) MRR decreases and the machining time increases with an increase in tool dipping length. The number of short circuits also increases with the tool dipping length even at lower feed rates. A short dipping length produces a precise hole with lower conicity and faster machining time but with greater side erosion.

(x) The effect of conical shaped microtool is also tested as a performance measure of combine effect of tool diameter and tool length. The result indicates that the angle of micro hole increases with decrease in tool feed rate. For better precision, the tool feed rate is kept as high as possible to reduce the side erosion and hence to obtain a precise conical microhole.

(xi) The feed rate (downward feed during microdrilling) needs to be adjusted to the MRR. Otherwise, the frequent occurrence of short circuit increases the machining time. After machining, the tool needs to be withdrawn (upward feed) from the machining zone immediately. Otherwise it enlarges the microhole entrance to some extent, i.e., conicity of microhole increases.

(xii) During microcutting or multiple hole drilling, the tool needs to be pulled over the electrolyte level while the tool advances from one machining position to another to avoid the microchannel formation.

Fabrication of microholes

By using the prefabricated microtools of cylindrical and conical shape, machining has been performed on nickel plate and stainless steel needle.

(i) The entrance and exit diameter of the machined microhole are not same even for a cylindrical microtool is used. To evaluate the total material removed during machining, both entrance and exit diameters need to be considered.

(ii) Conical shaped micro holes of different diameters and micro-nozzle array have been fabricated on nickel plate by ECM process. It is expected that various three dimensional shapes can be machined using the fabricated microtools. During machining, the tool should be fed along the workpiece and withdrawn after machining at a possible higher rate for better accuracy.

(iii) Various shaped microholes are also fabricated on high grade stainless steel (AISI 403) as a development of existing products. It can be concluded that electrochemical micromachining can be done in a confined zone with precision.

Process monitoring and control

This study details the development of in-process monitoring system based on a digital data storage oscilloscope during electrochemical microdrilling. The outcomes of the process, i.e., the MRR, machining time, the dimensions of fabricated microholes, etc., are predicted from the waveform generated during machining and control action has been taken accordingly. From these experiments, it is evident that the waveform generated during machining bears significant information about the MRR, machining time, and the dimension of fabricated microholes. During machining, frequently observed short circuit phenomenon can be monitored and controlled as well.

6.2 RESEARCH LIMITATIONS

During micromachining:

(i) It was not possible to determine the value of electrolyte resistivity to calculate the theoretical value of MRR and hence, to compare the theoretical value with actual value of MRR.

(ii) There was not any visual inspection facility to measure the gap between the tool and workpiece.

6.3 RECOMMENDATION FOR FUTURE WORK

Based on the findings of this study, following important issues to be resolved and needs further research on:

(i) fabrication of microtools providing rotation to the tool specimens and realization of microtool dimension under rotary motion, which is considered an important step towards achieving a high aspect ratio microtool.

(ii) comparison of microtools fabricated under AC, DC and pulsed voltage.

(iii) machining other materials under a chemically safe environment, i.e. use of safe and non-hazardous electrolytes for the fabrication of microproducts.

(iv) searching for possibility of a new electrolyte comparing its effectiveness for microtool fabrication with the existing electrolyte.

References

1. Jackson M.J., Micro- and nanofabrication, in: Jackson M.J. (ed.), Microfabrication and nanomanufacturing, Taylor & Francis Group, 2006, pp. 1–32.
2. Brown J.A., **Modern manufacturing processes**, 1st ed., Chapter 23, Computer integrated manufacturing, Industrial Press Inc, 1991
3. Ehrfeld W., Hessel V., Löwe H., **Microreactors – New technology for modern chemistry**, Wiley-VCH, Weinheim, 2000.
4. Ehrfeld W., Hessel V., Löwe H., "Extending the knowledge base in microfabrication towards themical engineering and fluid dynamic simulation", in: Proceedings of the 4th International Conference on Microreaction Technology, IMRET 4, Atlanta, 2000, pp. 3–22.
5. Wang Y., Yuan W., Jiang C., Prototyping of the computer integrated manufacturing processes of MEMS in a desktop micro-factory, in: Yan X. T., Jiang C., Eynard, B. (Eds.), Advanced design and manufacture to gain a competitive edge– New manufacturing techniques and their role in improving enterprise performance, Springer-Verlag London Ltd, 2008, pp. 767–773.
6. Cagnon L., Kirchner V., Kock M., Schuster R., Ertl G., Gmelin W. T., Kück H., "Electrochemical micromachining of stainless steel by ultrashort voltage pulses", *Z. Phys. Chem*., Vol. 217, 2003, pp. 299–313.
7. Hung J.C., Yan B.H., Liu H.S., Chow H.M., "Micro-hole machining using micro-EDM combined with electropolishing", *Journal of Micromechanics and Microengineering*, Vol. 16, 2006, pp. 1480–1486.
8. Masuzawa T., "State of the art of micromachining", *Annals of the CIRP*, Vol. 49, no. 2, 2000, pp. 473–488.
9. Bhattacharyya B., Doloi, B., Sridhar P. S., "Electrochemical micro-machining: new possibilities for micro– manufacturing", *Journal of Materials Processing Technology*, Vol. 113, 2001, pp. 301–305.
10. Chattopadhyay A.K., **Manufacturing Processes II**, Module 4, Non-conventional machining, Version 2 ME, IIT Kharagpur, India. Available on: http://nptel.iitm.ac.in/courses/Webcourse-contents/IIT%20Kharagpur/Manuf%20Proc%20II/pdf/LM-37.pdf
11. Lu X., Leng Y., **"**Electrochemical micromachining of titanium surfaces for biomedical applications", *Journal of Materials Processing Technology*, Vol. 169, no. 2, 2005, pp. 173–178.
12. El-Hofy H., **Advanced machining Processes**, McGraw-Hill, 2005, pp. 2–4.

13. Tanigushi N., “Current status in and future trends of ultra precision machining and ultra fine materials processing,” *Annals of the CIRP*, Vol. 32, no. 2, 1983, pp. 573–582.

14. Cone R.J., Barnes S., Patricia L**., How the new technology works: A guide to high-tech concepts**”, Greenwood Publishing Group, 1998, pp. 58–61.

15. Mahdavinejad R., Hatami, M., “On the application of electrochemical machining for inner surface polishing of gun barrel chamber*”, Journal of Materials Processing Technology*, Vol. 202, 2008, pp. 307–315.

16. Schmekel H., “Functional models and design solutions”, *Annals of the CIRP*, Vol. 38, no. 1, 1989, pp. 129–32.

17. Ulrich K.T., Eppinger S.D., **Product design and development**, McGraw-Hill, New York, 1995.

18. Alting L., Kimura F., Hansen H.N., Bissacco G., “Micro Engineering”, *Annals of the CIRP*, Vol. 52, no. 2, 2003, pp. 635–657.

19. Bhattacharyya B., Munda J., Malapati, M., “Advancement in electrochemical micro-machining”, *International Journal of Machine Tools & Manufacture*, Vol. 44, 2004, pp. 1577–1589.

20. Datta M., “Microfabrication by electrochemical metal removal”, *IBM Journal of Research and Development*, Vol. 42, no. 5, 1998, pp. 655–669.

21. Coetzee R., Beer D., Dimitrov D., Truscott M., Gorlach I., Van T.D., Schalkwyk, Land K., Micro-manufacturing strategy for South Africa, Micro-Manufacturing Strategy, Vol. 1.5, 2007, pp. 1–32.

22. Qin Y., Brockett A., Ma Y., Razali A., Zhao J., Harrison C., Pan W., Dai X., Loziak D., “Micro-manufacturing: research, technology outcomes and development issues”, *International Journal of Advanced Manufacturing Technology*, Vol. 47, 2010, pp. 821–837.

23. Bachmann M., EECSI 179 2006 in: Micro-manufacturing strategy for South Africa, Micro-Manufacturing Strategy, Vol. 1.5, 2007, pp. 1–32.

24. Datta M., Shenoy R.V., Romankiw L.T., “Recent advances in the study of electrochemical micromachining, *Journal of Engineering for Industry*, Vol. 118, 1996, pp. 29–36.

25. Purcar M., Bortels L., Bossche B.V., Deconinck J., “3D electrochemical machining computer simulations”, *Journal of Materials Processing Technology*, Vol. 149, 2004, pp. 472–478.

26. Data M., Harris D., “Electrochemical micromachiing: An environmentally friendly, high speed processing technology”, *Electrochimica Acta*, Vol. 42, no. 20–22, 1997, pp. 3007–3013.

27. Davydov A.D., Volgin V.M., Lyubimov V.V., “Electrochemical machining of metals: fundamentals of electrochemical shaping”, *Russian Journal of Electrochemistry*, Vol. 40, no. 12, 2004, pp. 1230–1265.

28. Ryu S.H., “Micro fabrication by electrochemical process in citric acid electrolyte”, *Journal of Materials Processing Technology*, Vol. 209, 2009, pp. 2831–2837.

29. Bhattacharyya B., Mitra S., Boro A.K., “Electrochemical machining: new possibilities for micromachining”, *Robotics and Computer Integrated Manufacturing*, Vol. 18, 2002, pp. 283–289.

30. Boden P.J., McGeough J.A., “Electrochemistry in the service of engineering”, *Philosophical Transactions of the Royal Society of London A*, Vol. 302, 1468, 1981, pp. 297–313.

31. Wang M.H., Zhu D., Peng W., “Experimental research on electrochemical micromachiningy”, in: Advanced design and manufacture to gain a competitive edge– New manufacturing techniques and their role in improving enterprise performance, Yan X.T., Jiang C., Eynard B. (Eds.), Springer-Verlag Ltd., 2008, pp. 775–784.

32. Costa H.L., Hutchings I.M., “Development of a maskless electrochemical texturing method*”, Journal of Materials Processing Technology*, Vol. 209, no. 8, 2009, pp. 3869–3878.

33. Klemm S.O., Pust S.E., Hassel A.W., Hüpkes J., Mayrhofe K.J.J., “Electrochemical texturing of Al-doped ZnO thin films for photovoltaic applications”, *Journal of Solid State Electrochemistry,* DOI: 10.1007/s10008-011-1313-z.

34. Glew, D.A., Staines A.D., Cannon A.J., Dunlop, R.N., “Electrochemical broaching apparatus”, United States patent 5314598, 1994. Available on: http://www.freepatentsonline.com/5314598.html

35. Aurich J. C., Dornfeld D., Arrazola P. J., Franke V., Leitz L., Min S., “Burrs–analysis, control and removal”, *Annals of the CIRP–Manufacturing Technology*, Vol. 58, 2009, pp. 519–542.

36. Kim B.H., Park B.J., Chu C.N., “Fabrication of multiple electrodes by reverse EDM and their application in micro ECM”, *Journal of Micromechanics and Microengineering*, Vol. 16, no. 4, 2006, pp. 843–850.

37. Wang M.H., Zhu D., “Fabrication of multiple electrodes and their application for micro-holes array in ECM”, *International Journal of Advanced Manufacturing Technology*, Vol. 41, 2009, pp. 42–47.

38. Zhu D. Wang W., Fang X.L., Qu N.S., Xu Z.Y., “Electrochemical drilling of multiple holes with electrolyte-extraction”, *Annals of the CIRP*, Vol. 59, no. 1, 2010, pp. 239–242.

39. El-Taweel T.A., Ebeid S.J., “Effect of hybrid electrochemical smoothing–roller burnishing process parameters on roundness error and micro-hardness”, *International Journal of Advanced Manufacturing Technology*, Vol. 42, 2009, pp. 643–655.

40. Osaka T., Yoshino M., “Electrochemical Fabrication Process for ULSI Interconnects”, in: Osaka T., Datta M., Diamand S.Y. (Eds), Electrochemical Nanotechnologies, Springer Science & Business Media, 2010, pp. 225–274.

41. Lim Y.J., Lim Y.M., Kim S.H., “Fabrication of tungsten micro-punch for micronozzles”, *Review of Scientific Instruments*, Vol. 72, No. 8, 2001, pp. 3470–3472.

42. Bayt R.L., Analysis, fabrication and testing of a MEMS-based micropropulsion system, Ph D Thesis, MIT, 1999. Access: 3 Nov 2011.

Available on: http://acdl.mit.edu/Technical_Reports/Bayt_Thesis.pdf

43. Louwerse M.C., Jansen H.V., Groenendijk M.N.W., Elwenspoek M.C., "Nozzle fabrication for micropropulsion of a microsatellite", *Journal of Micromechanics and Microengineering*, Vol. 19, no. 4, 2009, pp. 1–9.
44. Jung D., Wang W.L., Knafl A., Jacobs T.J., Hu S.J. Assanis D.N. "Experimental investigation of the abrasive flow machining effects on injector nozzle geometries, engine performance and emissions in a DI diesel engine', *International Journal of Automotive Technology*, Vol. 9, no. 1, 2008, pp. 9–15.
45. Kock M., Kirchner V., Schuster R., "Electrochemical micromachining with ultrashort voltage pulses–a versatile method with lithographical precision", *Electrochimica Acta*, Vol. 48, 2003, pp. 3213–3219.
46. Rahman M.A., Rahman M., Senthil Kumar A., Lim H.S., Asad A.B.M.A., "Development of micropin fabrication process using tool based micromachining", *International Journal of Advanced Manufacturing Technology*, Vol. 27, 2006, pp. 939–944.
47. Choi S.H., Ryu S.H., Choi D.K., Chu C.N., "Fabrication of WC micro-shaft by using electrochemical etching", *International Journal of Advanced Manufacturing Technology*, Vol. 31, 2007, pp.682–687.
48. Habib M.A., Gan S.W., Rahman M., 'Fabrication of complex shape electrodes by localized electrochemical deposition', *Journal of Materials Processing Technology*, Vol. 209, 2009, pp. 4453–4458.
49. Hobara R., Yoshimoto S., Hasegawa S., "Dynamic electrochemical-etching technique for tungsten tips suitable for multi-tip scanning tunneling microscopes", *e-Journal of Surface Science and Nanotechnology*, Vol. 5, 2007, pp. 94–98.
50. Fan Z.W. Hourng L.W., "The analysis and investigation on the microelectrode fabrication by electrochemical machining", *International Journal of Machine Tools & Manufacture*, Vol. 49, 2009, pp. 659–666.
51. Ozkeskin F.M., "Feedback controlled high frequency electrochemical micromachining", M Sc Thesis, Texas A&M University, 2008.
52. Mahalik N.P., **Micromanufacturing and nanotechnology**, Springer-Verlag, Heidelberg, 2006.
53. Schuster R., Kirchner V., Allongue P., "Electrochemical micromachining", *Science*, Vol. 289, no. 5476, 2000, pp. 98 – 101.
54. Kirchner V., Xia X., Schuster R., "Electrochemical nanostructuring with ultrashort voltage pulses", *Accounts of Chemical Research*, Vol. 34, no. 5, 2001, pp. 371–377.
55. Löwe H., Ehrfeld W., Schiewe J., Micro-electroforming of miniaturized devices for chemical applications, in: Schultze J.W., Osaka T., Datta M. (Eds.), Electrochemical Microsystems Technologies, Taylor & Francis, London, 2002, pp. 245–268.
56. Kang K.N., Jin Y., Goettert J., Ajmera P.K., "Shape controllable micro-nozzle fabrication", *Microsystems Technology*, Vol. 14, 2008, pp.1641–1646.

57. Datta M., Landalt D., “Fundamental aspects of electrochemical micro-fabrication”, *Electrochimica Acta*, Vol. 45, 2000, pp. 2535–2558.

58. Briston K.J., Cullis A.G., Inkson B.J., “Fabrication of a novel SEM microgripper by electrochemical and FIB techniques” *Journal of Micromechanics and Microengineering*, Vol. 20, no. 1, 2010, 28–32.

59. Brussel H.V., Peirs J., Reynaerts D., Delchambre A., Reinhart G., Roth N., Week M., Zussman E., “Assembly of microsystems”, *Annals of the CIRP*, Vol. 49, no. 2, 2000, pp. 451–472.

60. Todd R.H., Allen, D.K., Alting, L., **Manufacturing processes reference guide**, 1st ed., Industrial Press Inc., 1994, pp. 198–199.

61. History- from machining technique to versatile ECM technique, Access: 9 Nov, 2010. Available on: http://www.electrochemicalmachining.com/ecm/history

62. Li Z., Yuan G., “Experimental investigation of micro-holes in electrochemical machining using pulse current”, in Proceedings of the 3rd IEEE International Conference on Nano/Micro Engineered and Molecular Systems, January 6-9, 2008, China

63. McGeough J.A., “Electrochemical machining (ECM)”, Electrochemistry encyclopedia. Access: 9 Nov, 2010. Available on: http://electrochem.cwru.edu/encycl/art-m03-machining.htm

64. Data M., Harris D., “Electrochemical micromachiing: An environmentally friendly, high speed processing technology”, *Electrochimica Acta*, Vol. 42, nos. 20–22, 1997, pp. 3007–3013.

65. Wang J., **Analytical electrochemistry**, 3rd ed., John Wiley & Sons, Inc, 2006, pp. 2–24.

66. Wright M.R., **An Introduction to aqueous electrolyte solutions**, John Wiley & Sons Ltd, 2007, pp. 33–51.

67. McGeough J.A., **Advanced methods of machining**, 1st ed., Chapman and Hall Ltd, 1988, pp. 55-88.

68. Basu S.N., Sarin V.K., “Oxidation behavior of WC–Co”, *Material Science and Engineering A*, Vol. 209, 1996, pp. 206–212.

69. Andersson K.M., Bergstrom L., “Oxidation and dissolution of tungsten carbide powder in water”, *International Journal of Refractory Metals and Hard Materials*, Vol. 18, no. 2-3, 2000, pp. 121–129.

70. Girault H.H., **Analytical and physical electrochemistry**, 1st ed. EPFL Press, 2004, pp. 221–222.

71. Maeda R., Chikamori K., Yamamoto Y., “Feed rate of wire electrochemical machining using pulsed current”, *Precision Engineering*, Vol. 6, no. 4, 1984, pp. 193–199.

72. Li D., Zhu D., Li H., “Microstructure of electrochemical machining using inert metal mask”, *International Journal of Advanced Manufacturing Technology*, DOI: 10.1007/s00170-010-3025-4.

73. Newman J., Thomas-Alyea K.E., **Electrochemical systems**, 3rd ed., Wiley Interscience, Hoboken, 2004.

74. Hong S.Y., “Scanning tunneling microscopy for very large-scale integration (VLSI) inspection”, in: Cohen S.H., Lightbody M.L. (Eds.), Atomic force microscopy/ Scanning tunneling microscopy 2, Plenum Press, New York, 1997, pp. 7–22.

75. Bryant P.J., Kim H.S., Zheng Y.C., Yang R., “Technique for shaping scanning tunneling microscope tips”, *Review of Scientific Instruments*, Vol. 58, no. 6, 1989, pp. 1115.

76. Morikawa H., Goto K., “Reproducible sharp-pointed tip preparation for field ion microscopy by controlled ac polishing”, *Review of Scientific Instruments*, Vol. 59, no. 10, 1988, pp. 2195–2197.

77. Fotino M., “Calibration of atomic force microscope tips”, *Review of Scientific Instruments*, Vol. 64, no. 7, 1993, pp. 1868–1873.

78. Lim Y.M., Kim S.H., “An electrochemical fabrication method for extremely thin cylindrical micropin”, *International Journal of Machine Tools & Manufacture*, Vol. 41, 2003, pp. 2287–2296.

79. Lucier A.S., “Preparation and characterization of tungsten tips suitable for molecular electronics studies”, M Sc Thesis, McGill University, 2004.

80. Bai C., **Scanning tunneling microscopy and its applications**, 2nd ed, Shanghai Scientific and Technical Publishers, 1992, pp. 80–82.

81. Wickramasinghe H.K., Etensions of STM, in: Stroscio J.A., Kaiser, W.J., (eds), **Scanning tunneling microscopy**, Academic Press Inc., 1993, pp. 80–82.

82. Edwards G.J., Pearce P.R., “A comparison of AC and DC electrochemical etching techniques for the fabrication of tungsten whiskers”, *Journal of Physics D: Applied Physics*, Vol. 11, 1978.

83. Chen C.J., **Introduction to scanning tunneling microscopy**, Oxford University Press, 1993, pp. 282–290.

84. Garnaes J., Kragh F., Mørch K.A., Thölén A.R., “Transmission electron microscopy of scanning tunneling tips”, *Journal of Vacuum Science & Technology A*, Vol. 8, no. 1, 1990, pp. 441– 444.

85. Guise O.L., Joachim W.A., Jung M.C., Goughnour P.C., Yates Jr J.T., “Reproducible electrochemical etching of tungsten probe tips”, *Nanoletters*, Vol. 2, no. 3, 2002, 191–193.

86. Biegelsen D.K., Ponce F.A., Tramontana J.C., Koch S.M., “Ion milled tips for scanning tunneling microscopy”, *Applied Physics Letter*, Vol. 50, no. 11, 1987, pp. 696–698.

87. Ekvall I., Wahlström E., Claesson D., “Preparation and characterization of electrochemically etched W tips for STM”, *Measurement Science and Technology*, Vol. 10, no. 1, 1999, pp. 11–18.

88. Schulze H.-P., Borkenhagen D., Burkert, S., “Demands on process and process energy sources for the electro-erosive and electrochemical micro machining”, *International Journal of Material Formation*, Vol. 1, 2008, pp.1383 –1386.

89. Ibe J.P., Bey Jr. P.P., Brandow S.L., Brizzolara R.A., Burnham N.A., DiLella

D.P., Lee K.P., Marrian C.R.K., Colton R.J., “On the electrochemical etching of tips for scanning tunneling microscopy” *Journal of Vacuum Science and Technology A*, Vol. 8, no. 4, 1990, pp. 3570–3575.

90. Kerfriden S., Nahlé A.H., Campbell S.A., Walsh F.C., Smith J.R., “The electrochemical etching of tungsten STM tips”, *Electrochimica Acta*, Vol. 43, nos. 12–13, 1998, pp. 1939–1944.
91. Datta M., Landolt D., “Electrochemical machining under pulsed current conditions”, *Electrochimica Acta*, Vol. 26, no. 7, 1981, pp. 899–907.
92. Kenney J.A., Hwang G.S., “Electrochemical machining with ultrashort voltage pulses: modeling of charging dynamics and feature profile evolution”, *Nanotechnology*, Vol. 16, 2005, pp. s309–s313.
93. Ahn S.H., Ryu S.H., Choi D.K., Chu C.N., “Electro-chemical micro drilling using ultra short pulses”, *Precision Engineering*, Vol. 28, 2004, pp. 129–134.
94. Bard A.J., Faulkner L.R., **Electrochemical Methods: Fundamentals and Applications**, 2nd ed., John Wiley & Sons, New York, 2001.
95. Park B.J., Kim B.H., Chu C.N., “The effects of tool electrode size on characteristics of micro electrochemical machining”, *Annals of the CIRP*, Vol. 55, no. 1, 2006, pp. 197–200.
96. Bhattacharyya B., Munda J., “Experimental investigation into electrochemical micromachining (EMM) process”, *Journal of Materials Processing Technology*, Vol. 140, 2003, pp. 287–291.
97. Kozak J., Rajurkar K., P., Wei B., “Study of dimensional limitations of electrochemical micro-machining”, Transaction of the ASME, *Journal of Engineering for Industry*, Vol. 116, no. 3, 1994, pp. 316-323.
98. Kurita T., Chikamori K., Kubota S., Hattori M., “A study of three-dimensional shape machining with an ECμM system”, *International Journal of Machine Tools and Manufacture*, Vol. 46, 2006, pp. 1311–1318.
99. Kirchner V., Xia X., Schuster R., “Electrochemical nanostructuring with ultrashort voltage pulses”, *Accounts of Chemical Research*, Vol. 34, no. 5, 2001, pp. 371–377.
100. Rajurkar K.P., Wei B., Kozak J., McGeough J.A., “Modelling and monitoring interelectrode gap in pulse electrochemical machining”, *Annals of the CIRP*, Vol. 44, no. 1, 1995, pp. 177-180.
101. Kirchner V., Cagnon L., Schuster R., Etrl G., “Electrochemical machining of stainless steel microelements with ultrashort voltage pulses”, *Applied Physics Letter*, Vol. 79, 2001, pp. 1721–1723.
102. Kim B.H., Ryu S.H., Choi D.K., Chu C.N., “Micro electrochemical milling”, *Journal of Micromechanics and Microengineering*, Vol. 15, 2005, pp.124–129.
103. Zhang Z., Zhu D., Qu N., Wang M., “Theoretical and experimental investigation on electrochemical micromachining”, *Microsystems Technology,* Vol. 13, 2007, pp. 607–612.
104. Jo C.H., Kim B.H., Chu C.N., “Micro electrochemical machining for complex internal micro features”, *CIRP Annals–Manufacturing Technology*, Vol. 58,

2009, pp.181–184.

105. Zhu D., Wang K., Qu N.S., “Micro wire electrochemical cutting by using In-situ fabricated wire electrode”, *Annals of the CIRP*, Vol. 56, no. 1, 2007, pp. 241–244.
106. Kozak J., Gulbinowicz D., Gulbinowicz Z., “The mathematical modeling and computer simulation of pulse electrochemical micromachining”, *Engineering Letter*, Vol. 16, no. 4, November 2008.
107. Sen M., Shan H.S., “Analysis of hole quality characteristics in the electro jet drilling process”, International Journal of Machine Tools & Manufacture, Vol. 45, 2005, pp. 1706–1716.
108. Luo Y.F., “Differential equations for the ultra-fast transient migration in electrolytic dissolution”, *Electrochemistry Communications*, Vol. 8, 2006, pp. 353–358.
109. Uhlmann E., Doll U., Forster R., Schikofsky R., “High precision manufacturing using PEM”, Proceedings of the International Symposium for Electromachining (ISEM XIII), Bilbao, Spain (vol. 1), 2001, pp. 261–268.
110. Bilgi D.S., Jain V.K., Shekhar R., Kulkarni A., “Hole quality and inter-electrode gap dynamics during pulse current electrochemical deep hole drilling”, *International Journal of Advanced Manufacturing Technology*, Vol. 34, 2007, pp. 79–95.
111. Ali S., Hinduja S., Atkinson J., Pandya M., “Shaped tube electrochemical drilling of good quality holes”, *CIRP Annals - Manufacturing Technology*, Vol. 58, 2009, pp. 185–188.
112. Lee E.S., Shin T.H., Kim B.K., Baek S.Y., “Investigation of short pulse electrochemical machining for groove process on Ni-Ti shape memory alloy”, *International Journal of Precision Engineering and Manufacturing*, Vol. 11, no. 1, 2010, pp. 113–118.
113. Landolt D., Chauvy P.F., Zinger O., “Electrochemical micromachining, polishing and surface structuring of metals: fundamental aspects and new developments”, *Electrochimica Acta*, Vol. 48, 2003, pp. 3185–3201.
114. Perera K., Dissanayake M.A.K.L., “Conductivity variation of the liquid electrolyte, EC : PC : $LiCF_3SO_3$ with salt concentration”, *Sri Lankan Journal of Physics*, Vol. 7, 2006, pp. 1–5.
115. Osenbrugger C.V., Regt C., “Electrochemical micromachining”, *Philips Technical Review*, Vol. 42, 1985, pp. 22–32.
116. Datta M., Romankiw L.T., “Applications of chemical and electrochemical micromachining in the electronic industry”, *Journal of the Electrochemical Society*, Vol. 136, 1989, pp. 285c.
117. Jain V.K., Rajurkar K.P., “An integrated approach for tool design in ECM”, *Precision Engineering*, Vol. 13, no. 2, 1991, pp. 111–124.
118. Köhler M., **Etching in microsystems technology**, Wiley VCH, 1999, Germany, pp. 74–77.
119. Bhattacharyya B., Malapati M., Munda J., “Experimental study on electrochemical micromachining”, *Journal of Materials Processing*

Technology, Vol. 169, 2005, pp. 485–492.

120. Bard A.J., Inzelt G., Scholz F. (Eds), **Electrochemical Dictionary**, Springer-Verlag, Heidelberg, 2008
121. Strehblow H.H., "Passivity of metals", in: Alkire R.C., Kolb D.M. (Eds), Advances in electrochemical science and engineering, Wiley–VCH, Weinheim, 2003, pp. 271-374.
122. Strehblow H.H., "Mechanisms of pitting corrosion", in: Marcus P. (Ed), Corrosion mechanisms in theory and practice, Marcel Dekker, New York, 2002, pp. 243–285.
123. Williams K.R., Muller R.S., "Etch rates for micromachining processing", *Journal of Microelectrochemical Systems*, Vol. 5, no. 4, 1996, pp. 256–269.
124. Kikyuama H., Miki N., Saka K., Takano J., Kawanabe I., Miyashita M., Ohmi T., "Principles of wet chemical processing in ULSI microfabrication", *IEEE Transactions, Semiconductor Manufacturing*, Vol. 4, no. 1, 1991, pp. 26–35.
125. Fisher Chemical/Fisher Scientific, "Bottle label of potassium hydroxide, solid", Fisher chemical, Fair lawn, New Jersey, 1996.
126. Seidel H., Csepregi L., Heuberger A., Baumgärtel H., "Anisotropic etching of crystalline silicon in alkaline solutions I. Orientation dependence and behavior of passivation layers", *Journal of Electrochemical Society*, Vol. 137, no. 11, 1990, pp. 3612–3626.
127. Dickerson R.E., Gray H.B., Haight Jr. G.P., **Chemical Principles**, Menlo Park, CA: Benjamin/Cummings, 1979.
128. Glembocki O.J., Palik E.D., "Hydration model for the molarity dependence of the etch rate of Si in aqueous alkali hydroxides", *Journal of Electrochemical Society*, Vol. 138, no. 4, 1991, pp. 1055–1063.
129. Nielsen H., Hackleman D., "Some illumination on the mechanism of SiO_2 etching in HF solutions", *Journal of Electrochemical Society*, Vol. 130, no. 3, 1983, pp. 708–712.
130. Sampsell J.B., "The digital micromirror device and its application projection displays", in: 7th International Conference on Solid-state sensors and Actuators, Yokahama, Japan, June 1993, pp. 24–27.
131. Dabrowski L., Paczkowski T., "Computer simulation of two-dimensional electrolyte flow in electrochemical machining", *Russian Journal of Electrochemistry*, Vol. 41, no. 1, 2005, pp. 91–98.
132. Fahidy T.Z., Soida R.E., "The estimation of electrolyte temperature in small scale cell under electric current flow", *Electrochimica Acta*, Vol. 49, no. 7, 2004, pp. 1097–1103.
133. Rosenkranz C., Lohrengel M.M., Schultze J.W., "The surface structure during pulsed ECM of iron in $NaNO_3$", *Electrochimica Acta*, Vol. 50, 1995, 2009–2016.
134. Zhu S.M., Larsson C., Bannard J., "On the use of dilute solutions as ECM electrolytes, Proceedings of ISEM VII, 1983, pp. 405–415.
135. De Silva A.K.M., Altena H.S.J., McGeough J.A., "Influence of electrolyte

concentration on copying accuracy of precision–ECM" *CIRP Annals-Manufacturing Technology*, Vol. 52, no. 1, 2003, pp. 165–168.

136. Gamburg Y.D., Grosheva M.Y., Biallozor, S., Hass M., "The electrochemical deposition of nickel from electrolytes containing malonic acid", *Surface and Coatings Technology*, Vol. 150, 2002, pp. 95–100.
137. Reddy M.S., Jain V.K., Lal G.K., "Tool design for ECM: correction factor method", *Transactions of the ASME*, Vol. 10, 1998, pp. 111–118.
138. Zhu D., Yu C.Y., "Investigation on the design of tool shape in ECM", *ASME PED*, Vol. 58, 1992, pp. 181–190.
139. El-Hofy H., **Advanced machining processes– Nontraditional and hybrid machining processes**, McGraw-Hill, 2005, pp. 83–84.
140. Wang J., **Analytical electrochemistry**, 2nd ed, John Wiley & Sons Inc. New York, 2001, pp. 117–118.
141. Vitus C.M., Isaacs H.S., Schroeder V., "A study of the electrochemical behavior of tungsten in caustic solutions and platinum/iridium in chloride solutions", Informal report submitted to the United States Department of Energy, USA, 1994.
142. Wilson J.F., **Practice and theory of ECM**, John Wiley and sons, New York, 1971.
143. Zhang Y., Bulk titanium microfluidic devices, Ph D thesis, University of California, USA, 2006.
144. Aimi M.F., Bulk titanium microelectromechanical systems, Ph D thesis, University of California, USA, 2005.
145. Takami T., "DC etching tungsten tip preparation manual, version 1.0", prepared on February 18, 2009. Accessed: 9 May 2009.
Available on: www.ttakami.com/ DCtipEtching/DCtipEtching.html
146. Rajurkar K.P., Zhu D., McGeough J.A., Kozak J., De Silva A.K.M., "New developments in electrochemical machining", *Annals of the CIRP*, Vol. 48, no. 2, 1999, pp. 567–579.
147. Sorkhel S.K., Bhattacharyya B., "Computer aided design of tools in ECM for accurate job machining", Proceedings of the ISEM-9, Japan, 1989, pp. 240–243.
148. Chang C.S., Hourng L.W., Chung C.T., "Tool design in electrochemical machining considering the effect of thermal-fluid properties", *Journal of Applied Electrochemistry*, Vol. 29, 1999, pp. 321–330.
149. Chang C.S., Hourng L.W., "Two-dimensional two-phase numerical model for tool design in electrochemical machining", *Journal of Applied Electrochemistry*, Vol. 31, 2001, pp. 145–154.
150. Alder G.M., Clifton D., Mill F., "A direct analytical solution to the tool design problem in electrochemical machining under steady state conditions", Proceeding Institution of Mechanical Engineers Part B, Vol. 214, 2000, pp. 745–750.
151. Das S., Mitra A.K., "Use of boundary element method for the determination

of tool shape in electro-chemical machining", *International Journal for Numerical Methods in Engineering*, Vol. 35, no. 5, 1992, pp.1045–1055.

152. Lacey A.A., "Design of a cathode for an electromachining process", *IMA Journal of Applied Mathematics*, Vol. 34, 1985, pp. 259–267.
153. Dornfeld D., Min S., Takeuchi Y., "Recent advances in mechanical micromachining", *Annals of the CIRP*, Vol. 55, no. 2, pp. 745–768.
154. Albers A., Marz J., Burkardt N., "Design methodology in micro technology", 14th International Conference on Engineering Design, ICED 03, 2003.
155. Rahman M., Lim H.S., Neo K.S., Senthil Kumar A., Wong Y.S., Li X.P., "Tool-based nanofinishing and micromachining", *Journal of Materials Processing Technology*, Vol. 185, 2007, pp. 2–16.
156. Yamagata Y., Higuchi T., "Three-dimensional micro fabrication by precision cutting technique", *Journal of Japan Society of Precision Engineering*, Vol. 61, no. 10, 1995, pp. 1361–1364.
157. Waida T., Okano K., "Micro-grinding of micro-machine component", *Journal of Japan Society of Precision Engineering*, Vol. 61, no. 10, 1995, pp. 1365–1368.
158. Yong L., Yunfei Z., Guang Y., Liangqiang P., "Localized electrochemical micromachining with gap control", *Sensors and Actuators–A*, Vol. 108, 2003, pp. 144–148.
159. Masuzawa T., Kuo C.L., Fujinu I.I.S., "A combined electrical machining process for micronozzle fabrication, *Annals of the CIRP*, Vol. 43, no. 1, 1994, pp. 189–192.
160. Ohmori H., Uehara Y., Katahira K., Lin W., Watanabe Y., "Fabrication of ultra-fine tools using a desktop micro-grinding system", Proceedings of 12th International Conference on Monitoring and Automatic Supervision in Manufacturing, Kraków, 2004.
161. Mithu M.A.H., Fantoni G., "Etching behavior of tungsten microtool and its applications in electrochemical micromachining", *International Journal of Precision Technology*, Accepted (in press).
162. Mithu M.A.H., Fantoni G., Ciampi J., "Fabrication of micro nozzles and micro pockets by electrochemical micromachining", *International Journal of Machining and Machinability of Materials*, Accepted (in press).
163. Liu Y., Zhu D., Zeng Y., Yu H., "Development of microelectrodes for electrochemical micromachining" *International Journal of Advanced Manufacturing Technology*, doi: 10.1007/s00170-010-3035-2.
164. Hung W., Sundarram S., Ozkeskin F., Powers M., Manriquez J., Vasiraju V., "Electrochemical micro machining: A case study for synergistic international industry-academia collaboration", American Society for Engineering Education, AC 2009-2502 Past ASEE Annual Conferences & Expositions, June 14 - 17, 2009, Austin, TX.
165. Choi S.H., Ryu S.H., Choi D.K., Chu C.N., "Optimal machining condition of WC-microshaft using electrochemical machining", KSPE Fall Annual Meeting, 2002, pp. 245 –249.

166. Fan Z.W., Hourng L.W., Wang C.Y. “Fabrication of tungsten microelectrodes using pulsed electrochemical machining”, *Precision Engineering*, Vol. 34, no. 3, 2010, pp. 489–496.

167. Mammana S.S., Salvadon M.C., “Characterization of diamond sonic micronozzles and microtube”, *Journal of Vacuum Science & Technology B*, Vol. 21, no. 5, 2003, pp. 2034–2037.

168. Kim B.H., Ryu S.H., Choi D.K., Chu C.N., “Micro electrochemical milling”, *Journal of Micromechanics and Microengineering*, Vol. 15, no. 1, 2004, pp. 124–129.

169. Pust S.E., Salomo M., Oesterschulze E., Wittstock G., “Influence of electrode size and geometry on electrochemical experiments with combined SECM–SFM probes”, *Nanotechnology*, Vol. 21, 2010, 12pps.

170. N. Tenigyahi, “Current status in and future trends of ultra precision machining and ultra fine material processing”, *Annals of the CIRP*, Vol. 2, no.2, 1983, pp. 573–582.

171. Bhattacharyya B., Sorkhel S.K., “Investigation for controlled electrochemical machining through response surface methodology- based approach”, *International Journal of Materials Processing Technology*, Vol. 86, 1999, pp. 200–207.

172. Lee E.S., Park J.W., Moon Y.H., “A study on electrochemical micromachining for fabrication of microgrooves in an air-lubricated hydrodynamic bearing”, *International Journal of Advanced Manufacturing Technology*, Vol. 20, 2002, pp. 720–726.

173. Shin H.S., Kim B.H., Chu C.N., “Analysis of the side gap resulting from micro electrochemical machining with a tungsten wire and ultrashort voltage pulses”, *Journal of Micromechanics and Microengineering*, Vol. 18, 2008, 6pp.

174. Lescuras V., André J.C., Lapicque F., “Jet electrochemical etching of nickel in a sodium chloride medium assisted by a pulsed laser beam”, *Journal of Applied Electrochemistry*, Vol. 25, 1995, pp. 933–939.

175. Parshutin V.V., Bogdashkina N.L., Chernova G.P., “The effect of medium on the corrosion and electrochemical behavior of nickel”, *Protection of Metals*, 2007, Vol. 43, no. 1, pp. 59–65.

176. Arzhintar’ O.A., Dikusar A.I., Petrenko, V.I., “**Electrochemical machining of metals**”, Chisinau: Shtiintsa, 1974, p. 30.

177. Amirkhanova L.A., Sharikova L.P., Rafikova, L.G., **Electrochemical anodic machining of metals**, Ivanovo, 1988.

178. Shams El Din A.M., Al-Kharari F.M., Al-Fahd Z., El-Tantawy, Y.A., *Corrosion Prevention and Control*, Vol. 32, no. 5, 2007, p. 59-65.

179. Dubey J.S., Wadekar S.L., Chakravartty J.K., “Elevated temperature fracture toughness of AISI 403 martensitic stainless steel”, Journal of Nuclear Materials, Vol. 254, nos. 2-3, 1998, pp. 271–274.

180. Gupta C.K., **Materials in nuclear energy applications**, Vol. 1, CRC Boca Raton, FL, 1989.

181. Chikamori K., “Electrochemical wire cutting method”, United States patent no. 4,052,274, 1977, USA. Access: 3 March 2011. Available on: http://www.patentgenius.com/patent/ 4052274.html
182. Byrne G., Dornfeld D., Inasaki I., Ketteler G., Konig W., Teti R., “Tool condition monitoring (TCM) – the status of research and industrial application”, *Annals of the CIRP*, Vol. 44, 1995, pp. 541.
183. Ulsoy A.G., “Monitoring and control of machining”, in: Wang L., Gao R.X. (Eds.), Condition monitoring and control for intelligent manufacturing, Springer Series in Advanced Manufacturing, 2006, pp. 1–32.
184. Danai K., Ulsoy A.G., “An adaptive observer for on-line tool wear estimation in turning – part I: theory”, *Mechanical Systems and Signal Processing,* Vol. 1, no. 2, 1987, pp. 211–225.
185. Danai K., Ulsoy A.G., “An adaptive observer for on-line tool wear estimation in turning - part II: results”, *Mechanical Systems and Signal Processing,* Vol. 1, no. 2, 1987, pp. 227–240.
186. Du R., Elbestawi M.A., Wu S.M., “Automated monitoring of manufacturing processes, part 1: monitoring methods”, *ASME Journal of Engineering for Industry*, Vol. 117, 1995, pp. 121.
187. Ulsoy A.G., Koren Y., Rasmussen F., “Principal developments in the adaptive control of machine tools”, *ASME Journal of Dynamic Systems, Measurement, and Control*, Vol. 105, no. 2, 1983, pp. 107–112.
188. Park J.J., Ulsoy A.G., “On-line tool wear estimation using force measurement and a nonlinear observer”, *ASME Journal of Dynamic Systems, Measurement, and Control*, Vol. 114, no. 4, 1992, pp. 666–672.
189. Begnon C., Bedrin C., “Application of eddy currents to the in process measurement of the gap in ECM”, *Annals of CIRP*, Vol. 31, no. 1, 1982, pp.115–118.
190. Reddy M.S., Jain V.K., Lai G.K., “Tool design for ECM: correction factor method,” *ASME*, *Journal of Engineering for Industry*, Vol. 110, 1988, pp.111–118.
191. Rajurkar K.P., Schnacker C.L., “Some aspects of ECM performance and control,” *Annals of CIRP*, Vol. 37, no. 1, 1988, pp. 183–186.
192. El-Sayed E.M., “Towards better control of electrochemical machining (ECM) parameters by computer interfacing”, M. Sc Thesis, King Saud University 1989, Riyadh.
193. Sorkhel S.K., Bhattacharyya B., “Parametric control for optimal quality of workpiece surface in ECM,” *Journal of Material Processing Technology*, Vol. 40, 1994, pp. 271–286.
194. Kozak J., Dabrowiski L., Rusazj A., Slawinski R., “Computer simulation on numerically controlled electrochemical machining (ECM-NC) with a spherical tool electrode,” CAPE-11 Conference, 1995, pp. 205–210.
195. Amalnik M.S., McGeough J.A., “Intelligent concurrent manufacturability evaluation for design for electrochemical machining”, *Journal of Material Processing Technology*, Vol. 61, 1996, pp. 130–139.

196. Khayry A., “A knowledge-based system for electrochemical machining procedure”, *Journal of Material Processing Technology*, Vol. 58, 1996, pp.121–130.

197. Chikamori K., “Possibilities of electrochemical micromachining”, *International Journal of the Japan Society for Precision Engineering*, Vol. 32, no. 1, 1998, pp. 37–38.

198. Lu Y., Liu K., Zhao D., “Experimental investigation on monitoring interelectrode gap of ECM with six-axis force sensor*”, International Journal of Advanced Manufacturing Technology*, 2010. doi 10.1007/s00170-010-3105-5.

199. Zhu D., Rajurkar K.P., Wei B., “Modeling and monitoring and control systems”, *Journal of Manufacturing Science and Engineering*, *Transactions of ASME*, Vol. 119, no. 4, 1997, pp. 770–775.

200. Lu Y.H., Zhao D.B., Zhu D., “Mechanical property analysis of inter-electrode gap in electrochemical machining based on six force components”, *Chinese Journal of Mechanical Engineering*, Vol. 15, no. 23, 2004, pp. 2142–2145.

201. Rivera J.L., Michalek D.J., Sutherland J.W., “Air quality in manufacturing”, in: Kutz M. (Ed), Environmentally conscious manufacturing, John Wiley & Sons, New Jersey, 2007, pp. 145–178.

202. De Silva A.K.M., McGeough J.A., “Process monitoring of electrochemical micromachining”, *Journal of Material Processing Technology*, Vol. 76, 1998, pp. 165–169.

203. Kenney J.A., Hwang G.S., Shin W., “Two-dimensional computational model for electrochemical micromachining with ultrashort voltage pulses*”, Applied Physics Letter*, Vol. 84, no.19, 2004, pp. 3774–3776.

204. Berre M.L., Chen Y., Crozatier C., Zhang Z.L., “*Electrocapillary* force actuation of microfluidic elements”, *Microelectronic Engineering*, Vol. 78–79, 2005, pp. 93–99.

205. Sundarram S.S, “Development of electrochemical micro machining”, M Sc Thesis, Texas A&M University. Access 22 October, 2010. Available on: http://repository.tamu.edu/bitstream/handle/1969.1/86045/Sri.pdf?sequence=1

206. Kim S.H., Seidman D.N., “An electrochemical etching procedure for fabricating scanning tunnelling microscopy and atom-probe field-ion microscopy tips”, *Metals and Materials International*, Vol. 9, no. 4, 2003, pp. 399–404.

207. Moore W.J., **Physical chemistry**, Longmans, London, 1957.

Appendices

Appendix- A

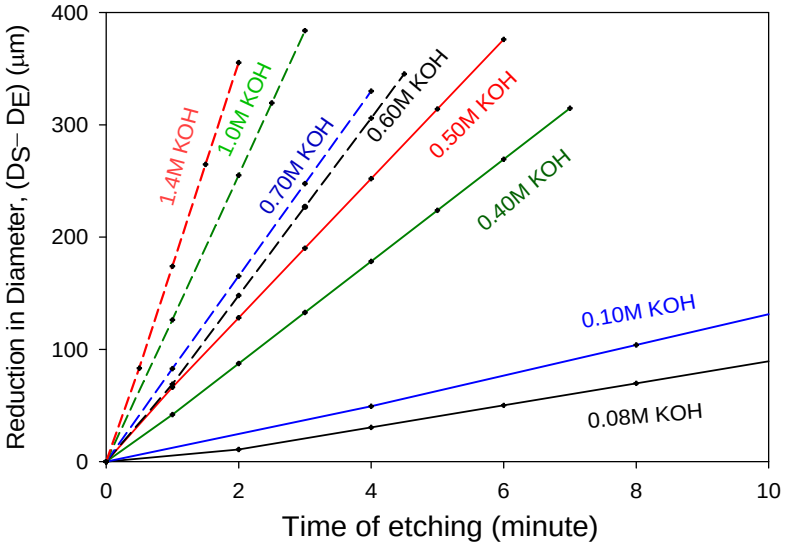

Fig. A.1 *Reduction in diameter (D_S—D_E) with etching time for various electrolyte concentrations and a 9 V constant applied potential.*

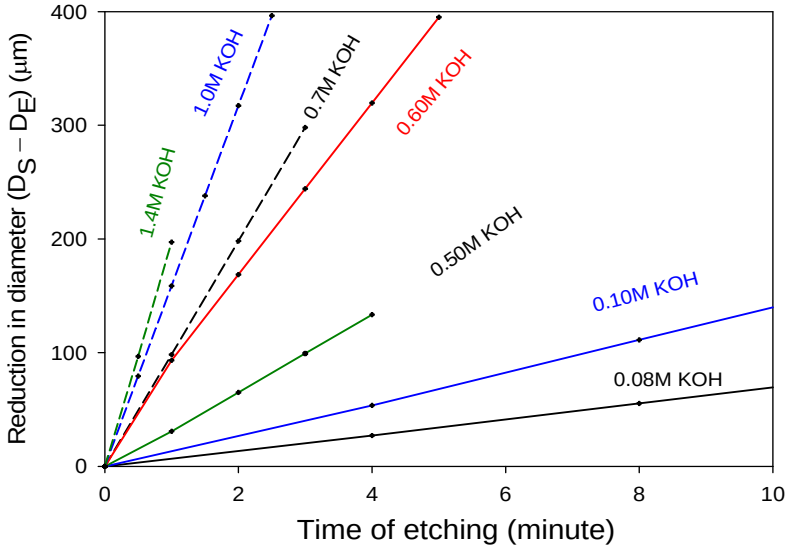

Fig. A.2 *Reduction in diameter (D_S—D_E) with etching time for various electrolyte concentrations and a 15 V constant applied potential.*

Appendix- B

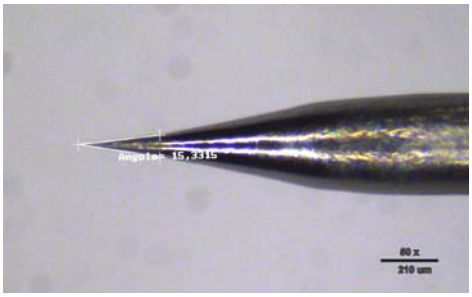

(a) 0.5M, 15V, 4.2 min, SS, 15.4^0 tip angle

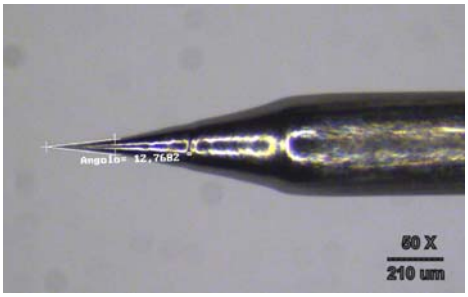

(b) 0.5M, 15V, 3.8 min, Tungsten, 12.8^0 tip

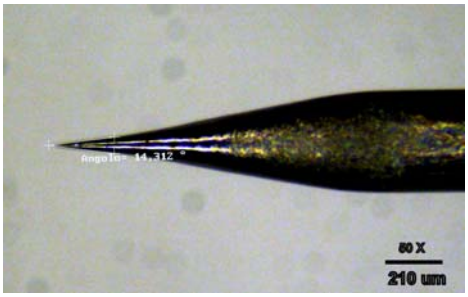

(c) 1.0M, 15V, 1.8 min, SS, 14.3^0 tip angle

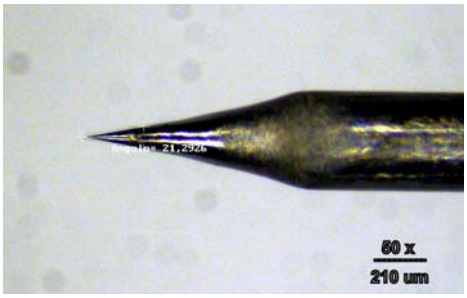

(d) 1.0M, 15V, 1.77 min, Tungsten, 21.3^0 tip

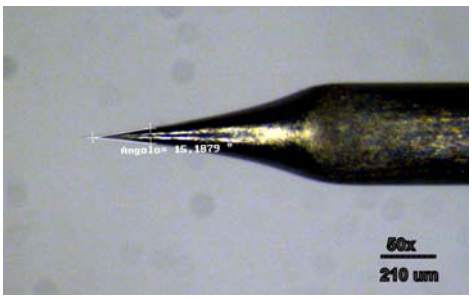

(e) 1.5M, 9V, 1.87 min, Tungsten, 15.2^0 tip

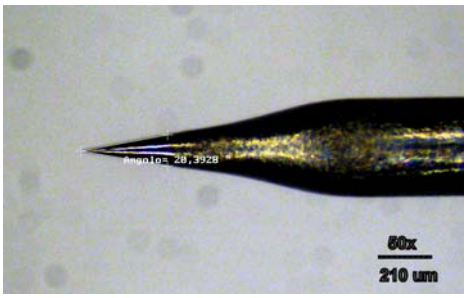

(f) 1.5M, 15V, 1.6 min, Tungsten, 20.4^0 tip

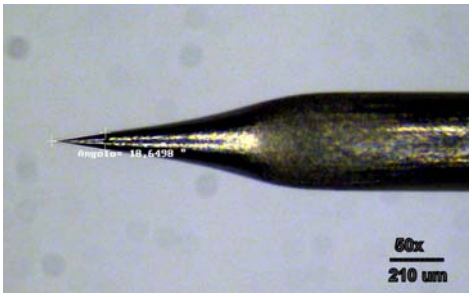

(g) 2.0M, 9V, 1.5 min, SS, 18.6^0 tip

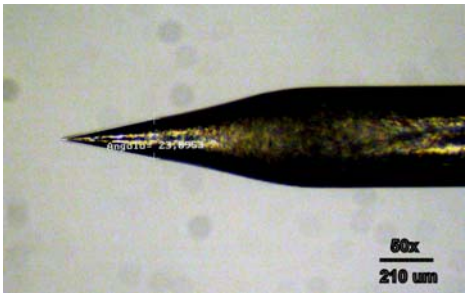

(h) 2.0M, 9V, 1.5 min, Tungsten, 23.9^0 tip

Fig. B *Pictorial illustration of some randomly selected microtool tip angles angle.*

Appendix- C

The nature of dynamic viscosity for Hydrochloric acid

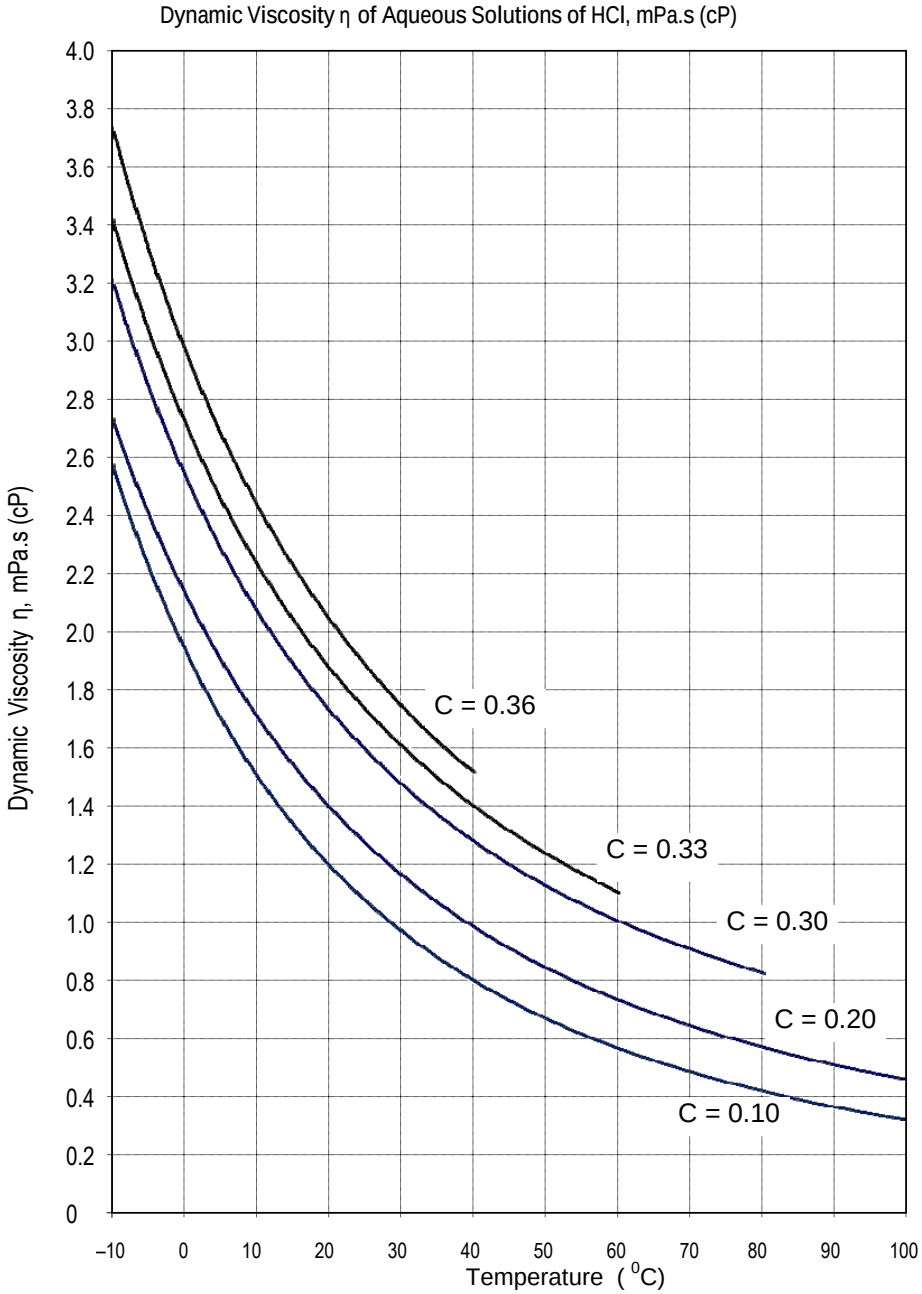

Source: http://www.solvaychlorinatedinorganics.com/docroot/chlo_inorg/static_files/